DISSERTATION

DEDICATED EXHAUST GAS RECIRCULATION APPLIED TO A RICH BURN INDUSTRIAL NATURAL GAS ENGINE

Submitted by

Chris Van Roekel

Department of Mechanical Engineering

In partial fulfillment of the requirements

For the Degree of Doctor of Philosophy

Colorado State University

Fort Collins, Colorado

Fall 2020

Doctoral Committee:

Advisor: Daniel B. Olsen

Shantanu Jathar
Anthony Marchese
Peter Young

Copyright by Christopher Allen Van Roekel 2020

All Rights Reserved

ABSTRACT

DEDICATED EXHAUST GAS RECIRCULATION APPLIED TO A RICH BURN INDUSTRIAL NATURAL GAS ENGINE

Rich burn natural gas engines provide power for industrial applications such as gas compression. In this application where exhaust oxides of nitrogen (NO_x) requirements can be critical, rich burn engines offer best in class aftertreatment emission reduction and operating cost capabilities by using a non-selective catalyst reduction (NSCR) or three-way catalyst system. However, due to high combustion temperatures associated with near stoichiometric air-fuel ratio (AFR) operation, rich burn engines are limited in brake mean effective pressure (BMEP) by combustion temperature. Consumers in the gas compression application are left to choose between engines that are capable of meeting even the most stringent emission requirements (rich burn) and engines with high BMEP rating (lean burn). Charge dilution by way of excess air (lean burn) or exhaust gas recirulation (EGR) is a common method used to lower combustion temperature with the purpose of limiting the production of engine out NO_x. Conventional configurations of EGR consist of high pressure loop (HPL) and low pressure loop (LPL), each of which rely on components exposed to relatively high temperatures to control the impact that EGR has on combustion. Dedicated EGR is a novel variant of conventional EGR configurations which allows for the impact that EGR has on combustion to be controlled by components exposed to ambient temperature natural gas while also lowering rich burn combustion temperatures. Due to the lack of published research on dedicated EGR applied to industrial natural gas engines and consumer driven need for technologies to increase rich burn industrial natural gas engine BMEP this work represents an initial investigation into challenges associated with and capabilities of dedicated EGR.

A Chemkin chemical kinetics model using the SI Engine Zonal, Flame Speed Calculator, and Equilibrium models was developed to quantify dedicated cylinder exhaust composition, laminar

flame speed, and equilibrium combustion composition, respectively. The Aramco 2.0 mechanism was used for natural gas kinetics and was modified to include Zel'dovich mechanism for NO_x formation. Engine experiments were conducted using a Caterpillar G3304 rich burn natural gas engine modified to operate with and without dedicated EGR. Initial tests that included power sweeps at fixed dedicated cylinder AFR revealed that operating conditions appropriate for dedicated EGR gasoline engines were not suitable for dedicated EGR natural gas engines. A response surface method (RSM) optimization was performed to find improved operating conditions at part load, 3.4 bar BMEP. Results showed that advanced spark timing and slightly rich dedicated cylinder AFR were optimal to achieve decreased coefficient of variance of indicated mean effective pressure (COV IMEP) and balanced cylinder IMEP output. In order to assess how operating with dedicated EGR would affect the performance of a NSCR system at 6.7 bar BMEP and fixed operating conditions engine AFR was swept between rich and lean conditions to quantify catalyst reduction efficiency and find the emissions compliance window. Without intentional AFR dithering the emissions compliance window was increased significantly. Finally, using best operating conditions from the RSM optimization and engine AFR sweep tests engine BMEP was increased beyond the 6.7 bar rating to find the possible increase in power density resulting from dedicated EGR.

ACKNOWLEDGEMENTS

In January 2015 I began the mechanical engineering masters degree program at CSU with Dr. Dan Olsen as my research advisor. At that time I had no experience in engine research, little knowledge of engines or combustion, and only second hand accounts of what work was being on at the Powerhouse. During the past five years Dr. Olsen has guided, advised, and mentored me through the completion of my masters degree, numerous conferences, publications, meetings, classes, engine tests, and now the completion of my doctoral degree. I am sincerely thankful and grateful for the time he invested in me during my graduate program. Much of the value of my work has come from collecting data from engines under test, and I am certain that there would be no engine data to present if it were not for the assistance of the Powerhouse staff of Mark James, James Tillotson, and Kirk Evans. Their patience in answering countless questions and assistance in troubleshooting issues helped me develop into the engineer I am today, but I am most thankful for the friendships I have been able to develop with each of them during my time at the Powerhouse. The funding for this work was provided by the Caterpillar Large Power Systems Division. Dave Montgomery, Jas Singh, and other Caterpillar employees provided me with helpful and critical feedback throughout the project and gave me opportunities to present this work, learn from themselves and other industry experts, and expand my understanding of industry perspectives. Especially during engine commissioning but throughout this work I was supported by staff at Woodward, Inc. Aaron Zimenoff provided numerous hours of technical product support, Erik Knudsen supplied funding and components, Don Grove and Tim Hinde help with engine commissioning and advising, and Greg Hampson loaned pre-chamber spark plugs. At my times during my work I was fortunate enough to have the assistance of so many undergraduate and graduate students, without which this work would not have been accomplished. All along the way, my parents Steve and Deanne with the rest of my family have been unwavering in their support of my time and work done at the Powerhouse. My deepest gratitude and love are for them.

DEDICATION

for His glory

TABLE OF CONTENTS

LIST OF TABLES

LIST OF FIGURES

Chapter 1

Introduction

Historically, exhaust gas recirculation (EGR) has been used to lower peak combustion temperatures in spark ignited (SI) and compression ignition (CI) engines with the intent of limiting the formation of engine out NO_x emissions.[1] SI rich burn natural gas engines are commonly found in an industrial oil and gas type setting. This class of engine is frequency used in gas compression and natural gas well service. To be considered a rich burn engine it must operate at an air-fuel ratio (AFR) of less than lambda 1.1,[2] and at these conditions NO_x is formed primarily by the Zel'dovich mechanism which has a rate of production that is a strong, non-linear function of temperature[3, 4, 5]. The method by which EGR lowers peak combustion temperatures is acting as a diluent in combustion reactants. Considering a constant volume, adiabatic system the general equation for calculating the adiabatic flame temperature during a combustion event can written by Equation 1.1[3]

$$H_{reac} - H_{prod} - R_u(N_{reac}T_{init} - N_{prod}T_{ad}) = 0 \tag{1.1}$$

Natural gas fuel composition can vary significantly based on the source but in general consists of methane (CH_4), ethane (C_2H_6), propane (C_3H_8), various C_{4+} hydrocarbons, nitrogen (N_2), and carbon dioxide (CO_2). Including considerations for dissociation of complete combustion products at high temperature and assuming no incomplete combustion of hydrocarbons, products resulting from these reactants consist primarily of N_2, CO_2, water (H_2O), carbon monoxide (CO), and nitric oxide (NO) at conditions near lambda 1. Standardized enthalpies and ratio of specific heats of common natural gas combustion reactants and products are found in Table 1.1. Recirculating complete combustion products such as CO_2 and H_2O act to lower the overall standardized enthalpy of combustion reactants, and following Equation 1.1 a decrease in standardized enthalpy of reactants leads to a lower adiabatic flame temperature and, in practice, a lower peak combustion temperature. In addition to the primary impact on general combustion thermochemistry, EGR

Table 1.1: Properties of common natural gas combustion reactants and products at varied temperature.

	Enthalpy of Formation @298K (kJ/kmol)	γ @298K	γ @2000K	γ @2500K
CH_4	-74,831	1.32	1.09	1.08
C_2H_6	-84,667	1.18	1.06	1.05
C_3H_8	-103,847	1.13	1.04	1.04
N_2	0	1.40	1.30	1.29
CO_2	-393,546	1.28	1.16	1.16
O_2	0	1.40	1.28	1.27
H_2O	-241,845	1.33	1.19	1.18
CO	-110,541	1.40	1.30	1.29
NO	90,297	1.40	1.29	1.29

also has secondary effects on other aspects of the combustion process including indicated thermal efficiency, heat loss during combustion, combustion burn duration, and heating value of the combustion charge. Thermal efficiency of a cycle in general terms is described in Equation 1.2[6]. Applying this to a theoretical Otto cycle while invoking assumptions such as combustion at constant volume and isentropic compression and expansion, through various steps Equation 1.2 can be simplified to Equation 1.3. The addition of exhaust products to the combustion charge act to increase the ratio of specific heats (γ) by decreasing combustion temperature. Values for gamma at a temperature of 298 K, 2000 K, and 2500 K are shown in Table 1.1. Increasing gamma due to decreased combustion temperature increases the theoretical achievable indicated thermal efficiency of the cycle. Instantaneous heat transfer from the combustion charge to the surrounding wall includes convective and radiative heat transfer. Detailed analysis of heat transfer coefficient correlations is outside of the scope of this work, but it is important to note that as described during discussion about peak combustion temperature, dilution of the combustion charge results in lower combustion temperature. Assuming a constant cylinder wall temperature, decreased peak combustion temperatures lead to lower heat transfer losses and increased total efficiency. A comparative analysis of the effects of increased γ and lower peak cylinder temperatures have on efficiency was done by Caton [7]. It was shown that for the conditions considered improvements in net indicated

thermal efficiency were achieved mainly through increases in γ (between 59-85$\%$ of the overall efficiency improvement).

$$\eta = \frac{work}{heatinput} = \frac{Q_H - Q_L}{Q_H} = 1 - \frac{Q_L}{Q_H} \tag{1.2}$$

$$\eta_{Otto} = 1 - \frac{1}{r^{\gamma-1}} \tag{1.3}$$

Where:

r = compression ratio

γ = ratio of specific heats of the unburned combustion charge

Another secondary effect of lower combustion temperature and changes in unburned charge chemistry due to EGR is prolonged combustion duration. The duration of combustion can be physically equated to cylinder geometry and turbulent flame speed. By dividing a turbulent flame into small discretized areas, it can be observed that the turbulent flame speed is a function of the laminar flame speed. Following work done by Mallard and Le Chatelier[8] laminar flame speed can be described by Equation 1.4 [4].

$$S_L = (\alpha \frac{\omega}{\rho})^{1/2} \tag{1.4}$$

Where:

α = thermal diffusivity

ρ = the unburned gas density

ω = reaction rate in terms of concentration

The thermal diffusivity term can further be simplified to Equation 1.5. It can now be observed that decreases in burned and interlayer temperature and increases specific heat which occur while using EGR act to decrease the thermal diffusivity of the combustion charge and in result the laminar flame speed. Decreased laminar flame speed leads to overall increased combustion duration.

$$\alpha = \frac{\lambda}{\rho c_p}(\frac{T_f - T_i}{T_i - T_0}) \tag{1.5}$$

Whether implemented on SI or CI engines EGR has been done so using high pressure loop (HPL) or low pressure loop (LPL). The difference between the two configurations is the physical location of exhaust gas extraction and introduction into the fresh-air fuel mixture. In a HPL configuration exhaust is taken from the exhaust manifold upstream of the turbine side of a turbocharger, cooled via a heat exchanger, metered across a valve, and finally introduced downstream of the compressor side of a turbocharger. The advantage of an HPL configuration is its ability to respond to necessary changes in EGR needs due to a relatively small volume of gas between the exhaust and intake manifolds. However, since the exhaust does not pass through any type of aftertreatment system it still includes all of the engine out composition. In a diesel application this can result in possible particulate matter fouling of the heat exchanger used to cool the exhaust. The primary disadvantage of a HPL configuration is the need for the exhaust gas upstream of the turbine must have a higher pressure than the air-fuel found in the intake manifold. Using a valve to meter EGR rate acts to enhance this issue due to inherent pressure drop across the valve. Higher exhaust pressure acts to increase pumping efficiency losses. For this reason, LPL EGR configurations are favored for many engine applications where higher efficiency is necessary. LPL EGR configurations extract exhaust from the post-aftertreatment exhaust stream, pass it through a heat exchanger, and mix it with fresh-air fuel upstream of a turbocharger compressor. Exhaust is essentially free of high levels of particulate matter and lowers the chance of EGR valve and heat exchanger fouling. The pumping losses associated with HPL are avoided using an LPL configuration. The disadvantage of LPL EGR is its inability to respond quickly to transient engine operating conditions due to the relatively long distance the exhaust must travel [1, 9, 10, 11]. It is appropriate here to mention that combined HPL and LPL EGR configurations or dual loop EGR have been researched in several publications. Detailed analysis of these configurations lie outside of the scope of this work, but an acknowledgement of these configurations is warranted [12, 13]. Figure 1.1 shows the general layout of HPL and LPL EGR systems. Key components to an HPL or LPL EGR system are the following:

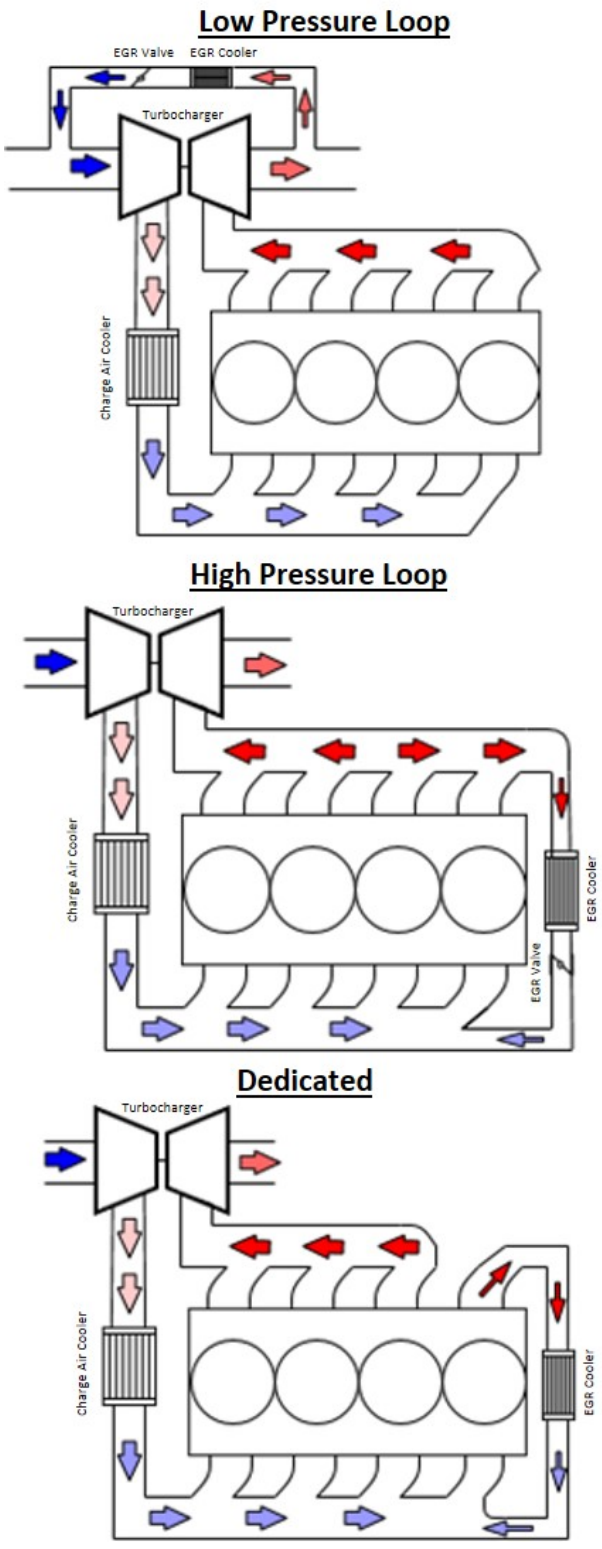

Figure 1.1: Schematic of LPL, HPL, and dedicated EGR techniques.

1. EGR Heat Exchanger. Regardless of combustion type (SI or CI) and type of conventional EGR configuration (HPL, LPL, or combined) cooling of exhaust prior to recirculation is necessary. The two most prominent design aspects of an EGR are cooler are the cooling capacity and fouling. First, given the range of exhaust volumetric flow and exhaust temperatures expected in an EGR system across the engine operating range an EGR cooler must be designed to adequately cool exhaust without dropping below the dew point temperature. Water condensation from exhaust is especially harmful due to the potential formation of sulfuric acid [14]. Conversely, exhaust temperatures must be kept low enough to protect the EGR valve and associated controls that are downstream of the EGR cooler and upstream of the intake manifold (HPL) or turbocharger compressor (LPL). Second, in CI HPL applications, consideration must be given to particulate matter concentration in the recirculated exhaust and possible fouling of the EGR heat exchanger.

2. EGR Metering Valve. Conventional LPL and HPL EGR systems rely on an EGR valve to meter the amount of exhaust recirculated to the intake manifold (HPL) or turbocharger compressor (LPL). To ensure acceptable engine operation and required NO_x reduction the amount of exhaust recirculated must be changed according to engine operating condition. At low power engine operating conditions less EGR can be tolerated by the engine due to relatively cool combustion temperatures which can result in unstable combustion. At high power conditions EGR acts to lower the energy available in the combustion charge and thus lowers peak power output so less EGR is used at this condition also. These limitations result in a general EGR rate range of 0-20$\%$ on a typical stoichiometric engine [1]. To avoid water condensation, the temperature of exhaust passing through the EGR metering valve can be in excess of 100 °C.[14] Based on discussion with industry partners exposure to temperatures in this range lead to failure of EGR metering valves.

First introduced in work done by Southwest Research Institute dedicated EGR is a variant on conventional HPL, LPL, and combined EGR systems [15]. A dedicated EGR system operates such that one or more of the engine cylinders is specified as a dedicated cylinder. All of the ex-

haust from dedicated cylinder(s) is recirculated back to the intake manifold of the engine at all engine operating conditions. Thus, a constant nominal EGR rate is realized. As mentioned, engine EGR tolerance changes with changes in engine operating conditions. Dedicated EGR operates on the principal that the effect that recirculated exhaust has on combustion is controlled via exhaust composition rather than exhaust quantity. The dedicated cylinder is operated at fuel rich conditions while the remaining cylinders operate near stoichiometric conditions. Rich burn combustion chemistry allows for the presence of partial oxidation combustion products of hydrogen (H_2) and CO to be part of the exhaust. These combustion products allow for increased tolerance of EGR as researched by Gerty and Ivanic [16, 17]. One of the indicators of poor EGR tolerance is coefficient of variation of indicated mean effective pressure (COV of IMEP). The work done by Ivanic et al. quantified a measure of H_2 enrichment in EGR diluted combustion as percent 'plasmatron', and as the 'plasmatron' fraction increased the amount of partial oxidation combustion products of H_2 and CO in the EGR gas increased. Figure 1.2 shows how increasing the fraction of 'plasmatron' affected the COV of IMEP at different EGR dilution rates. It is important to clarify that this work was done on a spark ignited, single cylinder research engine with a combustion chamber that featured a low swirl and high tumble turbulence design. Tumble was increased using a plate that was added to the intake manifold. The fuel used was Phillips Chevron UTG-96 which had a research octane number of 96.1, a lower heating value of 43.1 MJ/kg, and a H/C molar ratio of 1.93. This result demonstrates that increased EGR tolerance in terms of acceptable COV of IMEP can be realized by adding H_2 and CO to an EGR diluted turbulent combustion chamber. The addition of H_2 is also meant to offset longer combustion burn duration that is encountered while operating with EGR systems. Ivanic et al. demonstrated improvements in 0-10$\%$ and 10-90$\%$ burn duration when adding more 'plasmatron' to the combustion charge. Another publication by Alger et al.[15] where a single cylinder gasoline engine with an 11:1 compression ratio (CR) and a constant nominal EGR rate of 22$\%$ showed that the addition of H_2 to the EGR composition resulted in decreased 10-90$\%$ burn duration. Figure 1.3 shows this result from that publication. The experimental engine combustion chamber consisted of a flat, two valve head with shallow piston bowl which resulted in

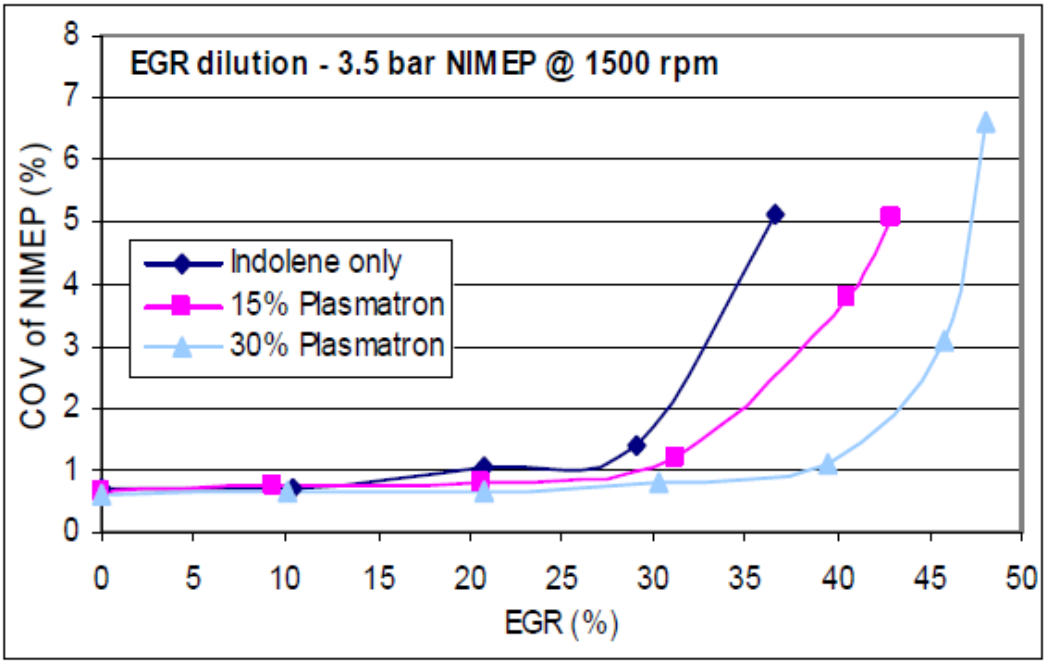

Figure 1.2: Quantifying COV of IMEP as a function of EGR dilution (%) given different partial oxidation products in the EGR [17].

low swirl and tumble ratios. The author notes that most of the charge motion came from the high squish area. A brief set of experiments was done to examine the effect of H_2 addition to natural gas combustion using the same single cylinder research engine. Natural gas EGR tolerance was improved by adding H_2 to the simulated EGR exhaust gas but the improvement was much less than what was shown for gasoline combustion. Interestingly, similar to the gasoline combustion tests the 10-90% burn duration for natural gas improved as move H_2 was added. Many other publications on the topic of dedicated EGR applied to gasoline engines were done by researchers at Southwest Research Institute. Their work focused mainly on the possibility of improving engine efficiency using dedicated EGR. Discussion of these publications can be found in section 4.8. By operating on the premise of EGR composition control rather than EGR quantity control, dedicated EGR has a significant advantage when compared to HPL, LPL, and combined systems, namely the removal of the EGR exhaust metering valve. Removing that valve eliminates a common warranty issue for engines operating with EGR systems. The two key components of a dedicated EGR system are the EGR heat exchanger and the dedicated cylinder fuel delivery system. The EGR heat

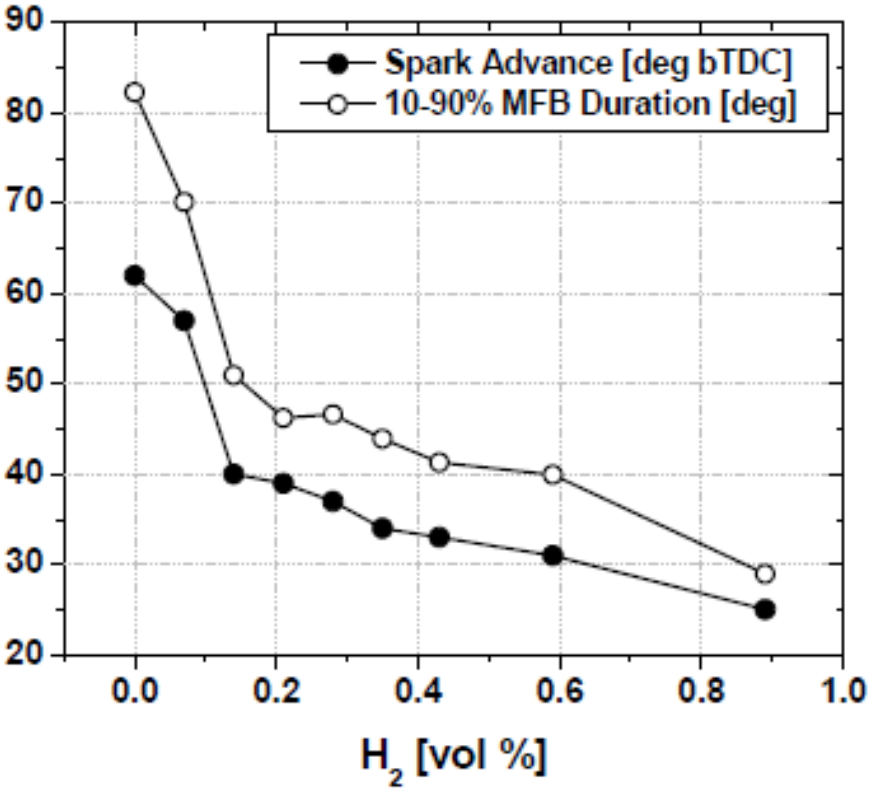

Figure 1.3: Examining the effect that H_2 has on 10-90% burn duration for a gasoline engine operating at 3.1 bar indicated mean effective pressure and 22% EGR rate. [15].

exchanger remains similar to a conventional EGR system. Fuel delivery to the dedicated cylinder can be done via port fuel injection if a low pressure fuel system is used. If port fuel inject or high pressure direct fuel injection are used delivery of additional fuel to the dedicated cylinder is straightforward. One of the less thought of fields where dedicated EGR can have an impact is the industrial natural gas engine industry. Industrial natural gas engines provide power in continuous prime, emergency, gas compression, and well service applications. Each of these applications has their respective hierarchy of design criteria such as continuous prime power where efficiency is most critical in cost of operation. In the gas compression application, reliably meeting site, state, and federal emissions regulations while also having high power density engines is most important. Meeting emissions regulations at gas compression sites regardless of location is done best by using a rich burn engine paired with a non-selective catalyst reduction (NSCR) or 3-way catalyst aftertreatment system. The tradeoff to operating a rich burn engine with best-in-class post catalyst

emissions is that these engines are currently limited in brake mean effective pressure (BMEP) due to combustion temperatures associated with near stoichiometric operation. In practice this can be most easily shown by comparison of natural gas engines in the oil & gas and electric production applications. The Caterpillar G3516TA is a stoichiometric gas engine intended to operate in the oil & gas field. Based on published engine data the rated power output at 1400 rpm is 1380 brake horsepower (bhp). The engine displacements is 69 liters (L) and is turbocharged [18, 19]. Conversely, the Caterpillar G3516C is a lean burn engine intended to operate in electric production (EP) applications. In this application efficiency is most important and emissions regulations are commonly met with no aftertreatment system using highly diluted (ultra lean burn) combustion. Similar to the G3516TA, the G3516C has a displacement of 69 L and turbocharged air system. It has different engine rotational speed options but the closest option to the G3516TA is 1500 rpm. At this speed the G3516C has a power rating of 1590 ekW or 2132 electric horsepower (ehp). If the assumption is made that bhp is equal to ehp this comparison shows that for a given displacement state of the art rich burn engines can produce only approximately 65% of lean burn engines.

Due to the impact that EGR has on combustion temperatures and the advantage that dedicated EGR has over conventional EGR systems, dedicated EGR may allow for rich burn natural gas engines to increase rated bmep while still offering low post aftertreatment emissions. With this in mind and considering the lack of published research on the topic of dedicated EGR applied to a multi-cylinder industrial natural gas engine the scope of this dissertation work includes the following:

1. Analysis of expected dedicated EGR exhaust composition and laminar flame speed with varying dedicated cylinder AFR. In chapter 2 of this work a Chemkin chemical kinetic model of a SI dedicated EGR engine is developed. It uses the Aramco 2.0 natural gas mechanism, the Chemkin SI zonal model for engine modeling and the Chemkin flame speed model for laminar flame speed calculations.

2. Previously published literature pertaining to the dedicated EGR concept applied to a gasoline engine showed improved combustion across all cylinders when the dedicated cylinder was

operated rich of stoichiometric conditions. A sweep of engine power at rated speed was done using a dedicated cylinder AFR similar to what was found in published literature. At varying engine power, combustion statistics of apparent heat release rate (AHRR), burn duration, and cylinder pressure are analyzed. In addition engine out emissions, engine efficiency, and exhaust temperatures are discussed.

3. The results from Chapter 3 pointed towards finding improved engine operating conditions, especially in terms of combustion statistics of COV IMEP and balanced cylinder IMEP. In Chapter 4 a RSM optimization is performed by incrementing variables of intake manifold temperature, spark timing, spark duration, and dedicated cylinder AFR at rated speed and 3.4 bar BMEP in an attempt to improve the aforementioned combustion statistics.

4. After finding improved operating conditions Chapter 5 builds off of the results from Chapter 4 using the improved conditions and exploring the performance of an NSCR catalyst at rated engine output of 6.7 bar BMEP. In this chapter the engine AFR is incremented rich and lean of stoichiometric to quantify the catalyst reduction efficiency and examine a typical post aftertreatment emissions compliance window.

5. Chapter 6 examines how dedicated EGR can extend the power output capabilities of a rich burn natural gas engine by lowering exhaust port temperature. Engine operating conditions were taken from the results of Chapter 4 and 5 to achieve what is thought to be the best combustion performance given the G3304 combustion chamber.

6. Finally, Chapter 7 concludes with a high level discussion of notable results and recommendations for future dedicated EGR work.

Chapter 2

Chemical Kinetic Modeling of Natural Gas Engine Combustion with Dedicated Exhaust Gas Recirculation

2.1 Summary

Using Chemkin chemical kinetics software, exhaust gas composition and combustion flame speed of a Caterpillar G3304 natural gas engine are modeled. The engine modeled is configured to operate with all exhaust from cylinder 1 routed back to the intake manifold. Equivalence ratio for cylinder 1 was varied between 0.5 and 1.8 while additional air or fuel was added to the remaining 3 cylinders to keep their combustion stoichiometric. The Spark Ignited Engine Zonal Model for Knock Assessment 0-D closed reactor is chosen for combustion simulation, and the Flame Speed Calculator is used to measure flame speed in the respective cylinders. Perfectly Stirred 0-D reactors are used to simulate cylinder 1 exhaust gas heat loss between the exhaust and intake manifold, and the mixing of exhaust products with intake reactants in a gas mixer. The AramcoMech 2.0 chemical kinetics mechanism is used to govern chemical reaction during combustion, and burn profile is based on the Wiebe function. Heat loss between intake valve close and exhaust valve open is calculated using the Woschni correlation. Results show cylinders operating at stoichiometric conditions demonstrated a 60% decrease in flame speed when exhaust gas recirculation is implemented. As excess fuel is added to cylinder 1 the flame speed of cylinders 2-4 showed a linear increase; conversely, the flame speed of cylinder 1 showed a near linear decrease. Operating cylinder 1 rich of stoichiometric results in excess elemental hydrogen and hydrogen radicals in exhaust products, which can dramatically increase flame speed in cylinders 2-4. [1]

[1]Sections 1-6 of this chapter are composed of paper written for the Western States Section of the Combustion Institue Spring 2018 Meeting. The citation for this paper is as follows: Van Roekel C, Montgomery DT, and Olsen DB.

2.2 Introduction

As the global demand for energy rises, market share between renewable energy sources and non-renewable energy sources such as natural gas is becoming increasingly competitive. It is expected that the global energy demand will rise from 575 quadrillion British thermal units (Btu) in 2015 to 735 quadrillion Btu in 2040, a 28% increase.[(1)] During this time the U.S. Energy Information Administration (EIA) projects that the fastest growing energy source will be renewables at an average rate of 2.3%/year. Natural gas is forecasted to be the fastest growing fossil fuel during this time with an average increase in consumption of 1.4% per year [(1)]. While non fossil fuel consumption in total is predicted to outpace fossil fuel consumption, fossil fuels are still presumed to account for 77% of energy use in 2040[(1)]. Due to the market presence that natural gas is expected to have in the future energy sector, development of novel natural gas combustion strategies to lower total emissions, cost of ownership, and increase overall efficiency is warranted. Exhaust gas recirculation (EGR) is a proven technology used in compression ignition (CI) and spark ignition (SI) engines to lower reactivity of the air fuel charge by recirculating a portion of the engine exhaust products back into the fresh air-fuel mixture. Overall lower reactivity of the air fuel charge results in increased knock suppression and lower rate formation of nitric oxide (NO), the primary component oxides of nitrogen (NO_x) which can react in the atmosphere to form smog and acid rain[(3)]. However, EGR also reduces the combustion rate which makes combustion at some engine operating conditions unstable. EGR requires control strategies to limit the fraction of exhaust being recirculated to the engine to maintain stable combustion, and also relies on a heat exchanger for cooling the exhaust gas before it mixes with fresh air and fuel[(2)]. Prior to research conducted by Southwest Research Institute (SWRi) in the late 2000s, EGR systems were configured as high pressure loop (HPL) or lower pressure loop (LPL) systems. In a HPL configuration exhaust gas is siphoned from the exhaust manifold upstream of the turbocharger turbine and mixes with a fresh air charge downstream of the turbocharger compressor. In a LPL configuration exhaust gas is re-

Chemical Kinetic Modeling of Natural Gas Engine Combustion with Dedicated Exhaust Gas Recirculation. #38CK-0007. Western States Section of the Combustion Institue Spring 2018 Meeting. March 25-27, 2018.

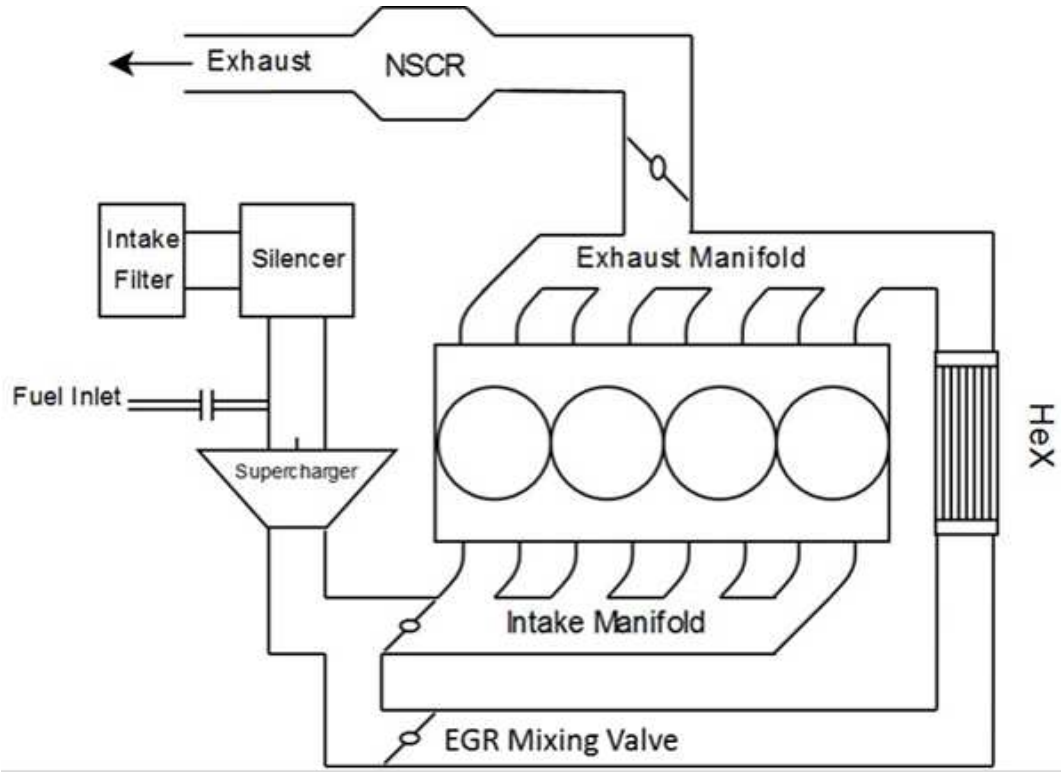

Figure 2.1: Schematic of a HPL EGR system equipped with a supercharger and exhaust back pressure valve to simulate a turbo charged system. A 3-way catalyst is used for reduction of regulated emissions.

moved downstream of the turbocharger turbine and returns to the fresh air charge upstream of the turbocharger compressor. In either configuration the composition of the recirculated exhaust gas is a fraction of the exhaust from each of the engine cylinders. Figure 2.1 shows a HPL EGR natural gas configuration which is equipped with a supercharger and exhaust back pressure valve to simulate a turbo compressor. This configuration is also equipped with a 3-way catalyst for emissions reduction which limits the equivalence ratio of the engine to 1.0 in order to simultaneously reduce emissions of carbon monoxide (CO), hydrocarbons (HC), and oxides of nitrogen (NO_x) in the catalyst. The work from SWRi introduced a novel variation of standard HPL and LPL EGR called dedicated EGR. Dedicated EGR functions on the following premise. One cylinder or group of cylinders is operated independently from the remaining engine cylinders in terms of equivalence ratio. At all engine conditions the entire exhaust charge from this cylinder or group of cylinders is mixed with the fresh intake charge in a unique EGR mixer, and results in a constant nominal 25% EGR rate. The dedicated cylinder can have an equivalence ratio that is rich of stoichiometric. The

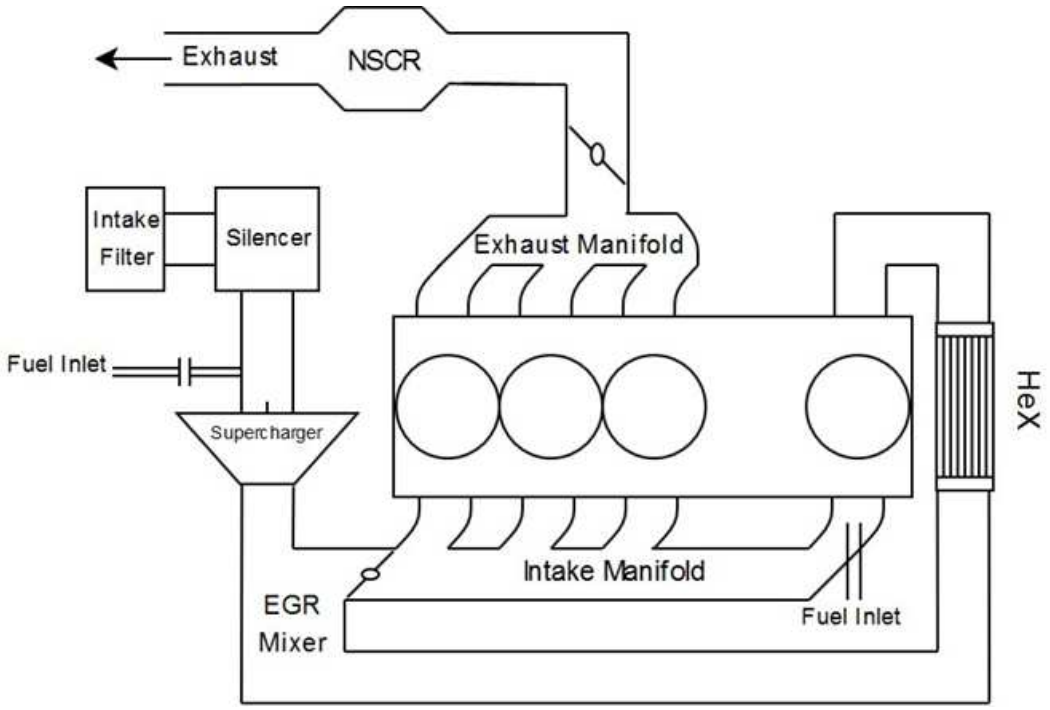

Figure 2.2: Schematic of a dedicated EGR system.

exhaust products of this rich combustion contain increased mole fractions of H_2 which increase the reactivity of the charge and allows the engine to operate at a 25% EGR rate. The remaining cylinders' fuel flow is maintained at a precise slightly lean setting which, with the addition of the donor cylinder's fuel laden exhaust, results in an engine exhaust equivalence ratio of 1.0. Thus, a 3-way catalyst can still be utilized to reduce engine out emissions. Figure 2.2 shows a schematic of a natural gas dedicated EGR system equipped with port fuel injection on the dedicated cylinder and specialized EGR mixer. The EGR mixer used in a dedicated EGR system must be able to mix exhaust gas spatially and temporally (radially and axially in the flow) due to the phased pulses of EGR returning to the intake manifold. Published work from SWRi on gasoline engines has shown that dedicated EGR technology can substantially increase knock suppression, allow for increased compression ratios, and stabilize engine operation near the EGR limit. This increase in compression ratio ultimately leads to higher engine efficiency while meeting regulated emissions standards[4–8]. However, little has been published on the applicability of a dedicated EGR system to a stoichiometric natural gas engine. The work presented in this paper aims to understand the

fundamental effects of a dedicated EGR system on the combustion products and flame speed in a stoichiometric natural gas engine. A Caterpillar G3304 engine was used as a model around which a dedicated EGR system was configured. The G3304 is a four cylinder engine so one cylinder is considered the dedicated cylinder (for EGR) and the remaining three cylinders are identified as stoichiometric cylinders.

2.3 Methods

ANSYS Chemkin-Pro version 18.1 was used to model combustion processes and flame speed in stoichiometric and dedicated cylinders. The first selection when modeling an engine combustion process is the reactor. Chemkin Pro 18.1 offers three closed 0-D reactors which are appropriate for modeling combustion within and engine cylinder. First, the Homogeneous Charge Compression Ignition (HCCI) Engine reactor can be used to simulate combustion under auto-ignition conditions between intake-valve closing (IVC) and exhaust valve opening (EVO). This reactor assumes that gas in the combustion chamber is homogeneous with uniform temperature, pressure, and gas composition. The Chemkin Pro 18.1 theory manual states that the single zone model can predict ignition when the initial conditions are known, but because it does not account for low-temperature regions within boundary layers and crevices it tends to under predict carbon monoxide and unburned hydrocarbon emissions while over predicting peak pressures[(9)]. Second, the Multi-Zone HCCI Engine reactor can be used when a balance between detailed temperature or composition inconsistencies and comprehensive kinetics models is required. The cylinder volume is divided into multiple zones according to a selected cylinder variable. Each zone is modeled as a closed homogeneous reactor where no mass nor heat transfer is allowed to cross a zone boundary. Pressure is equal among all zones, and pressure work is the only interaction between zones. Finally, the Spark Ignition (SI) Engine Zonal reactor is a zero-dimensional multi-zone model used to simulate spark ignited combustion in an engine cylinder. This reactor utilizes only two homogeneous zones. According to the Chemkin Pro 18.1 theory manual the SI reactor behaves in the following ways. Initially, unburned zone contains fresh air and fuel according to the equivalence ratio and gas

composition inputs. The burned zone contains no mass, but during combustion will be filled with combustion products. The unburned zone allows gas to exit but no gas can enter, and the burned zone acts inversely to this. A turbulent, premixed flame of trivial size separates the two zones after ignition and acts as an interface between zones. The premixed flame serves only to convert reactants of air and fuel to combustion products[9]. Further, the SI Engine Zonal reactor model can be divided into three stages. The first stage is the pre-combustion stage. During this stage the model acts similarly to the single zone HCCI model. The duration of this stage is governed by user defined properties of intake-valve closing (IVC) and start of combustion (SoC) timing. The second stage is the combustion stage. The Wiebe function governs the mass fraction burned at each crank angle. The SoC, burn duration, and Wiebe function coefficients are required inputs during the combustion stage. Lastly, the expansion stage spans the time between end of combustion (EoC) and EVO. During the combustion stage mass is transferred from the unburned zone to the burned zone. When the expansion stage begins the reactor model behaves like a single zone HCCI model.

The SI Engine Zonal reactor was selected to model the combustion process in this work because it most closely represented the characteristics of spark ignited natural gas combustion. Table 2.1 shows the physical properties of the SI Engine Zonal reactor. Properties of engine speed, compression ratio, bore, stroke, and connecting rod length are representative of a Caterpillar G3304 engine. The temperature and pressure properties were selected from data recorded in previous experiments. Convective heat transfer from combustion gases to cylinder walls was modeled in the SI Engine reactor via the Woschni correlation. This correlation represents spatially averaged combustion chamber heat transfer. Equation 2.1 shows the assumed Nussult number correlation. The SI Engine Zonal reactor model used a value of 0.8 for the Reynolds number exponential coefficient[2].

$$Nu = 0.035Re^{m} \tag{2.1}$$

Average cylinder gas velocity in the Woschni correlation is calculated using Equation 2.2 which was derived from heat transfer measurements made on a direct-injection four valve diesel engine without swirl [2]. In Equation 2.2 V_d is the displaced volume, p is the instantaneous cylinder

Table 2.1: Dedicated EGR Chemkin SI engine zonal reactor physical properties.

Caterpillar G3304	
Starting Crank Angle (°aTDC)	-170
End of Simulation Crank Angle (°aTDC)	160
Engine Speed (rpm)	1800
Compresssion Ratio	10.5
Bore (mm)	120.7
Stroke (mm)	152.4
Connecting Rod Length (mm)	243.7
Initial Temperature (°C)	70
Initial Pressure (kPa)	85.4

Table 2.2: Dedicated EGR Chemkin model Woschni correlation coefficients

Combustion Period	C1	C2
Gas Exchange	6.18	0
Compression	2.28	0
Combustion and Expansion	2.28	3.24E-03

pressure, p_r, V_r, T_r are the fluid pressure, volume, and temperature at a reference state, and p_m is the motored pressure at the same crank angle as the cylinder pressure, p. The Woschni correlation specifies different coefficients of C_1 and C_2 for the gas exchange, compression, and combustion periods. Coefficients for each of these periods were selected from Heywood and are shown in Table 2.2. The assumed wall temperature during combustion was 500 K, and the Prandtl Number was 0.7.

$$w = C_1 S_p + C_2 \frac{V_d T_r}{p_r V_r}(p - p_m) \tag{2.2}$$

The Wiebe function was used to govern the burn rate and duration profile in this work. Efficiency and form factors were chosen to be values of five and three, respectively, and the burn efficiency was assumed to be one. In addition to the efficiency and form factors the Wiebe function also requires that SoC and burn duration are specified. In the absence of in-cylinder combustion data

for the G3304 engine, burn duration data was selected from previous work performed by Sutley[10] at the Colorado State University Engines and Energy Conversion Lab. SoC for this model was set at 23 °bTDC which was just after the G3304 spark timing of 26 °bTDC. The mechanism used to describe chemical kinetic and thermodynamic properties of the gas composition during combustion was the Aramco 2.0 mechanism. According to[11] this mechanism was developed to represent numerous C_1 - C_4 hydrocarbon and oxygenated fuels over a range of experimental conditions. It has been validated through many experimental measurements including shock tube, rapid compression machines, flames, jet-stirred, and plug-flow reactors[12,13]. In addition to selecting the SI Engine Zonal model reactor for simulating combustion in a G3304 natural gas engine other reactors and simulators were required to accurately model a complete dedicated EGR system. Figure 2.3 presents the complete Chemkin model used to simulate dedicated EGR operation on a Caterpillar G3304 natural gas engine. The models used in this simulation include the dedicated cylinder that can be incremented between fuel rich and lean conditions, an EGR loop that recirculates exhaust products from the dedicated cylinder back to the intake of the dedicated and stoichiometric cylinders, a stoichiometric cylinder, and flame speed calculator for the dedicated and stoichiometric cylinders. The entire model can be separated into three subsystems. First, the dedicated cylinder subsystem is depicted in the shaded blue area of Figure 2.3. In this subsystem the equivalence ratio and inlet fuel composition are controlled via the external source of gas inlet simulator. This simulator also controls the oxidizer mixture and the expected complete combustion products. Following the external source of gas inlet is a perfectly stirred reactor (PSR) which acts as a mixer for the recirculated exhaust gas and incoming fresh air and fuel. The reactor has a fixed gas temperature and total volume which is representative of physical mixers used on previous on-engine experimentation. The PSR is an open 0-D reactor thus an outflow simulator is required, but is not utilized in this model. The resultant gas composition of this PSR is used as the initial conditions for the SI engine zonal model. The combustion products from SI engine zonal model feed into a gas inlet simulator where they remain unchanged. The PSR that follows acts as an EGR cooler where inlet conditions are representative of engine exhaust products. The exhaust is cooled to inlet air and

fuel conditions by specifying the heat loss, wall area, and residence time. Finally, the gas splitter directs 25% of the exhaust gas back to the inlet of the EGR mixer, 50% to the outflow simulator, and 25% to the stoichiometric cylinder. Only one of three stoichiometric cylinders is simulated so 50% of the EGR that would normally go to the other two stoichiometric cylinders is discarded through the outflow simulator. The green dashed line signifies the exhaust being routed out of the gas splitter into the EGR mixer. This process is repeated until the SI engine solution has converged adequately. The convergence criteria in this model consists of an absolute and relative tolerance. The absolute tolerance specifies the tolerance below which species fractions will be ignored, and the relative tolerance indicates the significant digits to the solution. The selected values for the absolute and relative tolerances in this work were 1.0E-10 and 1.0E-8, respectively. After the dedicated cylinder subsystem converges on a solution the stoichiometric cylinder subsystem shown in the red shaded area of Figure 2.3 begins. The exhaust products from the dedicated cylinder are circulated to a PSR with similar configuration to the dedicated subsystem with the exception that the equivalence ratio is kept at 1.0. In this PSR simulated mixing of fresh air and fuel, and dedicated cylinder exhaust products takes place and serves as initial conditions for the subsequent SI engine zonal model. Exhaust products from the SI engine zonal model shown in Figure 5 are representative of stoichiometric cylinders operating with a 25% nominal EGR rate. The final subsystem depicted in the grey area of Figure 2.3 contains the laminar flame speed calculators for the dedicated and stoichiometric cylinders. These calculators use gas temperature and pressure conditions near cylinder top dead center (TDC) to simulate a freely propagating flame. In this work the temperature and pressure was defined as 800 K and 18 atm, respectively. The point of reference is a fixed position on the flame, and the flame speed is defined as the inlet velocity of unburned gas moving towards the flame that allows the flame to stay in a fixed position[9]. The composition of the unburned fuel and air mixture used to calculate flame speed was taken directly from the PSR in the dedicated cylinder and stoichiometric cylinder subsystems. With the complete system model in place consideration was given to the sensitivity of the results with respect to the raw natural gas fuel composition. Initially, simulations were conducted with a fuel methane number (MN) of

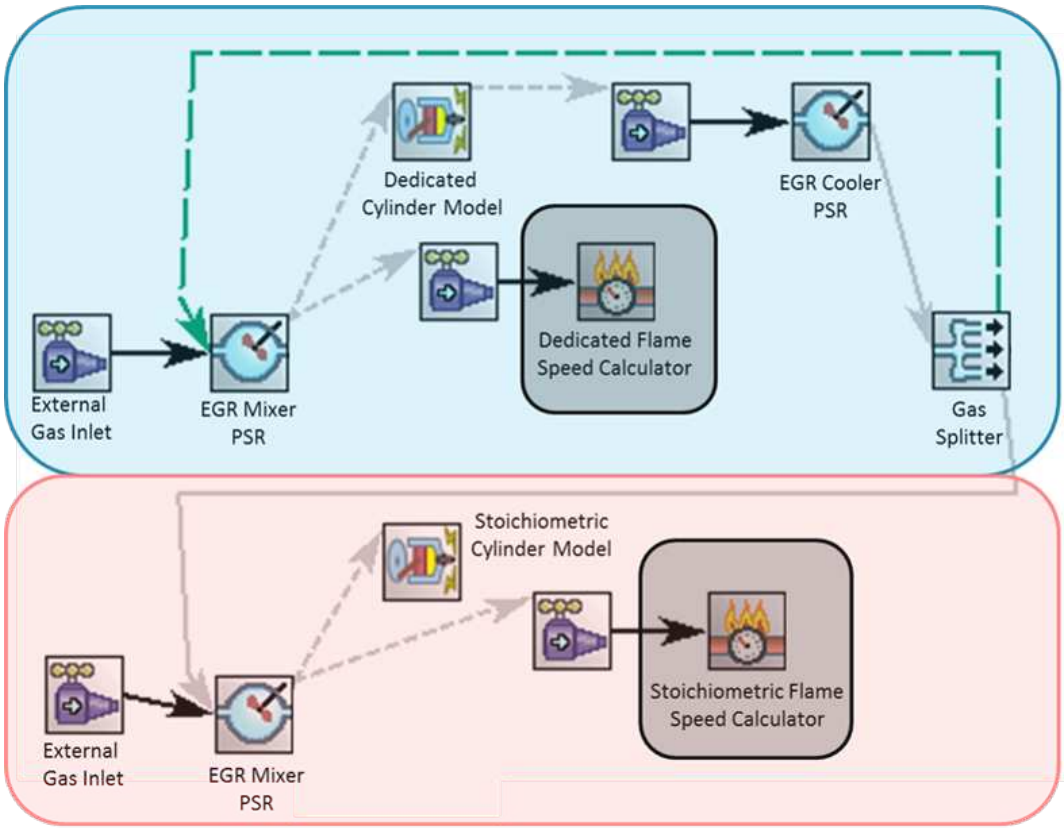

Figure 2.3: Chemkin model simulating dedicated EGR operation. The blue shaded area represents the dedicated cylinder portion in which 25% of the exhaust is routed back to the intake of the system via the green hashed line. The red shaded area represents the stoichiometric cylinders of the system that receive 25% of the dedicated cylinder exhaust. The grey shaded area shows the flame speed calculators for the dedicated and stoichiometric cylinders.

Table 2.3: Selected fuel composition for studying combustion products and flame speed in dedicated and stoichiometric cylinders in a dedicated EGR system using Chemkin chemical kinetics modeling software. Methane number (MN) was calculated using Westport fuel methane number calculator.

Fuel Composition			
Species	MN 75	MN 79	MN 85
CH_4	0.83	0.865	0.92
C_2H_6	0.14	0.105	0.05
C_3H_8	0.01	0.01	0.01
CO_2	0.017	0.017	0.017
N_2	0.003	0.003	0.003

79. This value was selected by analyzing previous gas chromatograph data on inlet fuel conditions during a G3304 engine test. Additional methane numbers of 75 and 85 were selected to evaluate the effect of methane number on combustion products and flame speed in the dedicated and stoichiometric cylinders. The composition of the selected fuels can be found in Table 2.3. With the Chemkin dedicated EGR system defined and a suite of fuel compositions selected the equivalence ratio of the dedicated cylinder was incremented by 0.1 between 0.5 and 1.8. The air-fuel ratio of the fresh charge entering the EGR mixer was adjusted such that the exhaust gas equivalence ratio was 1.0. The following results and discussion reflect the solutions from the dedicated EGR system model with a constant nominal 25% EGR rate as described in this section.

2.4 Results and Discussion

In an introduction to laminar flame speed Glassman[14] describes the development of equations governing calculation of flame speed. The work of Mallard and Le Chatelier led to an expression for calculating flame speed shown in Equation 2.3. A further simplification of this equation into measurable

$$w = (\frac{\lambda}{\rho c_p}\frac{T_f - T_i}{T_i - T_0}\frac{\omega}{\rho})^{0.5} \tag{2.3}$$

Where:

S_L = flame speed

λ = thermal conductivity

ρ = unburned gas density

c_p = unburned gas specific heat at constant pressure

T_f = final flame temperature

T_i = ignition temperature

T_0 = unburned gas temperature

ω = reaction rate in terms of concentration

terms can be found in the Glassman text, but Equation 2.3 allows insight into physical factors affecting flame speed. It is apparent from this equation that both unburned and burned gas temperature have a significant effect on flame speed due to the range of possible combustion temperatures. Further, a general statement of the impact of pressure on flame speed is described in Equation 2.4 where n is equal to the global reaction rate. This equation is rooted in the global reaction rate term, ω. In general, for hydrocarbon combustion the global reaction rate term is a second order term and thus flame speed is independent of pressure [14,15].

$$S_L = (P^{n-2})^{0.5} \tag{2.4}$$

Another consideration when calculating flame speed is equivalence ratio of the air-fuel mixture. The primary effect of equivalence ratio on flame speed is similar to that of the effect it has on adiabatic flame temperature due to the dependence of flame speed on final gas temperatures. Finally, fuel type has an effect on flame speed where alkanes, alkenes, and alkynes have slightly increasing flame speed, respectively, while hydrogen has a flame speed much greater than hydrocarbons. Turns[15] states that the factors leading to the increased laminar flame speed of elemental hydrogen are first, the thermal diffusivity of pure H_2 is many times greater than hydrocarbons. Second, the mass diffusivity of H_2 is much greater than hydrocarbons, and third, reaction kinetics for H_2 are much more rapid than hydrocarbons. The Chemkin flame speed calculator was used to calculate

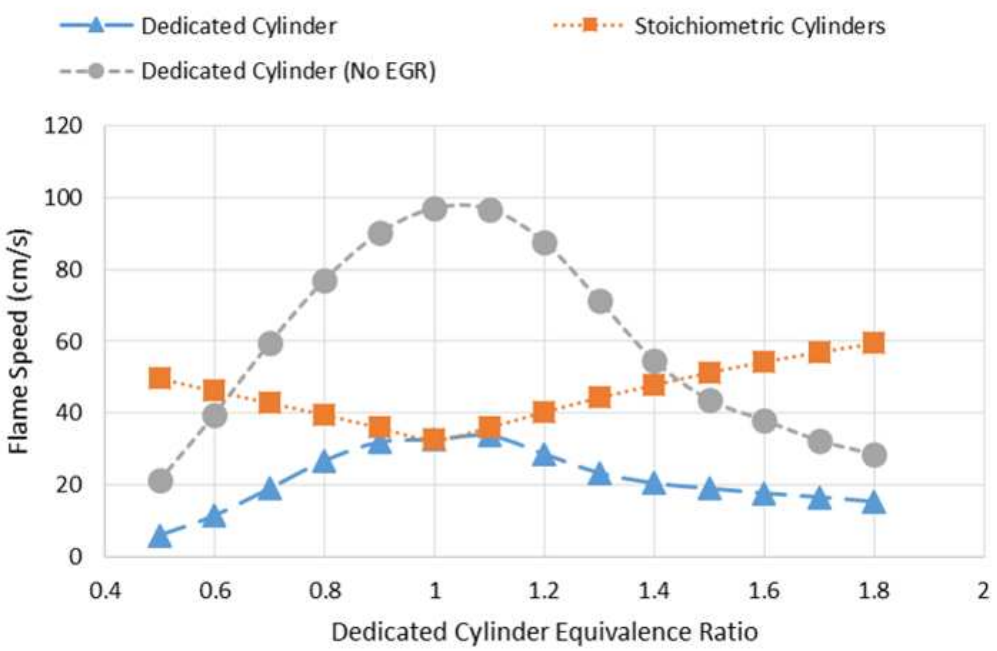

Figure 2.4: Flame speed as a function of dedicated cylinder equivalence ratio for natural gas with a MN of 79 for the dedicated cylinder with EGR, the dedicated cylinder without EGR, and the stoichiometric cylinder with EGR

flame speed across a range of dedicated cylinder equivalence ratios. Figure 2.4 plots laminar flame speed with respect to dedicated cylinder equivalence ratio for a fuel with MN 79. The grey, medium dashed line represents flame speed in the dedicated cylinder with no EGR present. This was done to provide a baseline against which flame speeds for mixtures including EGR could be compared. This flame speed trace shows the relationship between equivalence ratio and flame speed. The blue, heavy dashed line shows flame speed in the dedicated cylinder with a nominal 25% EGR present. The effects of non-reactive combustion products replacing fresh air-fuel mixture is apparent in the decrease in flame speed from the no EGR baseline. At stoichiometric conditions in the dedicated cylinder a decrease in flame speed of approximately 60 cm/s can be seen. Of further interest is the difference in the line slope of the dedicated cylinder with and without EGR. As the dedicated cylinder is operated more fuel rich or fuel lean complete combustion products of CO_2 and H_2O decrease and the presence of reactive molecules such as O_2 and H_2 increase. Table 2.4 shows the variation in complete combustion products and reactants in the dedicated cylinder with a fuel

Table 2.4: Combustion products for a dedicated cylinder with fuel MN of 79

Dedicated Cylidner Equivalence Ratio								
	1.8	1.6	1.4	1.2	1	0.8	0.6	0.5
H_2	13%	10%	7%	3%	0%			
O_2					0%	4%	8%	10%
H_2O	14%	15%	17%	18%	18%	15%	11%	10%
CO_2	3%	4%	5%	7%	10%	8%	6%	5%

methane number of 79 as the cylinder is operated from lean to rich conditions. At stoichiometric conditions CO_2 and H_2O are maximized at 10% and 18%, and decrease as the fuel composition becomes fuel rich or lean. At an equivalence ratio of 1.8 H_2 molecules represent 13% of the total combustion products. Similarly, during lean combustion O_2 represents 10% of the total combustion products. Both of these reactants are not present during stoichiometric combustion. This tradeoff can explain the reduced change in flame speed per change in equivalence ratio when moving further away from stoichiometric combustion conditions. The orange, light dashed line displays the flame speed in the stoichiometric cylinders as a function of dedicated cylinder equivalence ratio. Again, the increased presence of reactive molecules in the EGR mixture at lean and rich conditions results in an increased flame speed when compared to EGR from stoichiometric combustion. Figure 2.5 depicts the dedicated cylinder flame speed with EGR as a function of cylinder equivalence ratio while incrementing fuel methane number. Each of the flame speed traces follow a similar path with the lower methane number flame speeds being higher at each of the simulation points. The difference in fuel composition from MN 85 to MN 75 is an increase in ethane mole fraction and a decrease in methane mole fraction. The carbon-hydrogen bond in ethane is weaker than the carbon-hydrogen bond in methane[14] which can explain the increased reactivity of ethane and thus an increased flame speed given similar conditions. The stoichiometric cylinder flame speed is shown in Figure 2.6. In this figure fuel methane numbers 75, 79, and 85 are shown in the purple, yellow, and grey colors, respectively. The stoichiometric cylinder receives a nominal 25% EGR from the dedicated cylinder. The minimum flame speed occurs at a dedicated cylinder equivalence

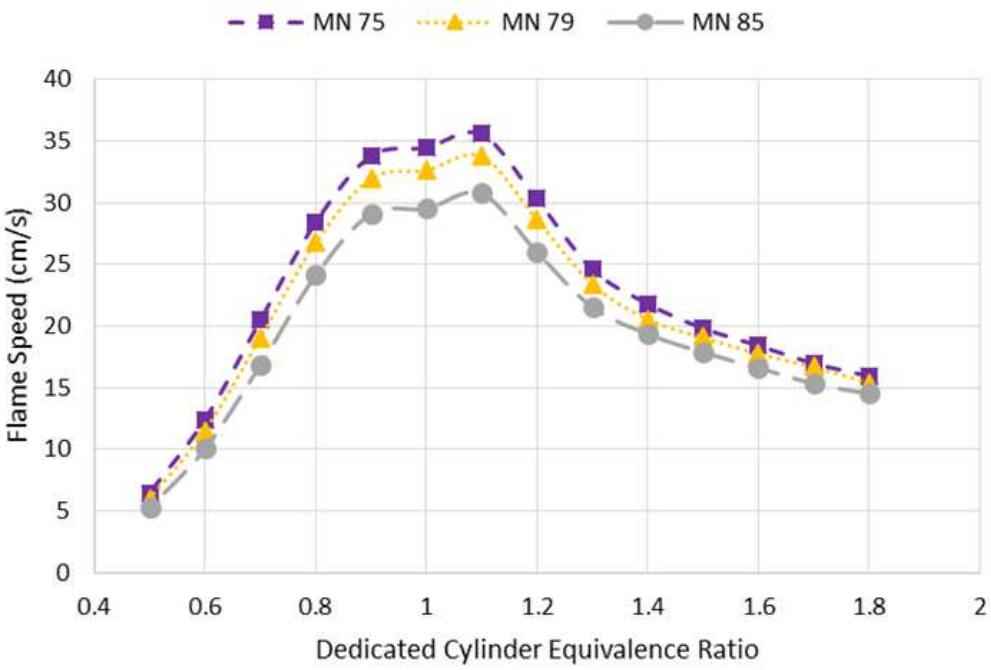

Figure 2.5: Dedicated cylinder flame speed as a function of dedicated cylinder equivalence ratio

ratio of 1.0 which is a result of the high mole fractions of complete combustion products such as CO_2 and H_2O. As stated earlier as the dedicated cylinder equivalence becomes fuel rich or fuel lean incomplete combustion leads to increased reactants of H_2 and O_2, respectively. Figure 2.7 shows the weighted average flame speed of the dedicated EGR system assuming a four cylinder engine operating with one dedicated cylinder and three stoichiometric cylinders. Figure 2.4 showed that in the absence of EGR a stoichiometric natural gas engine with operating conditions similar to the G3304 engine has a laminar flame speed of approximately 96 cm/s, and a 25% EGR rate results in a significant reduction in flame speed. Figure 2.7 provides insight into the optimal dedicated cylinder equivalence ratio considering the entire engine. It shows a minimum value at stoichiometric conditions, and shows a maximum value at a dedicated cylinder equivalence ratio of 1.8 which suggests that the best combustion performance would be attained at the most rich conditions within the dedicated cylinder. Final combustion products from the dedicated cylinder were analyzed to understand the composition of EGR being produced, and the effect of varied equivalence ratio on exhaust composition. The combustion products from the stoichiometric cylinders were also quan-

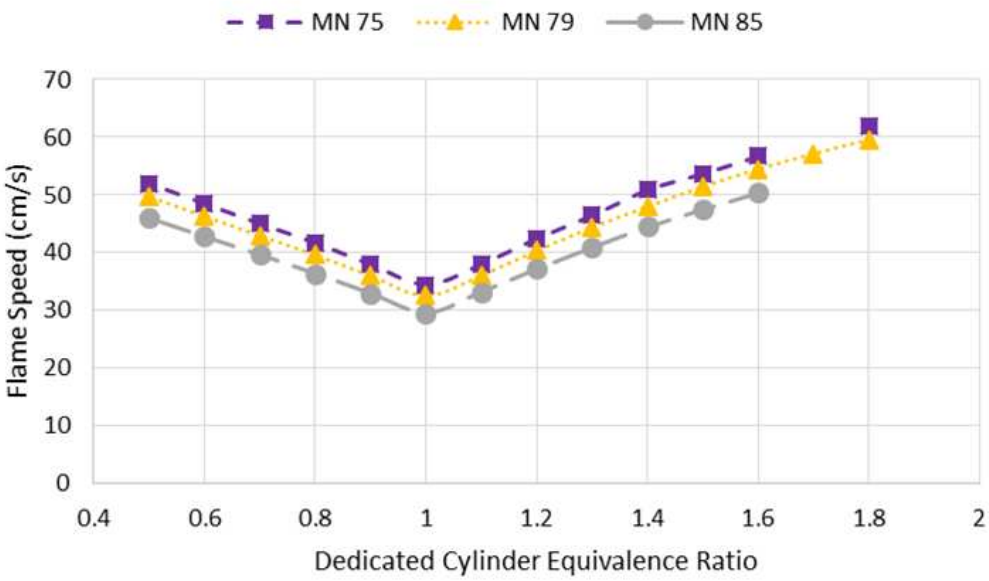

Figure 2.6: Stoichiometric cylinder combustion as a function of dedicated cylinder equivalence ratio for fuel methane numbers of 75, 79, and 85.

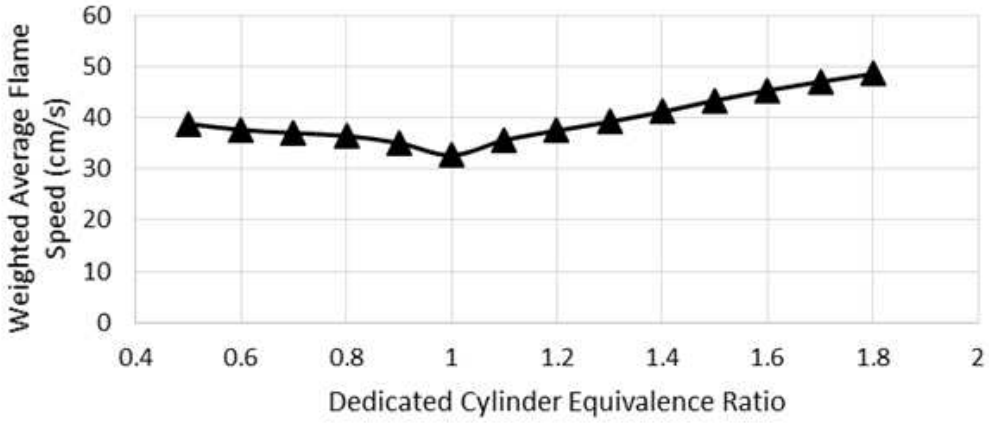

Figure 2.7: Weighted average cylinder flame speed assuming a four cylinder engine operating with one dedicated cylinder and three stoichiometric cylinders.

tified. The detailed low-temperature and high-temperature oxidation processes for hydrocarbons such as methane are beyond the scope of this work, but an understanding of basic oxidation pathways are critical to analysis of dedicated EGR combustion products. Glassman[14] provides major reaction pathways for high-temperature oxidation of methane which can be found in the reactions of Equations 5-13. In these equations X represents any OH, O, or H radical, and M represents a non-reactive molecule. Methane oxidation differs from that of other hydrocarbons because breaking the first C-H bond takes roughly 40kJ/mol more than the subsequent bonds, and much more than in other hydrocarbons[14]. Thus, the initiation step for methane oxidation is very slow and is governed by thermal decomposition of the methane molecule. Once H atoms are created from the reaction in Equation 5, H + O2 chain can begin and methane is destroyed via H-atom abstraction shown in Equation 2.6. The resulting methyl radicals are oxidized to form very unstable methoxy radicals and are quickly converted to formaldehyde in Equations 2.8 and 2.9. Formaldehyde is converted to the formyl radical, which is then converted to carbon monoxide in Equations 2.10 and 2.11. The reaction in Equation 2.12 shows the recombination of methyl radicals into ethane which is a pathway for soot production. Finally, carbon monoxide is oxidized to carbon dioxide in a chain terminating step shown in Equation 2.13.

$$CH_4 + M \rightarrow CH_3 + H + M \tag{2.5}$$

$$CH_4 + X \rightarrow CH_3 + XH \tag{2.6}$$

$$CH_3 + O_2 \rightarrow CH_3O + O \tag{2.7}$$

$$CH_3 + O_2 \rightarrow H_2CO + OH \tag{2.8}$$

$$CH_3O + M \rightarrow H_2CO + H + M \tag{2.9}$$

$$H_2CO + X \rightarrow HCO + XH \tag{2.10}$$

$$HCO + M \rightarrow H + CO + M \tag{2.11}$$

$$CH_3 + CH_3 \rightarrow C_2H_6 \tag{2.12}$$

$$CO + OH \rightarrow CO_2 + H \tag{2.13}$$

With this high temperature pathway considered the exhaust products from the dedicated and stoichiometric cylinders can be discussed. In Figure 2.8 exhaust products of CO_2, CO, and OH are considered. The mole fractions of each molecule are plotted as a function of dedicated cylinder equivalence ratio. The dedicated cylinder exhaust products are shown in green with square markers and the stoichiometric exhaust products are shown in black with circular markers. All data sets reflect the standard nominal 25% EGR rate. As dedicated cylinder conditions move away from stoichiometric conditions CO_2 products decrease by approximately 50% at extreme lean and rich conditions. This is due to the lack of available oxidizer and fuel to create radicals required for the final chain terminating step from CO to CO_2. The reduction in in CO_2 production is less pronounced in the stoichiometric cylinder when compared to the dedicated cylinder because while the dedicated cylinder may be operating at extreme lean or rich equivalence ratio the equivalence ratio of the stoichiometric cylinder does not change. The CO and OH plots in Figure 2.8 show visually the dependence of CO_2 production on these molecules. As the mole fraction of OH molecules decreases during rich combustion conditions the mole fraction of CO increases. This coincides with Equation 2.11 and is consistent with the expected reaction pathways in the Aramco 2.0 kinetic mechanism. Figure 2.9 displays exhaust products of H_2, H, and O_2 for dedicated and stoichiometric cylinders as a function of dedicated cylinder equivalence ratio. The results describe mole fractions of products at EVO. The dedicated exhaust products can be equated to the composition of exhaust gas being recirculated to an engine intake manifold. Most notably in Figure 2.9 is the increase in H_2 as equivalence ratio becomes richer. Hydrogen has a flame speed approximately 4-5 times that of methane at ambient air conditions so the increased H_2 mole fraction in recirculated exhaust gas leads to a higher flame speed in the stoichiometric cylinders as shown in Figure 2.4, which serves to offset the effects non-reactive constituents in the recirculated exhaust gas such as CO_2.

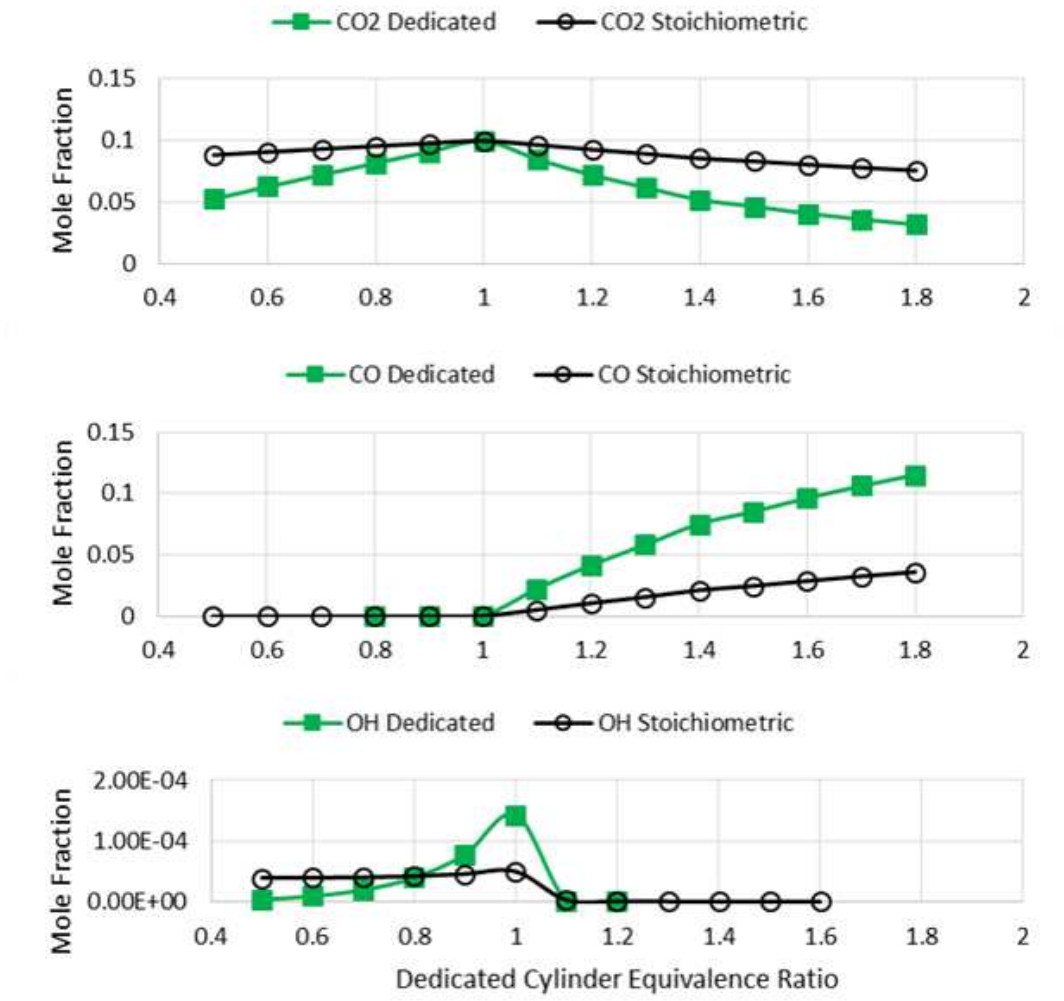

Figure 2.8: Exhaust products mole fraction for both dedicated and stoichiometric combustion with nominal 25% dedicated EGR as a function of dedicated cylinder equivalence ratio.

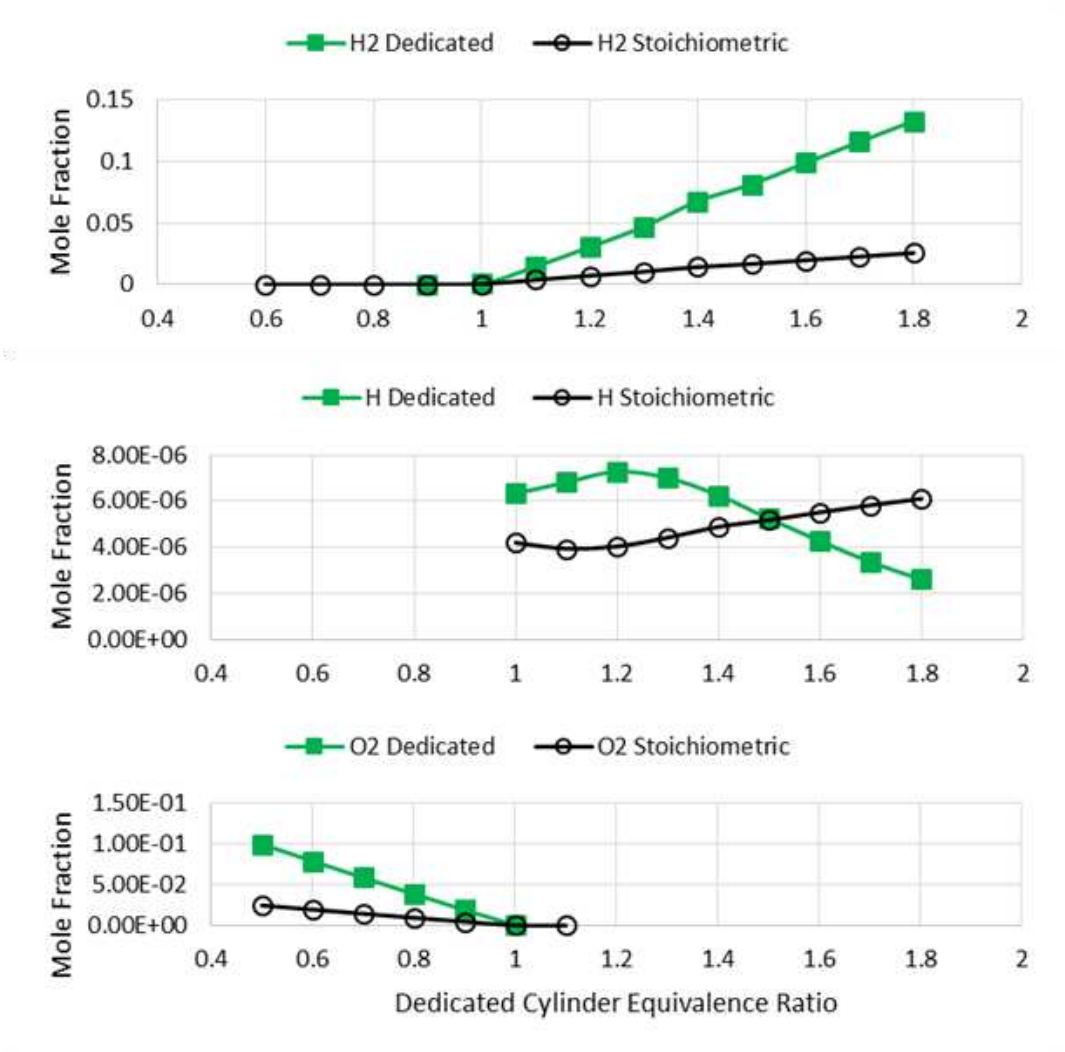

Figure 2.9: Exhaust products mole fraction for both dedicated and stoichiometric combustion with nominal 25% dedicated EGR as a function of dedicated cylinder equivalence ratio.

2.5 Conclusions

The effects of a dedicated EGR system on the combustion products and flame speed in a stoichiometric natural gas engine were studied using the AramcoMech 2.0 mechanism and Chemkin chemical kinetics software. The following conclusions were drawn from the results:

- Operating the dedicated cylinder rich or lean of stoichiometric led to a decrease in CO_2 combustion products, and an increase in reactive molecules such as O_2 and H_2.
- Flame speed in the dedicating cylinder and stoichiometric cylinder benefitted from decreased CO_2 and increased reactive molecules in the EGR composition.
- Natural gas fuel compositions with lower methane numbers demonstrated greater increase in flame speed in dedicated and stoichiometric cylinder conditions. However, given the small range of methane numbers considered a significant change in flame speed was not found.

The next step in this work is an on engine demonstration of a dedicated EGR system on a Caterpillar G3304 engine. During these test combustion products will be measured from the dedicated and stoichiometric exhaust flow streams, and resultant values will be compared to these model results.

2.6 References

1. "International Energy Outlook 2017." U.S. Energy Information Administration, 14 Sept. 2017, www.eia.gov/outlooks/ieo/.

2. Heywood, John B. Internal Combustion Engine Fundamentals. McGraw Hill. Print.

3. Hinds, William C. Aerosol technology properties, behavior, and measurement of airborne particles. Wiley-Interscience, 1999.

4. T .Alger, J. Gingrich, and B. Mangold. "The Effect of Hydrogen Enrichment on EGR Tolerance in Spark Ignited Engines" SAE 2007 World Congress. 2007-01-0475.

5. T. Alger and B Mangold. "Dedicated EGR: A New Concept in High Efficiency Engines" SAE International 2009-01-0694.

6. C. Chadwell, T. Alger, J Zuehl, and R Gukelberger. "A Demonstration of Dedicated EGR on a 2.0 L GDI Engine" SAE International 2014-01-1190.

7. R. Gukelberger, J. Gingrich, T. Alger, and S. Almaraz. " LPL EGR and D-EGR Engine Concept Comparison Part 2: High Load Operation" SAE International 2015-01-0781.

8. R. Gukelberger, J. Gingrich, T. Alger, S Almaraz, and B Denton. "LPL EGR and D-EGR Engine Concept Comparison Part 1: Part Load Operation" SAE International 2015-01-0783.

9. ANSYS Chemkin-Pro 18.1 Theory Manual. CK-TH-15181-1704-UG-1

10. F. Sutlety "Installation and Testing of a Cummins QSK19 Lean Burn Natural Gas Engine" Colorado State University. 2013

11. "Saudi Aramco Mechanism Release." Combustion Chemistry Centre, www.nuigalway.ie/c3/aramco2/frontmatter.html.

12. W.K. Metcalfe, S.M. Burke, S.S. Ahmed, H.J. Curran, " A hierarchical and comparative kinetic modeling study of C1–C2 hydrocarbon and oxygenated fuels", Int. J. Chem. Kinet. (2013) 45(10) 638–675.

13. A. Kéromnès, W.K. Metcalfe, K.A. Heufer, N. Donohoe, A.K. Das, C.J. Sung, J. Herzler, C. Naumann, P. Griebel, O. Mathieu, M.C. Krejci, E.L. Petersen, W.J. Pitz, H.J. Curran " An Experimental and Detailed Chemical Kinetic Modelling Study of Hydrogen and Syngas Mixtures at Elevated Pressures" Combustion and Flame (2013) 160 995–1011.

14. Glassman, Irvin, and Richard A. Yetter. Combustion. Academic Press, Elsevier, 2008.

15. Turns, Stephen R. An introduction to combustion: concepts and applications. McGraw-Hill, 2012.

Chapter 3

Evaluating Dedicated Exhaust Gas Recirculation on a Stoichiometric Indistrial Natural Gas Engine

3.1 Summary

Due to the market presence that natural gas has and is expected to have in the future energy sector, research and development of novel natural gas combustion strategies to increase power density, lower total emissions, and increase overall efficiency is warranted. Dilution whether by excess air or by exhaust gas recirculation has historically been implemented on diesel, natural gas, and gasoline engines to mitigate various regulated emissions. In the large industrial natural gas engine industry excess air dilution or ultra lean burn operation has afforded lean burn engines increased power density and reduced NO_x emissions. This advance in technology has allowed lean burn engines to compete in markets such as electrical power generation which previously they had not been able. However, natural gas engines utilizing a non-selective catalytic reduction system or 3-way catalyst must operate at stoichiometric conditions, and thus are limited in power density by exhaust gas temperatures. In previous gasoline small engine research a novel exhaust gas recirculation technique called dedicated exhaust gas recirculation was shown to have a positive impact on engine out emissions of NO_x and unburned hydrocarbons while also lowering exhaust component temperatures. This work seeks to understand the consequences of implementing a dedicated exhaust gas recirculation system on a multi-cylinder stoichiometric industrial natural gas engine. The results of this initial evaluation demonstrate reductions in engine-out NO_x and CO emissions and improvements in engine-out exhaust gas temperatures with the dedicated exhaust gas recirculation technique. However, in a low turbulence combustion chamber dedicated exhaust gas recirculation

significantly lowers the overall rate of combustion and results is significant differences in cylinder to cylinder combustion. [2]

3.2 Introduction

As the global demand for energy increases, market share between renewable energy sources and non-renewable energy sources such as natural gas is becoming increasingly competitive. It is expected that between 2015 and 2040 the global energy requirement will have increased by 28%. Natural gas is forecasted to be the fastest growing fossil fuel during this time with an average increase in consumption of 1.4% per year[(1)]. Domestically, the United States consumes approximately 27.5 trillion cubic feet of natural gas per year,[(2)] and in 2017 became a net exporter of natural gas[(3)]. The current rate of natural gas collection, reserves, and outlook on possible reserves have positively impacted the cost of industrial natural gas. When compared to refinery retail diesel fuel on a per energy basis natural gas is less expensive and has lower price volatility[(4,5)].

An important advancement in natural gas engine technology has been the introduction of charge dilution whether by lean burn combustion or adding exhaust gas recirculation (EGR) to stoichiometric combustion. This technology has allowed natural gas engines to operate at higher brake mean effective pressure (BMEP) and increased efficiency while also achieving low oxides of nitrogen (NO_x) emissions by reducing peak combustion temperatures and changing thermodynamic properties of the combustion charge[(6)]. However, there are challenges and disadvantages to charge dilution. The charge dilution effects of lean burn combustion have less impact at higher altitude because of the decreasing density of the intake air. The decrease in effectiveness is often made up for by adding additional supercharging capability to the engine. The design of the combustion chamber which includes the piston, piston rings, head, and ignition source is critical to lean burn combustion. Combustion heat release rate is an inverse function of air fuel ratio and a direct func-

[2]Sections 1-8 of this chapter are composed of a paper published in the International Journal of Engine Research. The citation for this publication is as follows: Van Roekel C, Montomgery DT, Singh J, and Olsen DB. Evaluating Dedicated Exhaust Gas Recirculation on a Stoichiometric Industrial Natural Gas Engine. (https://journals.sagepub.com/doi/10.1177/1468087419864733). International Journal of Engine Research. 2019.

tion of laminar flame speed thus as the air fuel ratio increases and the laminar flame speed decreases the flame area must increase. This can be achieved by adding more turbulence to the combustion chamber via piston bowl design and pre-chamber ignition. The disadvantages of adding EGR to stoichiometric combustion include additional components to direct exhaust gas back to the intake manifold, the possibility of durability issues due to contaminants in exhaust gases, and complex control systems for adjusting the amount of exhaust gas routed to the intake manifold at different engine operating conditions[7]. The amount of exhaust directed back to the intake manifold of the engine must also be changed at different engine operating conditions. Due to the negative impact EGR has on the lower heating value (LHV) of the combustion charge less EGR can be used at high BMEP conditions. At low BMEP conditions less EGR can be used because the lower reactivity of the combustion charge. Thus, an EGR valve must be used.

Stoichiometric combustion systems incorporating EGR conventionally have done so via high pressure loop (HPL) or low pressure loop (LPL). A high pressure loop system siphons exhaust gas directly from the exhaust manifold prior to a turbocharger while a low pressure loop system extracts exhaust downstream of a turbocharger[6]. A novel variant of conventional HPL and LPL EGR is dedicated EGR (dEGR).

Dedicated EGR systems are configured such that all of the exhaust from one or more cylinders of an engine is routed back to the intake manifold at all engine operating points. In a four cylinder engine with one cylinder designated as the dedicated cylinder this equates to a nominal 25% EGR rate across the entire engine operating range. Conventional HPL and LPL EGR systems control the effect that EGR has on the combustion process by changing the amount of exhaust routed back to the intake manifold. Conversely, dedicated EGR controls the effect that the recirculated exhaust has on the combustion process by changing the chemical composition of the exhaust gas. This is done by adding additional fuel to the dedicated cylinder or cylinders and changing the air fuel ratio (AFR) of these cylinder(s). Figure 3.1 shows a simplified diagram of HPL, LPL, and dedicated EGR systems and how they are implemented on a four cylinder engine. Combustion charge dilution by way of dedicated EGR offers distinct advantages when compared to standard

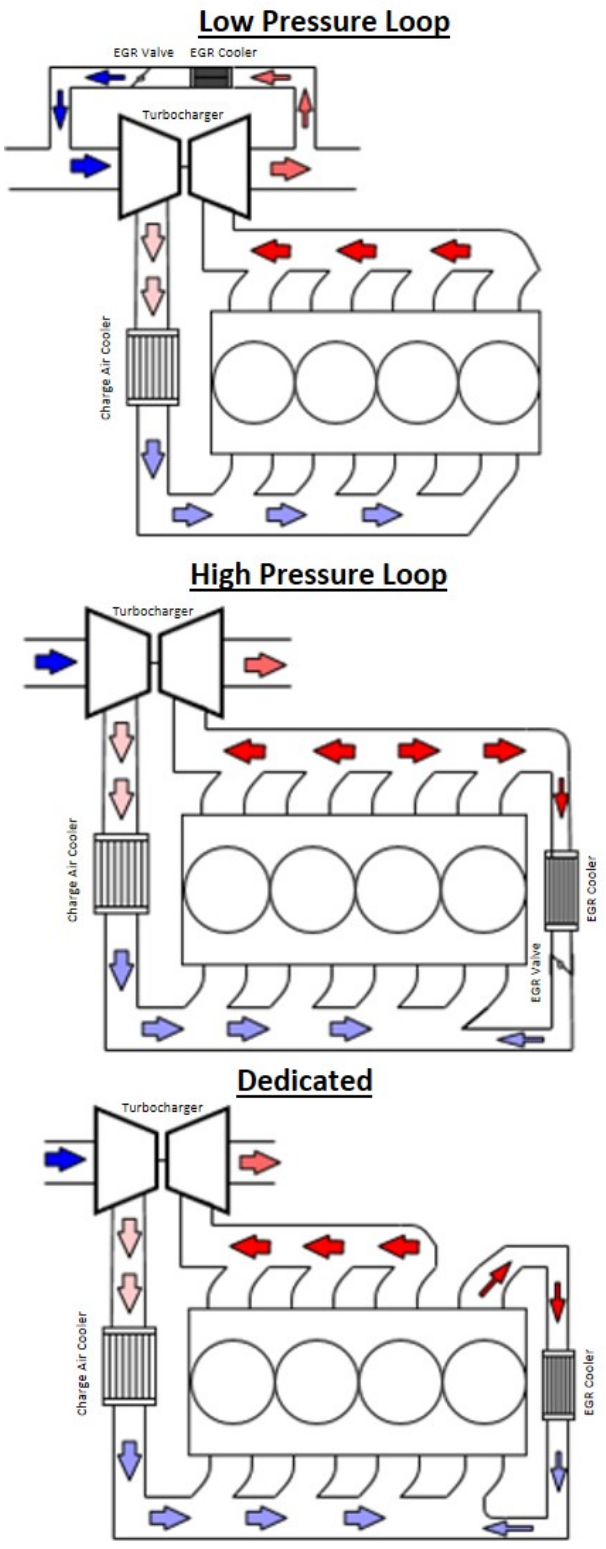

Figure 3.1: Schematic of LPL, HPL, and dedicated EGR techniques.

HPL and LPL EGR configurations. The first advantage is the ability to operate at a nominal 25% EGR rate across the entire operating range of the engine. This EGR rate surpasses conventional HPL and LPL EGR rates for natural gas engines which allows for lower combustion temperatures and thus lower component temperatures and lower NO_x emissions. The second advantage is the removal of an exhaust flow control valve and flow control strategy. On HPL and LPL EGR systems the exhaust flow control valve is positioned downstream of a heat exchanger as shown in Figure 3.1. Even with this heat exchanger in place the control valve can be exposed to exhaust temperatures near 100 °C which can limit the long term reliability of the control valve. A dedicated EGR system instead uses a mass flow controller and simple port fuel injection strategy to deliver additional fuel to the dedicated cylinder. The working fluid in the mass flow controller is natural gas at temperature and pressure similar the gas coming into the engine.

Accomplishing a nominal 25% EGR rate across the entire operating range requires that the effects of highly non-reactive molecules such as carbon dioxide (CO_2) and water (H_2O) be offset by highly reactive molecules. The general combustion reaction for an arbitrary hydrocarbon with air is shown in Equation 3.1.

$$C_xH_y + a(O_2 + 3.76N_2) \rightarrow bCO_2 + cCO + dH_2O + eH_2 + fO_2 + 3.76aN_2 \qquad (3.1)$$

For lean or stoichiometric conditions the reaction in Equation 3.1 can be simplified to the reaction in Equation 3.2, or for rich conditions can be simplified to the reaction shown in Equation 3.3[8]. The reaction in Equation 3.3 provides the increased reactivity required to operate an engine at a nominal 25% EGR rate since hydrogen is the highest reactivity primary reference fuel for methane number (MN) calculations[9]. As the air fuel ratio becomes more rich the presence of hydrogen (H_2) and carbon monoxide (CO) increase and the presence of inert complete combustion products of CO_2 and H_2O decrease. This shift from inert molecules in the recirculated exhaust to highly reactive molecules such as H_2 and molecules with some ability to participate in combustion such

as CO allow for the nominal 25% EGR rate to be achieved via increase in LHV and reactivity.

$$C_xH_y + a(O_2 + 3.76N_2) \rightarrow bCO_2 + dH_2O + fO_2 + 3.76aN_2 \tag{3.2}$$

$$C_xH_y + a(O_2 + 3.76N_2) \rightarrow bCO_2 + cCO + dH_2O + eH_2 + 3.76aN_2 \tag{3.3}$$

3.3 Background

While the addition of hydrogen to natural gas engines outfitted with EGR has not been well researched, investigations into the effects of hydrogen on gasoline engine combustion have been studied during the past 15 years.

In 2005 Ivanic et al.[10] performed experiments on a single cylinder research engine to study the effects of hydrogen enhancement with lean and EGR diluted mixtures on gasoline engine efficiency, NO_x emissions, and flame speed. The results showed that hydrogen has a significant impact on the 0-10 mass fraction burned (MFB) time, but the 10-90 MFB is less affected by hydrogen enrichment. He stated that hydrogen addition contributed more to speeding up the flame initiation phase (0-10 MFB) than to the flame propagation phase (10-90 MFB) because it increases the mixtures laminar flame speed, which has a greater effect on flame growth rate before the flame becomes fully turbulent[10]. Significant reductions in NO_x emissions on the order of a 90% reduction were also found at an EGR rate near 25%. Similar results of lower NO_x emissions due to fuel reforming with dilution were found by Jamal et al.[11].

In a similar study, Gerty et al.[12] investigated the effects of H_2 enrichment on gasoline engine knock characteristics. Considering the results published by Ivanic in 2005, it was concluded that the primary means by which hydrogen can reduce engine knock is the auto ignition chemistry. This chemistry was summarized to be the conversion of hydroxyl radicals to hydrogen radicals and water. Hydrogen radicals were stated to be not as effective at initiating chain branching reactions as hydroxyl radicals[12].

In 2007 Alger et al.[13] researched the effects of hydrogen enrichment on EGR tolerance in spark ignited engines. In this work the method of dedicated EGR was first introduced. Until this point, fuel was reformed separate from the engine being used to produce power. The experimental setup consisted of a single cylinder variable compression ratio gasoline engine which utilized a flat, two valve head and a shallow piston bowl. He found while operating the engine at 3.1 bar BMEP and a compression ratio (CR) of 11:1 the 0-2 MFB and 2-10 MFB duration decreased as H_2 was added to the combustion chamber. A brief set of experiments was done to examine the effect of H_2 addition to natural gas combustion. Natural gas EGR tolerance was improved by adding H_2 to the exhaust gases, but the improvement was only from 20% to 28% which was much less than the improvements shown for gasoline combustion. Interestingly, similar to the gasoline combustion tests, the 10-90 MFB of natural gas improved as more H_2 was added to the recirculated exhaust.

The next research step for Alger et al.[14] was to implement the dedicated EGR concept on a multi cylinder engine and operate one cylinder fuel rich to provide the partial oxidation fuel reformation required to create H_2, CO, and other partial combustion products. The engine used for this work was a 2.4L naturally aspirated gasoline engine. At part load operation minima in brake specific fuel consumption (BSFC) and coefficient of variation of indicated mean effective pressure (COV of IMEP) were found at a dedicated cylinder lambda of 0.8. At part load operation an improvement in overall burn duration was found. However, the reduction in burn duration was found to be more substantial in early combustion stages when compared to the 2007 single cylinder research[13]. The results from 2009 Alger publication[14] showed the necessity of a mixer that would mix EGR and fresh air-fuel mixture spatially and temporally. The temporal aspect of the mixer is required due to the inherent pulses of EGR coming from a single cylinder on an engine.

Further on engine demonstrations of dedicated EGR implemented on commercially available gasoline engines were performed by Alger and others at Southwest Research Institute[15–24]. These demonstrations continued to focus on improving engine efficiency by increased compression ratio, boosting, and the development of the patented dedicated EGR mixer.

In 2018, Liu et al.[25] researched the effects on knock and lean limit extension from the addition of equal amounts H_2 and CO to 99% CH_4 CNG gas. Experiments were done on a single cylinder spark ignited (SI) engine with displacement of 1.85 liters, CR of 10.5:1 , and flat combustion chamber design. It was found that at part load conditions when the H_2 and CO addition increased from 0 to 1% and 2% on a volume percentage basis the knock intensity increased from 4.8 to 5.5 and 24.9, respectively. Apparent heat release plots showed that the addition of H_2 and CO increased the flame speed, and the author suggested that the increased flame speed further compressed unburned mixture resulting in higher unburned gas temperature and pressure.

Given the amount of research on the topic of dedicated EGR applied to gasoline engines and the limited research on dedicated EGR applied to multi-cylinder natural gas engines this work seeks to evaluate dedicated EGR implemented on a stoichiometric industrial natural gas engine and answer the following research questions:

- What impact will dedicated EGR have on engine combustion metrics such as COV of IMEP, 10-90 MFB, and individual cylinder IMEP?
- What combustion products can be expected from a stoichiometric natural gas engine operating with dedicated EGR, and how will these compare to a conventional stoichiometric natural gas engine?
- What impact will dedicated EGR have on exhaust temperatures, and how will this compare to a conventional stoichiometric natural gas engine?

3.4 Methods

A Caterpillar G3304 natural gas engine was selected for the on engine demonstration of dedicated EGR. Physical properties of the G3304 can be found in Table 3.1. As a stock engine the G3304 is fully mechanical relying on a carburetor to perform fuel mixing, a fly ball governor to control engine speed, and a mechanical means of adjusting spark timing. The industry application for the G3304 engine is gas lifting and wellhead compression. Often this class of engine is

Table 3.1: Engine specifications for Caterpillar G3304 engine.

Caterpillar G3304	
Number of Cylinders	4
Rated Engine Speed	1800 rpm
Compression Ratio	10.5
Displacement	7.0 L
Bore	120.7 mm
Stroke	152.4 mm
Piston / Head Design	Flat
Spark Plug	Fine Wire (0.64 mm gap)

operated in remote areas with little or no access after the engine is installed. Because of this the engine must be able to run reliably on a wide variety of gas methane numbers. The variation in possible gas MN is reflected in the design choices for the G3304. The fully mechanical controls offer excellent reliability and the flat top piston and head with a relatively low compression ratio of 10.5:1 offer good knock resistance. Finally, the BMEP at wide open throttle (WOT) is 6.7 bar.

After installing the G3304, upgrades were made to the measurement and control capabilities. A Woodward large engine control module (LECM) was installed which allowed electronic control valves to be implemented for closed loop AFR and engine speed control. Closed loop AFR dithering was not used in this work. Instead a simple PID method was used to control AFR. Wide band oxygen sensors were installed on the stoichiometric cylinder and dedicated exhaust manifolds to monitor AFR. The LECM also controlled individual cylinder spark timing and spark duration. Fuel delivery to the engine was done via a low pressure intake system with fuel mixing with air upstream of a compressor. Additional fuel supplied to the dedicated cylinder was done via port fuel injection. Total fuel flow was measured using an orifice meter flow path designed and built according to the American Gas Association (AGA) Report No. 3 Part 1 and 2[26,27]. A stand alone turbocharger system was installed to provide increased intake manifold pressure to the engine. A Whipple WSC-140AXB compressor upstream of the intake manifold was paired with an Advanced

Valve Design high temperature wafer type valve downstream of the exhaust manifold to simulate a turbocharged configuration.

In cylinder combustion was measured on each cylinder by a National Instruments data acquisition system utilizing Kistler 6013C pressure transducers. Real time cylinder pressure was measured and combustion statistics such as IMEP, COV of IMEP, peak cylinder pressure (PCP), location of peak pressure (LPP), 10/50/90 MFB, and knock intensity (KI) were determined for all tests.

Engine exhaust gas species were analyzed using a Rosemount 5-gas analyzer rack with Siemens instrumentation. Species measured using this instrumentation were CO, CO_2, total hydrocarbons (THC), oxygen (O_2), and NO_x. Additional emissions such as methane, ethane, formaldehyde, and ammonia were measured using an MKS Fourier Transform InfraRed Spectrometer (FTIR). Natural gas fuel was taken directly from local natural gas pipeline feedstock. The composition of natural gas was measured using a Varian CP4900 mini gas chromatograph. Natural gas methane number was calculated using the MWM methane number method[28]. Details of the engine laboratory setup used in the experiments discussed in this work are shown in Figure 3.2. Figure 3.3 shows the EGR mixer used to mix exhaust from the dedicated cylinder with the fresh-air fuel mixture. Exhaust is accumulated in the inner cylinder where the inherent pulses from the dedicated cylinder are damped out. The exhaust then passes through orifices on the inner cylinder where it is then entrained in the fresh air-fuel passing through the interior of the outer cylinder. The inner cylinder on the EGR mixer has a volume 1.5 times that of the dedicated cylinder on the G3304 engine. This design allows exhaust and the premixed air-fuel to spatially and temporally mix. The experimental setup for this work is shown pictorially in Figure 3.4. Tests were conducted at steady state operating conditions. After reaching an operating point the engine was allowed to come to equilibrium for approximately 10 minutes prior to data collection. Emissions data presented is representative of pre catalyst, 5 minute collection times at 2 Hz, and combustion data presented is an average of 500 cycles. In this preliminary work while the engine was operating in the dedicated EGR mode the air fuel ratio for the dedicated cylinder was set at a lambda of 0.830 while the air fuel ratio of

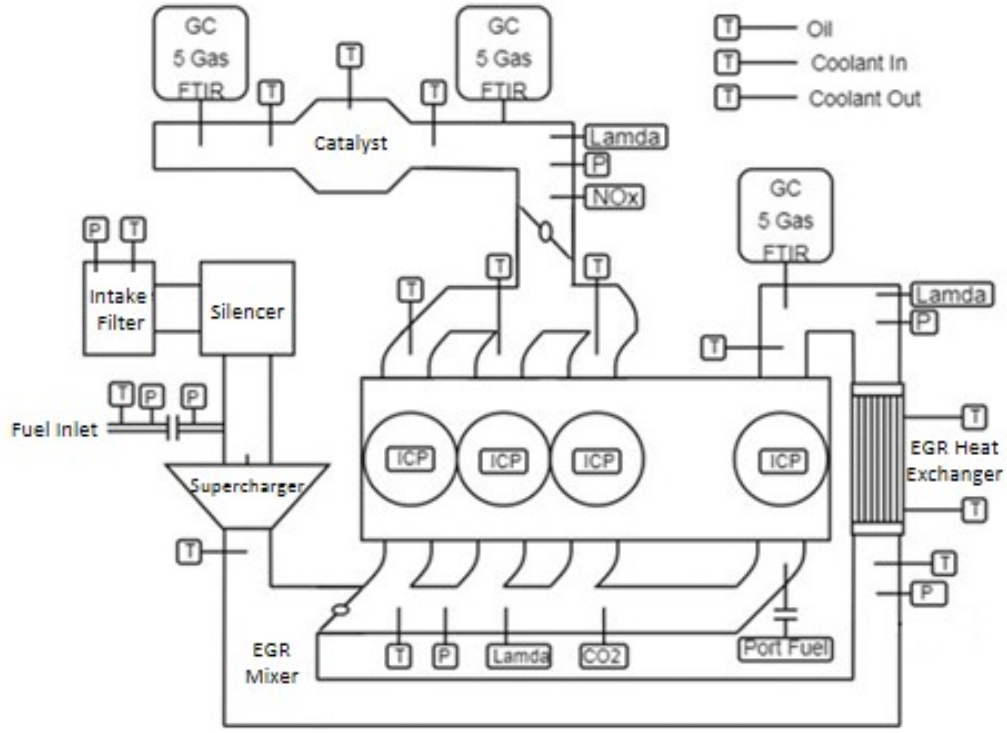

Figure 3.2: Schematic of measurement devices used on the G3304 engine.

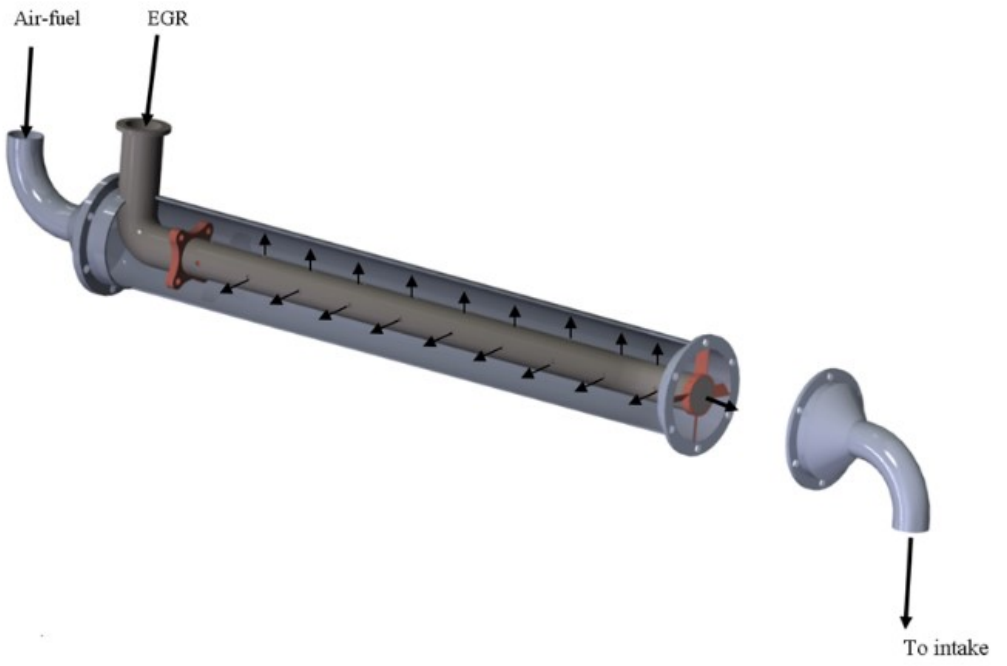

Figure 3.3: Dedicated EGR mixer design used in this work.

Figure 3.4: Experimental setup for the Caterpillar G3304 engine operating with dedicated EGR and upgraded measurement and control capabilities. The EGR mixer is shown in the red box.

the three remaining cylinders was held constant at lambda 1.000. The dedicated cylinder lambda value of 0.830 was selected based on previous engine tests performed by another team working on the G3304 engine. Using a similar dedicated cylinder AFR provided insight into the long term performance repeatability of the dedicated EGR concept. Spark duration and timing were kept at a constant value of 150 μs and 34° before top dead center (bTDC), respectively.

3.5 Results

3.5.1 Exhaust Emissions

Regulated engine emissions are critical to understanding the feasibility of dedicated EGR applied to a rich burn natural gas engine. Figures 3.5, 3.6, and 3.7 show brake specific emissions of NO_x, CO, and THC at part load operating conditions where spark timing was held constant. The formation of NO_x from hydrocarbon combustion is achieved through the Zel'dovich (thermal), Fenimore (prompt), N_2O intermediate, and NNH mechanisms. The Zel'dovich mechanism is the primary means of NO_x formation in high temperature combustion over a large range of equivalence ratios[8]. Both data sets in Figure 3.5 had stoichiometric AFR conditions. Thus, NO_x emissions are primarily formed by the Zel'dovich mechanism. The dEGR test points exhibited approximately one third the engine out brake specific NO_x of the no EGR test points which demonstrates the impact that high levels of dilution has on combustion temperatures. Error bars shown in Figures 3.5, 3.6, 3.7, 3.8, and 3.9 represent total uncertainty in the single sample measurements as defined by Kline, et al.[29]. The uncertainty shown is representative of calibration gas uncertainty and measurement instrument linearity. Figure 3.6 describes the engine out brake specific CO emissions. Similar to the engine out brake specific NO_x emissions, dEGR operation of the engine showed lower CO emissions compared to the no EGR operation at all part load test points. At stoichiometric conditions high amounts of CO are present in combustion products due to the dissociation of CO_2 at stoichiometric combustion temperatures. However, equilibrium concentration of CO decreases significantly as combustion temperature decreases.[8] Lower peak combustion temperature resulting in less dissociation of CO_2 to CO is likely a contributing factor to the lower brake

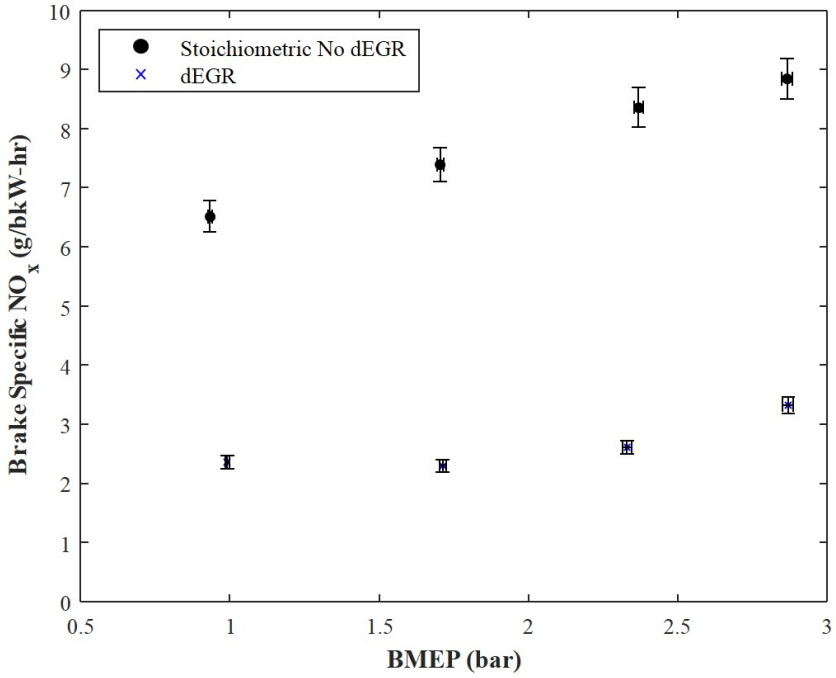

Figure 3.5: Engine out brake specific NOx emissions for stoichiometric and dedicated EGR operation.

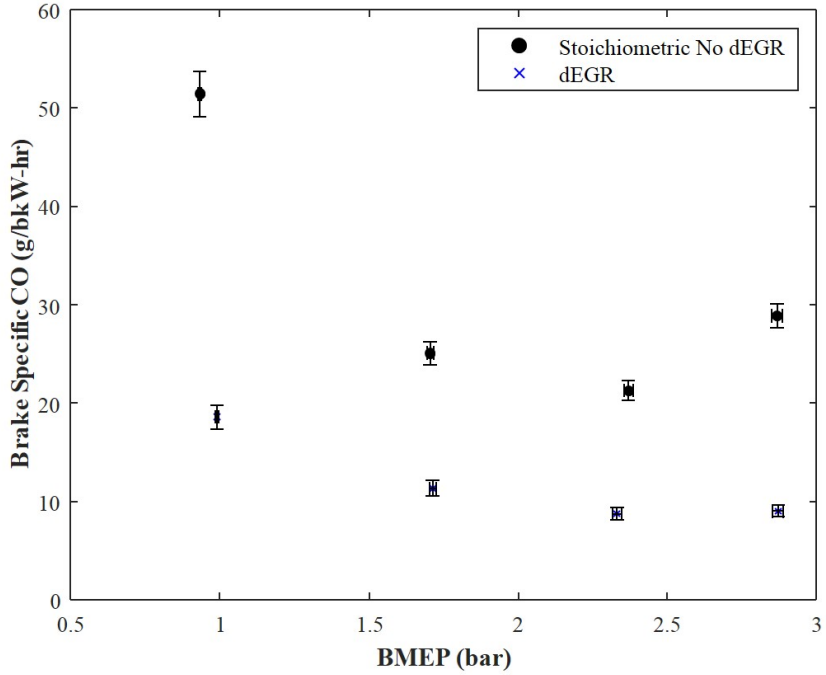

Figure 3.6: Engine out brake specific CO emissions for stoichiometric and dedicated EGR operation.

specific CO emissions found in all dEGR test points. Examination of engine out CO_2 emissions confirmed this explanation as each of the dEGR test points had a higher CO_2 emissions than their no EGR counterparts. The decrease in CO emissions as break mean effective pressure increases is an artifact of reduction in incomplete combustion as engine load increases. As a reference, at high speed full load conditions engine out brake specific CO emissions for no EGR operations were 4.45 g/bkW-hr, roughly ten times lower than the low load operating point.

Figure 3.7 shows the brake specific engine out unburned hydrocarbon emissions. Engine operating points incorporating the dEGR technology showed higher unburned hydrocarbon emissions than the no EGR operation at each respective point. The primary methods by which unburned hydrocarbons are produced during pre-mixed combustion are formation and retention in crevice volumes, adsorption and desorption in engine oil, poor combustion, and combustion chamber wall effects[6]. As will be outlined in subsequent figures and discussion in this work dEGR operation of the G3304 engine resulted in higher COV of IMEP and longer total burn duration. Both of these variables are markers of poor combustion which results in higher unburned hydrocarbon emissions. Similar the discussion of engine out CO emissions, unburned hydrocarbon emissions trend lower as engine load is increased in the no EGR and dEGR test cases due to increases in expansion and exhaust stroke temperatures, and in-cylinder oxidation rate of hydrocarbons[6].

A final consideration of the formation of unburned hydrocarbons in dEGR engines as compared to standard stoichiometric natural gas engines is the difference in quench gap, which is the distance from the wall where the flame is quenched, of the combustion charge. Processed natural gas is typically composed of $C_1 - C_5$ alkanes with fractions of N_2 and CO_2 also being present. The quench gap for these alkanes varies from 0.21 cm to 0.16 cm while the quench gap for H_2 is approximately 0.06 cm[30]. While operating as a dEGR engine rich combustion in the dedicated cylinder results in the presence of H_2 in the exhaust that is then recirculated back to the intake manifold. The smaller quench gap of H_2 and its presence as a combustion reactant in a dEGR engine results in a positive impact on unburned hydrocarbon emissions. Another important regulated emission for natural gas engines is formaldehyde. Formation of formaldehyde is prevalent in partial oxidation

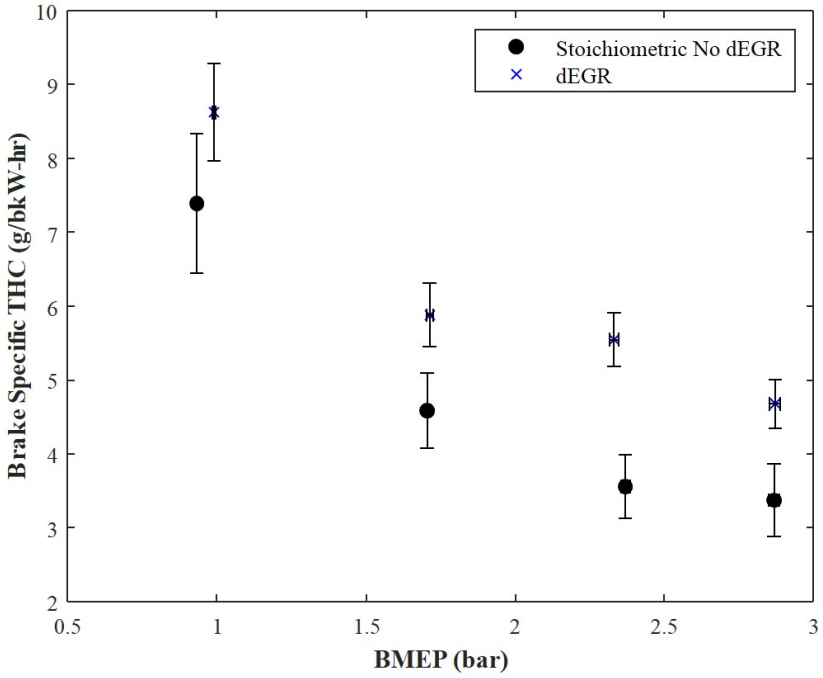

Figure 3.7: Engine out unburned hydrocarbon emissions. Results shown include dry methane and ethane.

combustion where the temperature is high enough for reactions to occur, but not high enough that formaldehyde destruction takes place[31]. Reduced combustion temperatures due to the high level of dilution in dEGR operation likely results in the increased engine out formaldehyde emissions shown in Figure 3.8. The final regulated emission considered in this work is volatile organic compounds (VOCs). In this work VOCs are defined as non-methane, non-ethane hydrocarbons and oxygenated hydrocarbons such as formaldehyde are excluded. Using the hydrocarbons quantified by the MKS FTIR, VOCs are a collection of ethylene, acetylene, propylene, and propane. The data shows a general trend of decreasing brake specific VOC emissions as engine load is increased. Contrary to the previous emissions data where statistical differences between dEGR and no EGR operation were found, the brake specific VOC emissions have no discernable statistical differences between results at any engine BMEP.

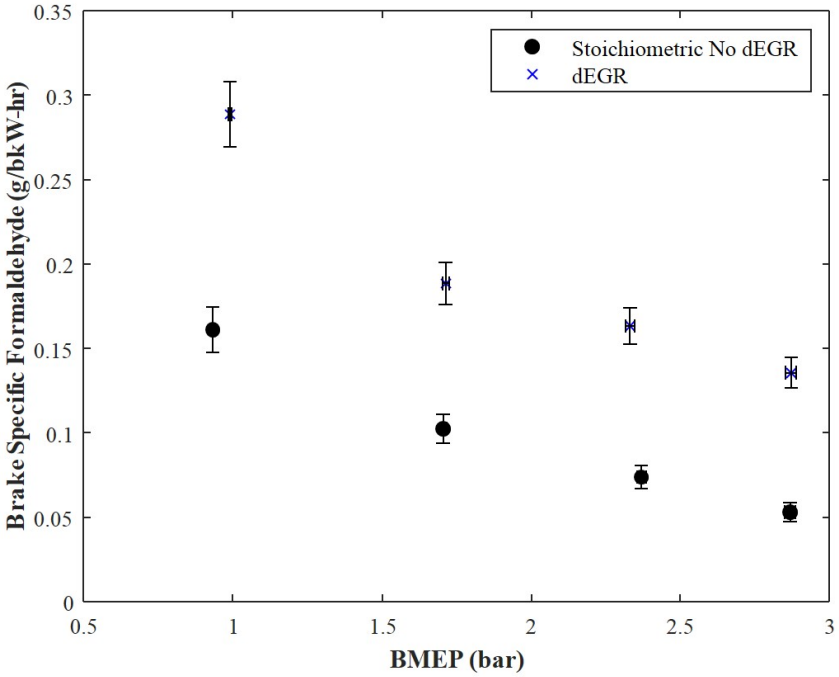

Figure 3.8: Engine out formaldehyde emissions.

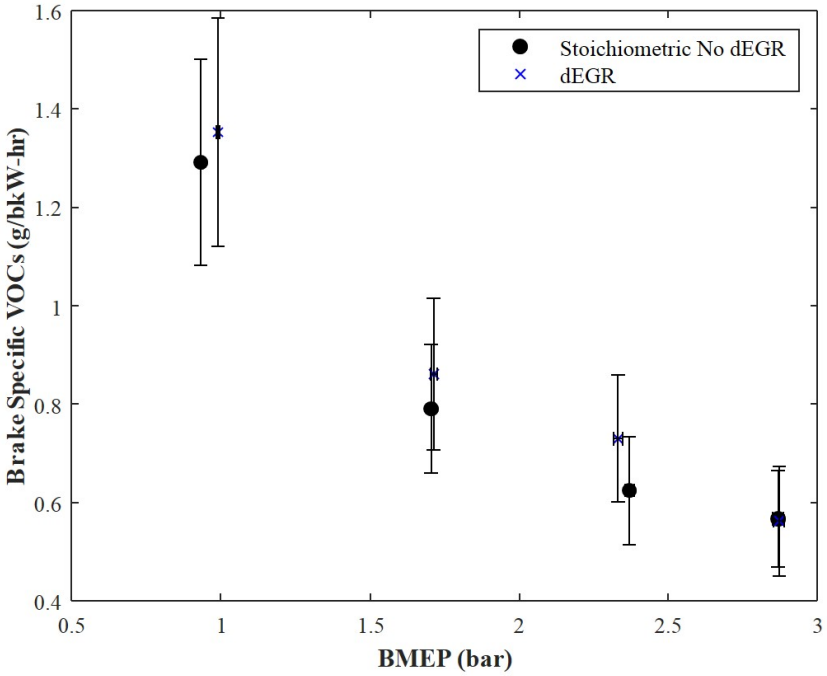

Figure 3.9: Engine out VOC emissions. VOCs included were ethylene, acetylene, propylene, and propane.

3.5.2 Combustion Metrics

High speed combustion data collected in this work included tenth crank angle resolution cylinder pressure, burn duration, and apparent heat release rate. Combustion statistics calculated were PCP, average location of peak pressure (LPP), average IMEP, COV of IMEP, NMEP, PMEP, and locations of 10, 50, and 90% mass fraction burned (MFB). While at rated speed the three engine operating points considered were 0.9, 2.4, and 6.7 bar BMEP. While operating in the dedicated EGR mode the rich burn dedicated cylinder AFR was held at 0.830 lambda. Spark timing and duration were again held at 34° bTDC, and 150 μs, respectively. Spark timing was not adjusted to match combustion phasing or achieve maximum brake torque between no EGR and dEGR tests. High speed and combustion statistics were collected on all four cylinders of the engine. The data presented in this section is divided into three subsets which are no EGR (average of all four cylinders at lambda 1.0) shown in black, dEGR stoichiometric cylinder average (of three cylinders) shown in blue, and dEGR dedicated (rich burn) cylinder shown in red. While operating in the dedicated EGR mode the variation in combustion among the three stoichiometric cylinders was low enough that combining the individual cylinder data into averaged data was appropriate. Figure 3.10 shows the cylinder pressure, apparent heat release rate, and mass fraction burned at rated engine speed and 0.9 bar BMEP. At this low engine load significant differences between the location of 10, 50, and 90% MFB for the no EGR and dEGR test cases is evident. First, comparing the no EGR MFB and dEGR stoichiometric cylinder burn rates the statistics showed that the 0-10 MFB duration differed by 4.97 crank angle degrees. The no EGR 10% MFB location was at 0.59 degrees °bTDC while the dEGR stoichiometric cylinder 10% MFB location was at 4.37 °aTDC. The disparity between the two test cases became larger at the 50% and 90% MFB locations. The location for 50% MFB was 19.73 and 27.52 °aTDC for the no EGR and dEGR test cases, respectively. The location for 90% MFB was 42.51 and 57.17 °aTDC for the respective test cases. The impact that a 25% nominal EGR rate has on stoichiometric combustion is clear in the slower rate of combustion during the entire event. The dedicated cylinder with an AFR of lambda 0.830 had even slower combustion with the 10, 50, and 90% MFB locations occurring at 10.10, 30.65, and 64.07

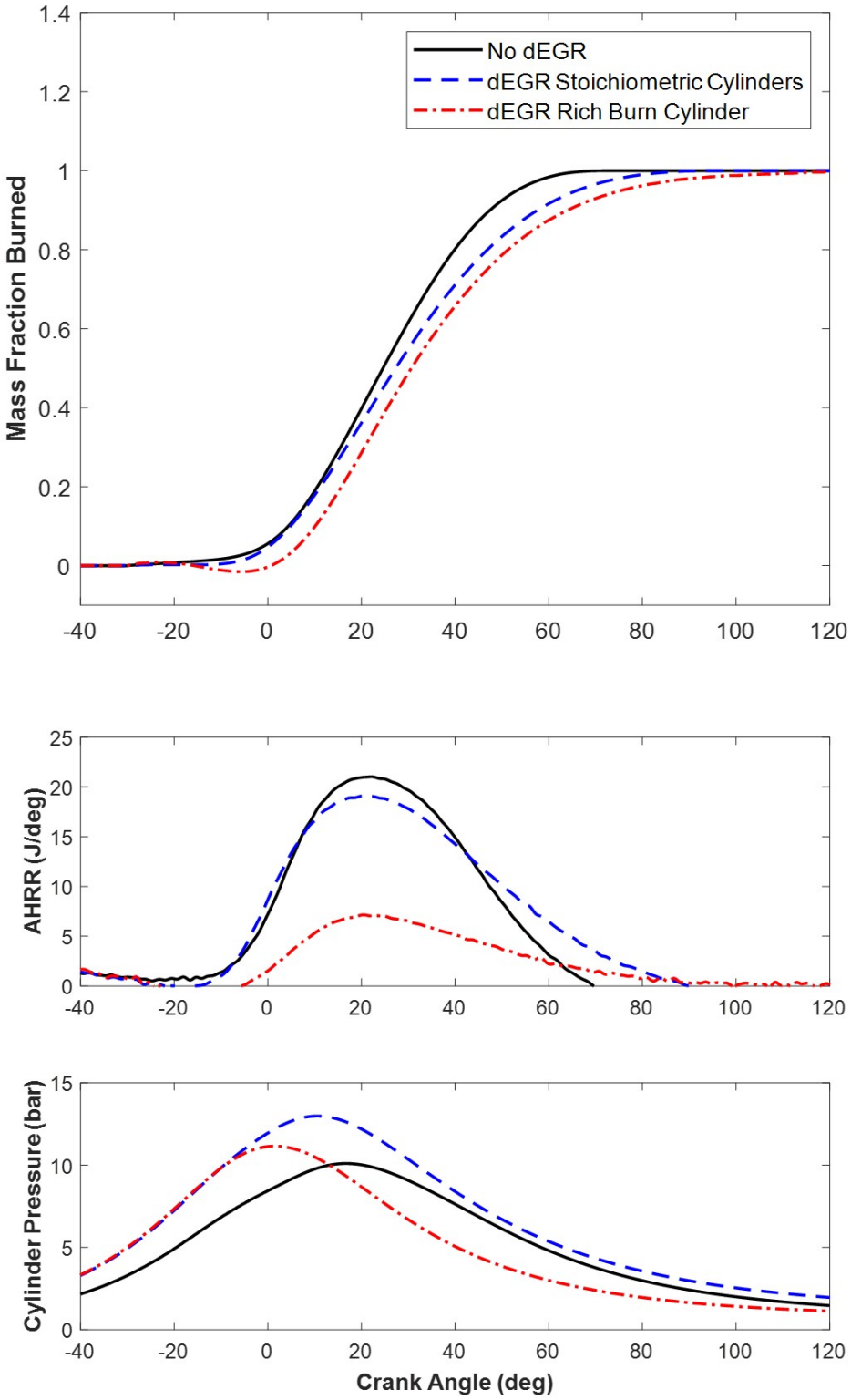

Figure 3.10: Combustion statistics at 0.9 bar BMEP. Dedicated EGR stoichiometric cylinder data is averaged from three cylinders operating at stoichiometric conditions, and no dEGR is averaged data from all four engine cylinders.

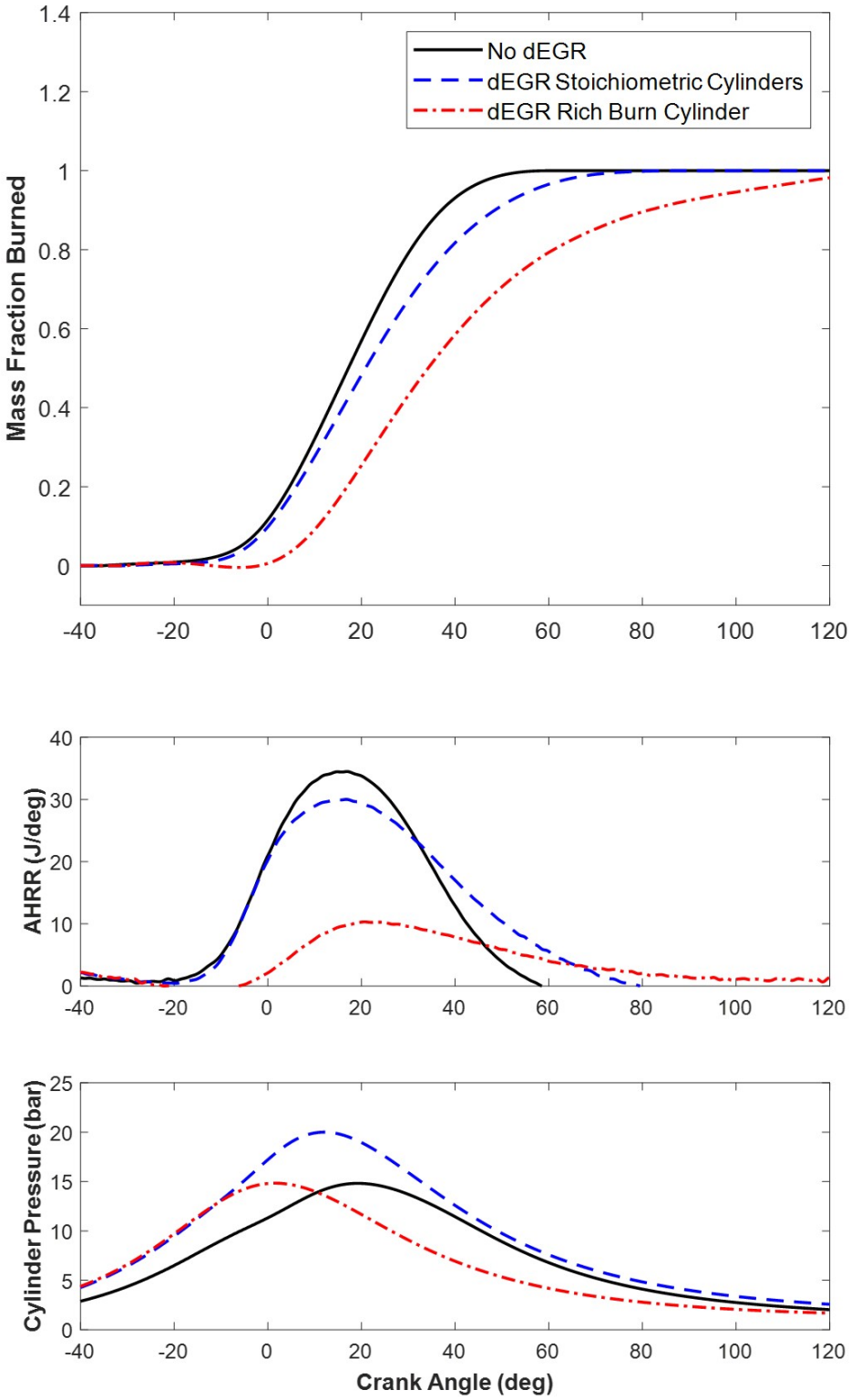

Figure 3.11: Combustion statistics at 2.4 bar BMEP. Dedicated EGR stoichiometric cylinder data is averaged from three cylinders operating at stoichiometric conditions, and no dEGR is averaged data from all four engine cylinders.

°aTDC, respectively. The AHRR sub figure in Figure 3.10 shows how the combustion in dEGR operation has a lower peak heat release rate and an extended heat release duration. The dedicated cylinder shows much lower and extended heat release rate due to partial burning when compared to the stoichiometric combustion traces. Finally, the cylinder pressure sub figure in Figure 3.10 shows how while operating with dEGR the three stoichiometric cylinders have a higher average peak pressure than the no EGR average test case. The engine power is similar between the two test cases, but because of the poor combustion in the dedicated cylinder during dEGR operation the stoichiometric cylinders must have higher power output to maintain the same total engine power output. The difference between pre-combustion pressures (motored pressures) of the dEGR and no EGR test cases is due to different intake manifold pressures. The dEGR intake manifold pressure was 1.56 psi higher than the no EGR test.

The second operating point where combustion metrics were considered was rated speed and 2.4 bar BMEP. In contrast to the low load condition, the dEGR stoichiometric cylinders 10% MFB location was 0.78 °bTDC and the no EGR location was 1.44 °bTDC. The location of 50% MFB was 18.80 °aTDC and 16.49 °aTDC for the dEGR and no EGR tests, respectively. These differences in MFB locations were much improved from the low load condition. However, the dedicated cylinder which again operated at an AFR of lambda 0.830 still suffered from slow, poor combustion as indicated in the MFB sub figure of Figure 3.11. The AHRR sub figure of Figure 3.11 shows how well the stoichiometric dEGR and no EGR test cases trended together during the first third of the combustion event. However, the dEGR stoichiometric test exhibits late heat release extending late into the expansion stroke. The AHRR of the dedicated cylinder shows the poor combustion in the dedicated cylinder. The onset of heat release is delayed by approximately 13.8 crank angle degrees and extends very late into the expansion stroke. The cylinder pressure sub figure of Figure 3.11 again shows while operating with dedicated EGR the stoichiometric cylinders must make up for the lack of combustion in the dedicated cylinder. This results in a higher intake manifold pressure and higher peak pressure in comparison to the no EGR test case.

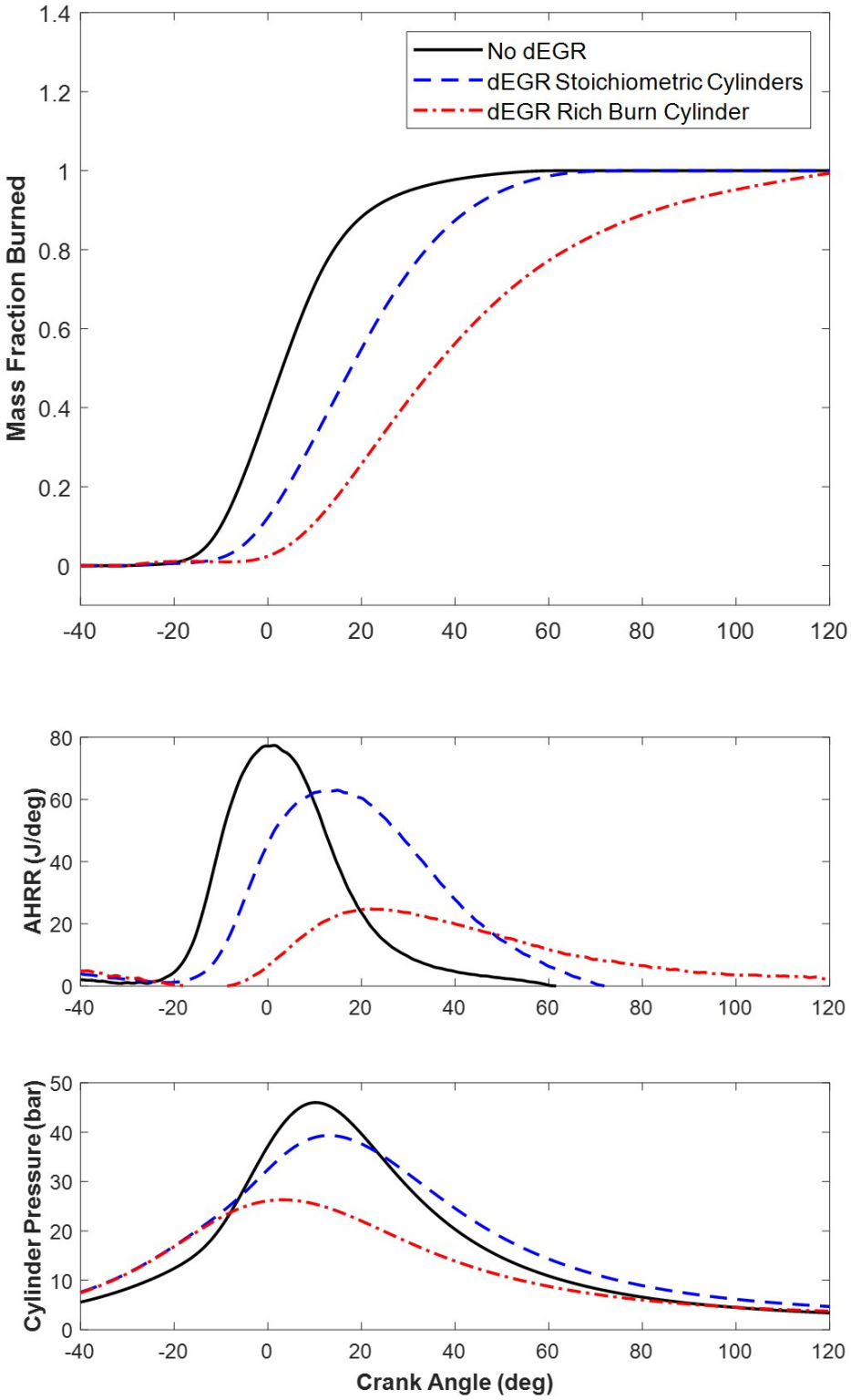

Figure 3.12: Combustion statistics at 6.7 bar BMEP. Dedicated EGR stoichiometric cylinder data is averaged from three cylinders operating at stoichiometric conditions, and no EGR is averaged data from all four engine cylinders.

The final operating condition considered was rated speed and 6.7 bar BMEP. This condition is the rated full power operating point for the G3304 engine. The improvements in burn rates shown at intermediate engine load shown in Figure 3.11 were not evident at the full power test point shown in Figure 3.12. The difference in 0-10 MFB (early combustion) between the no EGR and dEGR stoichiometric cylinders was 8.65 crank angle degrees. Early combustion burn rate in the no EGR operating condition improved by 8.33 crank angle degrees between the 2.4 bar and 6.7 bar BMEP test cases. The dEGR operating condition did not show this improved 0-10 MFB as the improvement between 2.4 and 6.7 bar BMEP was 0.33 crank angle degrees. The stoichiometric dEGR rate of combustion continued to be slower than the stoichiometric no EGR combustion as shown by the MFB 50 and 90 locations being 17.98 and 42.25 °aTDC, respectively. The no EGR MFB 50 and 90 locations were 3.23 and 21.25 °aTDC. The AHRR and cylinder pressure sub figures in Figure 3.12 showed similar trends to that of Figure 10 in that dEGR operation had slower combustion.

The COV of IMEP for test cases is shown in Figure 3.13. COV of IMEP defines the cyclic variability in indicated work per cycle[8]. The threshold for acceptable COV of IMEP used in this work is a value of 5. However, for different natural gas engine applications the acceptable threshold may be much lower (such as stationary power generation). Poor combustion in the dedicated cylinder across all engine operating points is evident in this figure. Also of note is the COV of IMEP of the stoichiometric dEGR cylinders. While COV of IMEP improves as engine load increases the lowest value observed was 6.17, just above the acceptable threshold. The last combustion metric considered for this work was individual cylinder IMEP. Figure 3.14 shows the averaged IMEP values for no EGR stoichiometric tests, stoichiometric cylinders on dEGR tests, and the dedicated cylinder on dEGR tests. Stoichiometric cylinders on dEGR tests showed higher IMEP values than the non dEGR counterparts. Due to poor combustion in the dedicated cylinder the remaining three stoichiometric cylinders had higher power output to make up for the lower power output of the dedicated cylinder. Imbalanced power output between the stoichiometric and dedicated cylinder during dEGR operation is an issue that must be resolved for the dedicated EGR

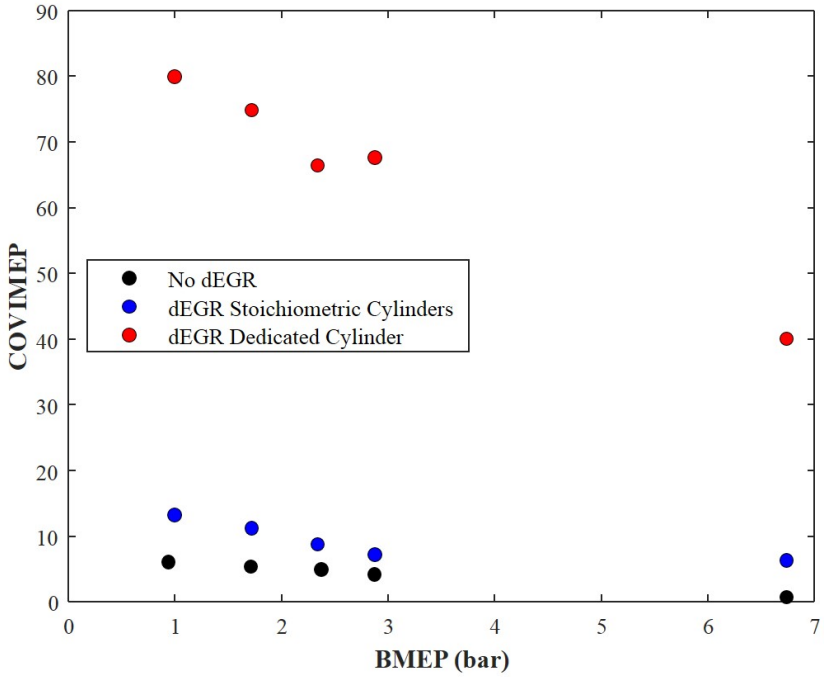

Figure 3.13: COV of IMEP as a function of BMEP. Threshold for acceptable COV of IMEP in this work was set at a value of 5.

technique to be implemented. A final consideration in the discussion of combustion metrics is the composition of the natural gas fuel. Gas composition was not controlled during these tests, but the composition which is shown in Table 3.2 was monitored and logged during each test. All dedicated EGR tests used fuel with lower levels of ethane, but higher levels of butane. Differences in mole fractions of inert species of CO_2 and N_2 were also evident between the no EGR and dEGR test cases. However, the MWM methane number calculated for each test case varied only between 69 and 72.

3.5.3 Exhaust Temperature and Efficiency

The impact that dedicated EGR has on exhaust component temperature is of key importance to this impact this technology can make on the stoichiometric natural gas engine industry. At the five operating conditions described in the combustion metrics section the exhaust port temperature of each cylinder was recorded. Figure 3.15 shows the average exhaust port temperature of all

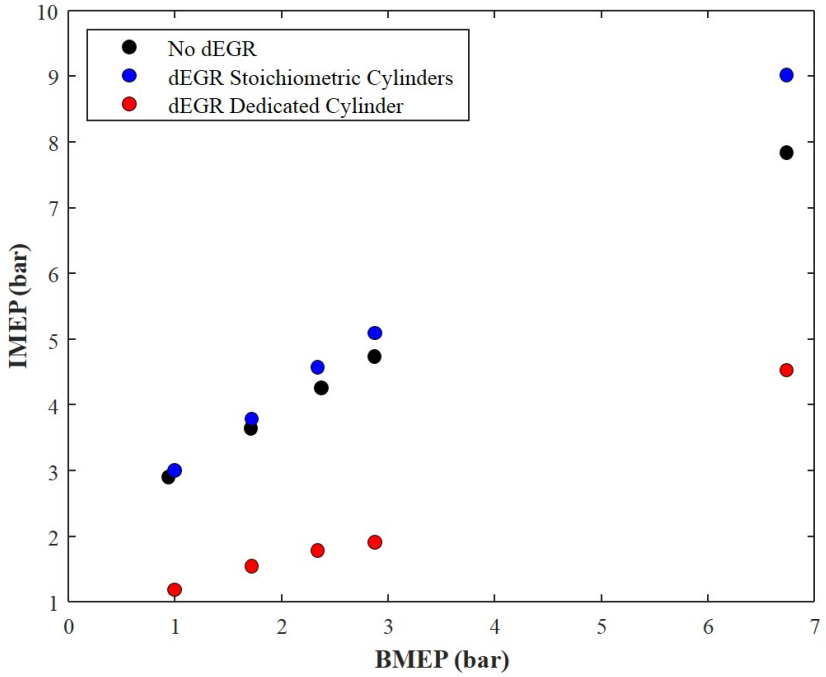

Figure 3.14: Cylinder IMEP as a function of engine BMEP. No EGR test points are averaged values from all cylinders.

Table 3.2: Fuel composition for the test cases considered in this work. Methane number was calculated using the MWM method.

Natural Gas Fuel Composition							
No dEGR Tests							
BMEP (bar)	N_2	CH_4	CO_2	C_2H_6	C_3H_8	C_4H_10	MN
0.9	0.40	82.23	2.37	12.48	2.33	0.09	71
1.7	0.39	81.75	2.39	12.75	2.50	0.09	70
2.4	0.36	81.45	2.41	12.86	2.70	0.10	70
2.9	0.36	81.38	2.34	12.82	2.85	0.11	70
6.7	0.38	82.40	2.50	12.62	1.95	0.07	72
dEGR Tests							
1.0	0.23	82.40	2.82	11.31	2.74	0.24	71
1.7	0.24	82.84	2.78	11.12	2.56	0.21	71
2.3	0.24	82.54	2.76	11.44	2.59	0.21	71
2.9	0.24	82.53	2.76	11.49	2.56	0.20	71
6.7	0.47	81.93	2.08	12.58	2.45	0.40	69

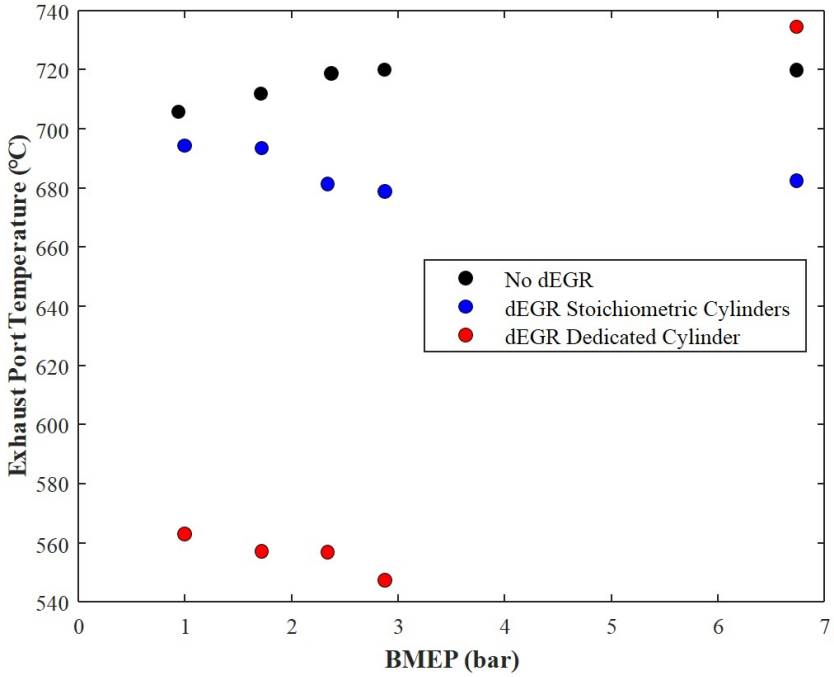

Figure 3.15: Exhaust port temperature at varied engine operating conditions. No dEGR test point data is averaged from all four engine cylinders.

four cylinders during stoichiometric no EGR operation, the average of the stoichiometric cylinders with dedicated EGR, and the dedicated cylinder with dedicated EGR. Beginning at intermediate load conditions of 2.37 bar BMEP and continuing to the full engine load condition of 6.7 bar BMEP the dedicated EGR technique lowers exhaust port temperatures by approximately 40 °C in the stoichiometric cylinders. However, the dedicated cylinder as shown in Figures 3.13 and 3.14 experienced very poor combustion. The decrease in exhaust temperatures ranged from 142 °C at 0.9 bar BMEP to 173 °C at 2.87 bar BMEP. At 6.7 bar BMEP the dedicated cylinder exhaust temperature was elevated to 734 °C which was above the average stoichiometric no EGR exhaust port temperature of 720 °C. Examining Figures 3.13 and 3.14 provide the rationale for this high exhaust port temperature. At the 6.7 bar BMEP operating point COV of IMEP of the dedicated cylinder is approximately 40%. This is an improvement from the average COV of IMEP of the lower BMEP operating points which is approximately 72%. Although a COV of IMEP of 40% is well above a desired COV of IMEP of less than 5% this decrease from 72% to 40% results in

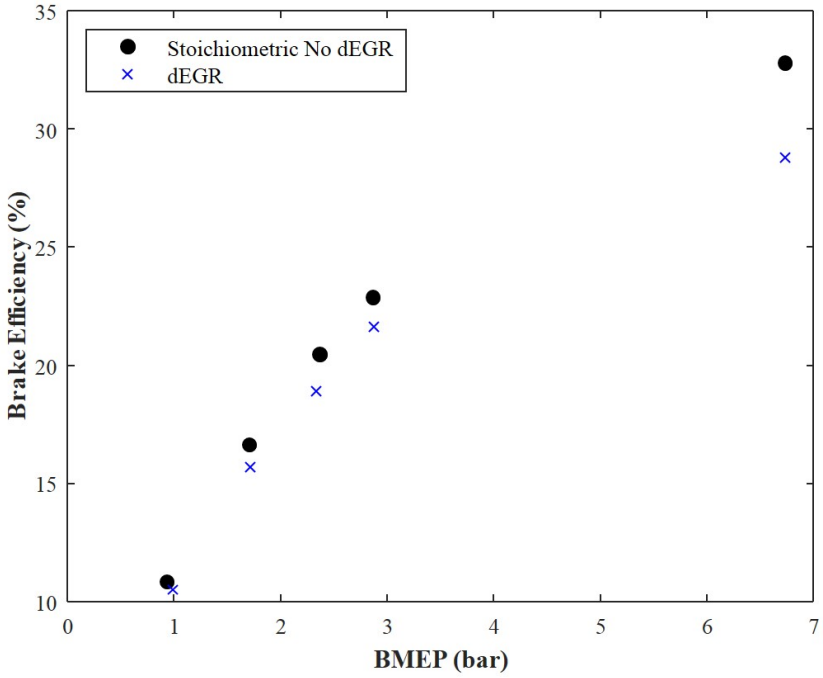

Figure 3.16: Brake efficiency as a function of engine operating condition.

more stable combustion and in turn a higher exhaust port temperature. If combustion phasing were to be controlled rather than spark timing the exhaust port temperatures of the dEGR test cases would be decreased further due to the advanced combustion phasing required to match non-dEGR and dEGR test cases. Brake efficiency comparisons at the five test points considered are made in Figure 3.16. This efficiency was calculated using the recorded fuel mass flow rate during the test and the fuel composition measured during the test. The decrease in efficiency while operating in the dedicated EGR condition can be explained primarily by the timing of the combustion heat release. Examination of the AHRR and MFB parts of Figures 3.10, 3.11, and 3.12 show combustion in the dedicated EGR test cases extending longer into the expansion stroke than the stoichiometric no dEGR test cases. As combustion happens in an expanding volume less useful work is applied to the piston and in turn the overall efficiency is decreased.

3.5.4 Conclusions and Next Steps

Dedicated EGR was implemented on a stoichiometric industrial natural gas engine and the effects on combustion metrics, engine out emissions, and exhaust temperatures were analyzed at low, part, and full load conditions. The dedicated cylinder AFR was held at a lambda 0.830 during dedicated EGR test while other cylinders operated at stoichiometric conditions, and during all tests the spark timing was held constant at 34 °bTDC. Results while operating with dedicated EGR were compared to stoichiometric no dEGR conditions at the same engine operating points. The following conclusions were drawn from this work:

- While operating under dedicated EGR conditions - emissions of NO_x and CO were reduced at all operating points considered due to decreased combustion temperatures associated with a nominal 25% EGR rate but, emissions of unburned hydrocarbons and formaldehyde were higher when compared to stoichiometric no dEGR operation.
- Utilizing fine wire spark plug ignition source and flat top head and piston design the dedicated EGR technique showed poor combustion in terms of COV of IMEP, balanced cylinder to cylinder IMEP, and rate of combustion. Specifically, the dedicated cylinder operating with a nominal 25% EGR rate and rich combustion conditions showed inadequate combustion.
- Due to the slow rate of combustion the dedicated EGR brake efficiency was lower than that of standard stoichiometric no dEGR operation.
- Dedicated EGR operation showed a marked decrease in exhaust port temperatures despite influences from slower combustion.

Challenges in optimizing this technology to meet acceptable combustion stability and balance between cylinders remain. This work demonstrates perhaps the worst case scenario for dedicated EGR to be implemented. Adding additional diluent to an already low reactivity fuel such as natural gas without making changes to the combustion chamber to improve turbulence and ultimately combustion rate proved to be feasible but not practical. The expected improvements in combustion rate

due to the partial oxidation combustion products from the dedicated cylinder were not sufficient in improving combustion rate nor stability. This initial work did not consider how adjustment to variables such as dedicated cylinder AFR, individual cylinder spark timing, various ignition technologies such as non-enriched pre chamber spark plugs, intake manifold conditions, and combustion chamber design could improve combustion stability and rate of combustion. In subsequent publications an optimization exercise will be demonstrated with variables of intake manifold charge temperature, cylinder spark timing, spark duration, and dedicated cylinder equivalence ratio. The choice of ignition system and combustion chamber design will also be considered.

3.6 References

1. U.S. Energy Information Administration. International Energy Outlook 2017, https://www.eia.gov/outlooks/archive/ieo17/ (2017, accessed March 11, 2018).

2. U.S. Energy Information Administration. Energy Explained, https://www.eia.gov/energyexplained/index.php?page=natural_gas_reserves (2018, accessed December 27, 2018).

3. U.S. Energy Information Administration. Today in Energy, https://www.eia.gov/todayinenergy/detail.php?id=37172 (2018, accessed December 22, 2018).

4. Energy Information Administration. U.S. No 2 Diesel Wholesale/Resale Price by Refiners, https://www.eia.gov/dnav/pet/hist/LeafHandler.ashx?n=pet&s=ema_epd2d_pwg_nus_dpg&f=m (2018, accessed December 17, 2018)

5. Energy Information Administration. Natural Gas Prices, https://www.eia.gov/dnav/ng/ng_pri_sum_dcu_nus_m.htm (2018, accessed December 17, 2018)

6. Heywood JB. Internal Combustion Engine Fundamentals. New York: McGraw-Hill, 1988.

7. Glewen W, Hoops C, Hiltner J, Flory M. Comparative Analysis of EGR and Air Dilution in Spark-Ignited Natural Gas Engines. 2017; ICEF2017-3608.

8. Turns S. An Introduction to Combustion Concepts and Applications. 3rd ed. New York: MeGraw Hill, 2012.

9. Leiker M, Christoph K, Rankl M, Cantellieri W, Pfeifer U. Evaluation of Anti-knocking Property of Gaseous Fuels by Means of Methane Number and Its Practical Application to Gas Engines. 1972; ASME-72-DGP-4.

10. Ivanic Z, Ayala F, Goldwitz J, Heywood JB. Effects of Hydrogen Enhancement on Efficiency and NOx Emissions of Lean and EGR-Diluted Mixtures in a SI Engine. SAE; 2005-01-0253.

11. Jamal Y, Wagner T, Wyszynski ML. Exhaust Gas Reforming of Gasoline at Moderate Temperatures. Hydrogen Energy 1996; 21: 507-519.

12. Gerty MD, Heywood JB. An Investigation of Gasoline Engine Knock Limited Performance and the Effects of Hydrogen Enhancement. SAE; 2006-01-0228.

13. Alger T, Gingrich J, Mangold B. The Effect of Hydrogen Enrichment on EGR Tolerance in Spark Ignited Engines. SAE; 2007-01-0475.

14. Alger T, Mangold B. Dedicated EGR: A New Concept in High Efficiency Engines. SAE; 2009-01-0694.

15. Alger T, Mangold B, Roberts C, Gingrich J. The Interaction of Fuel Anti-Knock Index and Cooled EGR on Engine Performance and Efficiency. SAE; 2012-01-1149.

16. Gingrich. EGR Distributor Apparatus for Dedicated EGR Configuration. United States patent 8,561,599 B2. Issued October 22, 2013.

17. Chadwell C, Alger T, Zuehl J, Gukelberger R. A Demonstration of Dedicated EGR on a 2.0 L GDI Engine. SAE; 2014-01-1190.

18. Gukelberger R, Gingrich J, Alger T, Almaraz S. LPL EGR and D-EGR Engine Concept Comparison Part 2: High Load Operation. SAE; 2015-01-0781.

19. Gukelberger R, Gingrich J, Alger T, Almaraz S, Denton B. LPL EGR and D-EGR Engine Concept Comparison Part 1: Part Load Operation. SAE; 2015-01-0783.

20. Alger T, Walls M, Chadwell C, Joo S, Denton B, Kleinow K, Robertson D. The Interaction between Fuel Anti-Knock Index and Reformation Ratio in an Engine Equipped with Dedicated EGR. SAE; 2016-01-0712.

21. Denton B, Chadwell C, Gukelberger R, Alger T. Design and Implementation of a D-EGR Mixer for Improved Dilution and Reformate Distribution. SAE; 2017-01-0647.

22. Robertson D, Chadwell C, Alger T. Dedicated EGR Vehicle Demonstration. SAE; 2017-01-0648.

23. Kalaskar V, Gukelberger R, Denton B, Briggs T. The Impact of Engine Operating Conditions on Reformate Production in a D-EGR Engine. SAE; 2017-01-0684.

24. Alger T, Gukelberger R, Gingrich J. Impact of EGR Quality on the Total Inert Dilution Ratio. SAE; 2016-01-0713.

25. AGA 3.1: Orifice Metering of Natural Gas and Other Related Hydrocarbon Fluids: Part 1. American Gas Association. 40 CFR 75, Appendix D.

26. AGA 3.2: Orifice Metering of Natural Gas and Other Related Hydrocarbon Fluids – Concentric, Square-edged Orifice Meters Part 2: Specification and Installation Requirements.

27. EUROMOT. MWM Methane Number Calculator, https://www.euromot.eu/publication-and-events/publications/ (2016, accessed November 2, 2018).

28. Kline SJ, McClinktock FA. Uncertainties in Single Sample Experiments. Mech Eng 1953; Jan: 3-8.

29. Glassman I. Combustion. 2nd ed. San Diego: Academic Press Inc, 1987.

30. Mitchell C, Olsen DB. Formaldehyde Formation in Large Bore Natural Gas Engines Part 1: Formation Mechanisms. ASME 2000; 122: 603-610

Chapter 4

Response Surface Method Optimization of a Natural Gas Engine with Dedicated Exhaust Gas Recirculation

4.1 Summary

Rich burn industrial natural gas engines rely on robust design to achieve consumer driven uptime requirements. Key to this design are exhaust components that are able to withstand high combustion temperatures found in this type of natural gas engine. The issue of exhaust component durability can be addressed by making improvements to materials and coatings or decreasing combustion temperatures. Among natural gas engine technologies shown to reduce combustion temperature, dedicated exhaust gas recirculation (EGR) has limited published research. However, due to the high nominal EGR rate it may be a technology useful for decreasing combustion temperature. In previous work by the author, dedicated EGR was implemented on a Caterpillar G3304 rich burn natural gas engine. Examination of combustion statistics showed that, in comparison to a conventional rich burn natural gas engine, operating with dedicated EGR requires adjustments to the combustion recipe to achieve acceptable engine operation. This work focuses on modifications to the combustion recipe necessary to improve combustion statistics such as coefficient of variance of indicated mean effective pressure (COV of IMEP), cylinder-cylinder indicated mean effective pressure (IMEP), location of 50% mass fraction burned, and 10-90% mass fraction burn duration. Several engine operating variables were identified to affect these combustion statistics. A response surface method (RSM) optimization was chosen to find engine operating conditions that would result in improved combustion statistics. A third order factorial RSM optimization was sufficient for finding optimized operating conditions at 3.4 bar brake mean effective pressure (BMEP). The results showed that in an engine with a low turbulence combustion chamber, such

as a G3304, optimized combustion statistics resulted from a dedicated cylinder air-fuel ratio of lambda 0.936, spark timing of 45 degrees before top dead center (°bTDC), spark duration of 365 μs, and intake manifold temperature of 62 °C. These operating conditions reduced dedicated cylinder COV of IMEP by 10% (absolute) and the difference between average stoichiometric cylinder and dedicated cylinder IMEP to 0.19 bar. [3]

4.2 Introduction

Development of technology such as horizontal drilling and hydraulic fracturing in the early and mid-2000s has led to a rapid increase in shale gas production from shale plays throughout the U.S[(1)]. Due to these developments the Marcellus, Permian, Utica, Haynesville, and Eagle Ford shale plays have each experienced significant growth since 2008 and to date account for nearly 80% of the U.S. dry shale gas production[(2)]. As shown in Figure 4.1 these shale plays cover large areas of land and cross multiple states in the U.S. [(3)] Industrial natural gas engines have come to play a critical role in providing on-site power for hydraulic fracturing processes. Natural gas engines are often the preferred power source at well sites due to the reduced operating expenses associated with replacing diesel fuel with natural gas. Federal, state, and well site specific laws regulate emissions from engines providing power to well servicing equipment at well sites. Federal requirements for natural gas engines at well sites are described in EPA 40 CFR 60 Subpart JJJJ[(4)]. However, state and well site specific regulations vary widely and can include total emission limits for the entire site[(5,6)]. It is not uncommon for natural gas engines to be moved between well sites over the life of the engine. Therefore, an engine that can meet state and site specific emissions requirements at any site is advantageous. Rich burn natural gas engines are able to utilize a three-way catalyst to achieve best in class post catalyst emissions and effectively meet even the most strict emissions requirements. However, since rich burn engines must operate near stoichiometric conditions to uti-

[3]Sections 1-10 of this chapter are composed of a paper submitted to the International Journal of Engine Research. The citation for this publication is as follows: Van Roekel C, Montomgery DT, Singh J, and Olsen DB. Response Surface Method Optimization of a Natural Gas Engine with Dedicated Exhaust Gas Recirculation. International Journal of Engine Research. 2019.

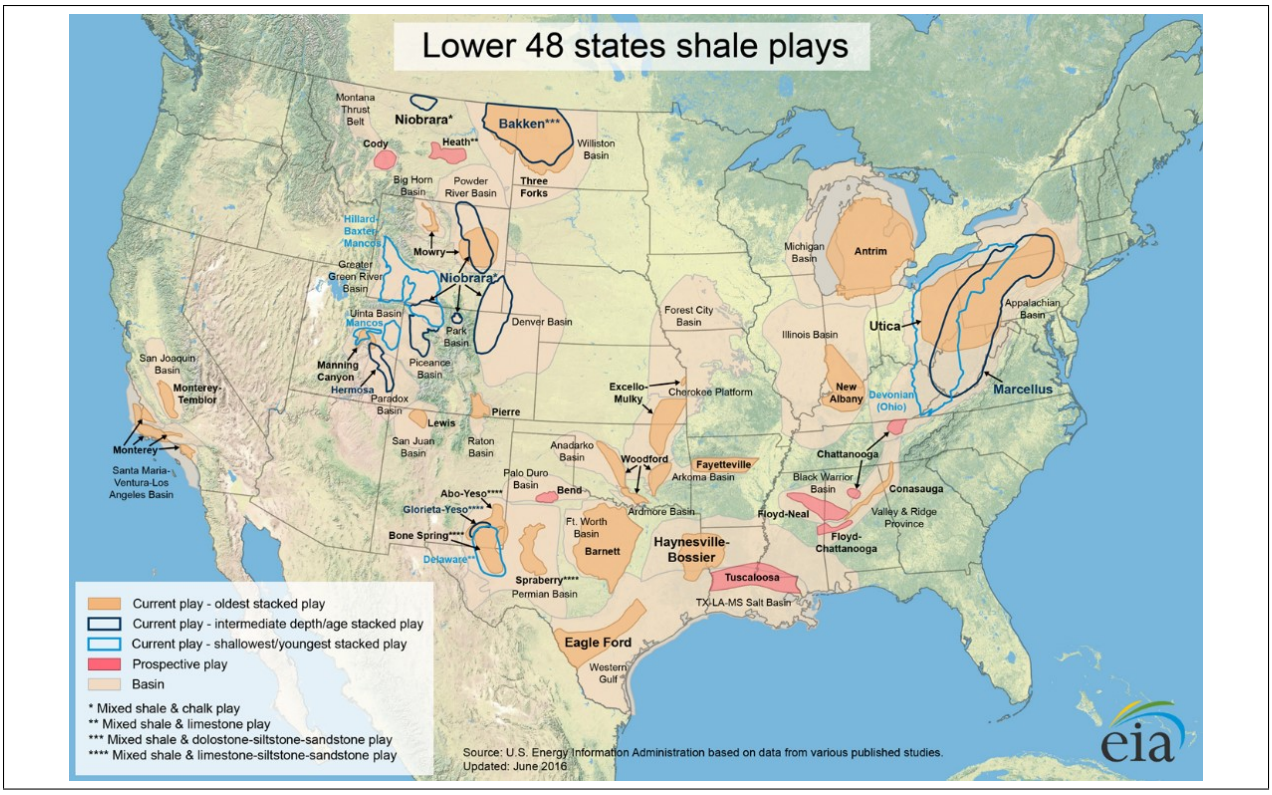

Figure 4.1: Natural gas shale plays in the US.

lize a three-way catalyst combustion temperatures are high when compared to lean burn natural gas engines. Higher combustion temperatures lead to shorter exhaust component life. Manufacturers of rich burn natural gas engines address this issue by limiting engine power density. It follows that a well site which requires a fixed amount of power to operate would need more rich burn engines than lean burn engines to meet a fixed site power requirement. This tradeoff between lower power density and decreased engine emissions provides motivation to investigate technologies that can be applied to rich burn natural gas engines which lower combustion temperature while still allowing the engines to operate near stoichiometric conditions. The ability for conventional low pressure loop (LPL) and high pressure loop (HPL) exhaust gas recirculation (EGR) to decrease combustion temperature is well understood [7,8], but less understood is how dedicated EGR can be applied to natural gas engines and its potential to lower combustion temperature.

Dedicated EGR is a novel variation on conventional low and high pressure loop EGR configurations. Rather than recirculating only a portion of the exhaust from all cylinders back to the intake

manifold, dedicated EGR recirculates all of the exhaust from one or more 'dedicated' cylinders of the engine at all engine operating points. The dedicated cylinder(s) are operated at fuel rich conditions which results in an exhaust composition that includes partial oxidation combustion products such as hydrogen (H_2) and carbon monoxide (CO)[9–11]. In contrast to the method of control that conventional HPL and LPL systems utilize, namely an EGR valve, a dedicated EGR system does not include components that are exposed to hot exhaust. This is a significant benefit in terms of the long term reliability of the EGR system.

4.3 Background

As outlined in a previous publication [12] most research of dedicated EGR has been focused on this technology applied to spark ignited (SI) gasoline engines. However, two publications, one by Van Roekel et al. [12] and another by Mitchell et al.[13] have demonstrated dedicated EGR implemented on multi-cylinder natural gas engines. The work by Mitchell et al. [13] was done on a 6 cylinder, 12 L Cummins ISX G engine. Two of the six cylinders were designated as 'dedicated' cylinders for a nominal 33% EGR rate. The objective of this research was to improve the engine efficiency by a relative 10% above the baseline. Notable results from this work were up to 11% relative improvements in brake thermal efficiency of the engine while operating with dedicated EGR. However, at high speed engine operating points the dedicated cylinder became unstable with increased fuel addition to that cylinder while the stoichiometric cylinder combustion stability improved. Overall, improved performance by the engine was limited by the dedicated cylinder and further research was planned to incorporate new ignition systems. Similar lack of combustion performance in the dedicated cylinder was found by Van Roekel et al. [12] In this work a 4 cylinder, 7 L Caterpillar G3304 engine with a low turbulence combustion chamber [12] was modified so that one cylinder was designated as the 'dedicated' cylinder. This resulted in a nominal 25% EGR rate. At rated speed and three difference engine brake mean effect pressure (BMEP) points a single dedicated cylinder air-fuel ratio (AFR) of lambda 0.830 was tested. At each point, combustion stability in the dedicated cylinder was well above the acceptable threshold of coefficienct of vari-

ance of indicated mean effective pressure (COV of IMEP) less than 5%. This work highlighted the need for a comprehensive assessment of dedicated EGR combustion recipe. The term recipe here is used to describe many variables that affect an engine combustion event. In general these variables would include things like the type of fuel used, physical combustion chamber geometry, and the initial conditions in the combustion chamber. The content of this paper is focused on finding a combustion recipe more suited to dedicated EGR operation in a low turbulence combustion chamber. The following research questions will be answered:

- In a low turbulence combustion chamber such as that in a G3304 engine what combustion recipe will result in most improved combustion?
- Will ignition sources such as non-enriched pre chamber spark plugs result in improved combustion when compared to a fine wire spark plug?

4.4 Experimental Setup

This work was carried out on a modified Caterpillar G3304 rich burn natural gas engine. Table 4.1 shows the specifications for the G3304, and an image of the engine installed in the test cell is shown in Figure 4.2. Key upgrades made to the stock G3304 engine were the addition of an engine control module, simulated turbocharger, and EGR mixer. The engine control module added capabilities such as independent cylinder timing offsets, and closed loop air-fuel ratio control. A turbocharger was simulated using a stand alone supercharger, driven by an AC motor, and a back pressure valve. The EGR mixer was designed to allow for adequate mixing of air, fuel, and exhaust in spite of inherent pulses of exhaust coming from a single dedicated cylinder. Further detail about the upgrades made to the engine, gaseous emissions measurement, and combustion statistics measurement can be found in a publication by Van Roekel et al.[12].

4.5 Response Surface Method

The response surface method (RSM) optimization performed in this work is modeled after the work published by Montgomery et al. and Brown et al.[14,15]. Critical to the setup of a RSM

Table 4.1: Engine specifications for Caterpillar G3304.

Number of Cylinders	4
Rated Engine Speed	1800 rpm
Rated BMEP	6.7 bar
Compression Ratio	10.5
Displacement	7.0 L
Bore	120.7 mm
Stroke	152.4 mm
Piston / Head Design	Flat

Figure 4.2: Experimental engine test cell used for this work.

optimization is defining boundaries, constraints, variables, and the merit or otherwise referred to as an objective function. Clear definition of these parts prior to carrying out the optimization ensures that the relevant research question will be answered at the end of the optimization. The objective function in the RSM optimization is described by the mathematical function shown in Equation 4.1. Acronyms seen in the equation are defined as follows: IMEP is the indicated mean effective pressure, COV IMEP is the coefficient of variance of indicated mean effective pressure, CA50 is the crank angle at which 50% of the total mass in the cylinder is burned, and 10 – 90 MFB is the time in crank angle degrees between 10% and 90% mass fraction burned in the cylinder.

$$f(x_n) = \frac{1000}{(\frac{|IMEP_{2-4} - IMEP_1|}{1.43})^2 + (\frac{COVIMEP_{MAX1-4}}{5})^2 + |CA50_{AVG} - 13.81| + \frac{10-90MFB_{AVG}}{35.38}} \tag{4.1}$$

Where:

$IMEP_{2-4}$ = the average IMEP of engine cylinders held at stoichiometric conditions

$IMEP_1$ = the IMEP of the dedicated cylinder

$COVIMEP_{MAX1-4}$ = the highest individual cylinder COV of IMEP recorded

$CA50_{AVG}$ = the average CA50 of all cylinders

$10\breve{}90MFB_{AVG}$ = the average 10 – 90 MFB of all cylinders

The terms included in the objective function were chosen based on the results from Van Roekel et al. [12] Figures 10-14 in this work showed the necessity for improving cylinder-cylinder IMEP, dedicated cylinder COV of IMEP, and the 10/50/90 MFB locations. Each term in the objective function includes a nominal 'target' value. The target for the difference between the average IMEP of cylinders 2 through 4 and the IMEP of cylinder 1 is 1.430 psi. The target for average CA50 location is 13.81 °aTDC, and the target for 10 – 90 MFB duration is 35.38 crank angle degrees. These target values were chosen from the baseline operation of the G3304 engine without EGR. The target for maximum COV of IMEP was set at a nominal value of 5. Further, the terms comparing IMEP and COV of IMEP are squared. Squaring these terms gives them priority during the optimization process. Overall, this objective function is designed such that a greater magni-

Table 4.2: Optimization variables incremented during the RSM optimization

Intake Manifold Temperature
Spark Timing
Spark Duration
Dedicated Cylinder Air-Fuel Ratio

tude solution means improved combustion (in terms of the combustion metrics listed) has been achieved.

Four variables were identified to have an effect on the combustion metrics and are listed in Table 4.2. Additional variables such as combustion chamber design were identified and are critical to a combustion recipe, but ultimately were deemed not feasible within the scope of this work. While the variables in Table 4.2 were incremented during the RSM optimization all other variables such as engine speed and brake mean effective pressure (BMEP) were held constant. The engine operation boundaries were set such that the maximum acceptable exhaust port temperature in any cylinder was 750 °C and a knock intensity (KI) of 50 was not exceeded. KI is a measure of the severity of knock based on calculated engine knock frequency and a specified number of cycles over which the magnitude of the knock event at the knock frequency is integrated. Further detail about the development of this method can be found be examining the dissertation of Wise[16]. A careful characterization of engine knock for the G3304 engine was performed where it was found that the knock frequency was 4.7 kHz and by advancing spark timing and increasing intake manifold temperature (IMAT) different levels of engine knock were induced. It was determined based on audible observations during a 200 combustion cycle window that heavy knock occurred at a KI of approximately 500, light knock at a KI of approximately 110, and incipient knock at approximately 39. During the entire optimization exercise the engine was operated at rated speed and 3.4 bar BMEP.

The workflow for the RSM optimization was as follows:

1. Initial conditions for the optimization variables found in Table 4.2 were selected and the objective function was solved in two consecutive tests.

2. The individual optimization variables were incremented and the objective function was solved at each point. Since there were four optimization variables this meant that there were 16 data points on the 'response surface'.

3. The engine was returned to the initial operating conditions and the objective function was solved again in two consecutive tests. A standard deviation of the objective function response at the initial conditions was calculated based on the four repeated tests. This standard deviation was compared to the standard deviation of the response from the 16 data points on the 'response surface'. If the standard deviation of the repeated initial condition points was greater than the standard deviation from the response surface points then the optimization exercise was complete. If the standard deviation of the repeated initial condition was less the optimization exercise continued.

4. The objective function gradient was calculated based on the objective function response of the 16 response surface points evaluated.

5. Initial conditions for the optimization variables were incremented in the direction and magnitude of the gradient until a maximum value of the objective function was found.

6. The values of the optimization variables where the maximum in the objective function was found were used as the initial conditions for a new factorial.

7. Steps 2 through 6 were repeated until the standard deviation of the initial condition objective function response was greater than the standard deviation of the response surface objective function.

4.6 Results and Discussion

4.6.1 First Factorial

The first RSM optimization was performed with fine wire spark plugs as an ignition source. These spark plugs are standard spark plugs for the G3304 engine. To initialize the RSM optimization values for optimization variables were chosen guided by the results from previous work[12]. Thus, the initial conditions were not arbitrarily chosen. Rather, it was suspected that these initial conditions would be closer to appropriate engine operating conditions than what was chosen in the previous work. These variables along with the other engine operating conditions can be found in Table 4.3.

In the first factorial the initial optimization variables were incremented around the center point in the following ways: dedicated cylinder AFR ratio was incremented $\pm$ 0.025 lambda, IMAT was incremented $\pm$ 5°C, spark timing was incremented $\pm$ 3 crank angle degrees, and spark duration was incremented $\pm$ 100 μs. Therefore, the objective function response is a function of four variables. To illustrate the objective function response in four dimensions the solution will be shown first as a function of dedicated cylinder lambda, ignition timing, and ignition duration. Then points sharing similar dedicated cylinder lambda, ignition timing, ignition duration, but different IMAT values will be compared. Figures 4.3 and 4.4 show the objective function response for an IMAT of 65 °C and 55°C, respectively.

The objective function response for the initial conditions found in Table 4.3 was a value of 4.78. In terms of physical combustion metrics the difference between the average IMEP of cylinder 2-4 and cylinder 1 (dedicated cylinder) was 18.42 psi, the highest cylinder COV of IMEP was 26.30, average location of CA50 was 27.74, and the average 10 – 90 MFB was 60.46 crank angle degrees. As expected the highest COV of IMEP was found in the dedicated cylinder. Independent of changes in IMAT, the results from the first factorial show clearly that conditions lean of the initial dedicated EGR AFR of 0.900 result in improved objective function response. Improvements in the IMEP comparison and COV of IMEP (both squared terms) in the objective function were responsible for the increase objective function response at lambda 0.925. Among points

Table 4.3: Initial engine operating conditions for the RSM optimization.

Speed	1800 r/min
BMEP	3.4 bar
IMAT	60°C
Ignition Timing	40°bTDC
Ignition Duration	400 μs
Dedicated Cylinder AFR	0.900 lambda
Jacket Water Outlet Temperature	95°C
Fuel Methane Number	71 (MWM)

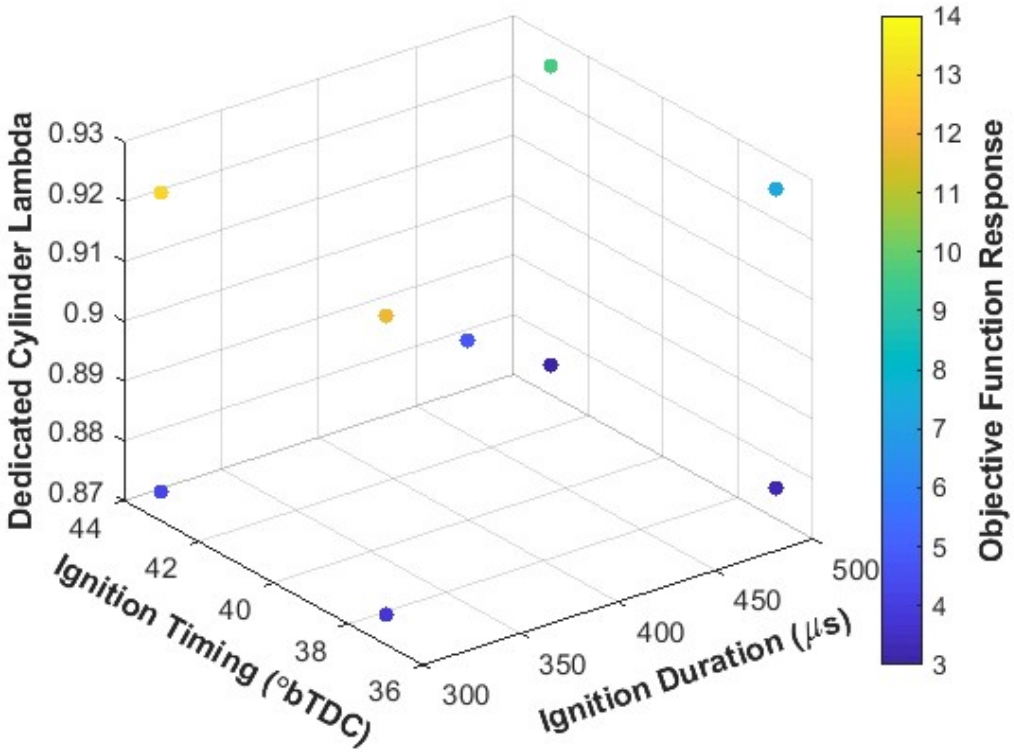

Figure 4.3: First factorial objective function response (solution) as a function of optmization variables ignition duration, ignition timing, and dedicated cylinder AFR at an IMAT of 65°C.

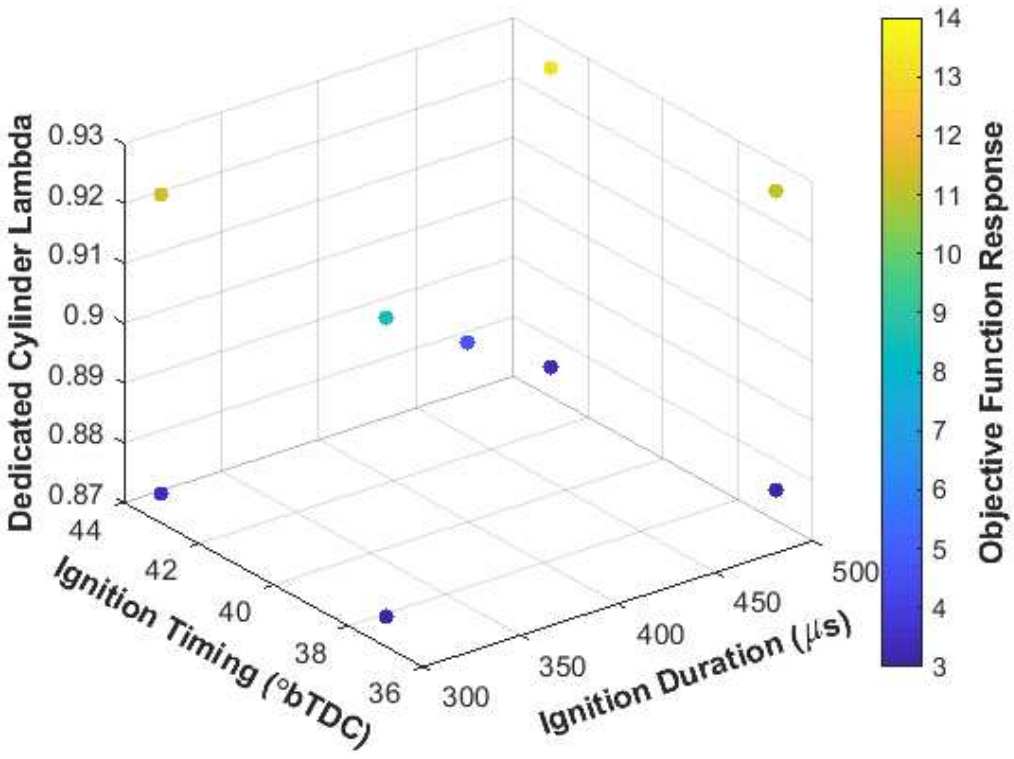

Figure 4.4: First factorial objective function response (solution) as a function of optmization variables ignition duration, ignition timing, and dedicated cylinder AFR at an IMAT of 55°C.

Table 4.4: Post factorial optimization steps. Direction and magnitude of the optimization variable steps representes the gradient calculated during the first factorial.

	1	2	3	4
IMAT (°C)	60.0	59.9	59.8	59.7
ID (μs)	400	391	382	373
IT (°bTDC)	40	40.5	41.0	41.5
DC AFR (Lambda)	0.90	0.93	0.95	0.98
OF Response	4.8	21.7	22.1	13.2

ID: ignition duration; IT: ignition timing; DC AFR: dedicated cylinder air-fuel ratio; OF: objective function

that included a dedicated cylinder lambda of 0.925, the average objective function response was 10.76 while the average objective function response for points that included a dedicated cylinder lambda of 0.875 was only 3.39. The first factorial also showed that advancing spark timing from 40 °bTDC was also beneficial in terms of location of CA50. This result is not surprising, but advancing timing can lead to increased COV of IMEP, which would decrease the objective function response. The results of this first factorial optimization showed that advancing timing had little to no impact on COV of IMEP. The impact of ignition duration had mixed results in the first factorial optimization. At increased IMAT a shorter ignition duration resulted in an improved objective function response, but at lower IMAT longer ignition duration showed an improved objective function response. However, objective function response due to changes in ignition duration were only observed at a dedicated cylinder lambda of 0.925. Similarly, changes in the objective function response when ignition timing was incremented were observed only at conditions more fuel lean of 0.900 lambda. This suggests that if improved objective function response were desired at conditions more fuel rich of 0.900 lambda other changes to the combustion recipe would need to be explored.

Examining points of similar optimization variables except for IMAT provides important insight into the results of the first factorial result. Figure 4.5 shows this comparison. Of note is the higher response of points 2, 4, 6, and 8. These points have a dedicated cylinder lambda 0.925. Points 6 and 8 had shorter ignition duration. It is clear that points with shorter ignition duration showed improved response at higher intake manifold temperatures while longer ignition duration showed improved response with lower intake manifold temperatures. The lower intake manifold temperatures of points 2 and 4 resulted in a slightly lower COV of IMEP which was the main contributor to a higher objective function response. Interestingly, the inverse is true that at points 6 and 8 the main contributor to higher objective function response was a slightly lower COV of IMEP. The resultant gradient from the first factorial exercise was a decrease in IMAT, shortened ignition duration, advanced timing, and increased dedicated cylinder AFR. Table 4.4 shows the gradient step magnitude and direction of the optimization variables and the objective function response

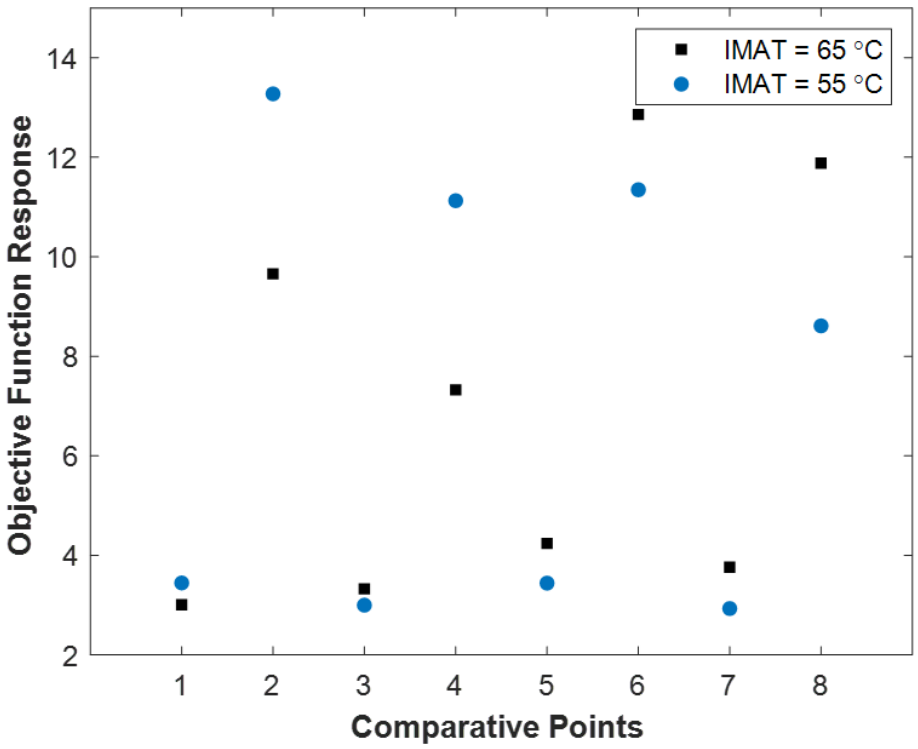

Figure 4.5: First factorial objective function response as a function of factorial points with similar IMAT. Comparitive points on the x axis have common ignition duration, ignition timing, and dedicated cylinder AFR. The impact that IMAT has on the response is shown by the difference in objective function response at 65 and 55°C.

results from the post factorial optimization exercise. The best objective function response found in the resultant direction was found in optimization step 3. Only one step after optimization step 3 was necessary to identify that a maximum objective function response was found. The optimization variables from optimization step 3 serve as the new initial conditions for the 2nd factorial of the RSM optimization exercise.

4.6.2 Second Factorial

The optimization variables selected from factorial 1 resulted in objective function response of 22.12. In terms of physical combustion metrics this was a difference between the average stoichiometric cylinder and dedicated cylinder IMEP of 4.04 psi, a maximum cylinder COV of IMEP of 22.12 (again from the dedicated cylinder), an average location of CA50 29.62 °aTDC, and an average 10 – 90 MFB duration of 65.23 crank angle degrees. In addition to new initial conditions the second factorial also featured slightly adjusted optimization variable increments. The intake manifold temperature increment was updated from $\pm$ 5 °C to $\pm$ 3 °C, the ignition timing increment from$\pm$ 3 crank angle degrees to $\pm$ 2 crank angle degrees, and the dedicated cylinder lambda increment from $\pm$ 0.025 to $\pm$ 0.01. Figure 4.6 and 4.7 show the objective function response at the 16 points evaluated during the second factorial. Points shown in Figure 4.6 were collected with an IMAT of approximately 63 °C and Figure 4.7 with an IMAT of approximately 57 °C. Analysis of Figures 4.6 and 4.7 reveal that the best dedicated cylinder lambda likely lies very close to the range of dedicated cylinder lambda examined. This can be deduced by the lack of significant difference between the objective function response at the high and low dedicated cylinder lambda points. The most obvious trend from Figures 4.6 and 4.7 is that improved objective function response comes from advancing spark timing. The improvement came not only from advancing location of CA50 but also decreased COV of IMEP. Ignition duration did not have a clear impact on the objective function response. Looking at Figure 4.7 the highest objective function responses are found at both the high and low ignition duration points. Contrary to factorial 1, examining points with similar optimization variables as a function of IMAT shows no obvious trend. This scattering of

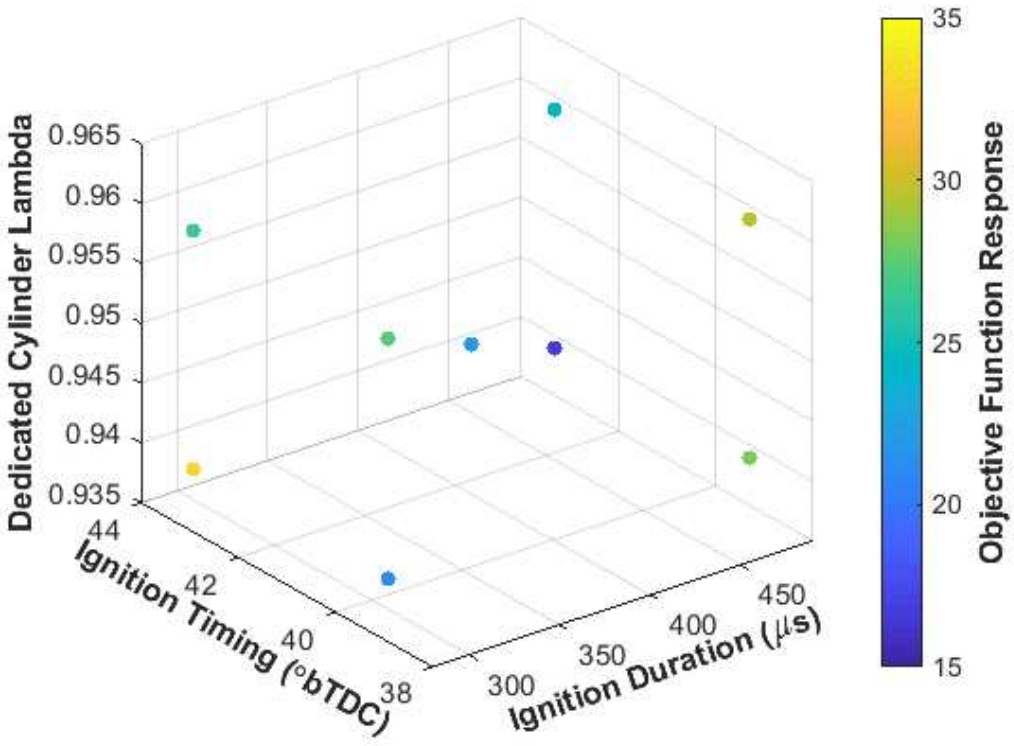

Figure 4.6: Second factorial objective function response (solution) as a function of optmization variables ignition duration, ignition timing, and dedicated cylinder AFR at an IMAT of 63°C.

objective function response data shown in Figure 4.8 indicates that the entire RSM optimization is approaching a final solution. The direction of the gradient after evaluating the 16 factorial 2 points was slightly increased intake manifold temperature, shortened ignition duration, advanced spark timing and slightly decreased dedicated cylinder lambda. Table 4.5 shows the gradient step magnitude and direction of the optimization variables and the objective function response results from the post factorial optimization exercise. The difference between target IMAT values in optimization steps 1-5 found in Table 4.5 were very small. These small increments were beyond the control capability of the engine test cell so an average IMAT of 60 °C was targeted for all tests found in Table 4.5. Optimization step 3 resulted in a maximum objective function response and was chosen as the new initial condition for the third factorial because the stop criteria of the RSM optimization was not yet met after the second factorial. Combustion metrics responsible for the objective function response of optimization step 3 were a difference between average stoichiomet-

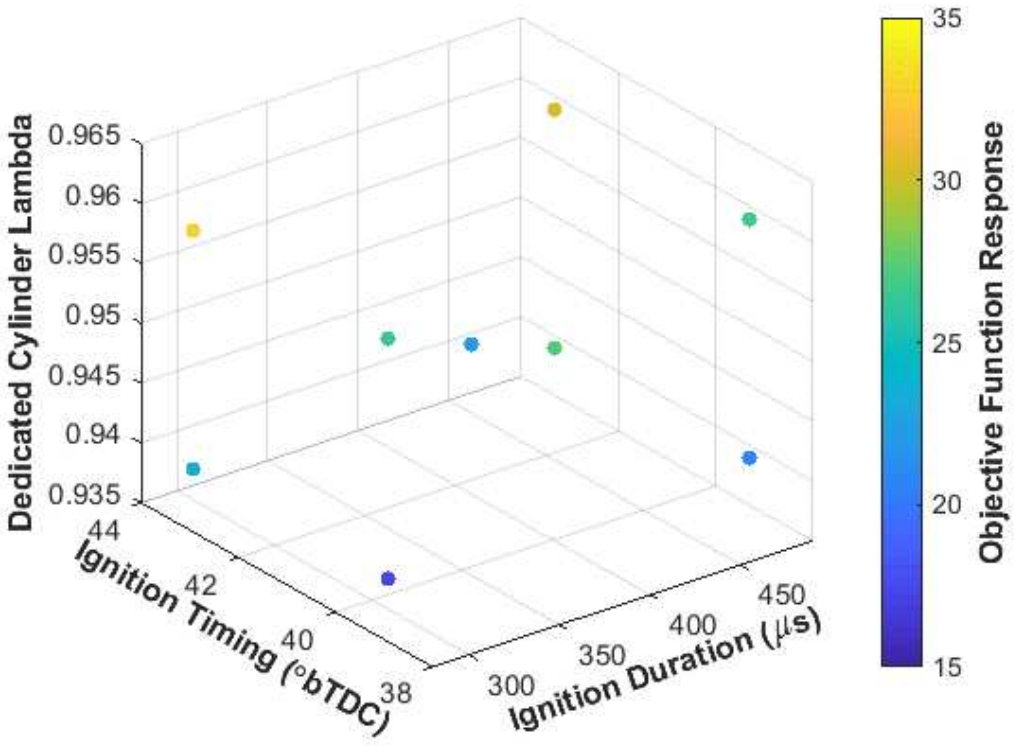

Figure 4.7: Second factorial objective function response (solution) as a function of optmization variables ignition duration, ignition timing, and dedicated cylinder AFR at an IMAT of 57°C.

ric cylinder and dedicated cylinder IMEP of 3.03 psi, the highest cylinder COV of IMEP of 17.33, the location of CA50 near 28° aTDC, and a 10 – 90 MFB duration of 63.4 crank angle degrees.

4.6.3 Third Factorial

The third factorial in the RSM optimization had similar optimization variable increments as the second factorial with initial conditions which came from post factorial optimization step three from the second factorial. Results from the 16 points factorial design are shown in Figures 4.9 and 4.10. The third factorial results were the first to show a discernable difference between objective function response at different IMAT. The average objective function response at an IMAT of 63 °C was 30.67 while the average response at 57 °C was 28.09 (25.89 vs 25.62 for the second factorial and 7.00 vs 7.14 for the first factorial). It appears that this impact is most apparent at more advanced spark timing which could explain why changes in IMAT had very little impact on

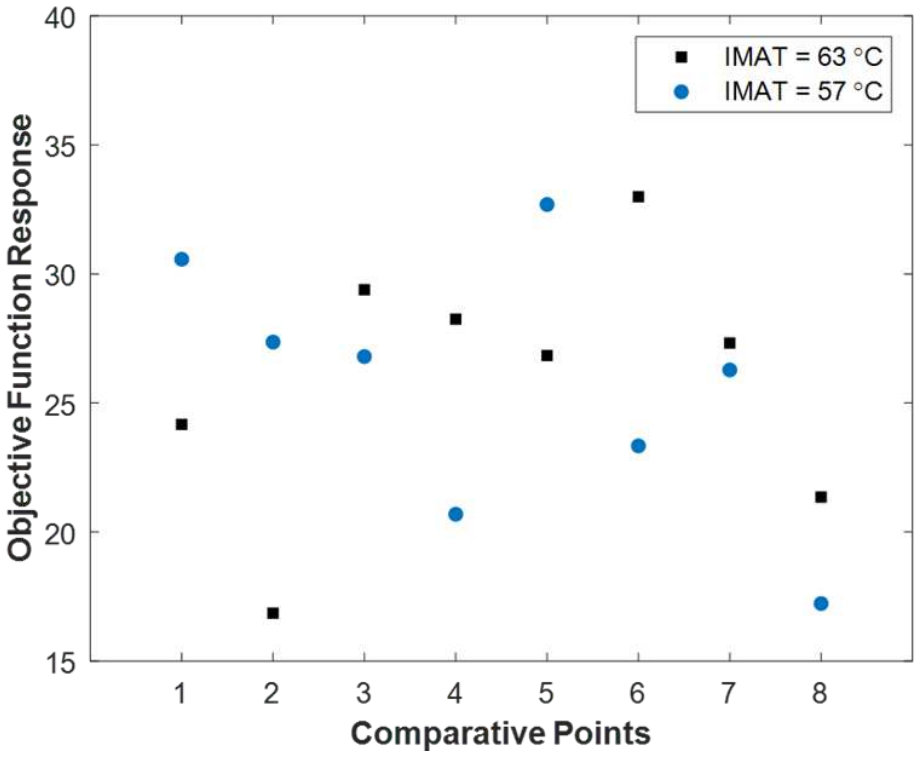

Figure 4.8: Second factorial objective function response as a function of factorial points with similar IMAT. Comparitive points on the x axis have common ignition duration, ignition timing, and dedicated cylinder AFR. The impact that IMAT has on the response is shown by the difference in objective function response at 63 and 57°C.

objective function response in the first two factorials. The most advanced spark timing considered in the first and second factorials was 43°bTDC. Figures 4.9 and 4.10 also show that similar to the second factorial advancing spark timing again leads to improved objective function response. However, in the third factorial the physical combustion metrics that were improved by advancing spark timing included 10 – 90 MFB duration in addition to the location of CA50 and COV of IMEP. By examining points where only ignition duration is varied it does appear from Figures 4.9 and 4.10 a wide range of ignition durations can be utilized to achieve improved objective function response. Comparing points where only IMAT was varied as shown in Figure 4.11 the impact that increased IMAT has on combustion performance is apparent. It should also be noted that the lack of impact that ignition duration has on objective function response can clearly be seen in Figure

Table 4.5: Post factorial optimization steps. Direction and magnitude of the optimization variable steps representes the gradient calculated during the second factorial.

	1	2	3	4	5
IMAT (°C)	59.8	59.9	60.0	60.1	60.2
ID (μs)	382	376	370	365	359
IT (°bTDC)	41.0	41.5	42.0	42.5	43.0
DC AFR (Lambda)	0.95	0.945	0.94	0.934	0.93
OF Response	22.2	27.1	30	26.8	23.5

ID: ignition duration; IT: ignition timing; DC AFR: dedicated cylinder air-fuel ratio; OF: objective function

4.11. The general trend of responses from points 1-4 which each have an ignition duration of 470 μs, match the trend of responses in points 5-8 which have an ignition duration of 270 μs.

The direction of the gradient calculated after the third factorial was that of increased IMAT, slightly decreased ignition duration, advanced timing, and slightly decreased dedicated cylinder lambda. The third factorial was the final factorial necessary for this RSM optimization. The standard deviation calculated for four repeated initial condition points (two prior to the 16 points factorial and two after) was 10.81. The standard deviation for the 16 factorial points was 4.59 and thus the variability in repeated points was greater than the variability found when changing optimization variables. Therefore, the RSM optimization was complete. Table 4.6 shows the post factorial optimization steps. The maximum objective function response was found at optimization step 3. Due to the stop criteria for the RSM optimization being met this point serves as the optimal operating condition for the G3304 engine while operating with dedicated EGR at rated speed and 3.4 bar BMEP.

The results of the RSM optimization can be summarized by examining the post factorial optimization steps for the first, second, and third factorials. Figure 4.12 shows the objective function response as a function of the post factorial optimization steps. The first factorial steps are shown in black, second factorial steps shown in red, and the third factorial steps shown in blue. The initial objective function response of the first factorial and the best objective function response of the third factorial are circled in the figure. While the improvement in objective function response is

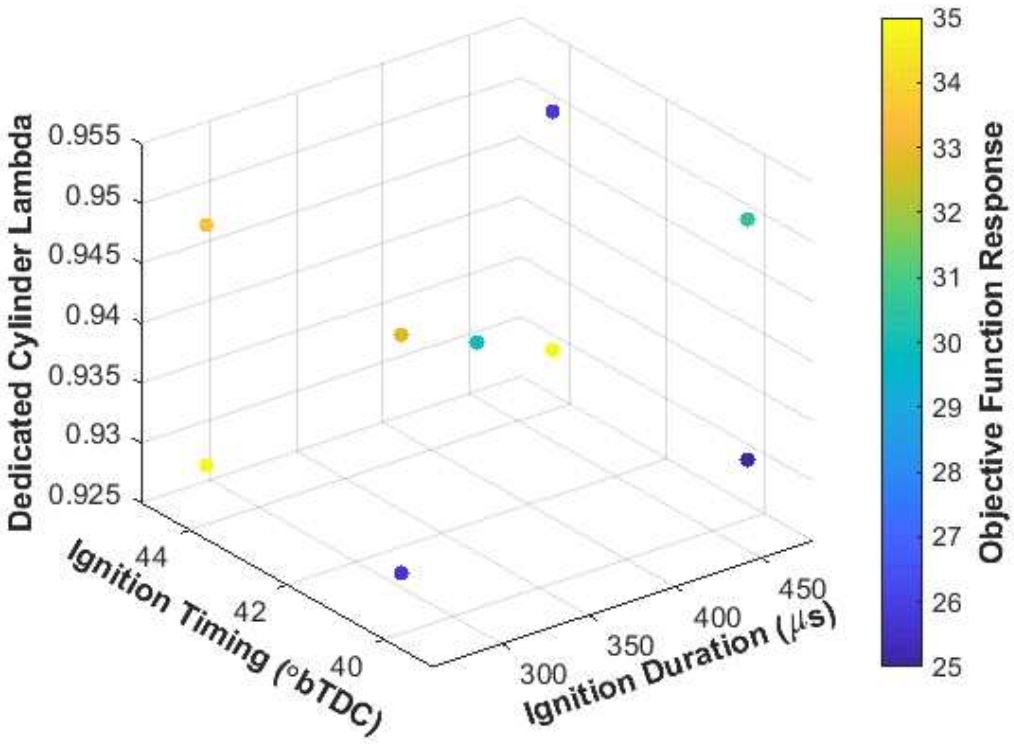

Figure 4.9: Third factorial objective function response (solution) as a function of optmization variables ignition duration, ignition timing, and dedicated cylinder AFR at an IMAT of 63°C.

key to understanding the success of this RSM optimization more important to understand is how the target combustion metrics found in the terms of the objective function were improved. Table 4.7 shows the initial and final combustion metrics for the RSM optimization as well as the initial and final optimization variables. Significant improvements in differences between average stoichiometric and dedicated cylinder IMEP and the highest cylinder COV of IMEP were observed after completing the RSM optimization. The design of the objective function placed more emphasis on these metrics by squaring the terms in the function and explains why these metrics were improved while the location of CA50 and 10 – 90 MFB location metrics were not improved rather only maintained.

Table 4.6: Post factorial optimization steps. Direction and magnitude of the optimization variable steps representes the gradient calculated during the third factorial.

	1	2	3	4	5
IMAT (°C)	60.0	61.1	62.3	63.4	64.5
ID (μs)	370	368	366	364	361
IT (°bTDC)	42.0	43.6	45.2	46.8	48.3
DC AFR (Lambda)	0.94	0.938	0.936	0.934	0.932
OF Response	30	32.4	33.5	27.4	26.9

ID: ignition duration; IT: ignition timing; DC AFR: dedicated cylinder air-fuel ratio; OF: objective function

Table 4.7: Pre and post-optimization combustion metrics as a function of optimization variables considered.

Combustion Metrics		
	IC	3^{rd}FO
Cylinder ΔIMEP (psi)	18.42	2.76
COV IMEP Max ($\%$)	26.3	16.26
Average CA50 (°aTDC)	27.74	27.6
Average 10-90 MFB (°)	60.46	61.94
Operating Condtions		
	IC	3^{rd}FO
IMAT (°C)	60	62
Spark Duration (μs)	400	365
Spark Timing (°bTDC)	40	45
DC AFR (Lambda)	0.900	0.936

IC: initial conditions; 3^{rd}FO: 3^{rd} order factorial optimized conditions

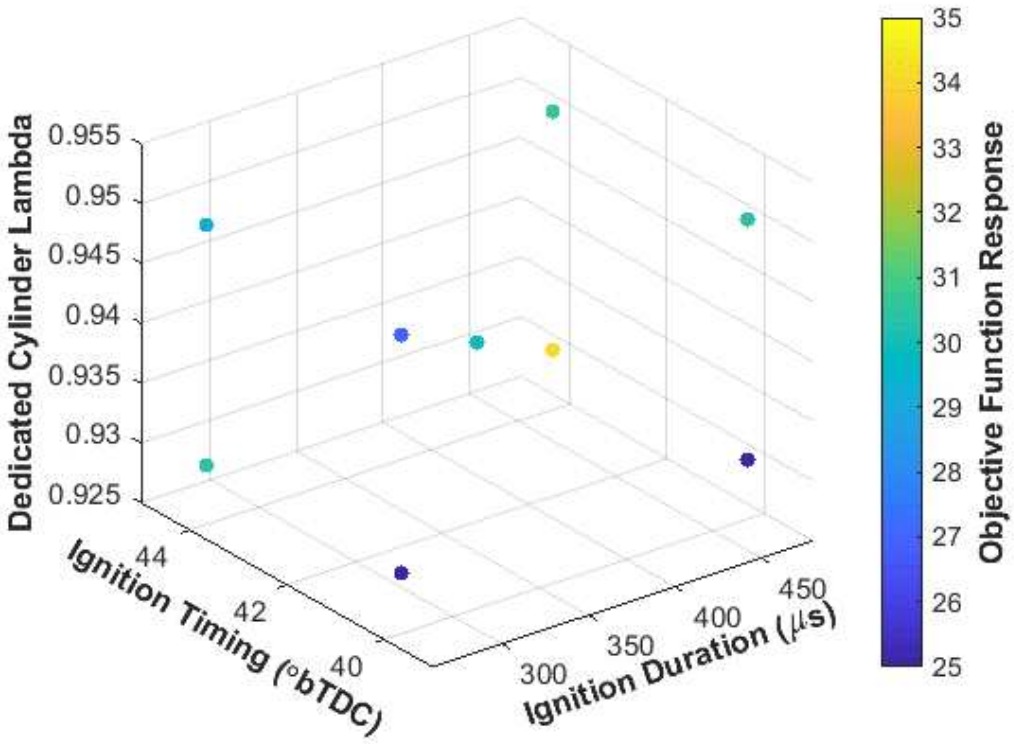

Figure 4.10: Third factorial objective function response (solution) as a function of optmization variables ignition duration, ignition timing, and dedicated cylinder AFR at an IMAT of 57°C.

4.6.4 Ignition Source Analysis

After the first RSM optimization was completed an evaluation was carried out of other ignition types and how they might further improve combustion in a dedicated EGR engine. Non-enriched pre chamber spark plugs were identified as an ignition source that may improve COV of IMEP by protecting the flame from being extinguished in early stages of combustion. It was also theorized that in a low turbulence combustion chamber such as the G3304 a non-enriched pre-chamber ignition source would provide turbulence to the combustion chamber via the flame jets leaving the pre chamber area through the orifices in the pre-chamber bowl. It would follow that 10-90 MFB duration would be shortened due to the increased turbulence. While considering a non-enriched pre-chamber spark plug the authors did recognize that the performance of these plugs are a complex function of conditions within a combustion cylinder and significant design work is done to match the pre-chamber design to the main chamber design. Such analysis was outside of the scope

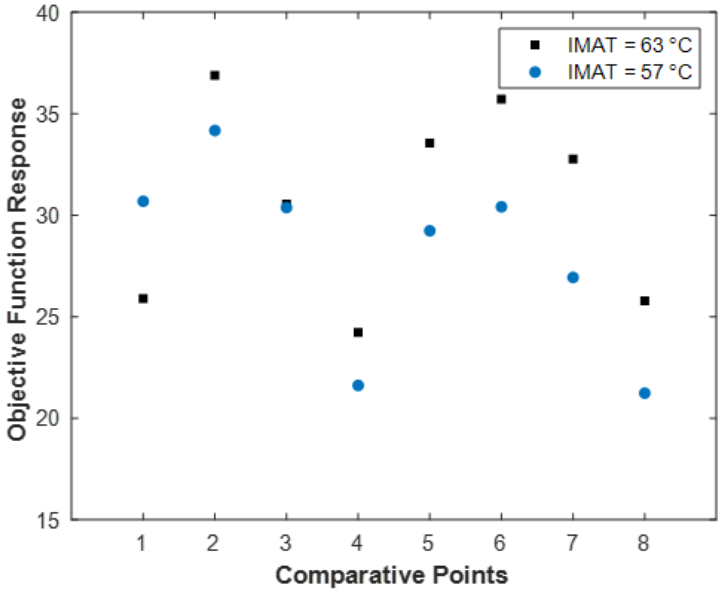

Figure 4.11: Third factorial objective function response as a function of factorial points with similar IMAT. Comparitive points on the x axis have common ignition duration, ignition timing, and dedicated cylinder AFR. The impact that IMAT has on the response is shown by the difference in objective function response at 63 and 57°C.

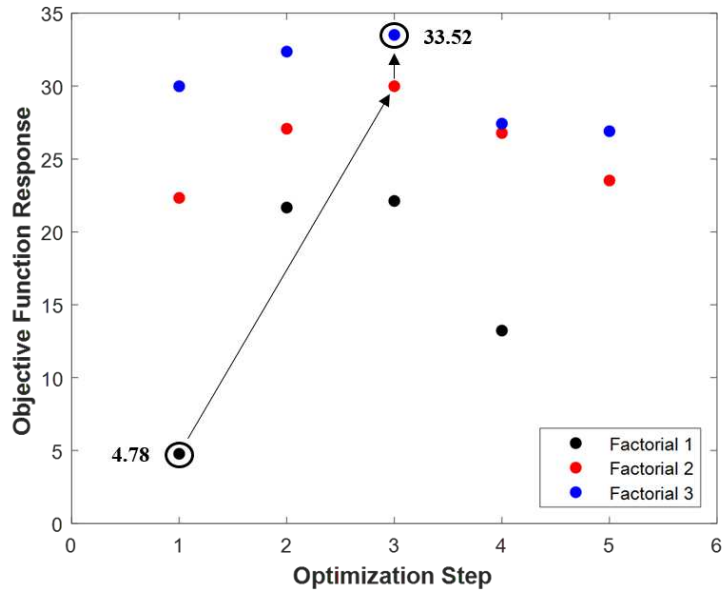

Figure 4.12: Objective function response as a function of post factorial optimization steps of the first, second, and third factorial.

of this work, but in lieu of such analysis multiple configuration of pre-chamber plugs were tested.

Two prototype non-enriched pre-chamber spark plugs were sourced from a supplier along with

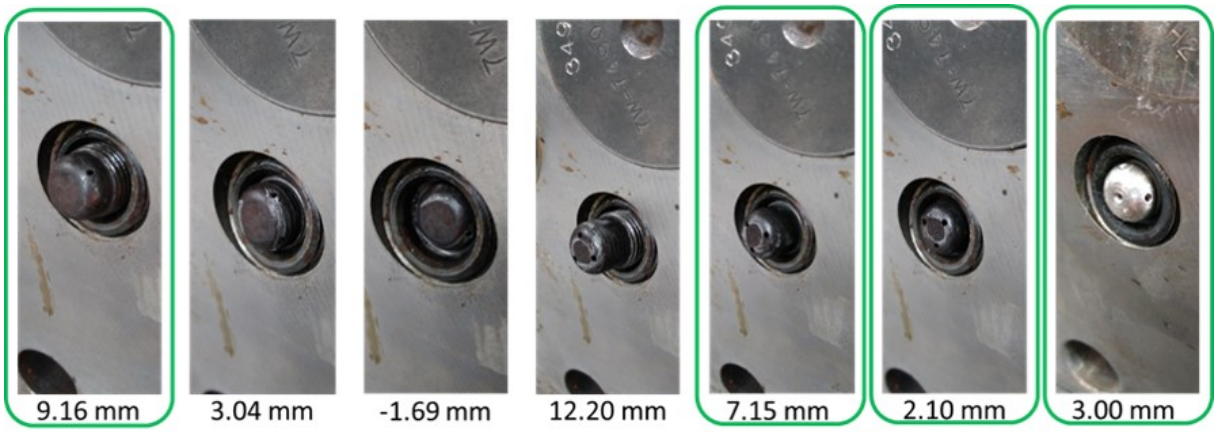

Figure 4.13: Non-enriched pre-chamber configurations considered in this work. Configurations boxed in green were chosen as the best candidates for on engine evaluation.

one production plug from a second supplier. The prototype plugs had a high thread count and were supplied with different copper spacers such that the pre-chamber bowl could be located further in or out of the combustion chamber. The production pre-chamber from the second supplier was only able to be installed at one depth into the combustion chamber. A two level screening process was subjected to the different configurations of pre-chamber plugs. The first screening was an examination of the physical installation of the plus on a stock G3304 head. Specific consideration was given to the location of the orifices of the pre-chamber relative to the deck height of the engine head. In some configurations the jets leaving the pre chamber through the orifices would have impinged directly on to the head. These types of scenarios were avoided. Figure 4.13 shows all of the configurations considered. The configurations with the green boxes designate that these passed the first screening process. The dimension associated with each plug denotes the distance to which the bowl of the plug protruded into the main combustion chamber. The four plugs chosen were thought to give a good representation of different non-enriched pre-chamber designs. The second screening process was evaluating the performance of each plug at a similar nominal engine operating point. It was unknown how the plugs would perform so the operating condition chosen to evaluate the plugs was taken from the third factorial optimized conditions found in the first RSM optimization. At this operating point combustion metrics of dedicated cylinder IMEP, stoichiometric cylinder IMEP, highest cylinder COV of IMEP, and 10 – 90 MFB duration were evaluated.

The performance of each plug was compared to the baseline operation of the engine without dedicated EGR and the performance of the engine using a fine wire spark plug at the same operating conditions. Figures 4.14, 4.15, and 4.16 show the results of the second screening process for the non-enriched pre-chamber spark plugs. Upon comparison at the engine operating condition

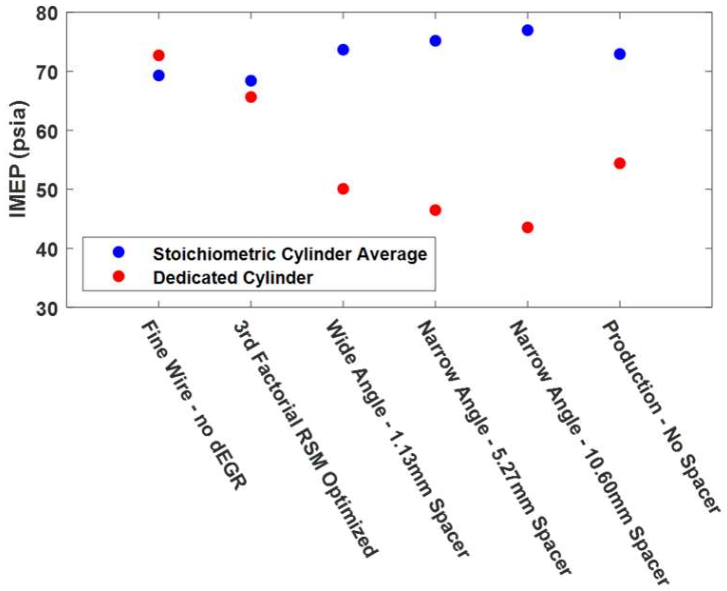

Figure 4.14: Average stoichiometric and dedicated cylinder IMEP as a function of ignition source. The 3^{rd} Factorial RSM Optimized, Wide Angle, both Narrow Angle, and Production data points were collected while the engine was operating at the same conditions with dedicated EGR.

Table 4.8: Initial engine operating conditions for the second RSM optimization that incorporated a production non-enriched pre-chamber spark plug as the ignition source.

Speed	1800 r/min
BMEP	3.4 bar
IMAT	60°C
Ignition Timing	42°bTDC
Ignition Duration	200 μs
Dedicated Cylinder AFR	0.940 lambda
Jacket Water Outlet Temperature	95°C
Fuel Methane Number	71 (MWM)

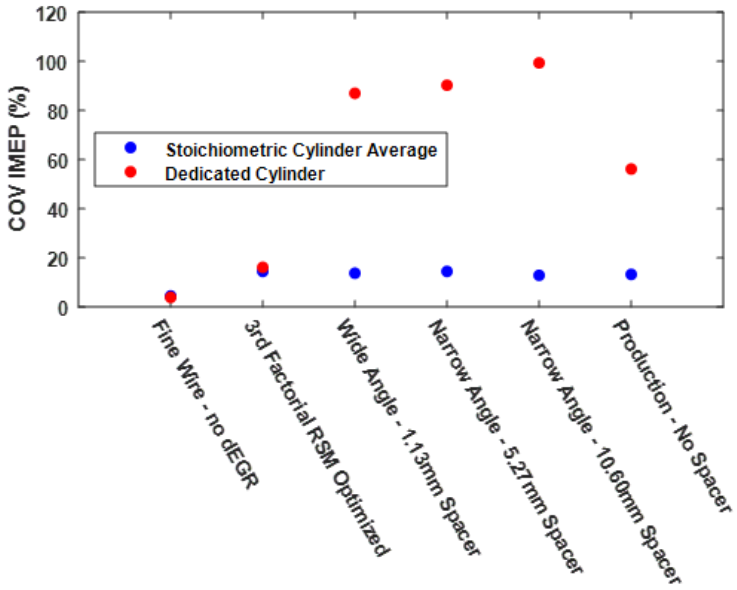

Figure 4.15: Average stoichiometric and dedicated cylinder COV of IMEP as a function of ignition source. The 3^{rd} Factorial RSM Optimized, Wide Angle, both Narrow Angle, and Production data points were collected while the engine was operating at the same conditions with dedicated EGR.

chosen the production pre-chamber plug performed better than the different configurations of the prototype plug from another supplier. Using the production plug the difference between dedicated cylinder IMEP and the average IMEP of the stoichiometric cylinders was 18.52 psi while that difference between cylinder power output for the prototype plugs ranged from 23.58 to 33.43 psia. The production pre-chamber plug also showed the most promise, though well outside of the acceptable range, when examining the COV of IMEP of the dedicated cylinder. Using the production plugs the COV of IMEP of the dedicated cylinder was 56.2 while the best performing prototype plug had a COV of IMEP of 87.1. Here it is appropriate to reiterate the necessity of tailoring the design of pre-chamber plugs to the rest of the combustion recipe based on the overall poor performance of each pre-chamber plug used in this screening process. However, it is important to take note of the positive results that the pre-chamber plug ignition source had on the 10-90 MFB duration shown in Figure 4.16 The shortest 10-90 MFB burn duration achieved during the first RSM optimization was 61.1 crank angle degrees. Using the pre-chamber plugs the shortest 10-90 MFB duration of 44.5 crank angle degrees was found using the wide angle plugs with the 1.13mm

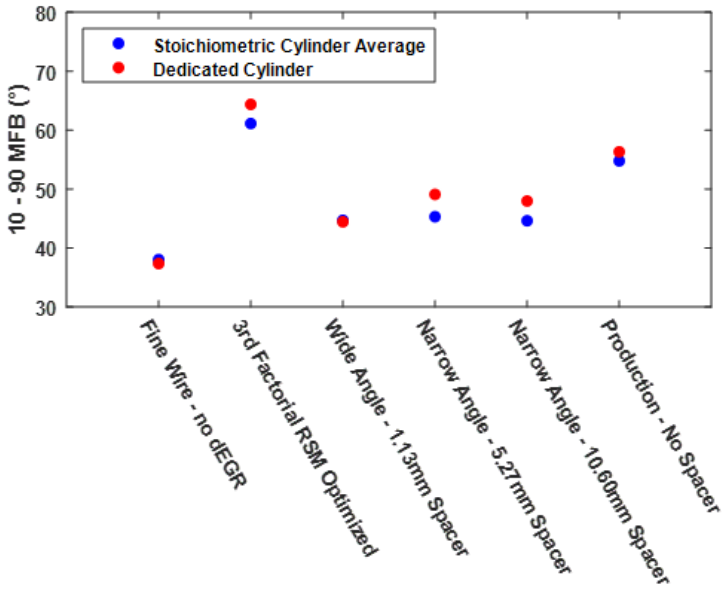

Figure 4.16: Average stoichiometric and dedicated cylinder 10-90 MFB duration as a function of ignition source. The 3^{rd} Factorial RSM Optimized, Wide Angle, both Narrow Angle, and Production data points were collected while the engine was operating at the same conditions with dedicated EGR.

spacer. The production plug showed a 10-90 MFB duration of 54.8 crank angle degrees. The impact that high levels of EGR dilution have on combustion duration was not able to be compensated for by using pre-chamber plugs as the no EGR 10-90 MFB duration was 38 crank angle degrees, but significant improvements over the use of fine wire spark plugs are shown. If further investigation into using non-enriched pre-chamber spark plugs with dedicated EGR were to be planned the results from this work suggest that the pre-chamber orifice location and number be closer to that of the production plug. These results also suggest that a pre-chamber that extends further into the main chamber may also provide improved results. The wide angle prototype plug with the 1.13mm spacer extended furthest into the combustion chamber and among prototype plugs showed the lowest dedicated cylinder COV of IMEP and the highest dedicated cylinder IMEP. Based on these results the production pre-chamber plug was chosen for a RSM optimization. Equation 1 was again used for the second RSM optimization exercise. Overall, a similar approach was used during the second optimization as was used during the first optimization including the optimization variables, constraints, boundaries, and completion criteria. The initial conditions were updated as

shown in Table 4.8. The optimization variable increments were set at IMAT of $\pm$ 10 °C, ignition duration of $\pm$ 100 μs, ignition timing of $\pm$ 2 crank angle degrees, and a dedicated cylinder lambda of 0.020. The increase in increment of IMAT was to ensure that fluctuations in IMAT during tests would not make up a significant fraction of the increment step.

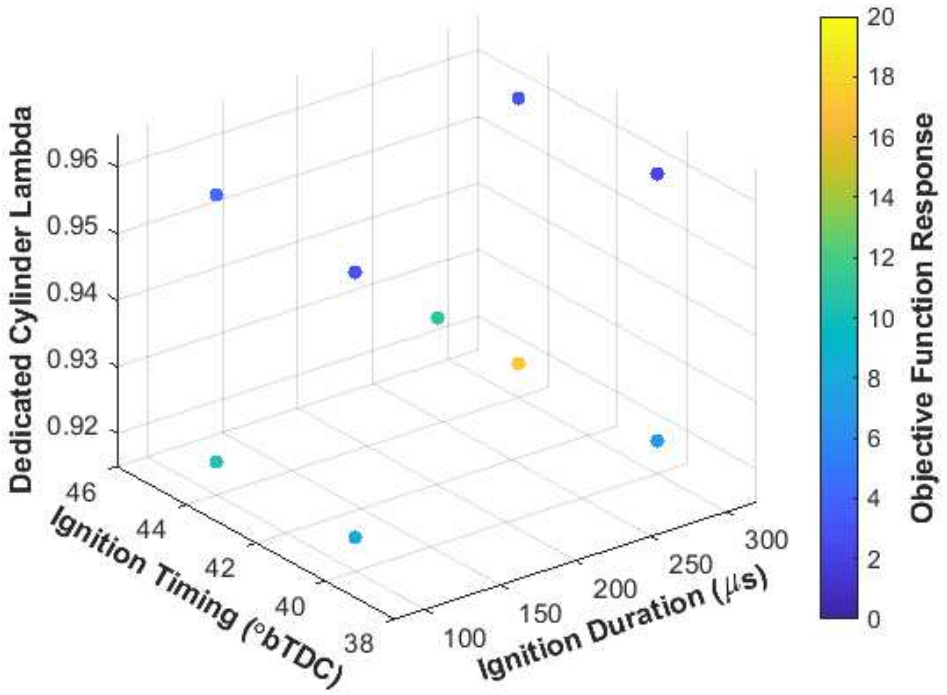

Figure 4.17: First factorial objective function response (solution) as a function of optmization variables ignition duration, ignition timing, and dedicated cylinder AFR at an IMAT of 70°C using non-enriched pre-chamber spark plugs.

Figures 4.17 and 4.18 depict the objective response based on incrementing optimization variables at 70 °C and 50 °C, respectively. The averaged objective function response of the four repeated initial condition was 11.01. Notably, in this first factorial of the second RSM optimization the arbitrarily chosen initial condition resulted in an objective function response higher than all but one of the 16 factorial surface points. In this optimization exercise there was no clear trend towards operating conditions of improved response. This can be further seen by examining points where all optimization variables were held constant except IMAT. Figure 4.19 shows this data which is chaotic. As discussed earlier non-enriched pre-chamber spark plugs must be designed to function

well with not only the combustion chamber design but also variables such as the cylinder air-fuel ratio. The objective function for this RSM optimization was designed with the idea that overall the combustion in the dedicated cylinder would be worse than that of the stoichiometric cylinders. However, in this second RSM optimization at times combustion in one of the stoichiometric cylinders was much more unstable than what was happening in the dedicated cylinder. For example, the 12th point tested during this second optimization had promising combustion metrics except that the highest COV of IMEP recorded was a value of 66.62. This came from cylinder 4 which was operating at stoichiometric conditions. The COV of IMEP in the dedicated cylinder at this operating point was 17.40. This type of good performance in the dedicated cylinder coupled with poor performance in one or more of the stoichiometric cylinders occurred multiple times during this optimization and can be blamed for the overall poor performance of the dedicated EGR concept.

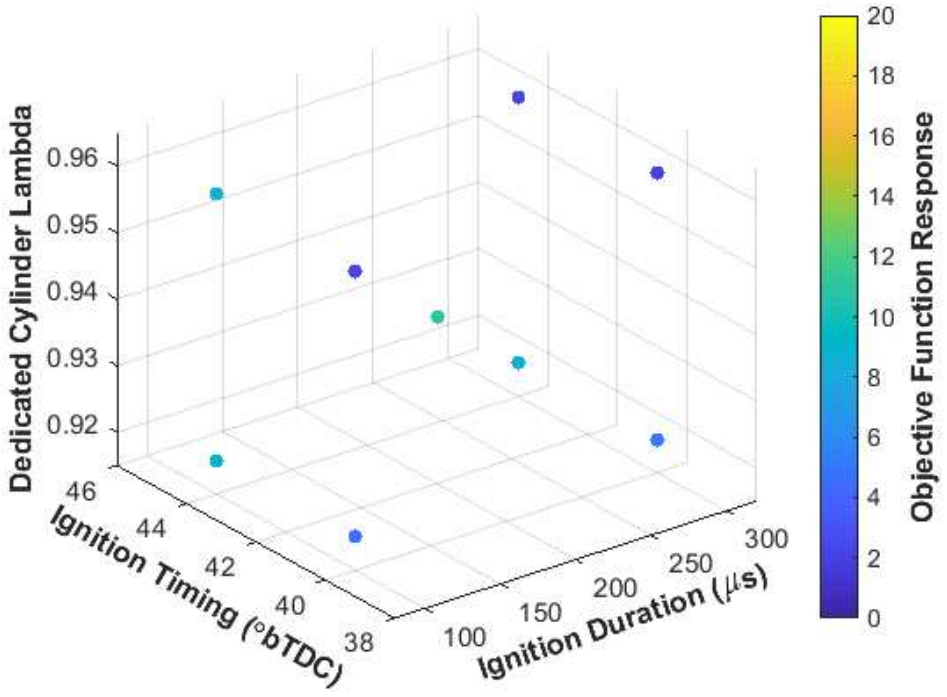

Figure 4.18: First factorial objective function response (solution) as a function of optmization variables ignition duration, ignition timing, and dedicated cylinder AFR at an IMAT of 50°C using non-enriched prechamber spark plugs.

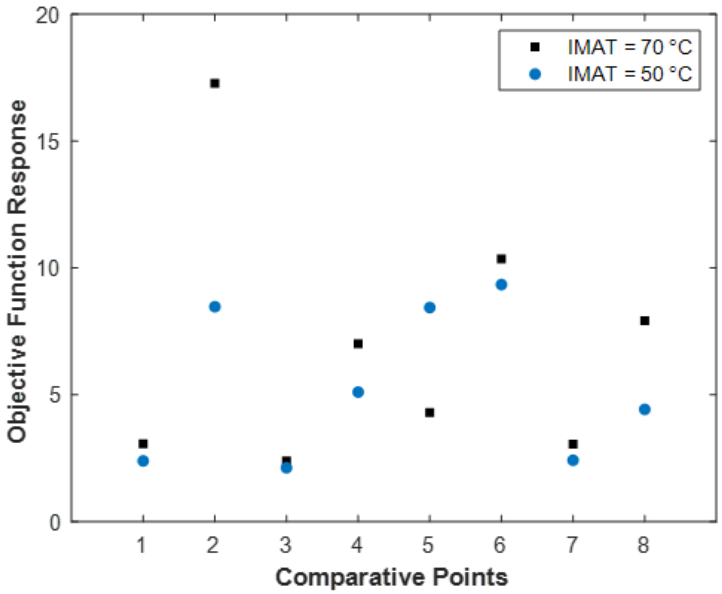

Figure 4.19: First factorial objective function response as a function of factorial points with similar IMAT using pre-chamber spark plugs. Comparitive points on the x axis have common ignition duration, ignition timing, and dedicated cylinder AFR. The impact that IMAT has on the response is shown by the difference in objective function response at 70 and 50°C.

Not surprisingly the optimization completion criteria was met only after one factorial. Therefore, no additional work could be done to attempt to improve the performance of the dedicated EGR concept while using the selected non-enriched pre-chamber spark plug. Table 4.9 shows a summary of the initial and final optimization variables and the resultant combustion metrics. The initial condition combustion metrics are shown as the average of four data points collected. Only slight improvements in each of the combustion metrics was realized in this first and only factorial.

4.7 Dedicated Cylinder Exhaust Composition

Finally, additional consideration was given to examining the dedicated cylinder exhaust composition at the post factorial optimization operating points. Since the composition of the dedicated cylinder is the control mechanism used in dedicated EGR systems it was of interest to understand what composition led to the most improved combustion. After the initial RSM optimization exercise the post factorial operating points were repeated. The repeated tests included all of the

Table 4.9: Pre and post-optimization combustion metrics as a function of optimization variables considered. These results come from the second RSM optmization performed where non-enriched pre-chamber spark plugs were used as an ignition source.

Combustion Metrics		
	IC	3^{rd}FO
Cylinder ΔIMEP (psi)	9.44	7.75
COV IMEP Max (%)	32.88	25.85
Average CA50 (°aTDC)	31.97	31.05
Average 10-90 MFB (°)	64.84	62.72
Operating Condtions		
	IC	3^{rd}FO
IMAT (°C)	60	62.6
Spark Duration (μs)	200	194
Spark Timing (°bTDC)	42	43.5
DC AFR (Lambda)	0.940	0.960

IC: initial conditions; 3^{rd}FO: 3^{rd} order factorial optimized conditions

same data acquisition as the initial RSM optimization but sampling of the dedicated cylinder exhaust, stoichiometric cylinder exhaust, and intake manifold composition was added. This section is meant to display the post factorial dedicated and average stoichiometric cylinder exhaust composition at the post factorial RSM optimization points. The optimization points considered and their associated values for the optimization variables can be found in Tables 4.3, 4.4, 4.5, and 4.6. The exhaust gas composition is representative of FTIR measurements. FTIR data was chosen to present because the unburned hydrocarbons are speciated. Table 4.10 displays the exhaust gas composition from the first post factorial optimization points. For reference the optimization combustion statistics from Equation 4.1 at each post factorial optimization step are also included. Since multiple variables were changed between post factorial optimization steps, analysis of the impact of changes in single variables on results can't be considered conclusive. However, the data presented in Tables 4.10, 4.11, and 4.12 can be useful for future modeling of the dedicated EGR concept and when selecting calibration gases to be used in FTIR and 5-gas sampling of dedicated cylinder and stoichiometric cylinder exhaust.

Table 4.10: Dedicated and average stoichiometric cylinder exhaust composition for the first post factorial optimization steps in the RSM optimization exercise. Engine operating conditions for the results displayed can be found in Tables 4.3 and 4.4.

	F1_O1		F1_O2		F1_O3		F1_O4	
	ASC	DC	ASC	DC	ASC	DC	ASC	DC
CO (ppm)	951	18054	1000	13932	1037	10521	1026	4553
CO_2 (%)	9.24	7.83	9.20	8.38	9.13	8.59	8.98	9.00
NO (ppm)	56	28	48	32	44	36	43	43
NO_2 (ppm)	11	13	12	11	13	9	13	8
CH_4 (ppm)	1259	2152	1603	1461	1927	1175	2611	1086
C_2H_4 (ppm)	99	213	113	148	130	133	142	114
C_2H_6 (ppm)	137	169	177	117	214	90	300	95
C_3H_6 (ppm)	10	8	11	8	12	7	13	3
CH_2O (ppm)	31	37	36	26	39	24	45	24
H_2O (%)	18.89	18.92	18.77	18.97	18.75	19.97	18.85	19.95
C_3H_8 (ppm)	15	16	20	12	25	8	37	9
NH_3 (ppm)	0	1	0	0	0	0	0	0
C_2H_2 (ppm)	19	57	21	43	23	36	24	30
O_2 (%)	0.56	0.54	0.70	0.35	0.83	0.29	1.08	0.29
IMEP (psia)	71.9	56.9	69.2	63.1	68.8	65.3	67.1	70.1
COV IMEP (%)	14.0	22.7	17.6	18.5	18.4	16.8	20.5	16.6
CA50 (°aTDC)	27.1	33.6	28.5	31.5	29.3	31.9	30.0	29.4
10-90 MFB (°)	60.7	81.3	63.7	72.2	65.5	73.1	68.0	67.9

ASC: Average Stoichiometric Cylinder; DC: Dedicated Cylinder; F1_O1: Factorial 1 - Optimization Step 1; F1_O2: Factorial 1 - Optimization Step 2; F1_O3: Factorial 1 - Optimization Step 3; F1_O4: Factorial 1 - Optimization Step 4;

Table 4.11: Dedicated and average stoichiometric cylinder exhaust composition for the second post factorial optimization steps in the RSM optimization exercise. Engine operating conditions for the results displayed can be found in Tables 4.3 and 4.5.

	F2_O1		F2_O2		F2_O3		F2_O4	
	ASC	DC	ASC	DC	ASC	DC	ASC	DC
CO (ppm)	1028	11096	1027	11814	1022	12978	1006	13664
CO_2 (%)	9.14	8.66	9.15	8.56	9.16	8.50	9.19	8.44
NO (ppm)	47	36	48	35	50	34	52	33
NO_2 (ppm)	12	10	12	10	12	10	12	10
CH_4 (ppm)	1903	1179	1812	1271	1943	1296	1828	1330
C_2H_4 (ppm)	123	128	123	135	118	141	116	145
C_2H_6 (ppm)	212	92	203	101	220	101	209	102
C_3H_6 (ppm)	11	8	11	8	11	8	11	8
CH_2O (ppm)	40	22	39	25	38	24	37	25
H_2O (%)	18.71	19.17	18.71	19.34	18.60	18.93	18.60	18.98
C_3H_8 (ppm)	26	9	24	9	26	9	25	9
NH_3 (ppm)	0	0	0	0	0	0	0	0
C_2H_2 (ppm)	22	34	22	37	21	36	21	36
O_2 (%)	0.81	0.29	0.79	0.31	0.82	0.31	0.78	0.31
IMEP (psia)	67.8	67.0	68.0	66.4	69.1	65.2	69.8	63.2
COV IMEP (%)	19.5	17.4	18.4	17.3	19.1	17.6	17.5	18.4
CA50 (°aTDC)	28.8	30.0	28.2	29.7	27.4	29.9	27.2	30.8
10-90 MFB (°)	65.0	69.4	64.2	69.1	62.9	70.3	62.1	73.6

ASC: Average Stoichiometric Cylinder; DC: Dedicated Cylinder; F2_O1: Factorial 2 - Optimization Step 1; F2_O2: Factorial 2 - Optimization Step 2; F2_O3: Factorial 2 - Optimization Step 3; F2_O4: Factorial 2 - Optimization Step 4;

Table 4.12: Dedicated and average stoichiometric cylinder exhaust composition for the third post factorial optimization steps in the RSM optimization exercise. Engine operating conditions for the results displayed can be found in Tables 4.3 and 4.6.

	F3_O1		F3_O2		F3_O3		F3_O4	
	ASC	DC	ASC	DC	ASC	DC	ASC	DC
CO (ppm)	923	12346	898	12277	896	12158	896	12798
CO_2 (%)	9.19	8.44	9.22	8.42	9.14	8.43	9.19	8.44
NO (ppm)	55	34	60	35	62	37	68	36
NO_2 (ppm)	12	11	12	9	11	8	11	11
CH_4 (ppm)	1482	1326	1416	1294	1657	1348	1718	1383
C_2H_4 (ppm)	108	154	102	151	102	143	100	152
C_2H_6 (ppm)	163	93	155	91	187	105	198	103
C_3H_6 (ppm)	11	7	11	7	11	7	11	8
CH_2O (ppm)	33	26	31	26	33	26	33	27
H_2O (%)	19.01	19.56	18.88	19.93	19.27	20.01	18.84	19.36
C_3H_8 (ppm)	12	8	18	8	23	10	25	9
NH_3 (ppm)	0	0	0	0	0	0	0	0
C_2H_2 (ppm)	20	36	19	34	19	32	18	31
O_2 (%)	0.65	0.32	0.62	0.31	0.70	0.33	0.72	0.34
IMEP (psia)	70.3	61.9	70.5	61.5	70.8	61.6	70.9	61.9
COV IMEP (%)	15.0	19.7	16.2	18.4	15.3	18.5	15.1	18.8
CA50 (°aTDC)	27.1	29.6	26.1	28.4	23.4	25.0	21.7	23.7
10-90 MFB (°)	61.9	72.8	60.3	69.7	61.9	76.3	74.2	74.1

ASC: Average Stoichiometric Cylinder; DC: Dedicated Cylinder; F3_O1: Factorial 3 - Optimization Step 1; F3_O2: Factorial 3 - Optimization Step 2; F3_O3: Factorial 3 - Optimization Step 3; F3_O4: Factorial 3 - Optimization Step 4;

4.8 Conclusions

A response surface method optimization was performed on a rich burn natural gas engine while operating with dedicated EGR. An initial optimization was completed with fine wire spark plugs as the ignition source while optimization variables of IMAT, spark timing, spark duration, and dedicated cylinder AFR were changed. After a screening process a production non-enriched pre-chamber spark plug was chosen as the ignition source to be used in a second response surface method optimization. The following conclusions were drawn from this work:

- Response surface method optimization was found to be appropriate for finding engine operating conditions for improved combustion metrics in a dedicated EGR engine.
- Based on the design of the objective function in the RSM optimization a higher solution meant an improvement in combustion described in Table 7. The objective function increased from an initial value of 4.8 to a final value of 33.5. This improvement was due to minimizing the difference between cylinder-cylinder IMEP and a reduction in COV of IMEP in the dedicated cylinder.
- The region of best response using fine wire spark plugs was at an ignition timing of 45 °bTDC, ignition duration of 365 μs, IMAT of 62 °C, and a dedicated cylinder lambda of 0.936.
- The use of non-enriched pre-chamber spark plugs resulted in unpredictable combustion behavior, especially in cylinder that were operated at stoichiometric AFR conditions. The stop criteria for the RSM optimization was met after only one factorial. The results from that factorial showed no appreciable improvement in overall combustion performance as defined by the objective function.

4.9 References

1. US Environmental Protection Agency. Unconventional Oil and Natural Gas Development. URL https://www.epa.gov/ uog. [Online; accessed 02-August-2019].

2. US Energy Information Administration. Natural GasExplained: Where Our Natural Gas Comes From. URL https://www.eia.gov/energyexplained/index.php?page=natural_gas_where. [Online;accessed 02-August-2019].

3. US Energy Information Administration. Maps: Oil and GasExploration, Resources, and Production. URL https:// www.eia.gov/maps/maps.htm. [Online; accessed 03-August-2019].

4. US Environmental Protection Agency. Understandingthe Stationary Engines Rules. URL https: //www.epa.gov/stationary-engines/understanding-stationary-engines-rules.[Online; accessed 05-August-2019].

5. Ohio Administrative Code 3745-110. RACT Requirementsand/or Limitations for Emissions of NOx from Stationary Sources. URL https://www.epa.ohio.gov/dapc/regs/3745_110. [Online; accessed 06-August-2019].

6. Commonwealth of Pennsylvania Department of EnvironmentalProtection: Bureau of Air Quality. General Plan Approvaland/or General Operating Permit BAQ-GPA/GP-5.

7. Heywood JB. Internal Combustion Engine Fundamentals,1988. New York: McGraw-Hill.

8. Turns S. An Introduction to Combustion Concepts and Applications, 2012. 3rd ed. New York: MeGraw Hill.

9. Alger T and Mangold B. Dedicated EGR: A New Concept in High Efficiency Engines. SAE Paper 2009-01-0694.

10. Alger T, Gukelberger R, and Gingrich J. Impact of EGR Quality on the Total Inert Dilution Ratio. SAE Paper 2016-01-0713.

11. Robertson D, Chadwell C, Alger T, Zuehl J, Gukelberger R, Denton B, and Smith I. Dedicated EGR Vehicle Demonstration. SAE Paper 2017-01-0648.

12. Van Roekel C, Montomgery DT, Singh J, and Olsen DB. Evaluating Dedicated Exhaust Gas Recirculation on a Stoichiometric Industrial Natural Gas Engine. URL https://journals.sagepub.com/doi/10.1177/1468087419864733. International Journal of Engine Research.

13. Mitchell R and Kocsis M. Performance Evaluation of Dedicated EGR on a 12 L Natural Gas Engine. SAE Paper 2019-01-1143.

14. Montgomery DT and Reitz RD. Effects of Multiple Injections and FlexibleControl of Boost and EGR on Emissions and Fuel Consumption of a Heavy-Duty Diesel Engine. SAE Paper 2001-01-0195.

15. Brown J, Mizia J, Olsen D, Wilson B. On-Engine Demonstration of Micro-Pilot Ignition System for a Cooper-Bessemer GMV-4TF. ICEF 2003-762.

16. Wise DM. Investigation into Producer Gas Utilization in High Performance Natural Gas Engines. Dissertation, Colorado State University, 2013.

Chapter 5

Analysis of Non-Selective Catalyst Reduction Performance with Dedicated Exhaust Gas Recirculation

5.1 Summary

Rich burn industrial natural gas engines achieve low post catalyst emissions by using a non-selective catalyst reduction (NSCR) aftertreatment technology. However, they operate with reduced power density when compared to lean burn engines. Dedicated exhaust gas recirculation (EGR) offers a possible pathway for rich burn engines to use NSCR aftertreatment technology without sacrificing power density. In order to achieve low post catalyst emissions the precious metals and washcoat of a NSCR catalyst must be designed according to the expected exhaust composition of an engine. In this work a rich burn industrial natural gas engine operating with dedicated EGR was paired with a commercially available NSCR catalyst. At rated BMEP conditions the air-fuel ratio (AFR) was swept between rich and lean conditions to compare the catalyst conversion efficiency and post catalyst emissions of rich burn and dedicated EGR combustion. It was found that due to low engine out NO_x emissions across the entire air-fuel ratio range, dedicated EGR offers a much larger range of air-fuel ratios where regulated emissions levels can be met. Low engine out NO_x also points towards a possibility of using an oxidation catalyst rather than a non-selective catalyst for dedicated EGR applications. The location of the NO_x-CO tradeoff point was shifted to more rich conditions using dedicated EGR. [4]

[4]Sections 1-7 of this chapter are composed of a paper submitted to the ASME Journal of Energy Resource Technology. The citation for this publication is as follows: Van Roekel C, Montomgery DT, Singh J, and Olsen DB. Analysis of Non-Selective Catalyst Reduction Performance with Dedicated Exhaust Gas Recirculation. ASME Journal of Energy Resource Technology. 2019.

5.2 Introduction

Rich burn natural gas engines play a necessary and prominent role in power generation for the oil and gas industry. The EPA defines rich burn engines as any engine that is designed and operated at an air-fuel ratio of less than lambda 1.1[(1)]. Because rich burn engines typically operate near stoichiometric conditions a three-way, also known as a non-selective catalyst can be used to reduce emissions of oxides of nitrogen (NO_x), unburned hydrocarbons (THC), and carbon monoxide (CO). A well designed non-selective catalyst can achieve near 99% catalyst reduction efficiency of NO_x and CO when applied correctly to an engine[(2)]. However, the current tradeoff of rich burn natural gas engines is their limited power density due to high combustion temperatures that occur when operating at near stoichiometric conditions. Thus, consumers must decide between a natural gas engine that can achieve best in class post catalyst emissions, and a natural gas engine with increased power density such as a lean burn. Exhaust gas recirculation has conventionally been implemented on engines in high pressure or low pressure loop configurations to limit the formation of NO_x. Dilution of the combustion charge using recirculated exhaust changes the thermodynamic properties of the combustion charge and effectively lowers peak combustion temperature which results in lower engine out emissions of NO_x. High and low pressure loop EGR configurations rely on an EGR valve to meter the amount of exhaust recirculated back to the intake manifold at different engine operating conditions. A heat exchanger is used to reduce the temperature of the recirculated exhaust, but the EGR valve can often be exposed to gas temperatures in excess of 100 °C. Being exposed to high gas temperatures for an extended period of time can limit the long term reliability of an EGR valve. Some industrial natural gas engines are expected to operate at rated power nearly year round, and because of this long term reliability of components is a critical design criterion. Dedicated EGR is a variation of conventional high and low pressure loop configurations. The dedicated EGR method designates one or more engine cylinder(s) exhaust to be recirculated back to the intake manifold of the engine at all operating conditions. No EGR valve is used so the engine operates at a fixed effective EGR rate at all times. The impact that the recirculated exhaust gas has on combustion is controlled by changing the air-fuel ratio of the dedicated cylinder(s).

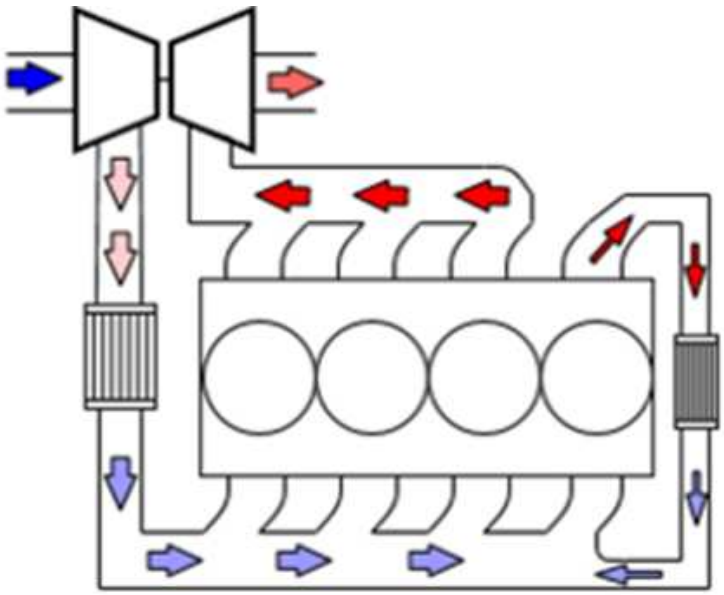

Figure 5.1: Dedicated EGR Layout

Additional fuel is added to the dedicated cylinder(s) while the other cylinders remain at near stoichiometric conditions. A general schematic of dedicated EGR applied to a four cylinder engine can be found in Figure 5.1. Fuel rich combustion conditions produce partial oxidation combustion products such as hydrogen (H_2) and CO. At engine operating conditions where an effective lower EGR rate is necessary for acceptable engine performance, additional fuel is added to the dedicated cylinder(s). This results in fewer inert combustion product species of carbon dioxide (CO_2) and water (H_2O) and more species that have higher reactivity such as H_2 and CO. If dedicated EGR is to be successfully implemented on an industrial natural gas engine a better understanding is needed of how a typical non-selective catalyst will perform when exposed to combustion products from a dedicated EGR engine is required. In this work an industrial natural gas engine was reconfigured to operate with dedicated EGR, and a commercially available non-selective catalyst was installed on the engine.

5.3 Methods

The engine used for this work was a Caterpillar G3304 rich burn industrial natural gas engine. As a stock engine a G3304 engine is naturally aspirated with a 7.0 liter displacement and a low

rated brake mean effective pressure (BMEP) of 6.7 bar at wide open throttle (WOT). The engine is spark ignited (SI) utilizing fine wire spark plugs as an ignition source. The quiescent combustion chamber is achieved through single intake and exhaust valves and a flat top piston design. Overall, the G3304 as a stock engine is a low technology engine utilizing a carburetor for air and fuel mixing, a fly-ball governor for engine speed control, and mechanical means of controlling spark timing. Operating the G3304 as a dedicated EGR engine required a number of changes to the engine design. The first was the addition of an engine control module (ECM). This allowed for electronic control of spark timing, closed loop air-fuel ratio control, and monitoring of numerous other engine operating conditions. The second was the addition of a simulated engine turbocharger. A turbocharger was simulated using a standalone supercharger and a back pressure valve. Another notable change made to the engine was that a port fuel injection system was added to the dedicated cylinder. This allowed the dedicated cylinder to operate at a different air-fuel ratio than the other three engine cylinders. Finally, based on previously published literature an EGR mixer was added to the engine[3]. Due to the expected intermittent pulses of exhaust coming from the dedicated cylinder a mixer was designed to dampen these pulses and allow for adequate mixing of dedicated cylinder exhaust and fresh air-fuel mixture. Table 5.1 shows general engine specifications for the G3304 engine used during this work. Figure 5.2 shows a schematic for the engine while operating as a dedicated EGR engine. Key components on the engine are labeled. In this work air-fuel ratio dithering to achieve improved catalyst efficiency was not implemented. However, the closed loop air-fuel ratio control used a PID control scheme in which the air-fuel ratio did oscillate slightly rich and lean about a chosen lambda. The magnitude and frequency of these oscillations were not modified at any time. After tests were conducted an analysis of the magnitude and frequency of the PID loop was done. It was found that the frequency with the largest power spectral density was 0.175 Hz. The magnitude of the oscillations varied over the course of the four minute test analyzed so a frequency distribution of the magnitude of the oscillations was was calculated. It was found that the magnitude of oscillations within two standard deviations (95% confidence interval) was $\pm$ 0.008 lambda. In previous work done at the CSU Powerhouse

Table 5.1: Caterpillar G3304 rich burn industrial natural gas engine specifications

Caterpillar G3304	
Number of Cylinders	4 (inline)
Rated Engine Speed	1800 rpm
Rated BMEP	6.7 bar
Compression Ratio	10.5
Displacement	7.0 L
Bore	120.7 mm
Stroke	152.4 mm
Piston / Head Design	Flat

Engines Lab a study of dithering and steady state AFR control was done on a 7.5 L rich burn engine. This study used the same catalyst as was used in this work. After sweeping dithering frequency and magnitude, results showed optimial catalyst conversion efficiency at a dithering frequency of 0.5 Hz and a magnitude of 0.005 lambda[4]. One of the key considerations when modifying the G3304 engine to operate at a dedicated EGR engine was the mixing of fuel and air. A low pressure fuel and air mixing system was built for the G3304 engine. As shown in Figure 5.2 downstream of the fuel control valve, fuel and air were mixed in the stock carburetor for the G3304 engine. After this the then mixed fuel and air passed through a supercharger and a charge air cooler before entering the EGR mixer. The general design of the EGR mixer is shown in Figure 5.3. The dedicated cylinder exhaust enters the mixer and is accumulated in a volume approximately 1.5 times that of the dedicated cylinder while the piston is at bottom dead center (BDC). The exhaust is entrained in the premixed fuel and air via orifices at various locations. The nature of this design ensured that the dedicated cylinder exhaust remained at a higher pressure than the incoming air and fuel at all operating conditions. Then the mixed fuel-air-exhaust exited the EGR mixer and passed over a butterfly valve used to control engine speed before finally entering the intake manifold of the engine. Together the carburetor, supercharger, charge air cooler, EGR mixer, and associated piping created a tortuous path for the air-fuel mixture and it was assumed that there was no stratification of gases. The fuel supply for this natural gas engine was taken

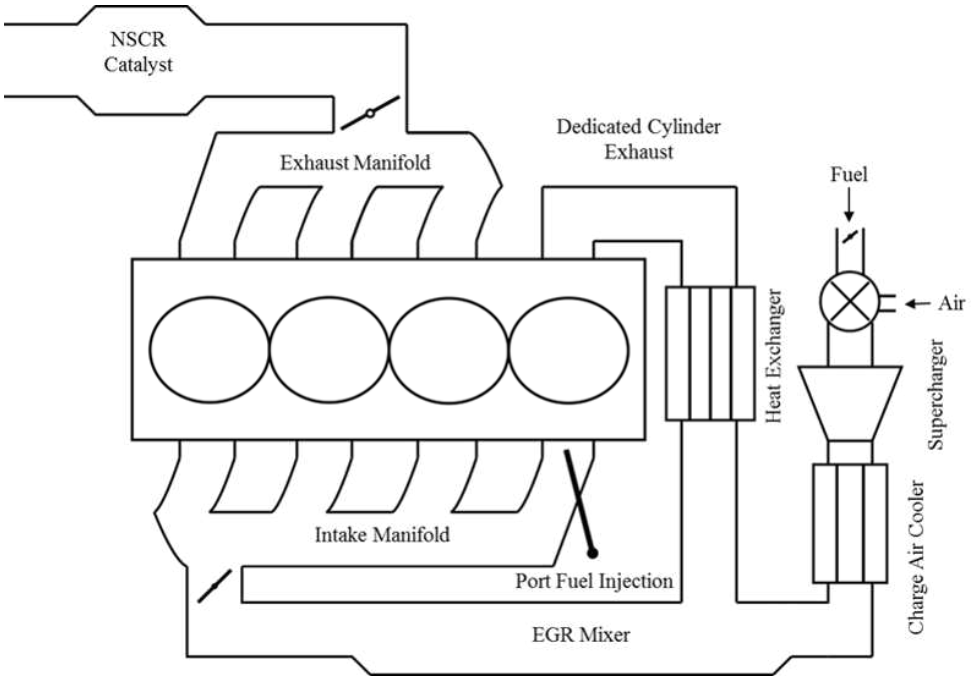

Figure 5.2: G3304 engine schematic while operating with dedicated EGR

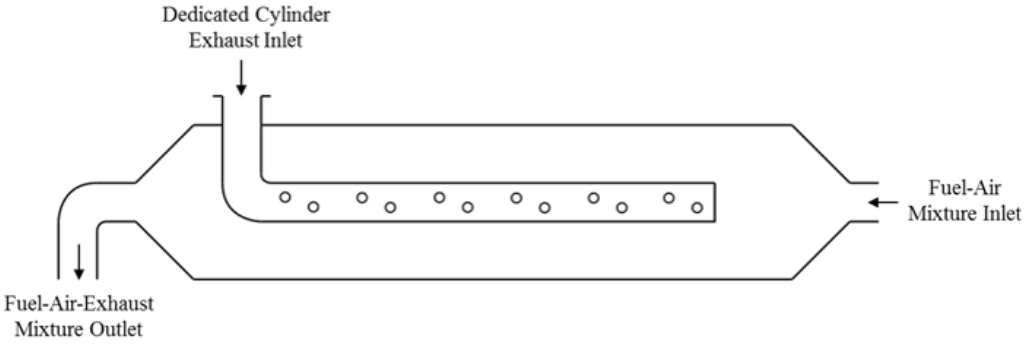

Figure 5.3: Dedicated EGR Mixer

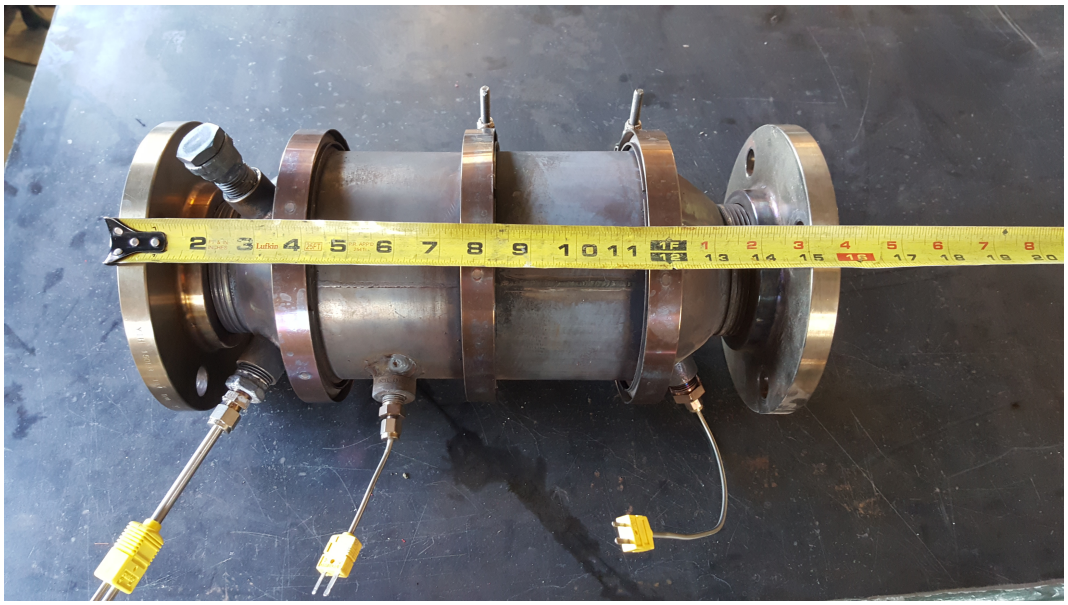

Figure 5.4: NSCR catalyst used with the G3304 engine.

directly from a natural gas pipeline source. Gas composition was measured using a Varian CP4900 mini gas chromatograph. Methane number (MN) calculations were done using the MWM methane number method[5]. Gaseous engine emissions were analyzed using two instruments. The first, a Rosemount five-gas rack measured CO, CO_2, total hydrocarbons (THC), oxygen (O_2), and oxides of nitrogen (NO_x). The second, an MKS Fourier transform infrared (FTIR) spectrometer was used to measure emissions such as species of volatile organic carbons (VOCs), nitric oxide (NO), and nitrogen dioxide (NO_2). A complete list of species quantified by the MKS FTIR is shown in Table 5.2. The FTIR method used to analyze spectra was developed by MKS for exhaust species typically found in rich burn natural gas combustion. At selected engine operating points a third gaseous engine emissions measurement instrument, an ECOM J2KN Pro Series, was used. This portable emissions analyzer uses an electrochemical method to quantify species such as CO, NO, and NO_2. Each of these analyzers shared a common, heated sample line between the engine and the respective instruments. Gaseous emissions were sampled using averaging probes designed to collect gas from three different locations in the exhaust stream. The probes were placed upstream of the catalyst, downstream of the catalyst, and just downstream of the exhaust leaving the dedicated cylinder. The catalyst used was designed and manufactured by DCL International, delivered to

Table 5.2: Combustion exhaust species quantified using MKS rich burn natural gas FTIR method

Species Quantified
Carbon monoxide (CO)
Carbon Dioxide (CO_2)
Nitric Oxide (NO)
Nitrogen Dioxide (NO_2)
Nitrous Oxide (N_2O)
Ammonia (NH_3)
Formaldehyde (CH_2O)
Methane (CH_4)
Ethane (C_2H_6)
Propane (C_3H_8)
Acetylene (C_2H_2)
Ethylene (C_2H_4)
Propylene (C_3H_6)
Water (H_2O)

CSU in 2015. Having been utilized on several research projects the catalyst performance was expected to be partially degraded. Figure 5.4 shows a picture of the catalyst and the flange-flange length of the catalyst for reference. Given typical engine out emissions from a rich burn natural gas engine it was originally designed to reduce post catalyst emissions of CO and NO_x below 4 and 2 g/bhp-hr, respectively for engines of similar power to the G3304. The space velocity of the catalyst at the operating conditions tested in this work was approximately 30,000/hr, and the cell density was approximately 200 cells per square inch. Specific catalyst precious metals and wash coat composition was not available, but based on discussion with the catalyst manufacturer, typical non-selective catalyst materials such as rhodium, platinum, palladium, cerium, and various promoters and stabilizers were used in this catalyst. The catalyst housing contains two substrates separated by a small volume. Exhaust gas temperature measurements were made at the inlet to the catalyst housing, between the substrates, and at the outlet of the catalyst housing. Emissions data presented is representative of a 5 minute collection at a rate of 2 Hz, and unless otherwise noted the data was collected by the Rosemount 5-gas analyzer. Uncertainty shown in emissions figures

Table 5.3: Engine operating conditions during the air-fuel ratio sweep

Operating Conditions		
	Baseline	Dedicated EGR
Speed (rpm)	1800	1800
BMEP (bar)	6.7	6.7
Power	71 kw	71 kw
IMAT (°C)	40	62
IMAP (psia)	11-13	17-18.5
Spark Timing (°bTDC)	30	45
Spark Duration (μs)	150	365
Dedicated Cylinder AFR (Lambda)	—	0.936
Global Lambda	Varied	Varied
MWM Methane Number	70-71	70-71

comes from instrument linearity and calibration gas uncertainty and was calculated using the Kline and McClinktock method[6]. Information about operating conditions of the engine while under test can be found in Table 5.3.

5.4 Results and Discussion

An initial evaluation of the catalyst performance was done by sweeping the air-fuel ratio of the engine while holding all other operating variables found in the 'Baseline' column of Table 5.3 constant. Based on observations made on previous engine tests on the G3304 is was anticipated that the air-fuel ratio that would result in the best post catalyst emissions was lambda 0.990. Due to this observation lambda was incremented in very small steps (0.001) around that value and step size increased as lambda moved away from a value of 0.990. The largest step size taken was 0.005 lambda. Prior to doing the lambda sweep an initial evaluation of pre and post-catalyst engine emissions was done at 0.990 lambda. This test was repeated after the lambda sweep to ensure that no significant variation of engine performance had occurred over the course of the lambda sweep. Figure 5.5 shows the post catalyst emissions of NO, CO, THC, and VOCs. Species considered VOCs here are propane, acetylene, ethylene, and propylene. The target emissions selected for this

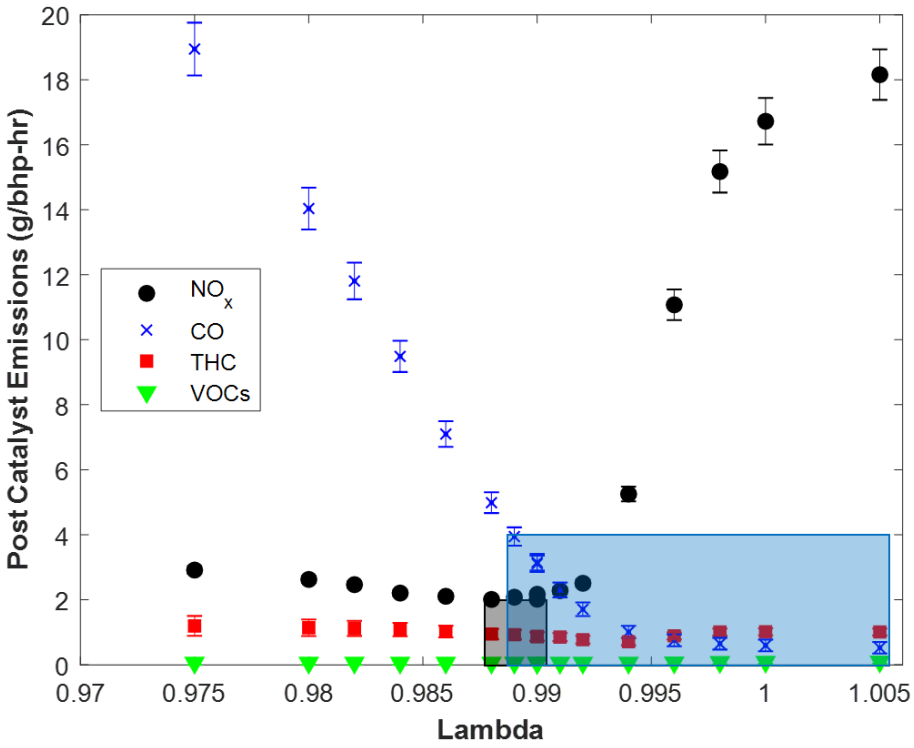

Figure 5.5: Rich burn baseline post catalyst emissions for the G3304 engine

work were not to exceed 4.0 g/bhp-hr CO, 2.0 g/bhp-hr NO_x, and 0.7 g/bhp-hr VOCs post catalyst. The range of lambda values in which post catalyst CO emissions requirements are met is shown in the area shaded blue, and the range of lambda where post catalyst NO_x emissions requirements are met is shown in the area shaded black. The overlapping area is then the acceptable range of engine operation in terms of air-fuel ratio where post catalyst emissions targets are met. Post catalyst VOC emissions were less than 0.1 g/bhp-hr across the entire lambda sweep. Thus, the window of acceptable lambda for this engine-catalyst pair without dithering was small with a range only between 0.990 and 0.989 lambda. Examination of catalyst efficiency as a function of lambda shows how the catalyst performed across the range of lambda values tested. On a fundamental level a catalyst simply provides area for gaseous molecules to meet, react with other molecules, and ultimately shift the composition of the gas towards equilibrium concentrations. The precious metals included in a wash coat provide reaction pathways for emission such as NO and CO with a lower activation energy and at an increased rate. However, a non-selective catalyst such as the one used in this work

must be designed such that the catalyst area or in another sense the number of sites available for reaction is adequate for the concentration of species passing through the catalyst. This measure is quantified in space velocity and as mentioned was approximately 30,000/hr for the catalyst and engine. Per discussion with the manufacturer of this catalyst a space velocity of 30,000/hr was well within the acceptable range that would result in good performance. Of specific note in any catalyst reduction efficiency study is the NO_x-CO tradeoff. The results shown in Figure 5.6 demonstrate the non-linear response that NO_x and CO have at only slightly fuel rich conditions between 0.990 and 0.995 lambda. At conditions rich of this range a high catalyst reduction of NO_x is shown. Examination of FTIR results in which a distinction between NO and NO2 was made shows that across the entire range of lambda values NO was by far the primary constituent in the NO_x measurement. The highest NO2 concentration measured in this lambda sweep was a concentration of 10 ppm while the pre catalyst NO values ranged from 2500 – 3000 ppm. Break down of NO in a 3 way catalyst is done primarily by reactions taking place with the precious metal rhodium where nitrogen and oxygen atoms are separated and attached to different sites. Monatomic nitrogen atoms are able to move freely on the catalyst surface, recombine with other monatomic nitrogen atoms and leave the catalyst. However, conditions in the catalyst are not sufficient for oxygen to be removed in this way. The presence of CO in the exhaust allows for oxygen to be liberated from the catalyst surface, and at rich engine operating conditions CO is abundant. Thus, at rich conditions a high catalyst reduction efficiency of NO is possible. Similarly, at rich conditions a low catalyst reduction efficiency of CO is seen due to the high concentration of CO and the lack of available oxygen to oxidize CO to CO_2. At conditions lean of the 0.990 – 0.995 lambda range catalyst reduction efficiency of CO is high due to the increased availability of oxygen in the exhaust that can be used to oxidize CO. Due to the limited number of reaction sites available on a catalyst surface, at lean conditions where there is excess O_2 catalyst reduction efficiency of NO_x is low because of a competition for sites that takes place between these two species. It follows that if reaction sites on the catalyst are occupied by O_2 molecules the NO_x molecules are not able to be destroyed. When designed properly, non-selective catalysts are capable of achieving 98-99$\%$ reduction efficiency for

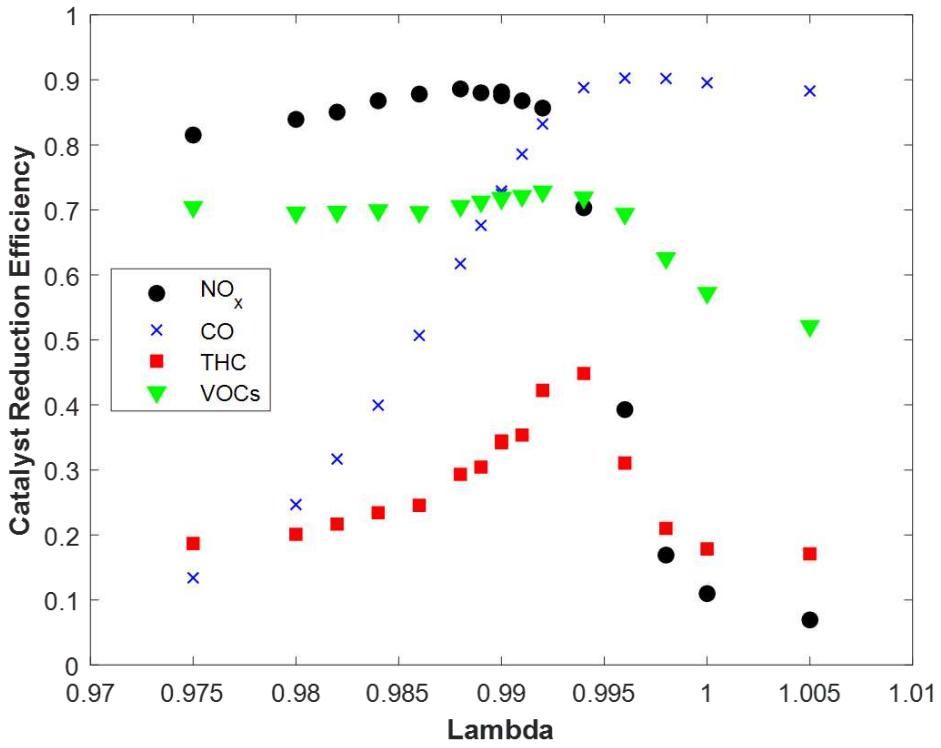

Figure 5.6: Catalyst reduction efficiency as a function of rich burn engine air-fuel ratio.

NO_x and CO. Examining the catalyst performance in this work reveals that in the range of optimal performance for both NOx and CO conversion the best reduction efficiency achieved was 86% and 83% for NO_x and CO, respectively. High reduction efficiency not only necessitates a well-designed catalyst but also careful management of oxygen within the catalyst. Decreased reduction efficiency in this work is likely a product of variations in cylinder to cylinder combustion, lack of tuned air-fuel ratio dithering, and partial catalyst degradation. The performance of catalyst VOC reduction efficiency at conditions lean of approximately 0.995 lambda was unexpected. The expected result was that VOC reduction efficiency would trend similarly to CO reduction efficiency, but Figure 5.6 shows that as conditions became more lean VOC reduction efficiency decreased. This behavior can likely be attributed to the combination of precious metals present in the catalyst not being correct for this particular exhaust composition. Pre-catalyst concentrations of formaldehyde ranged from less than 1 ppm to approximately 10 ppm. Post-catalyst measurement showed only trace amounts of formaldehyde which suggested that it was successfully oxidized in the catalyst.

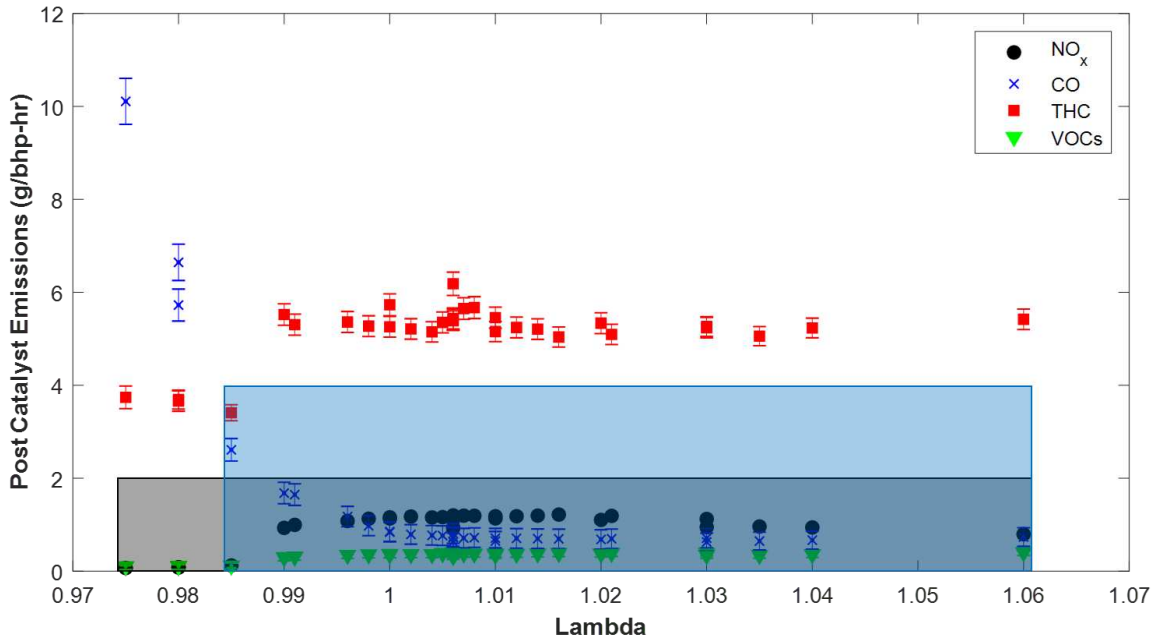

Figure 5.7: Post catalyst emissions as a function of air-fuel ratio. The engine was operating with dedicated EGR. The dedicated cylinder was held at a constant air-fuel ratio of 0.936 lambda while the three remaining cylinder air-fuel ratio was adjusted.

Following the baseline air fuel ratio sweep the G3304 engine was reconfigured to operate with dedicated EGR. Engine operating conditions for dedicated EGR included in Table 5.3 were identified via a response surface method optimization to be optimized operating conditions for the G3304 engine with dedicated EGR. Engine BMEP of 6.7 bar was held constant between the baseline and dedicated EGR tests while intake manifold pressure (IMAP) was varied to achieve the same engine BMEP. Natural gas fuel composition varied only slightly between 70 and 71 MWM methane number and fuel concentrations of methane, ethane, and propane remaining near 83%, 11%, and 2%, respectively. The specific fuel concentrations were very similar to the baseline engine operating fuel concentrations. Prior to performing the dedicated EGR air fuel ratio sweep it was observed in other tests that the engine air-fuel ratio that resulted in a pre-catalyst CO to NO_x ratio of 2:1 was approximately 0.996 lambda. This air fuel ratio was chosen as the 'center' of the dedicated EGR air-fuel ratio sweep. Four repeated tests at this air-fuel ratio were done during the sweep shown in Figure 5.7. Similar to the baseline air-fuel ratio sweep small steps in lambda were taken around the

center point with the steps between test points getting larger further away from lambda 0.996. Operating the G3304 engine with dedicated EGR results in large differences in the acceptable range of air-fuel ratio when compared to operating as a conventional rich burn engine. The range of acceptable air-fuel ratio where CO emissions are less than 4.0 g/bhp-hr, NO_x emissions are less than 2.0 g/bhp-hr, and VOC emissions are less than 0.7 g/bhp-hr is 0.075 lambda. Theoretically, this range could be even larger as an upper limit on lambda was not found within the scope of this study. The means by which this range was achievable was clearly due to low NO_x emissions. The highest post-catalyst NO_x emissions of 1.21 g/bhp-hr found were at an air-fuel ratio of lambda 1.016. This was approximately 16 times lower than the highest post-catalyst NO_x emissions found in the baseline air-fuel ratio sweep. A notable decrease in NO_x emissions was expected due to the impact that exhaust gas recirculation in general has on peak combustion temperatures during a combustion event. Near stoichiometric conditions the Zel'dovich mechanism, which is a strong function of temperature, accounts for the majority of NO and NO_2 production, and it follows that when peak combustion temperatures are lowered engine out NO_x emissions decrease. Another notable difference between the baseline and dedicated EGR post-catalyst emissions was the high unburned hydrocarbon emissions found in the dedicated EGR tests. This can be explained by incomplete combustion of methane and ethane fuel while operating with dedicated EGR. Pre-catalyst baseline concentration of methane and ethane was on the order of 300 and 30 ppm, respectively with low catalyst reduction efficiency near 20%. Pre-catalyst methane and ethane dedicated EGR emissions were on the order of 1500 and 150 ppm, respectively with very low catalyst reduction efficiency near 10%. While possible, oxidation of methane in a catalyst is much more difficult than other hydrocarbons because breaking the first C-H bond takes roughly 40kJ/mol more energy than the subsequent bonds, much more than in other hydrocarbons[7]. It is clear that conditions in the catalyst while operating with exhaust coming from the dedicated EGR configuration were not adequate to allow significant oxidation of methane and ethane to take place. As methane is now recognized as a major greenhouse gas[8] this result is not desirable. However, as outlined in previous work by the author[9,10] there is ample opportunity to improve combustion efficiency of

natural gas dedicated EGR engines that would result in lower engine out hydrocarbon emissions of methane and ethane.

Figure 5.8 shows the catalyst reduction efficiency for the G3304 engine while operating with dedicated EGR. Catalyst reduction efficiency of the G3304 engine operating with dedicated EGR had similar general trends to the baseline reduction efficiency for CO, THC, and VOCs. The air fuel ratio where the NO_x-CO tradeoff occurred, 0.985 lambda, was slightly more rich conditions than the baseline air-fuel ratio which occurred at 0.992 lambda. At conditions more rich of 0.985 lambda catalyst reduction efficiency of NO_x and VOCs were between 80-90$\%$ while the reduction efficiency of CO changed drastically from less than 50$\%$ at the most rich conditions of 0.970 lambda to nearly 80$\%$ at lambda 0.985. At all conditions more lean than 0.985 lambda Figure 5.8 shows a catalyst NO_x efficiency of 0. Data collected in this range showed a relatively small increase in NO across the catalyst. This result was confirmed by all three measurement methods described previously in the 'Methods' section of this work. Taking the uncertainty of the measurement methods and the uncertainty associated with the standard deviation of the repeated 'center' points the result did prove to be statistically significant. Using Chemkin 19.2 Equilibrium model and the known combustion charge composition a study was done to find the expected equilibrium NO concentration in the post combustion gases. This study revealed that at all air-fuel ratios the calculated equilibrium concentration of NO was higher than that of the measured engine out concentration. If a catalyst simply accelerates and allows for chemical equilibrium to be achieved then theoretically an increase in NO emissions is possible. However, discussion with the catalyst manufacturer indicated that the catalyst temperature is too low for NO to be created within the catalyst in the time required. Without a clear explanation as to how this can occur in a non-selective catalyst at lean conditions a minimum efficiency value of 0 was imposed on these results for plotting. The notable result from this figure is that the best operating conditions in terms of catalyst reduction efficiency for a natural gas engine using dedicated EGR appear to be a rich conditions near 0.985 lambda. A direct comparison of post catalyst baseline and dedicated EGR NO_x, CO, THC, and VOC emissions is shown in Figure 5.9. The impact of natural gas dedicated

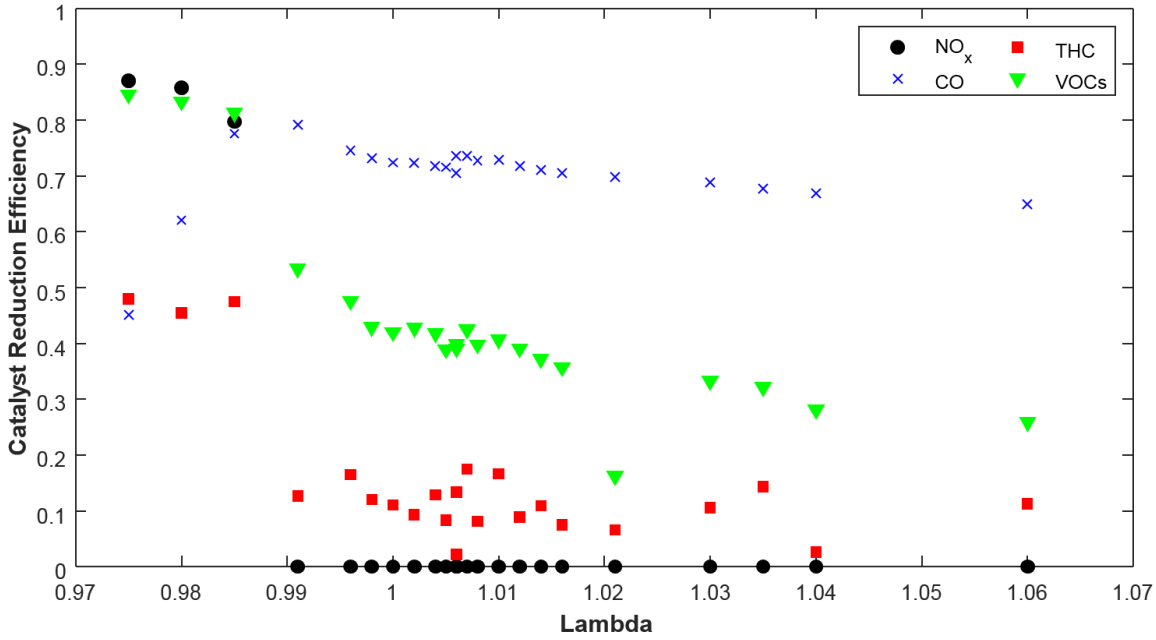

Figure 5.8: Dedicated EGR catalyst reduction efficiency as a function of lambda.

EGR combustion when paired with a common non-selective catalyst is clearly illustrated. In the subfigure of the upper left it is evident that post catalyst emissions on NO_x remain low over a wide range of air-fuel ratios. In fact, the pre-catalyst NO_x values are similar to that of post-catalyst dedicated EGR results which means that in order to meet a 2.0 g/bhp-hr limit of NO_x a catalyst would not be needed. This opens up the possibility to use an oxidation catalyst rather than a non-selective catalyst on dedicated EGR engines. Examining the subfigure of the upper right it is seen that at rich conditions post catalyst dedicated EGR emissions of CO are lower than that of the baseline engine operation. This is primarily due to the increased availability of oxygen in the pre and post catalyst exhaust of dedicated EGR tests. Even at the most fuel rich dedicated EGR conditions at least 0.50% oxygen was available in the pre-catalyst exhaust. This available oxygen allowed for high concentrations on the order of 5000 ppm to be oxidized in the catalyst while operating with dedicated EGR. The available oxygen content in dedicated EGR exhaust may be a function of poor combustion efficiency and thus would not be advantageous for the overall operation of the engine. Certainly, a dedicated EGR operating condition that has an

air-fuel ratio lean of 0.985 lambda could be chosen to meet CO emissions requirements. The two lower subfigures of Figure 5.9 depict a comparison of dedicated EGR and rich burn post catalyst VOC and THC emissions. Unburned hydrocarbon emissions found in premixed combustion are produced mainly by physical means within a combustion chamber. That is, they are protected from burning by the cold wall effects in crevice volumes, absorbed and desorbed in engine oil, etc[(11)]. Figures 5.6 and 5.8 show that the catalyst reduction efficiency of VOCs and THC emissions was higher while the engine was operating at baseline conditions (lower efficiencies for dedicated EGR). This decreased reduction efficiency paired with higher engine out THC and VOC emissions from the dedicated EGR configuration lead to the poor result shown in the lower two subfigures of Figure 5.9. The final consideration given when comparing catalyst performance was an analysis of the exhaust temperature at the catalyst inlet, between the two catalyst substrates, and at the catalyst outlet. Figure 5.10 shows the catalyst temperatures for baseline and dedicated EGR as a function of air-fuel ratio lambda. At each temperature measurement location the dedicated EGR configuration results in catalyst temperatures that are between 100 and 150 °C higher than baseline conditions. Per the catalyst manufacturer specifications temperatures in that catalyst should not exceed 730 °C to ensure designed catalyst life. The three richest conditions tested using dedicated EGR resulted in catalyst temperatures in excess of this specified upper limit. Temperatures at these three test cases were slightly higher than 750 °C. The presence of increased levels of VOCs and THC in dedicated EGR tests and associated oxidation of hydrocarbons likely contributed to the higher catalyst temperatures observed. Based on these results design of a catalyst to be used with dedicated EGR would need to include a consideration of using materials were greater tolerance for high temperatures. However, if combustion performance in a dedicated EGR engine were to be improved it is likely that lower catalyst temperatures would be observed.

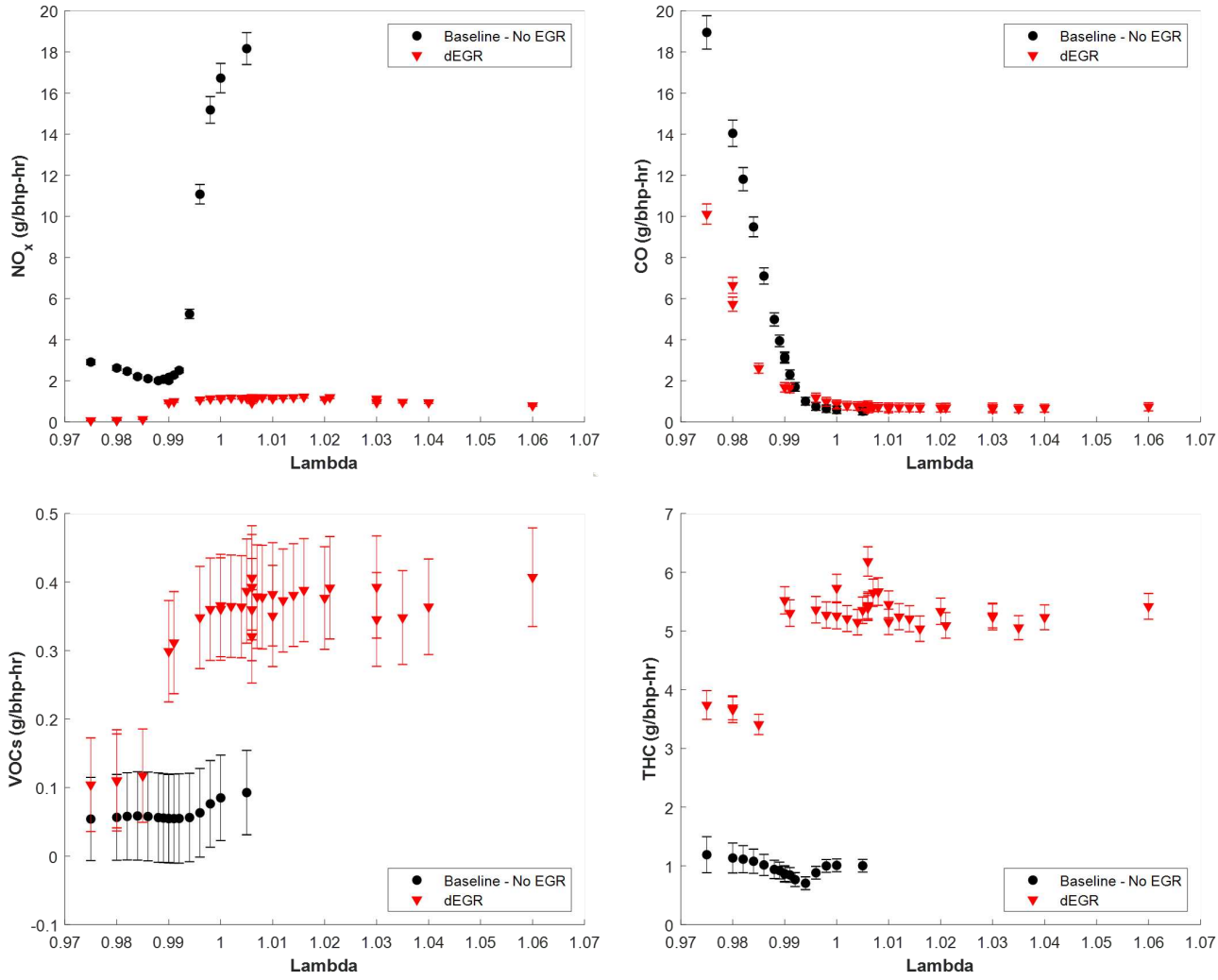

Figure 5.9: Post catalyst emissions of NO_x, CO, THC, and VOCs as a function of lambda. Dedicated EGR results are shown in red and rich burn baseline results are shown in black.

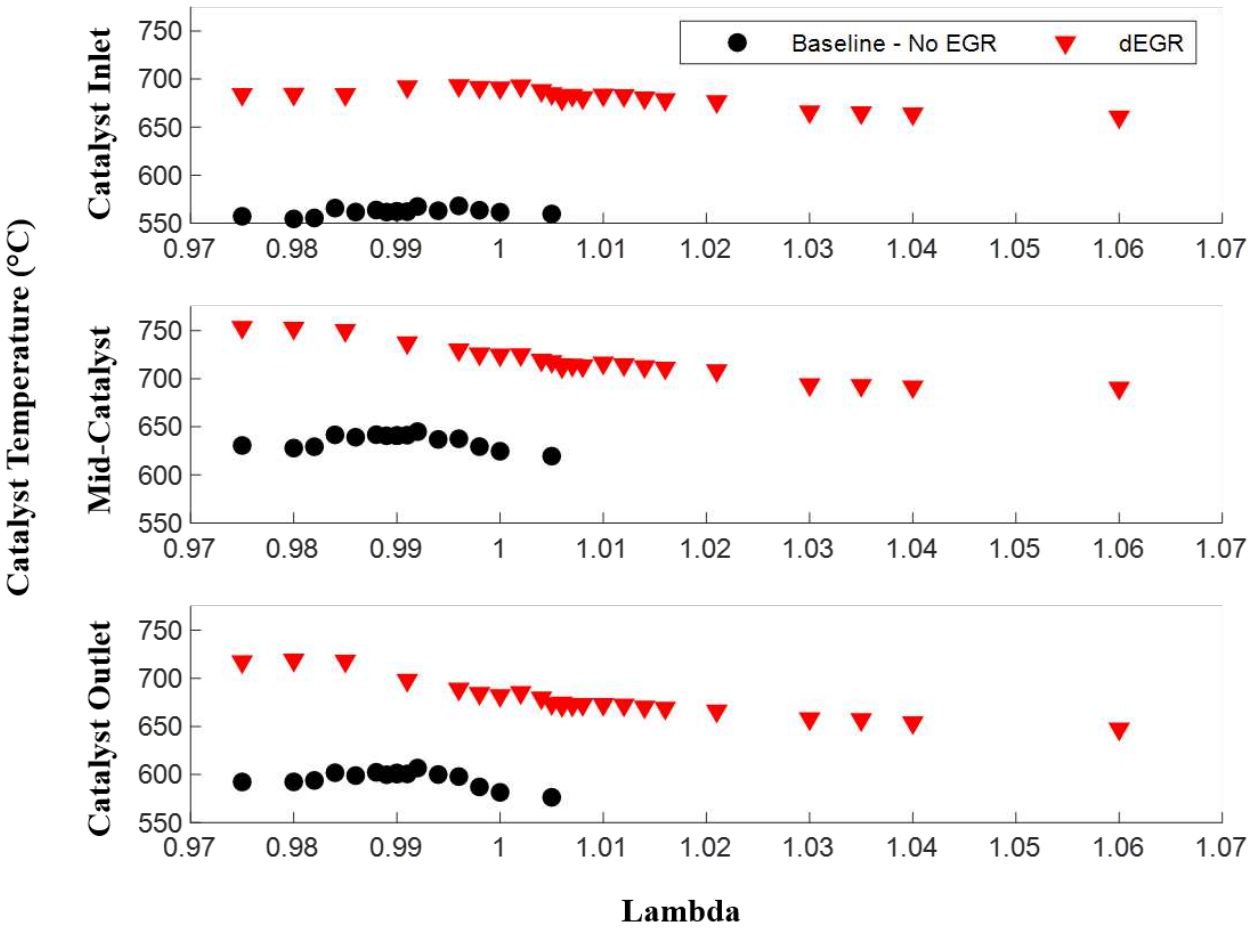

Figure 5.10: Exhaust gas temperature at the catalyst inlet, between catalyst substrates, and at the catalyst outlet as a function of lambda.

5.5 AFR Dithering and NO_x Considerations

As noted in the 'Methods' section of Chapter 5 the AFR control strategy used during this work did not include dithering. However, there was variation in AFR due to the PID control method of the software. Figure 5.11 shows how lambda varied over a four minute test. The raw data used to calculate lambda was collected using a 5-gas rack. During this test the target AFR was set at a value of 0.990 while the average lambda during the four minute collection time was 0.9917 as calculated using the Brettschneider method from pre-catalyst exhaust emissions data. One of the considerations made during analysis of the catalyst efficiency was the relatively low efficiency while the engine was operating without dedicated EGR in the range of the NO_x -CO tradeoff. One of the contributing factors to the low catalyst efficiency observed is the PID dithering frequency observed and how it relates to the optimal dithering frequency found in previous work by Finke et al[(4)]. At lambda greater than approximately 0.990 Figure 5.8 showed a catalyst reduction efficiency of NO_x equal to zero. The associated analysis as published in the paper simply noted that at these operating points the post catalyst NO_x was found to be greater than pre catalyst NO_x. Figure 5.13 shows the pre and post catalyst brake specific NO_x emissions while the engine was operating with dedicated EGR at varying stoichiometric cylinder lambda. The data shown is representative of NO_x emissions measured by a 5-gas rack. The error bars show that based on a single set of tests the results are statistically significant. However, the brake specific calculation does take into account other factors that could skew the results of pre and post catalyst results such as fuel consumption and engine power. The influence of these factors is unlikely due to the fact that the only difference between pre and post catalyst data was the sampling location of the emissions sample line. Figure 5.14 shows the raw NO data as collected by the 5-gas rack. Between lambda 0.990 and 1.020 the 5-gas rack measured an approximate increase of 30-40 ppm NO across the catalyst. When lambda was increased above 1.020 an increase of approximately 15 ppm NO was observed. The increase in NO emissions across the catalyst was affirmed by reviewing the FTIR measurements. The absolute values of pre and post catalyst NO measurements shown in Figure 5.15 are slightly different than what was measured by the 5-gas analyzer, but the

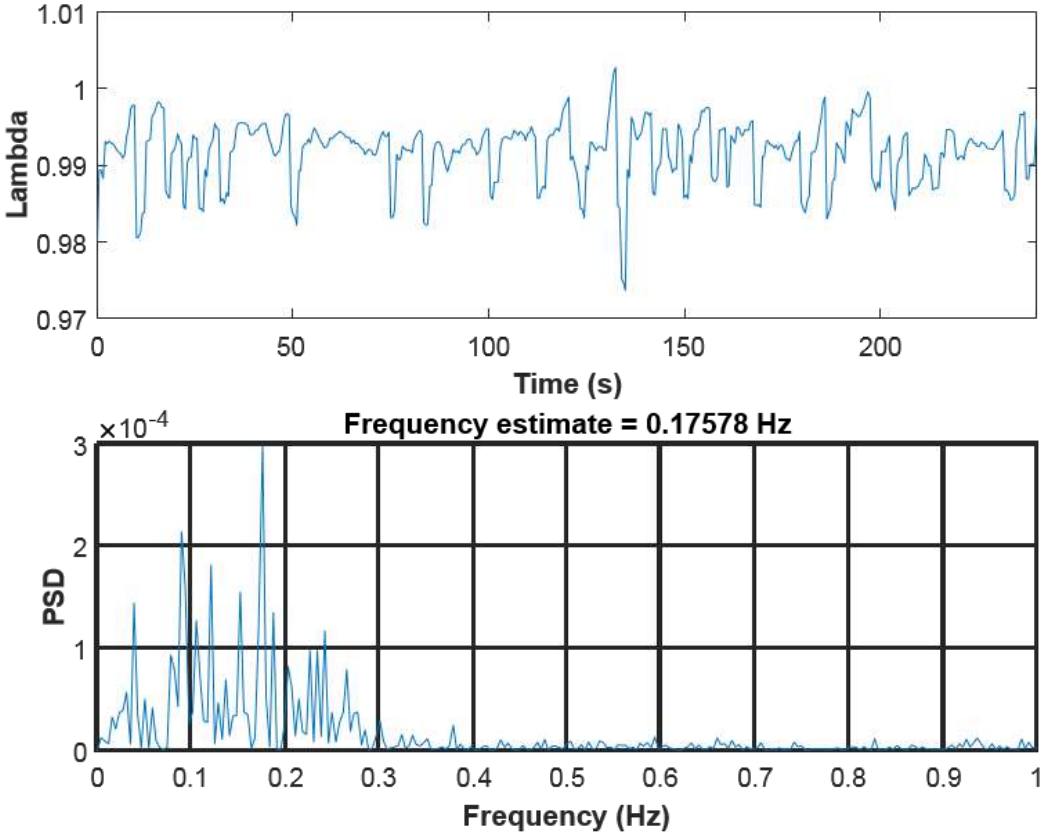

Figure 5.11: Sample AFR dithering raw data and power spectrum density for a single dedicated EGR test. The targeted AFR set for the test was lambda 0.990. The average lambda over a four minute average was 0.9917 as calculated using the Brettschneider method from pre catalyst exhaust emissions data.

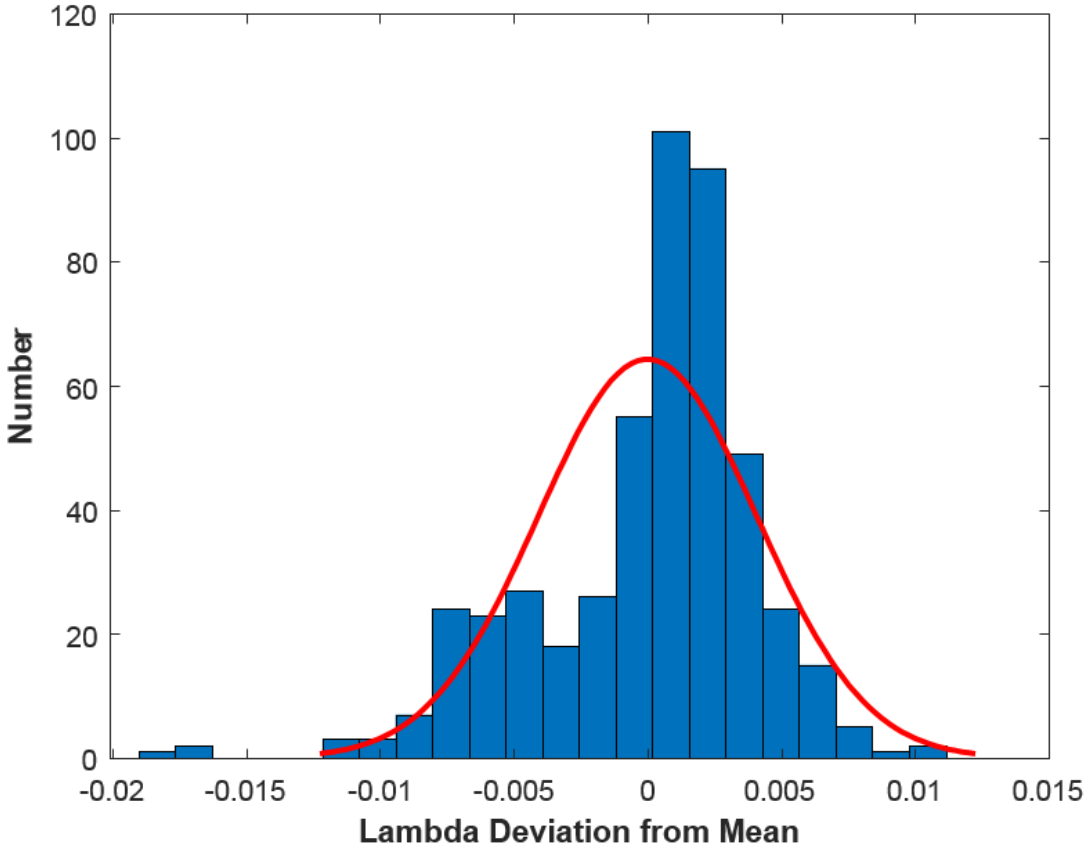

Figure 5.12: Frequency distribution data for the AFR data collected and shown in Figure 5.11

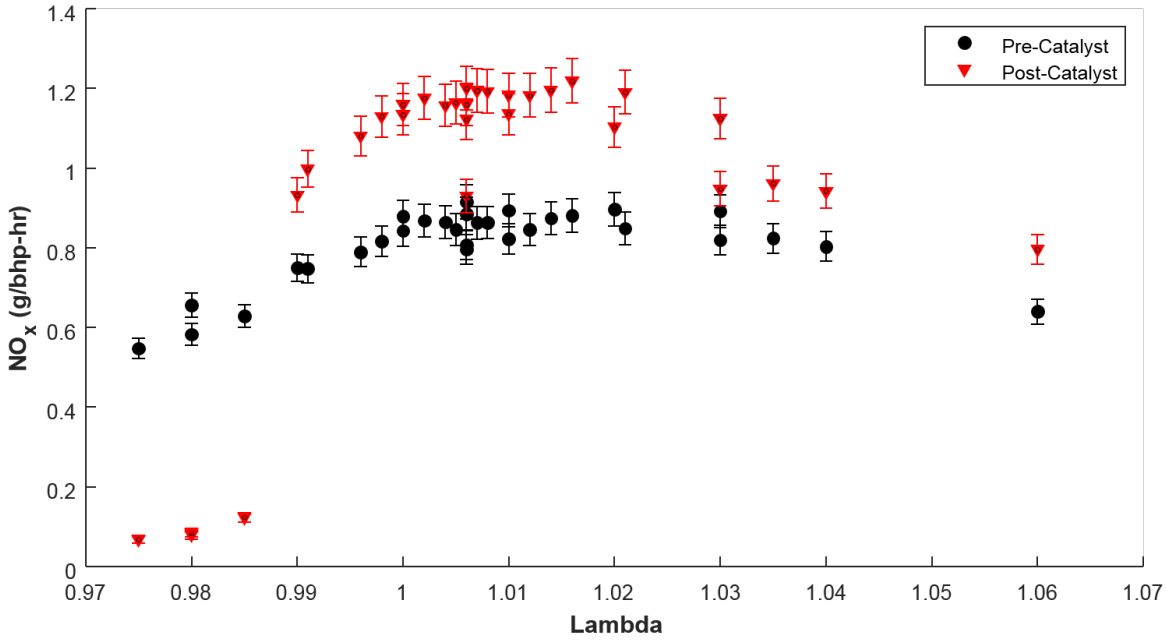

Figure 5.13: Pre and post catalyst brake specific NO_x data as collected by the 5 gas analyzer during the dedicated EGR air-fuel ratio sweep.

difference between pre and post catalyst measurement is nearly identical. After observing this phenomena the dedicated EGR lambda sweep was repeated a week after the initial data was taken. The repeated tests showed similar results. After this second data set was collected it was decided to use a third measurement method and repeat part of the test matrix. The third measurement method is explained in the 'Methods' section of Chapter 5. There was not enough test time left to repeat the entire test matrix so seven points which spanned the test range were selected. Figure 5.16 shows the ECOM raw NO results. These results again affirmed an increase in NO emissions across the catalyst at lambda greater than 0.990. After having a third measurement method confirm an increase in NO across the catalyst other measured emissions were analyzed across the lambda sweep in an attempt to explain this phenomena. The first data analyzed was NO_2 measurements across the lambda sweep. It was theorized that dissociation of NO_2 to NO could lead to an increase in NO across the catalyst. Across the lambda sweep the FTIR showed that there was a decrease in NO_2 across the catalyst between 5 and 10 ppm. Even if all of the NO_2 dissociated and remained NO this decrease could not fully account for the increase in NO across

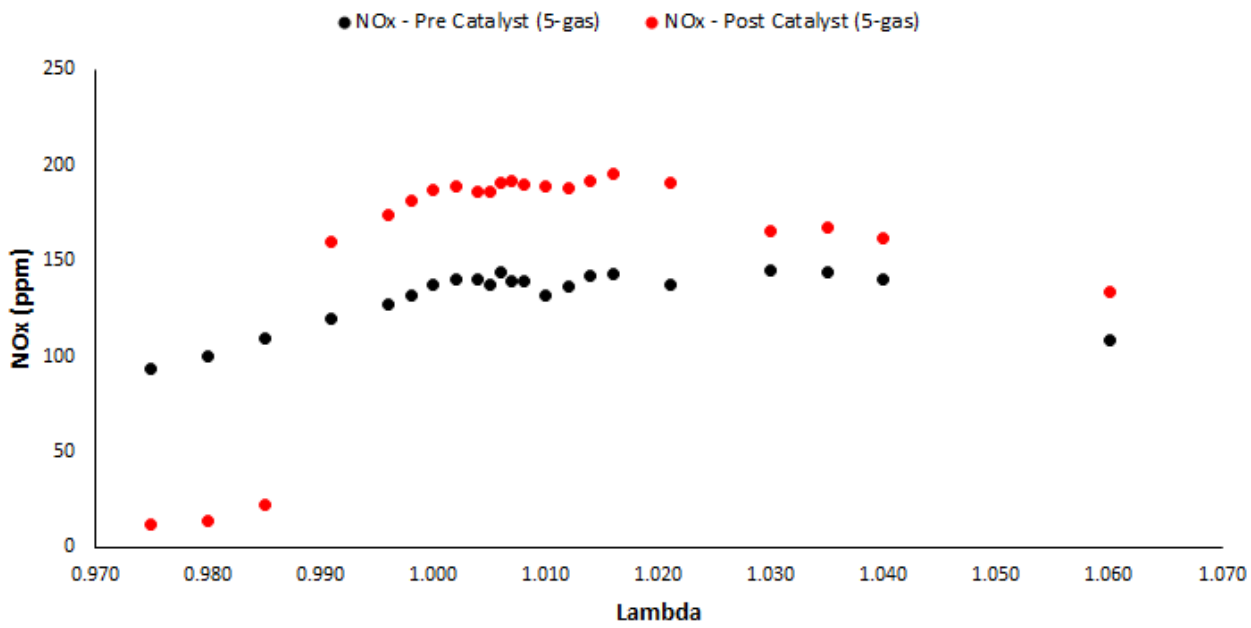

Figure 5.14: Pre and post catalyst raw NO data as collected by the 5 gas analyzer during the dedicated EGR air-fuel ratio sweep.

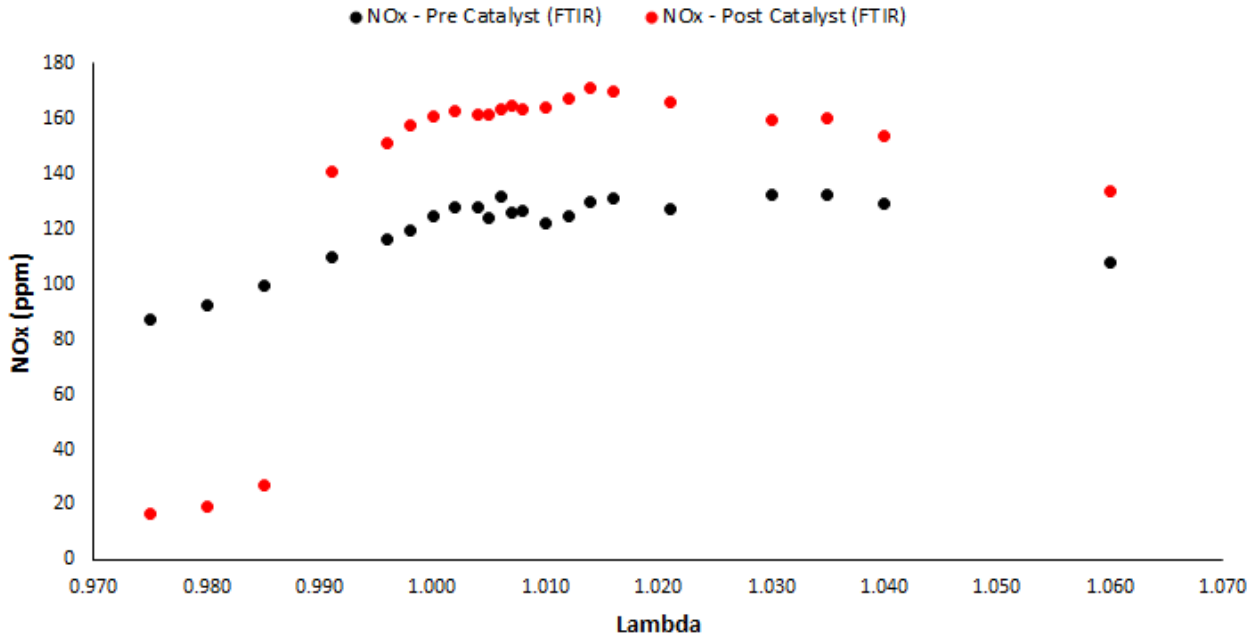

Figure 5.15: Pre and post catalyst raw NO data as collected by the FTIR analyzer during the dedicated EGR air-fuel ratio sweep.

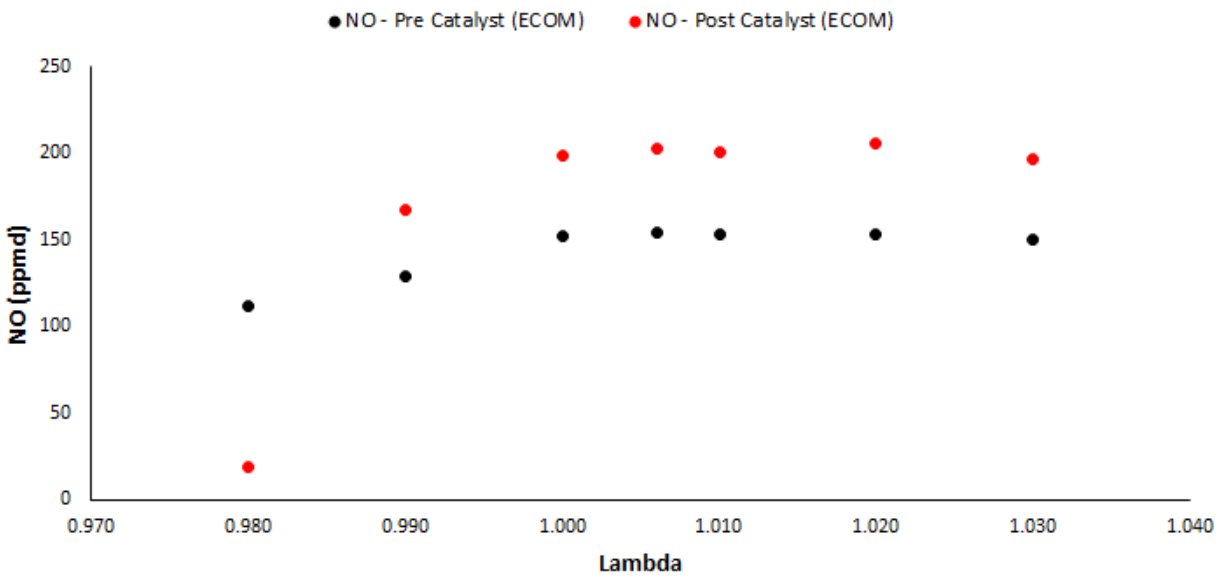

Figure 5.16: Pre and post catalyst raw NO data as collected by the ECOM analyzer during the dedicated EGR air-fuel ratio sweep.

the catalyst. Furthermore, the change in NO_2 did not follow the trend found in the NO data in that there was no significant change near lambda 0.990. The second theory that was explored was dissociation of ammonia across the catalyst. Pre and post catalyst ammonia while the engine was operating with dedicated EGR was less than 1ppm, respectively in the range of lambda where NO increased across the catalyst so it was determined that dissociation of ammonia was not the cause. Figures 5.18 and 5.19 show pre and post catalyst ammonia concentration for dedicated EGR and no EGR tests, respectively. Finally, since a common operating point was collected across the three separate tests days a statistical analysis of the spread of the data was done. Figure 5.20 shows the common operating point of lambda 1.006. Including all of the measurement uncertainties and the statistical uncertainty given the three test conducted at this operating point the results were statistically significant due to no overlap of the uncertainty ranges. Pre and post catalyst brake specific concentrations of CO, THC, and VOCs awhile the engine was operating with dedicated EGR are shown in Figures 5.21, 5.22, and 5.23. The notable outcome from these results is the high post catalyst THC emissions due to low catalyst efficiency.

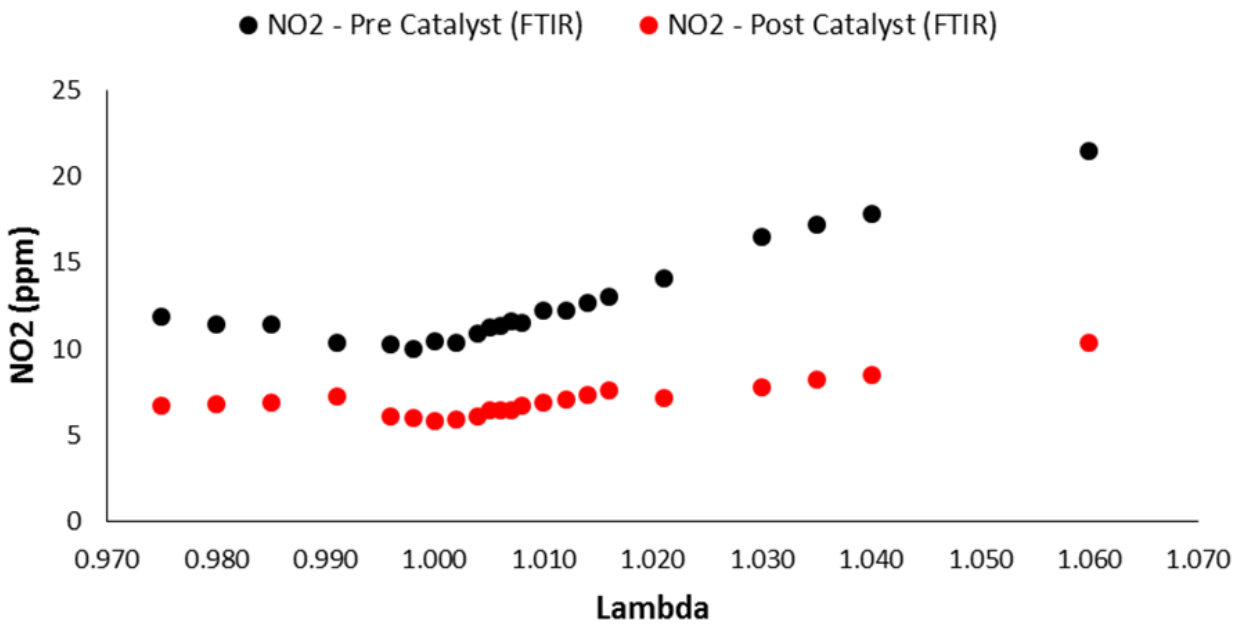

Figure 5.17: Pre and post catalyst raw NO_2 data as collected by the FTIR analyzer during the dedicated EGR air-fuel ratio sweep.

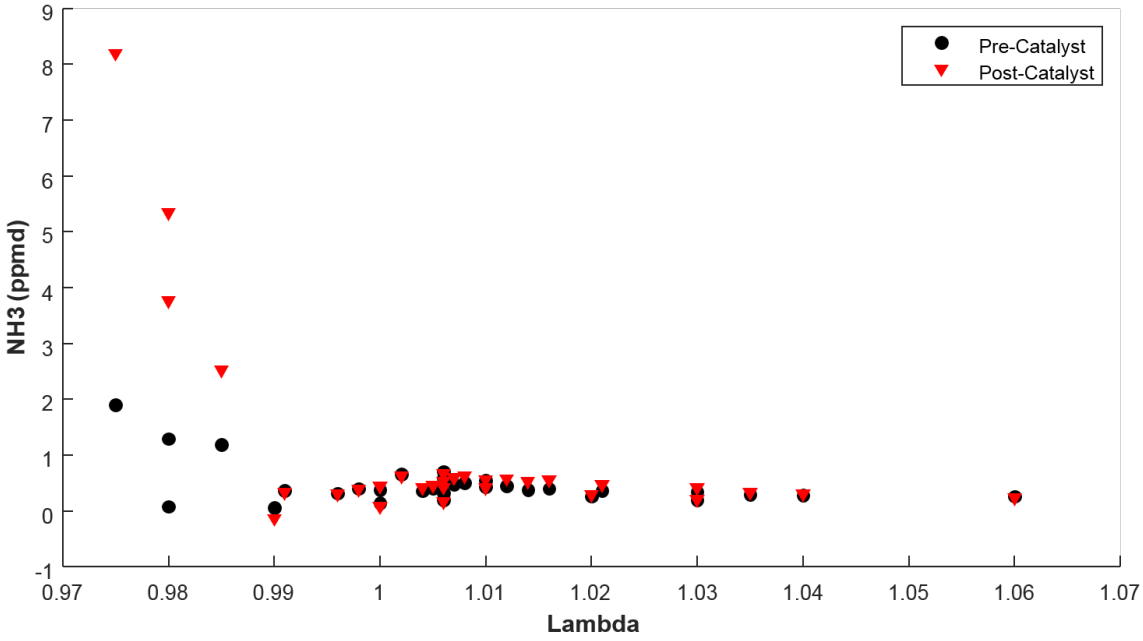

Figure 5.18: Pre and post catalyst NH_3 data as collected by the FTIR analyzer during the dedicated EGR air-fuel ratio sweep.

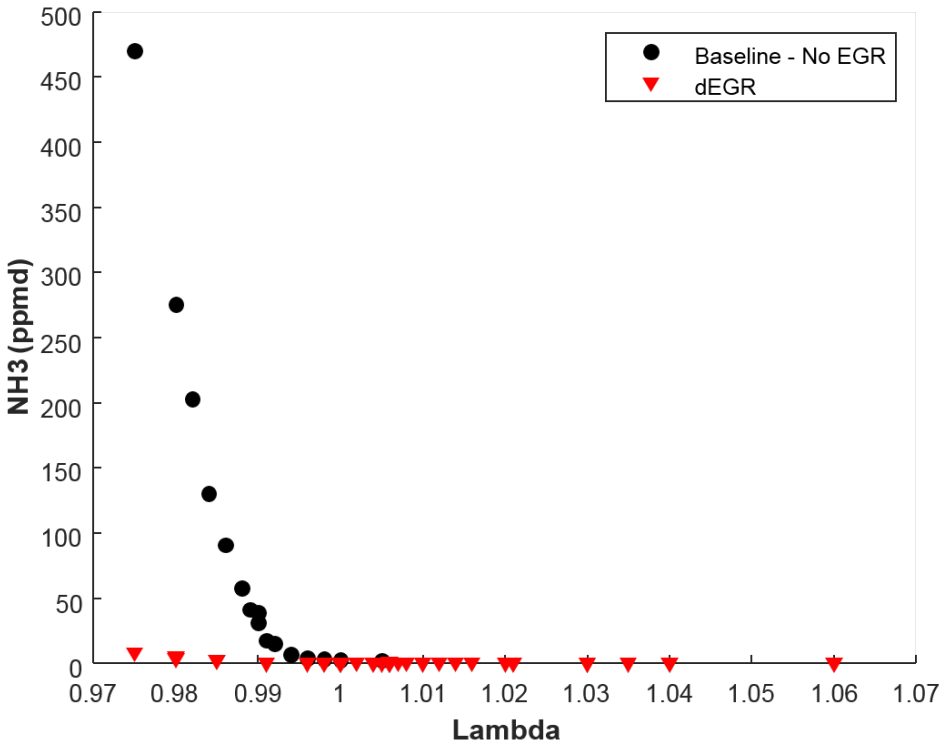

Figure 5.19: Post catalyst NH_3 data for the baseline and dedicated EGR test cases as collected by the FTIR analyzer.

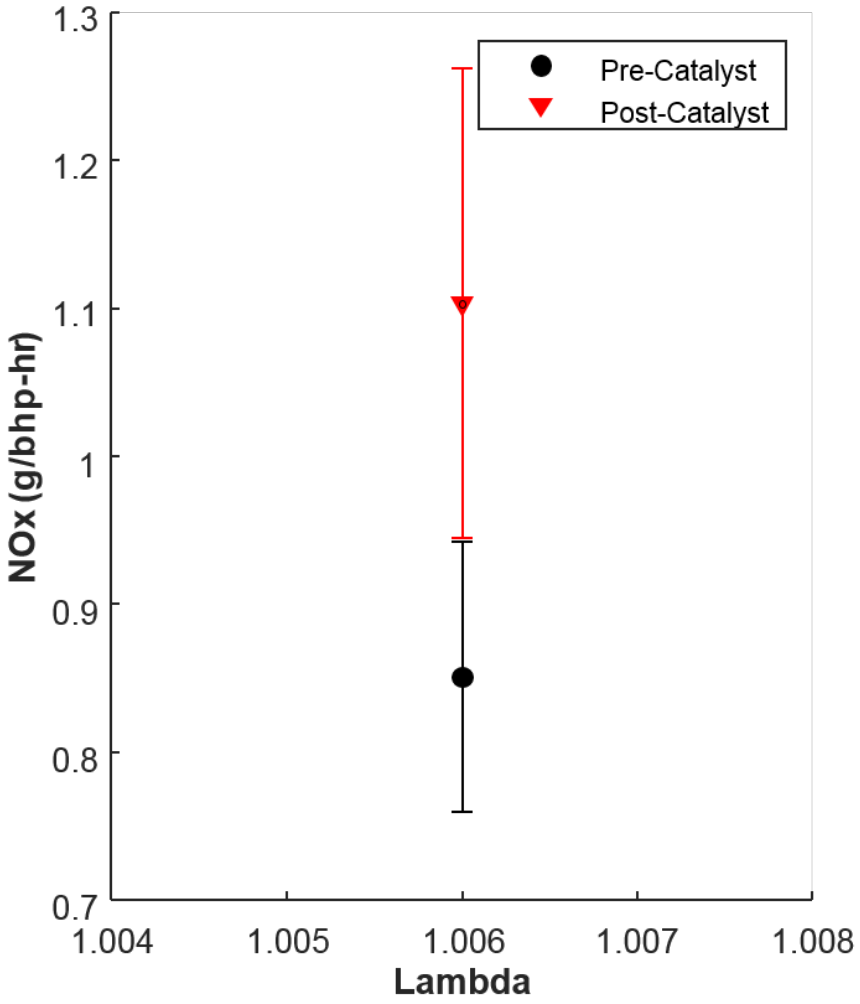

Figure 5.20: Full uncertainty analysis of pre and post catalyst NO_x emissions

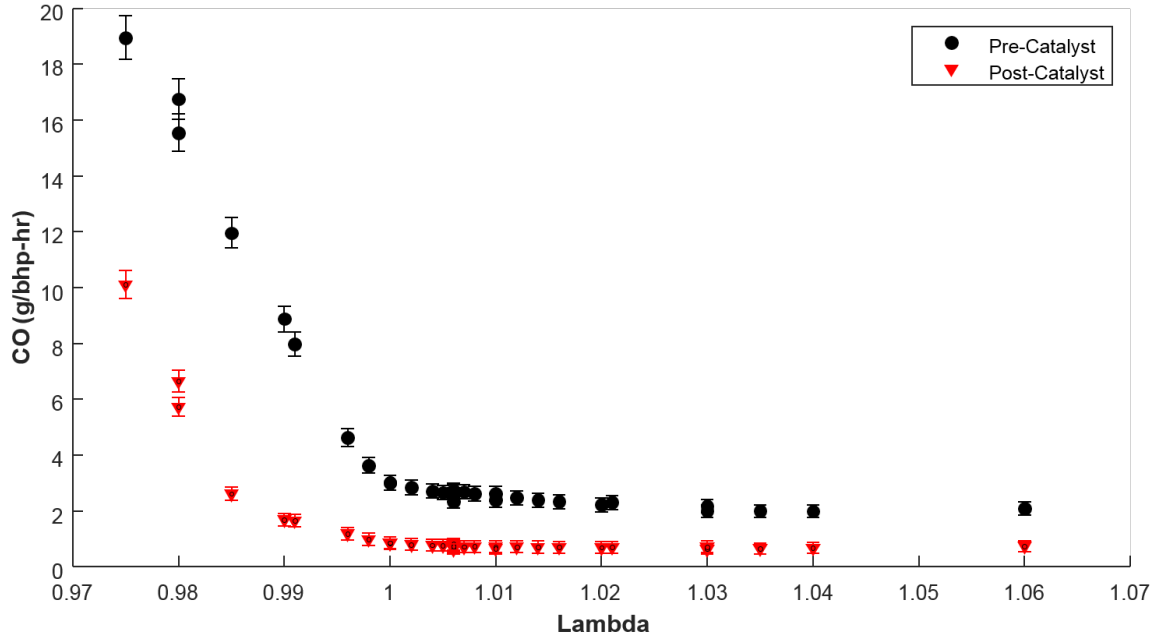

Figure 5.21: Pre and post catalyst CO data as collected by the 5 gas analyzer during the dedicated EGR air-fuel ratio sweep.

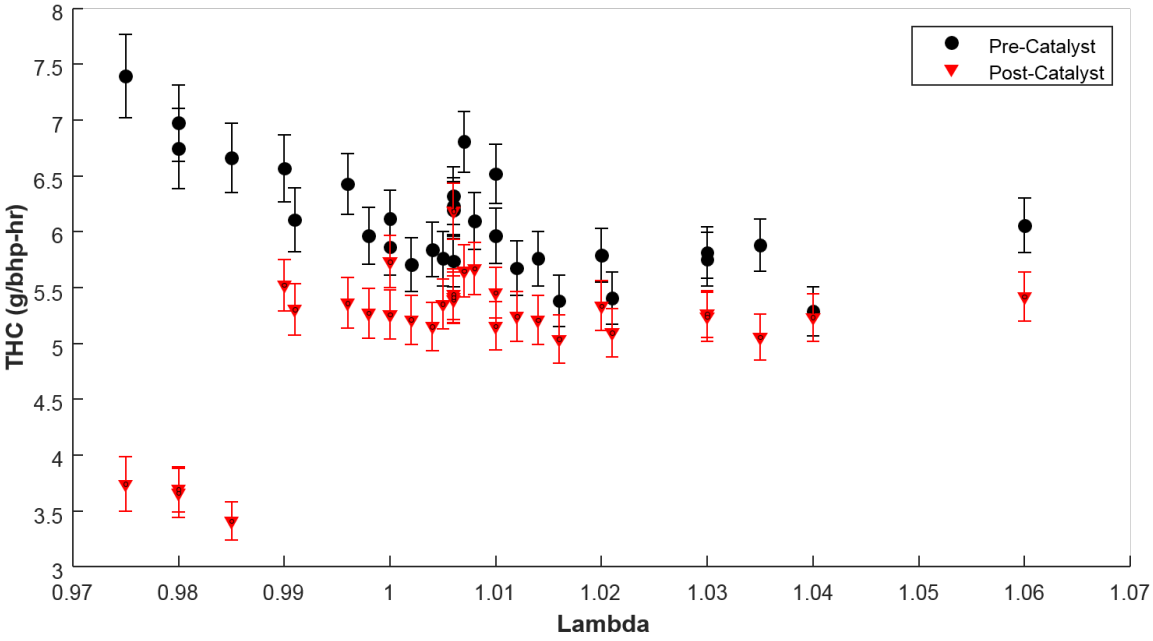

Figure 5.22: Pre and post catalyst THC data as collected by the 5 gas analyzer during the dedicated EGR air-fuel ratio sweep.

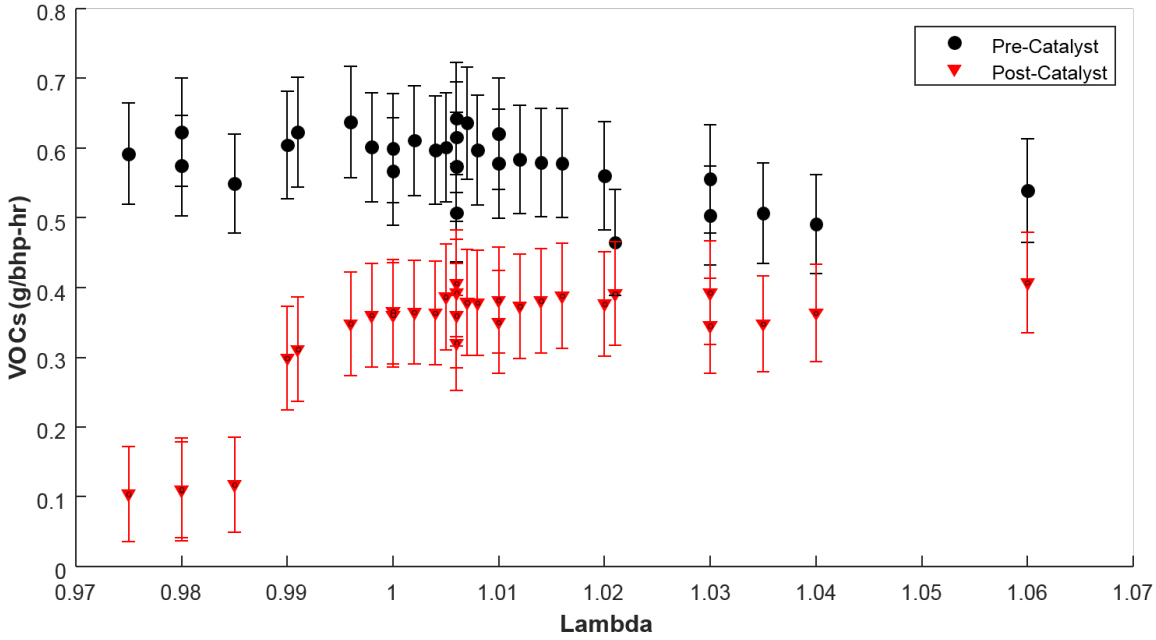

Figure 5.23: Pre and post catalyst VOC data as collected by the FTIR analyzer during the dedicated EGR air-fuel ratio sweep.

5.6 Conclusions

A rich burn industrial natural gas engine was modified to operate with dedicated exhaust gas recirculation. A commercially available non-selective catalyst was paired with then engine to understand how catalyst reduction efficiency and post catalyst emissions would be affected by operating an engine with dedicated EGR. While holding all other conditions constant an air-fuel ratio sweep was carried out on the engine operating as stock rich burn and with dedicated EGR. The following conclusions can be made based on the results from this work.

- Based on regulated post catalyst emissions, the range of air-fuel ratio in which emissions criteria were met was increased from 0.001 lambda while operating as a rich burn engine to 0.075 lambda while operating with dedicated EGR. This was due to the low post catalyst NO_x emissions across the entire lambda sweep.

- Across the entire dedicated EGR lambda sweep (0.970 – 1.06) pre-catalyst NO_x emissions remained below 1.3 g/bhp-hr. This was below the target of 2.0 g/bhp-hr and suggests that

only an oxidation catalyst may be used for dedicated EGR engine to meet low emissions requirements targeted in this study.

- The location of the NO_x-CO tradeoff was shifted from approximately 0.992 lambda at baseline conditions to approximately 0.985 lambda using dedicated EGR
- Dedicated EGR catalyst temperatures remained higher at all air-fuel ratios. Catalyst materials suited to exposure to higher temperatures should be considered while operating this engine with dedicated EGR.

5.7 References

1. EPA CFR 40 Part 60 Subpart JJJJ. https://www.ecfr.gov/cgibin/retrieveE CFR?gp=&SID=5cad118045b921585dbef4079dc88e3a&r=SUBPART&n=40y7.0.1.1.1.99#se40.8.60_14233

2. DCL International. Catalyst Specifications. https://www.dcl-inc.com/catalyst-specifications/#three-way-catalysts

3. Design and Implementation of a D-EGR Mixer for Improved Dilution and Reformate Distribution. Denton B, Chadwell C, Gukelberger R, and Alger T. SAE Paper 2017-01-0647.

4. Comparison of Dithering and Steady State NSCR Catalyst Control on a 7.5L Rich Burn Engine. Finke J, Olsen DB, Glover E, and Hanson K. Proceedings of the 2016 Gas Machinery Conference. October2-3,2016. Denver, CO.

5. EUROMOT. MWM methane number calculator.https://www.euromot.eu/publication-an d-events/publications/ (accessed 2 November 2018).

6. Kline SJ and McClinktock FA. Uncertainties in single sample experiments. Mech Eng 1953; 75: 3–8.

7. Glassman, Irvin, and Richard A. Yetter. Combustion. Academic Press, Elsevier, 2008.

8. Methane: The other important greenhouse gas. EDF. https://www.edf.org/climate/methane-other-important-greenhouse-gas

9. Evaluating Dedicated Exhaust Gas Recirculation on a Stoichiometric Industrial Natural Gas Engine. Van Roekel C, Montgomery, DT, Singh J, and Olsen DB. International Journal of Engine Research DOI: 10.1177/1468087419864733

10. Response Surface Method Optimization of a Natural Gas Engine with Dedicated Exhaust Gas Recirculation. Van Roekel C, Montgomery, DT, Singh J, and Olsen DB. International Journal of Engine Research

11. Heywood JB. Internal combustion engine fundamentals. New York: McGraw-Hill, 1988.

Chapter 6

Considerations on dedicated EGR Impact on Exhaust Gas Temperature

6.1 Exhaust Temperature at Rated Power

After finding improved engine operating conditions and compliance windows for baseline rich burn and dedicated EGR an analysis of the impact that dedicated EGR has on exhaust temperatures was done. Initially, exhaust port temperatures were thought to give a good representation of how dedicated EGR might be able to lower combustion temperatures and increase the rated power of rich burn industrial natural gas engines. However, after examination it was determined that during this work using the G3304, combustion chamber exhaust port temperatures were not necessarily an appropriate means to measure how dedicated EGR had an impact on combustion temperature. Appendix B includes detailed information about the knock margin tests performed on the G3304 engine prior to converting it to a dedicated EGR engine. A result from those tests is shown in Figure 6.1. In this figure a comparison is made between two no-dEGR tests. The operating conditions for each test are as follows: rated engine power of 6.7 bar bmep and rated speed, similar fuel composition of a MWM fuel methane number of 72, an intake manifold temperature of 30 °C, intake manifold pressure of 12.1 psia, and jacket water outlet temperature of 95 °C. The only difference between the two tests is the spark timing. The legend in Figure 6.1 lists advanced timing which means a spark timing of 34 °bTDC and retarded timing which means a spark timing of 24.5 °bTDC. The average decrease in exhaust port temperature seen in Figure 6.1 resulting from advanced combustion phasing is 29 °C. Examining the combustion statistics of 10, 50, and 90% reveals that there was no change in rate of combustion between the two tests. The average location of 10, 50, and 90% burn locations for the advanced timing tests was -9.76, 2.79, and 21.21 °aTDC, respectively. While the average location of 10, 50, and 90% burn locations for

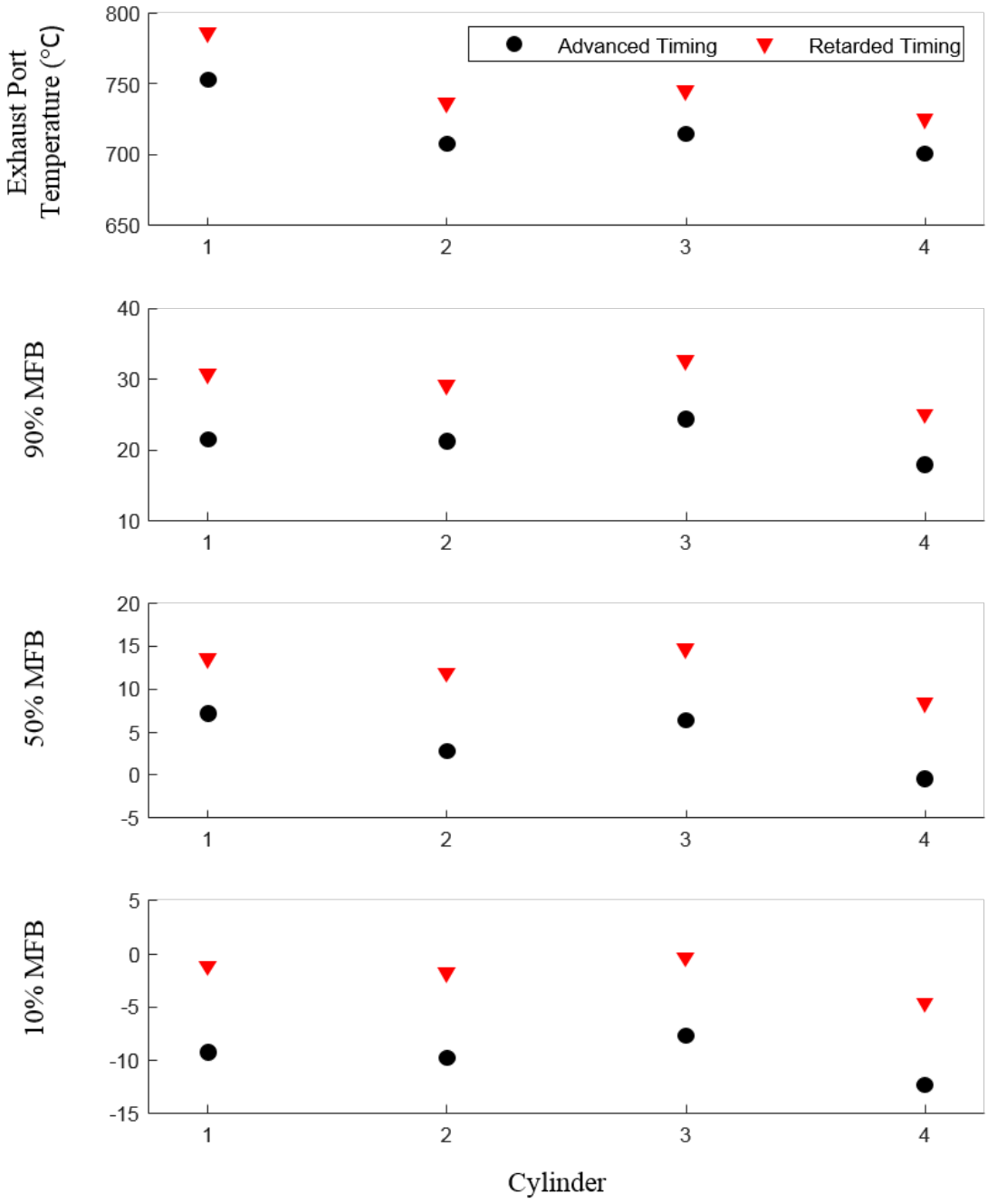

Figure 6.1: Exhaust port temperature and combustion statistics as a function of spark timing while the G3304 engine was operating without dedicated EGR. Operating conditions other than spark timing were held constant between the two tests. The impact that combustion phasing has on exhaust port temperature is apparent.

Table 6.1: Engine operating conditions for the test results shown in Figure 6.2

Operating Conditions		
	Baseline	Dedicated EGR
Speed (rpm)	1800	1800
BMEP (bar)	6.7	6.7
IMAT (°C)	40	62
IMAP (psia)	12.0	18.3
Spark Timing (°bTDC)	30	45
Spark Duration (μs)	150	365
Dedicated Cylinder AFR (Lambda)	—	0.94
Global Lambda	0.990	0.990
MWM Methane Number	71	71

the retarded timing was -1.85, 11.89, and 29.05 °aTDC, respectively. Differences in exhaust port temperatures due to changes in combustion phasing are one of the reasons why comparing different engine operating conditions is normally done using similar locations of 50% burn location. With the relationship between combustion phasing and exhaust port temperature laid out for the G3304 engine, the impact that dedicated EGR has on exhaust port temperatures can be examined. Figure 6.2 displays exhaust port temperatures and 10, 50, and 90% burn locations for dedicated EGR and baseline no-EGR tests. The points of operation displayed were selected to allow a direct comparison between baseline and dedicated EGR. Table 6.1 shows the operating conditions for the test results shown in Figure 6.2. The global AFR of 0.990 was chosen because it lies within the baseline, no-EGR and dedicated EGR compliance windows as demonstrated by Figures 5.5 and 5.7. The other dedicated EGR operating conditions were chosen from the best performance results from Chapter 4. It is important to note here the difference in spark timing. The no-EGR spark timing is 30 °bTDC and the dedicated EGR spark timing is 45 °bTDC. Beginning with the location of 10% burn location a clear difference in overall burn rate and differences in cylinder-cylinder burn rate is observed. First, cylinder four shows the largest discrepancy between the no-EGR and dedicated EGR 10% MFB location. The 0-10% burn duration for the no-EGR test was approximately 20 crank angle degrees while the dedicated EGR duration was approximately 45. Longer

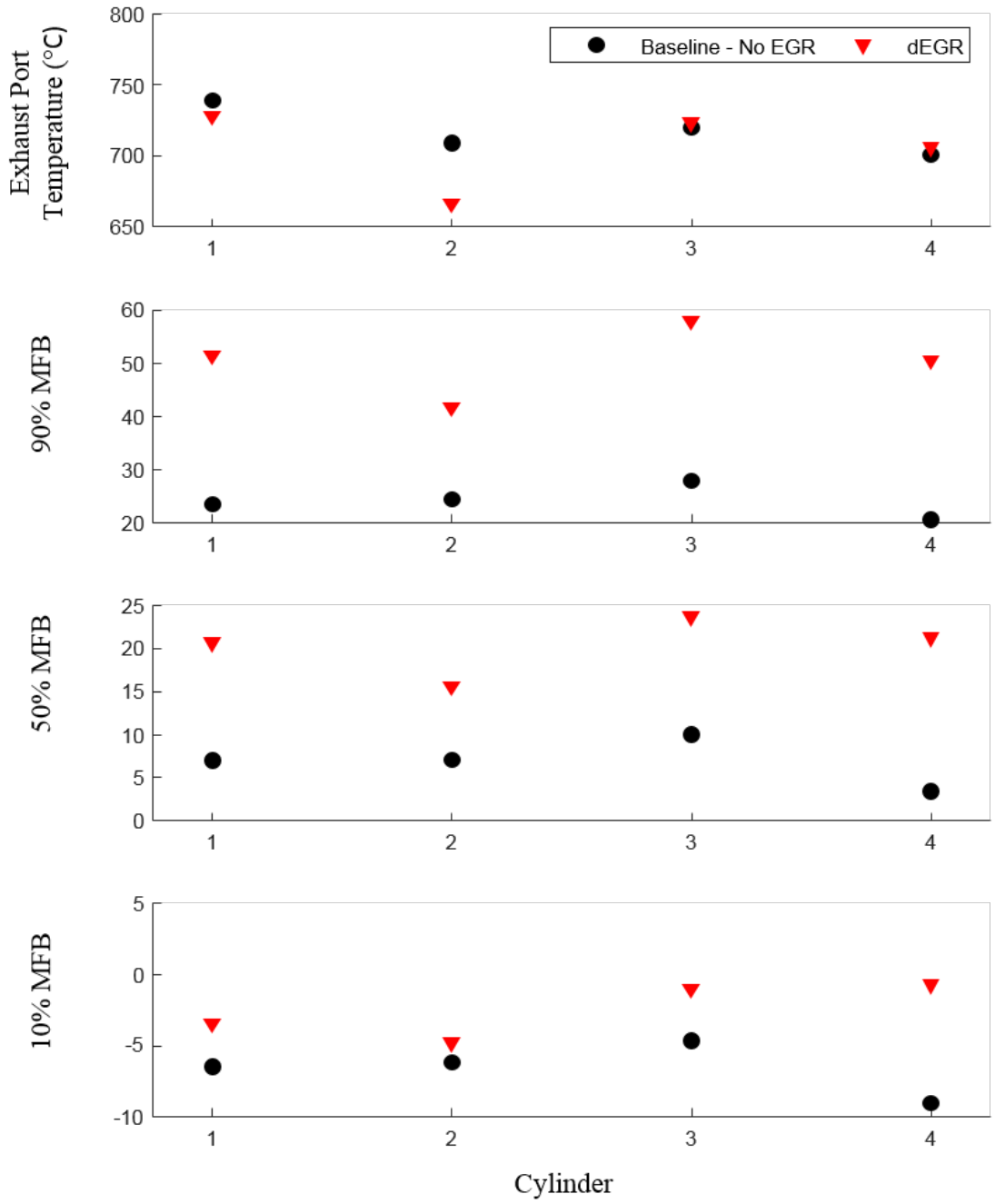

Figure 6.2: Exhaust port temperature and combustion statistics as a function of spark timing while the G3304 engine for no-EGR operating conditions and dedicated EGR operating conditions.

burn duration was also observed in the 10-90 MFB burn duration where the no-EGR duration for cylinder four was approximately 30 crank angle degrees and the dedicated EGR duration was approximately 51 crank angle degrees. Ultimately, the prolonged burn duration of cylinder 4 during the dedicated EGR test resulted in a similar exhaust port temperature to the no-EGR test. Due to the intake manifold design cylinder two showed faster rate of combustion while operating with dedicated EGR. The 0-10% burn duration for the no-EGR test was 24 crank angle degrees and the dedicated EGR duration was approximately 40 crank angle degrees. Shortened burn duration in cylinder 2 during the dedicated EGR test can also be seen by comparing the location of the 90% MFB location which was 41 °aTDC and 50 °aTDC for cylinder 4. Based on examining exhaust port temperatures alone it does not appear that dedicated EGR improves combustion temperature and ultimately exhaust component temperature. However, as mentioned, when comparing exhaust temperatures of differing engine operating conditions it is recommended to match the location of 50% burn location. Based on the the results shown in Figure 6.1 if the location of 50% burn location were to be matched a decrease in dedicated EGR exhaust port temperature would be observed. When comparing the dedicated EGR results to the baseline results it is more appropriate to match the location of 90% burn location rather than the 50% burn location based on the varying burn rates. Excluding results from cylinder two the average difference between dedicated EGR and no-EGR 50% burn location is approximately 15 crank angle degrees and the difference between 90% burn location is approximately 30 crank angle degrees. Thus, matching the location of 90% MFB to make exhaust temperature comparisons is preferred. Due to the discrepancy between location of 90% MFB in tests shown in Figure 6.2 the impact that dedicated EGR can have on lower combustion temperatures can't be accurately assessed using exhaust port temperatures alone.

A more conclusive measure to quantify the positive effect that dedicated EGR can have on combustion temperatures (ultimately exhaust component temperatures) is peak combustion temperature. The Chemkin SI Zonal reactor described in Section 2.3 was used to model combustion from the tests described in Table 6.1. The reactant species fuel composition and dedicated EGR composition were updated per measurements made during the physical engine test. The combus-

tion burn profile was updated with 10, 50, and 90% mass burned locations per measurements by the high speed combustion analyzer during the engine test. The combustion chamber heat transfer properties remained the same as described in Section 2.3. Based on this model the peak combustion temperature achieved with dedicated EGR was 2100 K and the peak combustion temperature achieved without using EGR was 2580 K. A decrease in combustion temperature using EGR was expected, but its impact on the longevity of exhaust components remains inconclusive from this analysis. Even without a significant decrease in exhaust port temperature combustion temperature is decreased based on the significant reduction in engine out NO_x as shown in Figure 5.9 and the results from the Chemkin SI Zonal reactor model.

A final highlight of the improvements made to dedicated cylinder combustion and consolidating individual cylinder power output is shown in Figure 6.3. Data presented in this figure is the mass fraction burned, apparent heat release rate, and cylinder pressure of the two test conditions described in Table 6.1. The dedicated EGR data has been separated into the dedicated cylinder and the average 'stoichiometric' (lambda 0.990) cylinder data sets. Combustion statistics of 10, 50, and 90% burn location are presented in Figure 6.2 are shown graphically in Figure 6.3. The results shown here can be compared to the initial combustion statistics at 6.7 bar BMEP shown in Figure 3.12 where operating conditions of the dedicated cylinder and other cylinders were chosen with little insight into how a dedicated EGR natural gas engine would operate. After the RSM optimization completed in Chapter 4 the dedicated cylinder combustion statistics of mass fraction burned, apparent heat release rate, and cylinder pressure have all been matched to the 'stoichiometric' cylinder statistics. This result also shows how the RSM optimization operating conditions translate to other engine operating points. The RSM optimization was done at 3.4 bar and rated engine speed while this data was collected at 6.7 bar and rated engine speed.

6.2 Increased BMEP

As described in Chapter 1 the primary industry motivation for exploring dedicated EGR is increasing rich burn engine BMEP without increasing exhaust component temperature. The final

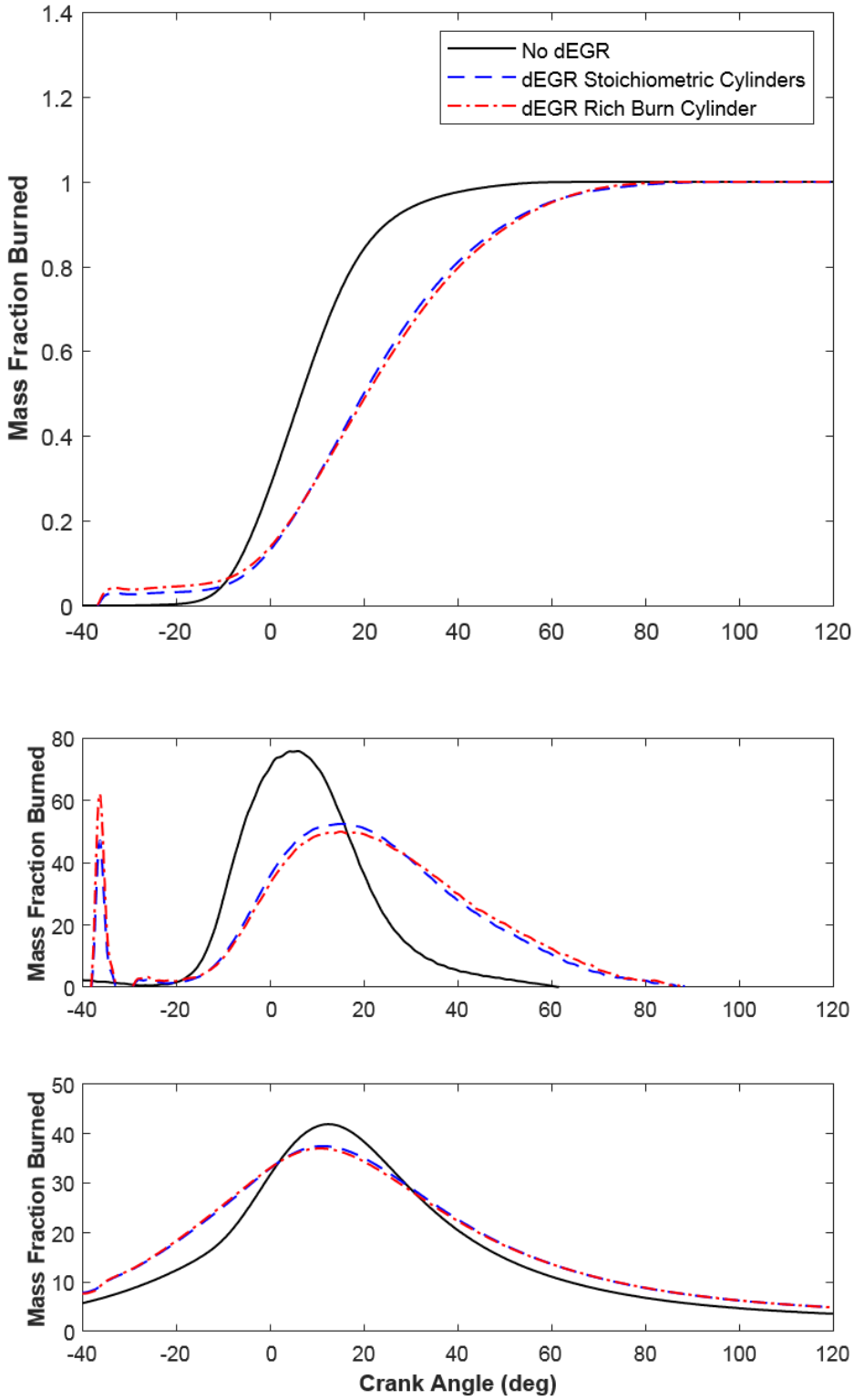

Figure 6.3: Combustion statistics at 6.7 bar BMEP and engine operating conditions described in Table 6.1. Stoichiometric cylinder data is averaged from the three near stoichiometric cylinders, and the no dEGR data is averaged from all four engine cylinders.

Table 6.2: Engine operating conditions for tests at increased engine BMEP.

Operating Conditions		
	Increased BMEP 1	Increased BMEP 2
Speed (rpm)	1800	1800
BMEP (bar)	7.1	7.4
IMAT (°C)	64	62
IMAP (psia)	18.9	19.5
Spark Timing (°bTDC)	45	45
Spark Duration (μs)	365	365
Dedicated Cylinder AFR (Lambda)	0.94	0.94
Global Lambda	0.990	0.990
MWM Methane Number	71	71

engine tests conducted on the G3304 were done to understand how much the engine BMEP could be increased before exceeding exhaust temperatures found in the no-dEGR conditions. The baseline reference exhaust temperatures can be found in Figure 6.2 and are 739, 709, 720, and 701 for cylinders 1, 2, 3, and 4, respectively. The baseline operating conditions which produced these exhaust temperatures are found in Table 6.1. While operating with dedicated EGR, the engine speed was maintained near rated speed and torque was increased. The simulated turbocharger system described in Chapter 3 was used to increase intake manifold pressure to allow for additional torque to be added to the engine. Two increased BMEP data points were collected. Table 6.2 shows the two operating conditions for these two points. In Figure 6.4 baseline reference exhaust port temperatures are compared to the 7.1 and 7.4 bar BMEP dedicated EGR exhaust port temperatures. Discussion of these results follows that of the discussion in the previous section with regards to differences in cylinder burn rates resulting in varying exhaust port temperatures and dedicated EGR results being skewed by long burn duration. It was argued in the previous section that due to longer burn rates associated with dedicated EGR analysis of the location of 90% burn fraction explained unexpectedly high exhaust port temperatures in cylinders 1, 3, and 4. At the 7.4 bar BMEP dedicated EGR operating point the location of 90% burn fraction in cylinder 2 was 40 °aTDC. This was 10 degrees advanced of the 90% burn fraction location in cylinders 1 and 4, and 16 degrees

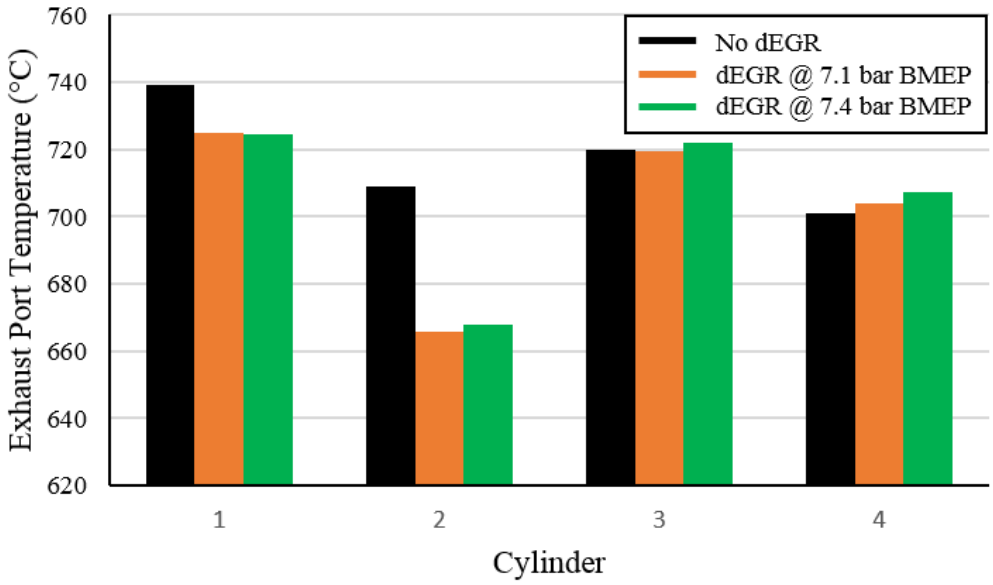

Figure 6.4: Exhaust port temperatures for dedicated EGR engine operating points at 7.1 and 7.4 bar BMEP. The reference no-dEGR data is shown in black.

advanced 90% burn fraction location in cylinder 3. Increasing BMEP based the rated BMEP for the G3304 engine was limited to 7.4 bar due to exhaust port temperatures in cylinders 3 and 4. However, results from cylinder 2 show again that if burn duration of dedicated EGR combustion would be shortened the engine power output could be increased even more.

Chapter 7

Conclusions and Recommendations

7.1 Overview

In an effort to assess the viability of dedicated EGR to lower combustion temperatures to increase exhaust component life, tests were carried out on a four cylinder, rich burn industrial natural gas engine and a Chemkin chemical kinetics model was developed. The industrial natural gas engine sector expects robust engine design and components with long life. In comparison to other EGR systems dedicated EGR does not expose control components to high temperature gases. This gives dedicated EGR an advantage over conventional LPL and HPL EGR systems. Dedicated EGR systems have been applied to small gasoline engines and shown that improvements in efficiency can be achieved. This work represents some of the first to apply dedicated EGR to a natural gas engine and explore the capabilities and challenges of the technology.

7.2 Conclusions

Based on this work, the following conclusions about dedicated EGR can be drawn:

1. A Caterpillar G3304 industrial rich burn natural gas engine was converted to operate with dedicated EGR. Based on a literature review, initial power sweeps were conducted at rated speed while operating with dedicated EGR. Combustion in the dedicated cylinder at each operating condition was poor based on combustion statistics of COV of IMEP and IMEP.

2. A RSM optimization was performed to find an improved combustion recipe by changing engine IMAT, spark timing, spark duration, and dedicated cylinder AFR at rated speed and 3.4 bar. Using the stock fine wire spark plugs the RSM optimization was successful at finding an improved combustion recipe. Non-enriched pre-chamber spark plugs were installed and a second RSM optimization was done. The results from the pre-chamber RSM optimization showed no improvement in rate of combustion or COV of IMEP.

3. At rated speed and power (6.7 bar) an AFR sweep of the three non-dedicated cylinders was done. The results showed that dedicated EGR offers low engine out NO_x across a wide range of AFR. This showed that dedicated EGR engines can have a wide emissions compliance window and possibly use only an oxidation catalyst to meet emissions regulations.

4. Analysis of exhaust port temperatures showed that without further improvement to the rate of combustion only a small improvement in exhaust port temperatures can be realized with dedicated EGR. The Chemkin chemical kinetics model was used to show that peak combustion temperatures are lower, but due to the slow rate of combustion exhaust port temperatures remained nearly unchanged when compared to the no-EGR baseline.

7.3 Research Recommendations

1. A large part of this work was focused on improving the combustion recipe of the G3304 engine. Changes were made to the recipe that were within a reasonable scope of this work, but further improvements can be made. As mentioned the combustion chamber did not feature any design that would increase combustion rate. Diluted charge combustion, including any form of EGR, results in slower combustion. Design of a combustion chamber that includes turbulence improvements such as swirl and squish could result in lower exhaust port temperatures by increasing the overall duration of combustion. Swirl could be introduced by modifications to intake runner design or by removing material asymetrically from intake valves. As intake manifold runners are commonly cast into the block of heavy duty natural gas engines making changes to intake valves to promote swirl is recommended. Adding squish to a combustion chamber is accomplished by designing bowl type geometry into the piston. The area of annulus around the bowl dictates and amount of squish. The more area in the annulus the more squish in the design. A second consideration when designing a piston bowl with squish is the transition between the bowl geometry and annulus (squish) area. A common design feature meant to break up combustion charge flow as it exists the squish volume and enters the bowl volume is a re-entrant angle. Detailed analysis of the

effect of re-entrant angle is far outside of the scope of this work, but in general this angle is meant to break up bulk flow into smaller eddies and further promote turbulence in the combustion chamber. An excellent diagram of varying levels of squish and re-entrant bowl geometry can be found in work published by Aldercreutz et al. [20]. The ability for differing amounts of squish and swirl to decrease combustion duration in spark ignited engines has been well documented by numerous authors [1, 20, 21, 22]. However, the addition of swirl has a a drawback of higher heat transfer losses due to increased convective heat transfer to the cylinder walls. [23] Thus, there is a tradeoff between increasing rate of combustion and increasing heat transfer to the cylinder walls when adding swirl to a combustion recipe. The recommendation of the author is that prior to further on engine testing of dedicated EGR simulation and analysis of varying degrees of swirl and squish be performed. The results from that simulation should be used to develop a piston design that results in increased rate of combustion. Further, that simulation should be performed for near stoichiometric cylinders and dedicated cylinder(s) on a dedicated EGR engine due to the different AFR in the respective cylinders.

2. Ignition of diluted, rich combustion in the dedicated cylinder proved to be difficult and limited the amount of additional fuel able to be added to that cylinder. The best combustion was found with fine wire spark plugs and a dedicated cylinder AFR of lambda 0.936. Further improvements in rate of combustion and COV of IMEP can be realized by increasing the additional fuel delivered to the dedicated cylinder. Future work should explore higher energy ignition systems capable of igniting combustion charge at non-optimal conditions. Perhaps, the first step in ignition source work should be the exploration of performance of j-gap spark plugs. Due to relatively low cost and reliability, j-gap type spark plugs are used throughout the industrial natural gas engine industry.

3. The G3304 engine featured a relatively low compression ratio of 10.5. It was found that dedicated EGR mitigated engine knock and allowed for very advanced spark timing. A higher compression ratio could be explored to improve engine efficiency.

Bibliography

[1] Heywood JB. *Internal Combustion Engine Fundamentals*. McGraw-Hill, 1988.

[2] United States Environmental Protection Agency. Subpart jjjj-standards of performance for stationary spark ignition internal combustion engines, January 2008. https://www.ecfr.gov/cgi-bin/retrieveECFR?gp=&SID=5cad118045b921585dbef4079dc88e3a&r=SUBPART&n=40y7.0.1.1.1.99.

[3] Turns SR. *An Introduction to Combustion: Concepts and Applications*, volume 3. McGraw-Hill, 2012.

[4] Yetter RA Glassman I. *Combustion*, volume 5. Academic Press, 2014.

[5] Grumstrup T. *NOx Formation in Methyl Ester, Alcohol, and Alkane Droplet Autoignition and Combustion: PLIF Measurements and Detailed Kinetic Modeling*. PhD thesis, Department of Mechanical Engineering, Colorado State University, Fort Collins, CO, 2014.

[6] Shapiro HN Moran MJ. *Fundamentals of Engineering Thermodynamics*, volume 7. John Wiley & Sons, Inc., 2011.

[7] Caton JA. Quantification of efficiency gains for dilute ic engines due to increases of theratio of specific heats. *Proceedings of the ASME 2014 Internal Combustion Engine Division Fall Technical Conference*, pages ICEF2014–5403, 2014.

[8] Le Chatelier H Mallard E. *Annals of Mines*, volume 4. 1883.

[9] Hoops C Glewen W. Comparative analysis of egr and air dilution in spark-ignited natural gas engines. *Proceedings of the ASME 2017 Internal Combustion Engine Division Fall Technical Conference*, pages ICEF2017–3608, 2017.

[10] Choi Y Lim G. Effects of hpl and lpl egr gas mixed supply on combustion and emissions in automotive diesel engine. *SAE International*, pages SAE 2011–01–1831, 2011.

[11] Zongjie L Chao Y. Comparison of fuel economy improvement by high and low pressure egr system on a downsized boosted gasoline engine. *SAE International*, pages SAE 2017–01–0682, 2017.

[12] Yin L Svensson E. Combined low and high pressure egr for higher brake efficiency with partially premixed combustion. *SAE International*, pages SAE 2017–01–2267, 2017.

[13] Macek J Vitek O. Comparison of different egr solutions. *SAE Technical Paper Series*, pages SAE 2008–01–0206, 2008.

[14] Baar R Gonzalez N. Thermodynamics of exhaust gas condensation. *SAE International*, pages SAE 2017–01–9281, 2017.

[15] Gingrich J Alger T. The effect of hydrogen enrichment on egr tolerance in spark ignited engines. *SAE Technical Paper Series*, pages SAE 2007–01–0475, 2007.

[16] Heywood JB Gerty M. An investigation of gasoline engine knock limited performance and the effects of hydrogen enhancement. *SAE Technical Paper Series*, pages SAE 2006–01–0228, 2006.

[17] Heywood JB Ivanic Z. Effects of hydrogen enhancement on efficiency and nox emissions of lean and egr-diluted mixtures in a si engine. *SAE Technical Paper Series*, pages SAE 2005–01–0253, 2005.

[18] Caterpillar. G3516 ta, 2017. https://www.cat.com/en_US/products/new/power-systems/oil-and-gas/gas-compression-engines/1000034159.html.

[19] Caterpillar. Caterpillar oil & gas introduces g3516 ta stoichiometric gas engine, 2017. https:// www.cat.com/en_US/news/engine-press-releases/caterpillar-oil–gas-introduces-g3516-ta- stoichiometric-gas-engine.html.

[20] Stenlaas O Adlercreutz L, Cronhjort A. Variation in squish length and swirl to reach higher levels of egr in a cng engine. *SAE International*, pages SAE 2019–01–0081, 2019.

[21] Okumura T Ueda T. Effets of squish area shape on knocking in a four-valve spark ignition engine. *SAE International*, pages SAE 1990–01–1494, 1990.

[22] Kadota T Fukano Y, Hisaki H Kida S. Two-dimensional in-cylinder flow field in a natural gas fueled spark ignition engine probed byparticle tracking velocimetry and its dependence on engine specifications. *SAE International*, pages SAE 1999–01–1534, 1999.

[23] Martin J Olmeda P. A combination of swirl ratio and injection strategy to increase engine efficiency. *SAE International*, pages SAE 2017–01–0722, 2017.

[24] Kocsis M Mitchell R. Performance evaluation of dedicated egr on a 12 l natural gas engine. *SAE International*, pages SAE 2019–01–1143, 2019.

Appendix A

Test Cell Development

Prior to conducting engine tests on the Caterpillar G3304 work was done to upgrade the measurement and control capability of the test cell which the engine was installed. Documentation of this upgrade is useful for future engine installations which will need to interface with the National Instruments input/output hardware. The following are lists and pictures of the available input/output hardware currently installed (as of 5-21-19) on the small engine test cell at the Powerhouse.

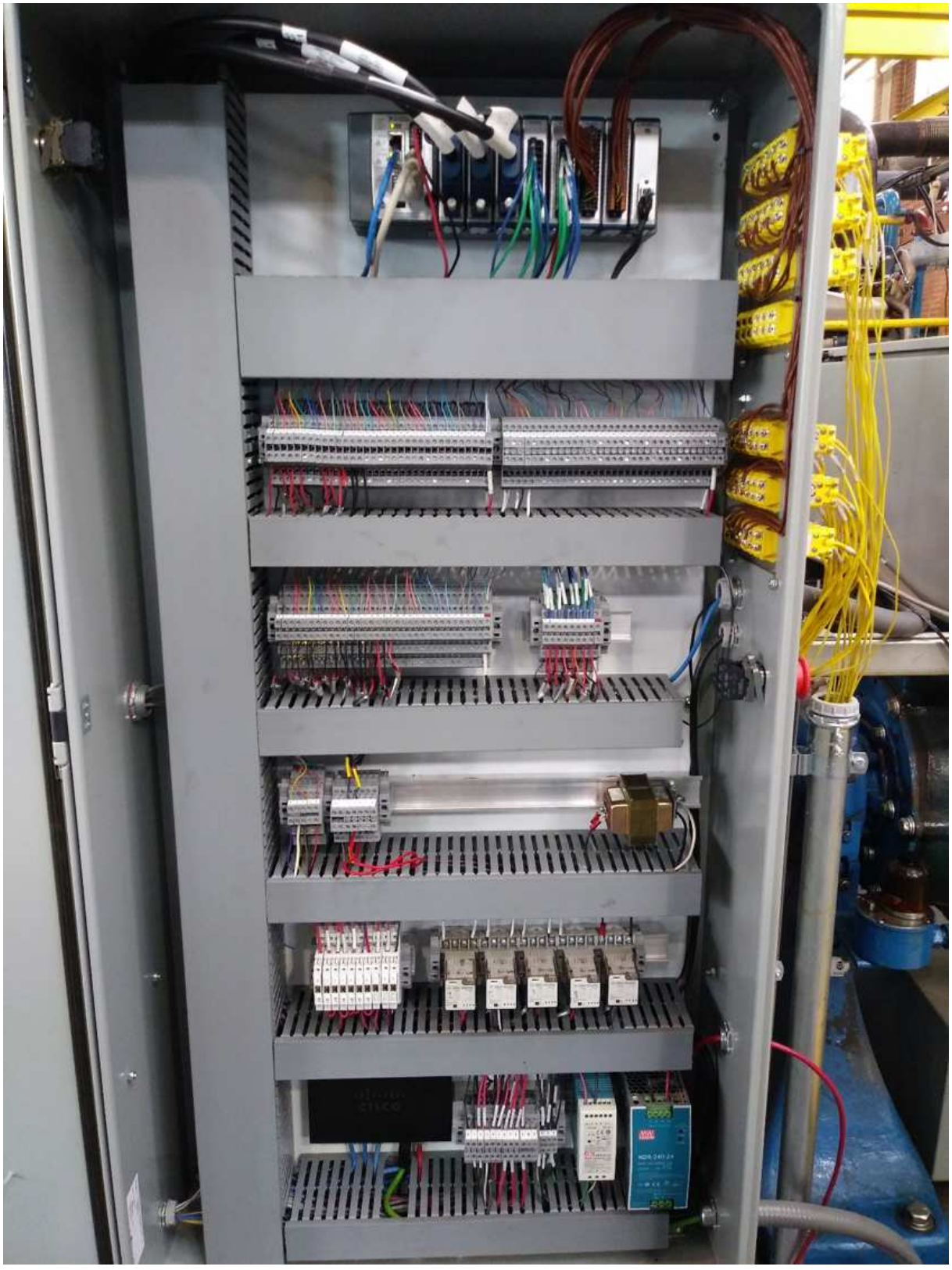

Figure A.1: The upgraded NI (National Instruments) test cell control cabinet.

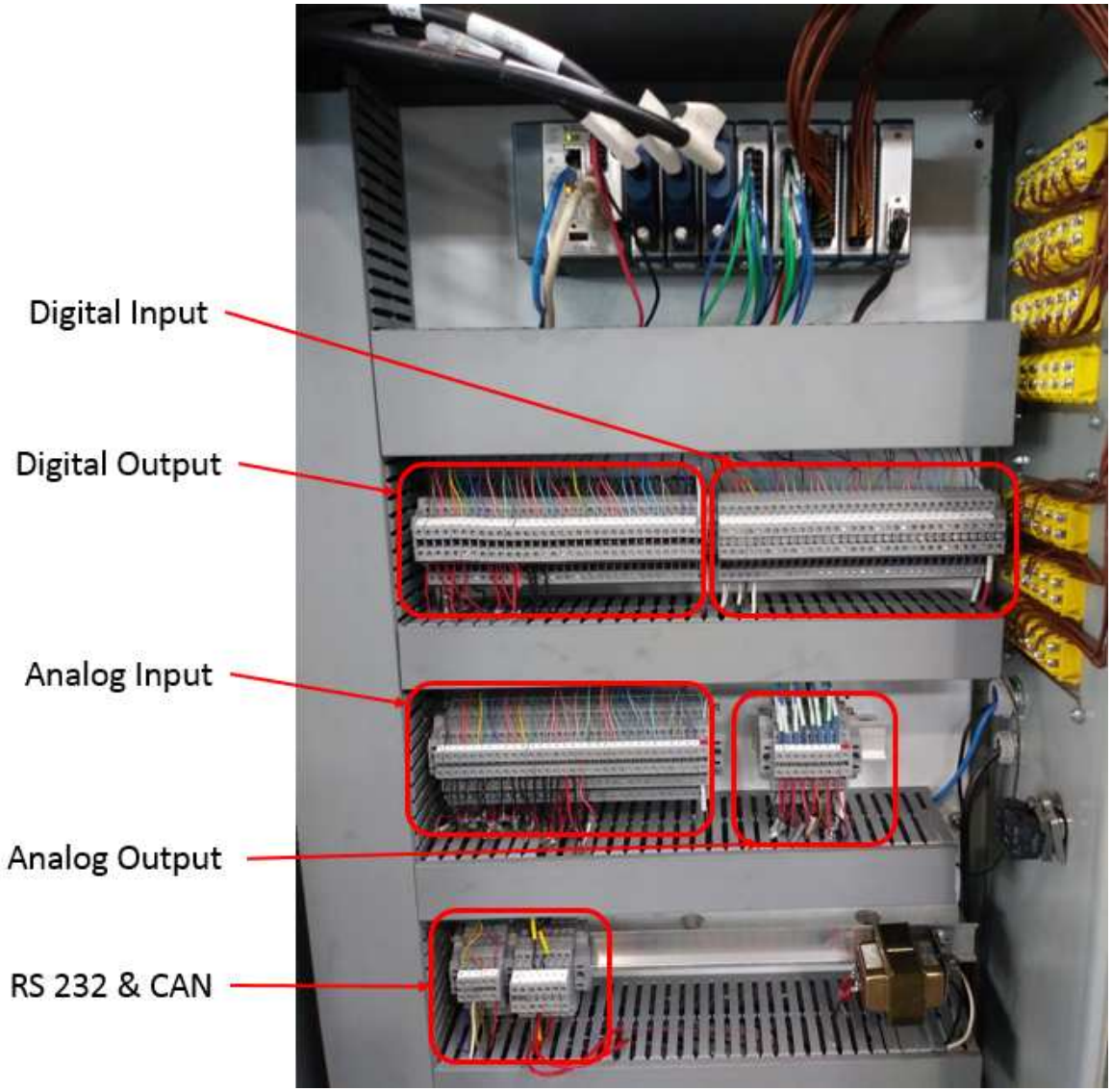

Figure A.2: Digital and analog input/output terminal blocks in the test cell control cabinet. The cabinet also has capabilities to communicate with devices via RS232 and high speed CAN (given that the correct NI card is installed).

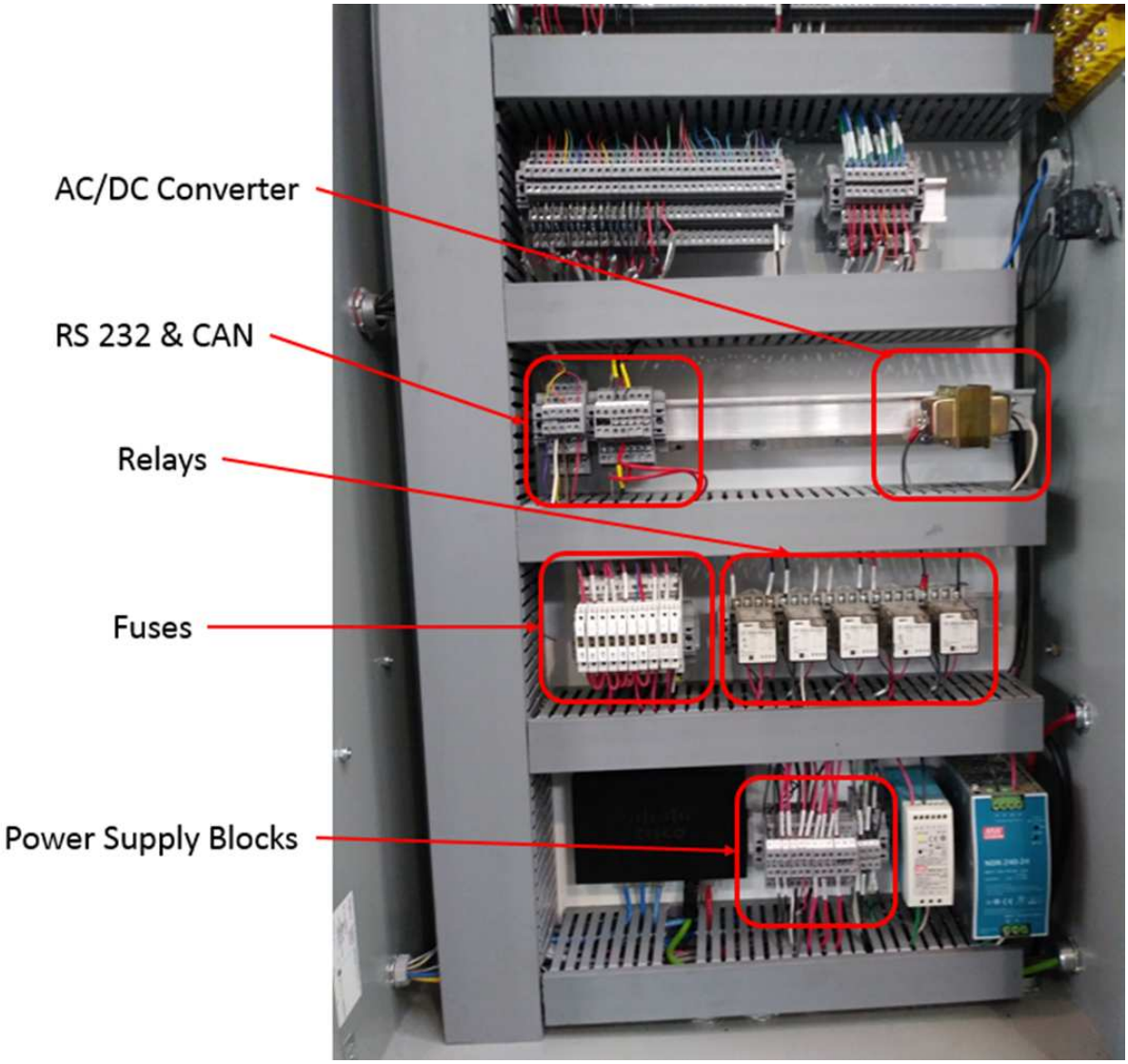

Figure A.3: The lower half of the cabinet contains test cell power management hardware. 120 VAC, 12 VDC, and 24VDC power supply is available in the cabinet.

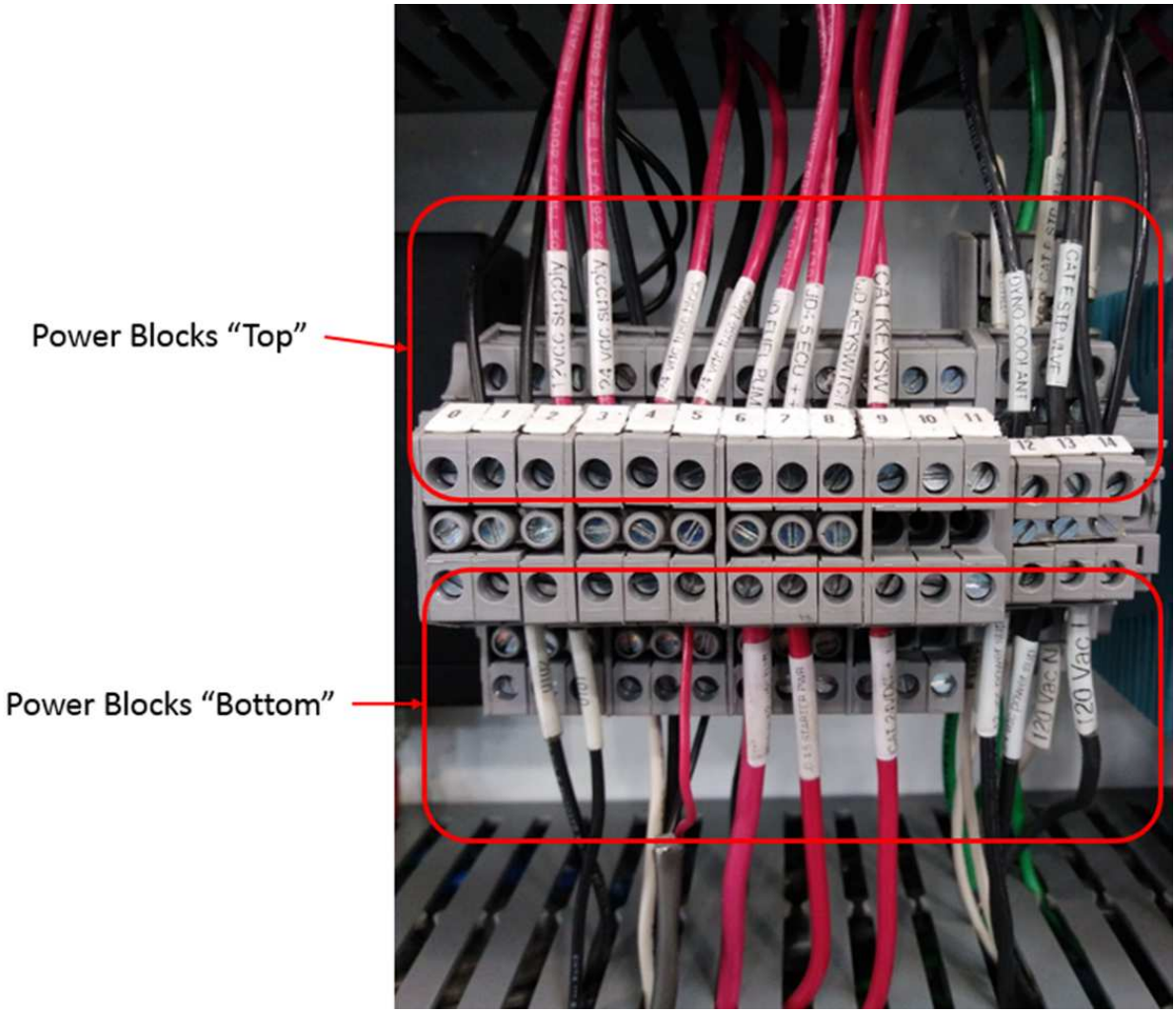

Figure A.4: The power supply area divided into upper and lower terminal block connections.

NI 9425 DI (Chassis 01)	CAT or JD I/O	Description	
0100	CAT	CAT LECM Keyswitch power on/off	KSW on = signal true
0101	CAT	Test Cell Emergency Stop button signal	Hit button = signal true
0102	JD	Test Cell Emergency Stop button signal (John Deere 4.5L side)	Hit button = signal true
0103	CAT	LECM LS05 Alarm Signal	
0104	CAT	LECM LS06 Alarm Signal	
0105			Unused
0106			Unused
0107			Unused
0108			Unused
0109			Unused
0110			Unused
0111			Unused
0112			Unused
0113			Unused
0114			Unused
0115			Unused
0116			Unused
0117			Unused
0118			Unused
0119			Unused
0120			Unused
0121			Unused
0122			Unused
0123			Unused
0124			Unused
0125			Unused
0126			Unused
0127			Unused
0128			Unused
0129			Unused
0130			Unused
0131			Unused

Figure A.5: Digial input channels used.

NI 9476 DO (Chassis 02)	CAT or JD I/O	Description	
0200	JD	Relay #1	JD 4.5 L Keyswitch On and Fuel Pump On
0201	BOTH	Relay #2	Dyno Coolant Tap Water Valve Open/Close
0202	CAT	Relay #3	CAT Emergency Fuel Valve
0203	CAT	Relay #4	CAT Drive Enable
0204	BOTH	Relay #5	Test Cell Jackwater Coolant Pump On/Off
0205			Unused
0206			Unused
0207	CAT		CAT Engine Starter
0208	JD		JD Engine Starter
0209	CAT	CAT VFD	AC Motor Run Enable CW
0210	CAT	CAT VFD	AC Motor Run Enable CCW (correct direction)
0211	CAT	CAT Engine Run Command	
0212	CAT	CAT Emergency LECM Stop	Digital signal sent directly to LECM. True signal = run permissive to LECM
0213	CAT	LECM Fault Clear (AL82)	Used to clear the Emergency Stop Fault
0214			Unused
0215			Unused
0216			Unused
0217			Unused
0218			Unused
0219			Unused
0220			Unused
0221			Unused
0222			Unused
0223			Unused
0224			Unused
0225			Unused
0226			Unused
0227			Unused
0228			Unused
0229			Unused
0230			Unused
0231			Unused

Figure A.6: Digial output channels used.

NI 9205 AI (Chassis 03)	CAT or JD I/O	Description	Measurement Range	Signal Range
0300	JD	JD Intake Manifold Pressure	0-50 psig	1-5 Vdc
0301	JD	JD Exhaust Manifold Pressure	0-50 psig	1-5 Vdc
0302	JD	JD Stack Exhaust Pressure (not used	0-5 psig	1-5 Vdc
0303	JD	JD Oil Pressure	0-100 psig	1-5 Vdc
0304	JD	JD Post Turbo Exhaust Pressure	0-50 psig	1-5 Vdc
0305	JD	JD Open	0-50 psig	1-5 Vdc
0306	JD	JD Open	0-50 psig	1-5 Vdc
0307	JD	JD Post Compressor / Pre Intercooler Pressure	0-50 psig	1-5 Vdc
0308	CAT	CAT Gas Flow Differential Pressure	0-40 Inches H2O	1-5 Vdc
0309	CAT	CAT Gas Flow Absolute Pressure	0-50 psiA	1-5 Vdc
0310	CAT	CAT Intake Manifold Air Pressure	0-50 psiA	1-5 Vdc
0311	CAT	CAT 3 Cylinder Exhaust Manifold Pressure	0-50 psiA	1-5 Vdc
0312	CAT	CAT Donor Cylinder Exhaust Pressure	0-50 psiA	1-5 Vdc
0313		Left wire in place but it is not connected to a sensor		Unused
0314	CAT	CAT Back Pressure Valve Position Feedback	Fully Closed-Fully Open	1-5 Vdc
0315	CAT	CAT VFD	Actual Speed	0 - +10Vdc
0316	CAT	CAT Post Blower Pressure	0-150 psiA	1-5 Vdc
0317	BOTH	Test Cell Jacket water bypass valve position feedback	Unsure of the sign convention (fully open = 10vdc?)	0-10 Vdc
0318				Unused
0319				Unused
0320				Unused
0321				Unused
0322				Unused
0323				Unused
0324				Unused
0325				Unused
0326				Unused
0327				Unused
0328				Unused
0329				Unused
0330				Unused
0331				Unused

Figure A.7: Analog input channels used.

NI 9263 AO (Chassis 04)	CAT or JD I/O	Description	Measurement Range	Signal Range
0400	BOTH	Test cell Jacket Water bypass valve position control		2-10 Vdc
0401	CAT	CAT VFD		0 - +10 Vdc
0402	CAT	CAT stoichiometric Exhaust Manifold Pressure	0-50 psiA	0 - + 10 Vdc
0403	CAT	CAT Dedicated Exhaust Pressure	0-50 psiA	0 - + 10 Vdc

NI 9265 AO (Chassis 05)	CAT or JD I/O	Description	Measurement Range	Signal Range
0500	JD	JD Intercooler Coolant Control Valve		4-20 mA
0501	CAT	Alicat Analog set point input	0-50 SLPM	4-20 mA
0502	CAT	CAT Back Pressure Valve Position		4-20 mA
0503	CAT	CAT LECM Speed Set Point	Need to Set the Range in Toolkit	4-20 mA

Figure A.8: Analog output channels used.

NI 9213 TC (Chassis 06 & 07)	CAT or JD I/O	Description
0600	JD	JD 4.5 EGR (post EGR cooler)
0601	BOTH	Dyno Coolant Outlet
0602	JD	JD Jacket Water Outlet
0603	JD	JD Intercooler Coolant Outlet
0604	JD	JD Exhaust Gas Aftertreatment Inlet
0605	JD	JD Jacket Water Inlet
0606	BOTH	Dyno Coolant Inlet
0607	JD	JD Oil
0608	JD	JD Cylinder 3 exhaust
0609	JD	JD Post Intercooler Intake Air
0610	JD	JD Intke Ambient Air (Pre compressor)
0611	JD	JD Cylinder 2 exhaust
0612	JD	JD Exhaust Gas Aftertreatment Outlet
0613	JD	JD Post Compressor (Pre Intercooler) Intake Air
0614	JD	JD Cylinder 4
0615	JD	JD Cylinder 1
0700	CAT	CAT EGR Coolant Inlet
0701	CAT	CAT Cylinder 2 Exhaust
0702	CAT	CAT Cylinder 4 Exhaust
0703	CAT	CAT Cylinder 3 Exhaust
0704	CAT	CAT Cylinder 1 Exhaust
0705	CAT	CAT Post Catalyst Exhaust Temp
0706	CAT	CAT Mid Catalyst Exhaust Temp
0707	CAT	CAT Pre Catalyst Exhaust Temp
0708	CAT	CAT Intake Air-Fuel Post Intercooler Temp
0709	CAT	CAT Intake Air-Fuel Pre Intercooler
0710	CAT	CAT EGR Coolant Outlet
0711	CAT	CAT Natural Gas Temp
0712	CAT	CAT Jacket Water Inlet
0713	CAT	CAT Jacket Water Outlet
0714		Unused
0715	CAT	Intake Manifold (air+fuel+EGR)

Figure A.9: Thermocouple channels used.

Power Blocks	CAT or JD I/O	Description	Voltage
0 (Top)	BOTH	Ethernet Switch +/-	12 vdc (power supply)
0 (Bottom)		Unused	12 vdc (power supply)
1 (Top)	BOTH	Dyno Controller Ethernet to serial converter +/-	12 vdc (power supply)
1 (Bottom)	JD	12 vdc power supply for JD test cell emergency stop DI	12 vdc (power supply)
2 (Top)	BOTH	12 vdc Input to power block group 0-2	12 vdc (power supply)
2 (Bottom)	CAT	12 vdc power supply for CAT test cell emergency stop DI	12 vdc (power supply)
3 (Top)	BOTH	24 vdc Input to power block group 3-5	24 vdc (power supply)
3 (Bottom)	BOTH	Ground for RS232 block group	
4 (Top)	BOTH	24 vdc power supply to fuse blocks 0-6	24 vdc (power supply)
4 (Bottom)	CAT	Common ground from DAQ box to CAT LECM box	
5 (Top)	BOTH	24 vdc power supply to fuse blocks 0-6	24 vdc (power supply)
5 (Bottom)	BOTH	24vdc power supply for NI 9862 CAN card (chassis 08)	24 vdc (power supply)
6 (Top)	JD	Fuel pump +/-	12 vdc (JD battery)
6 (Bottom)	JD	JD 12 vdc battery +/-	12 vdc (JD battery)
7 (Top)	JD	JD ECU +/-	12 vdc (JD battery)
7 (Bottom)	JD	JD Starter Power +/-	12 vdc (JD battery)
8 (Top)	JD	JD Keyswitch +/-	12 vdc (JD battery)
8 (Bottom)		Unused	12 vdc (JD battery)
9 (Top)	CAT	CAT Keyswitch +	24 vdc (CAT battery)
9 (Bottom)	CAT	CAT 24 vdc battery +	24 vdc (CAT battery)
10 (Top)		unused	
10 (Bottom)		unused	
11 (Top)		unused	
11 (Bottom)		unused	
12 (Top)	BOTH	Dyno coolant valve power supply	120 VAC
12 (Bottom)	BOTH	12 vdc power supply	120 VAC
13 (Top)	CAT	CAT emergency gas valve	120 VAC
13 (Bottom)	BOTH	24 vdc power supply	120 VAC
14 (Top)		(1) goes to AC/DC convertor for test cell jacket water bypass valve (2) goes to CAT back pressure valve power	120 VAC
14 (Bottom)	BOTH	120 VAC supply to blocks 12-14 (CBPB06 Breaker #30)	120 VAC

Figure A.10: AC and DC power terminals used.

Ethernet Switch	CAT or JD I/O	Description
1		unused
2	BOTH	Connection to NI DAQ
3	BOTH	Connection to test cell dyno controller
4	BOTH	Supply connection to the switch
5		unused
6	CAT	Connection to CAT LECM
7	CAT	Connection to combustion cart
8		unused

Figure A.11: Ethernet terminals used.

Fuses	CAT or JD I/O	Description	Fuse Rating/Voltage
0	BOTH	DAQ Main Power	5A/250V
1	BOTH	DAQ Chassis 01 (DI)	3A/250V
2	BOTH	DAQ Chassis 03 (AI)	3A/250V
3	BOTH	DAQ Chassis 04/05 (AO)	3A/250V
4	BOTH	DAQ Chassis 02 (DO)	3A/250V
5	CAT	Alicat Power supply	3A/250V
6	BOTH	DAQ NI 9265 AO Direct 24vdc power supply	2A/250V
7	JD	JD ECU Main Power	No Fuse in place
8	JD	JD Keyswitch Power	No fuse in place
9	CAT	CAT back pressure valve	1A/250V

Figure A.12: Fuse connections

Relays	CAT or JD I/O	Decription
1	JD	JD Keyswitch & Fuel Pump
2	BOTH	Dyno coolant tap water valve
3	CAT	CAT emergency natural gas fuel valve
4	CAT	CAT keyswtich
5	BOTH	Pump start for engine jacket water heat exchanger shell side

Figure A.13: Relay connections

RS232 (Pin #)	CAT or JD I/O	Decription	Wire Color
1	CAT	CAT Alicat Communication	Black
2	CAT	CAT Alicat Communication	Brown
3	CAT	CAT Alicat Communication	Red
4	CAT	CAT Alicat Communication	Orange
5	CAT	CAT Alicat Communication	Yellow (Ground)
6	CAT	CAT Alicat Communication	Green
7	CAT	CAT Alicat Communication	Blue
8	CAT	CAT Alicat Communication	Purple
9	CAT	CAT Alicat Communication	Gray

Figure A.14: RS232 pin-wire color code

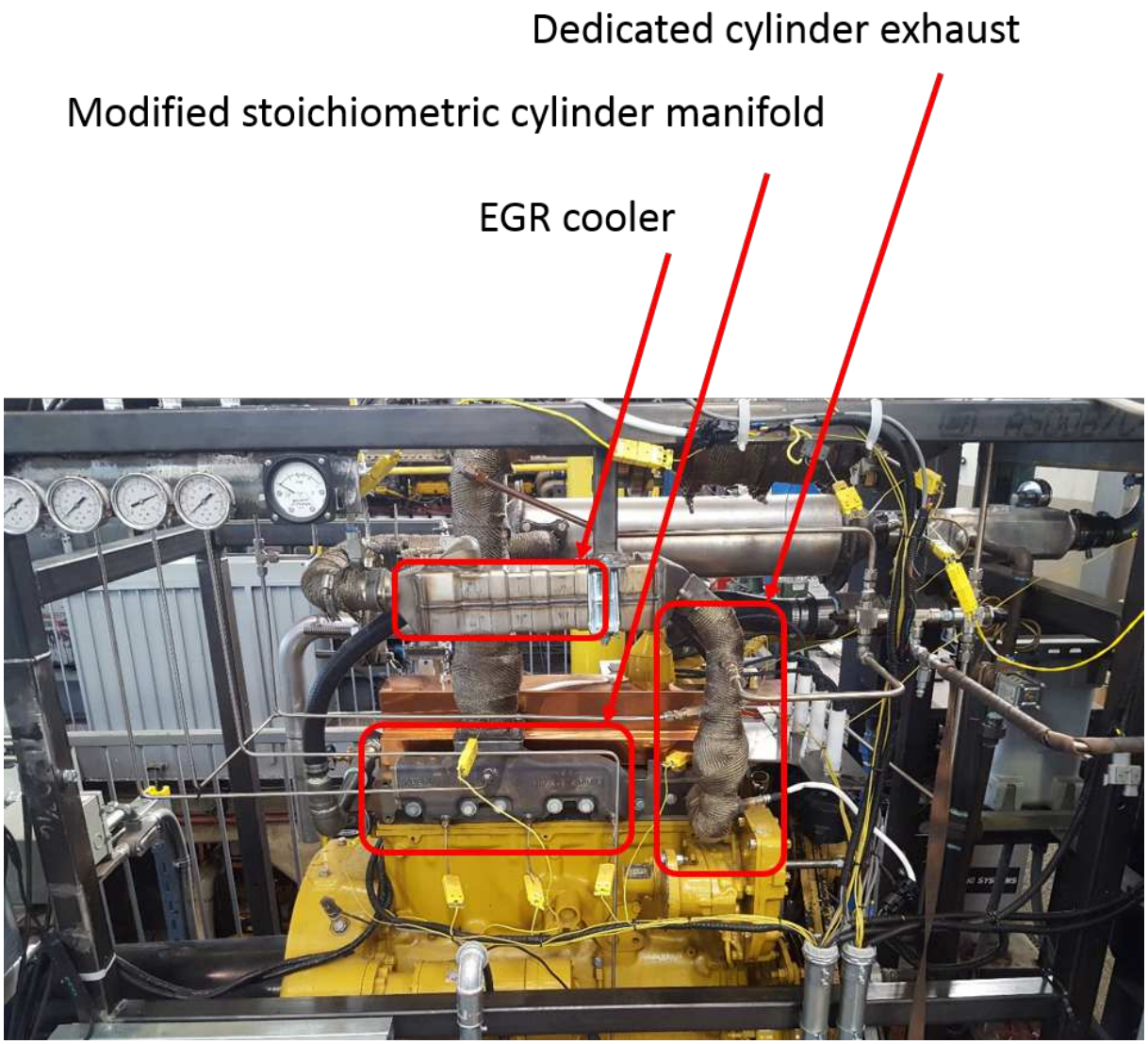

Figure A.15: 'Hot side' of the G3304 engine. Dedicated cylinder exhaust piping, EGR cooler, and modified stoichiometric cylinder manifold components are highlighted.

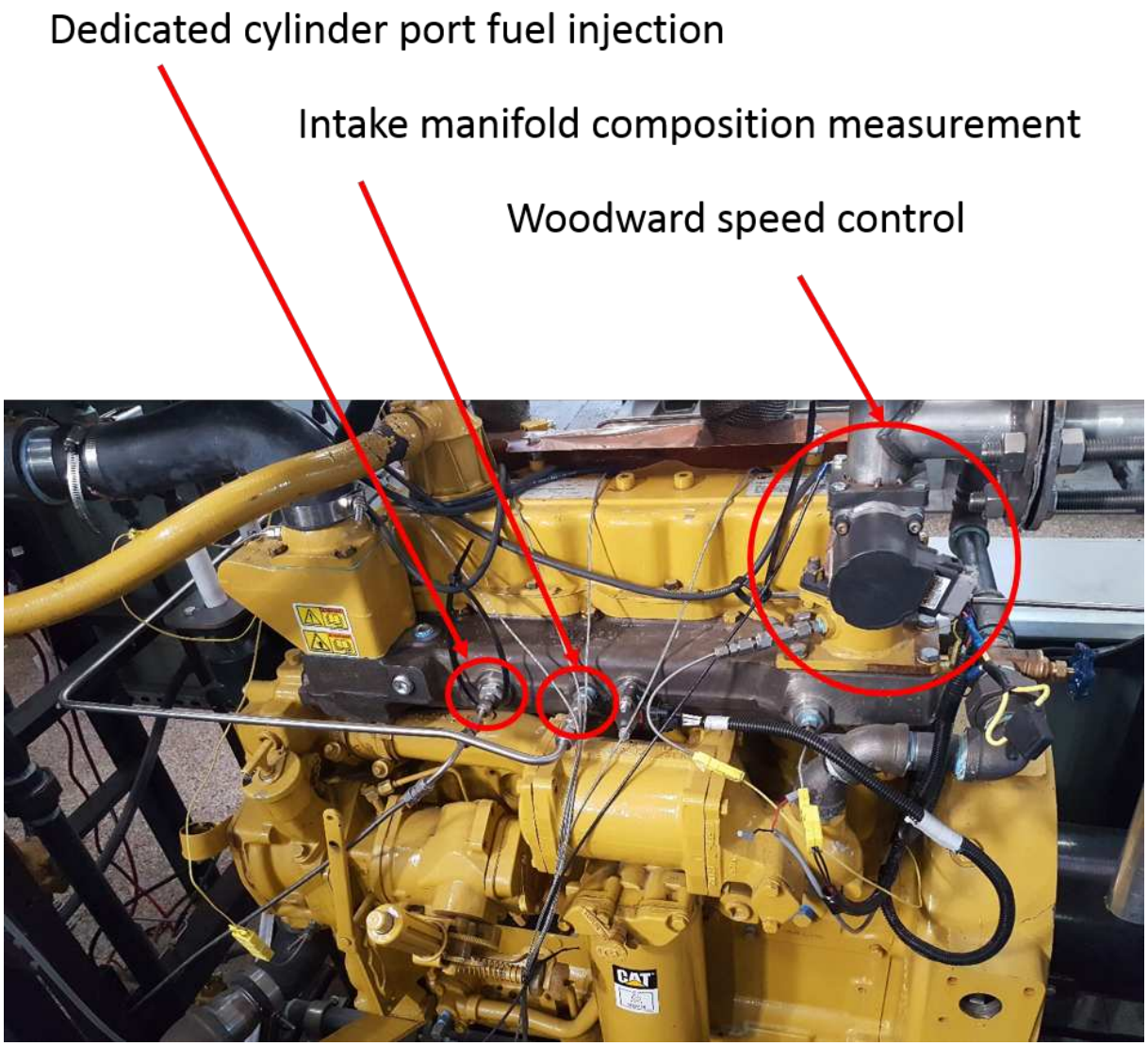

Figure A.16: 'Cold side' of the G3304 engine. The delivery of additional fuel to the dedicated cylinder via port fuel injection is highlighted. The intake manifold composition measurement and engine speed control are also highlighted.

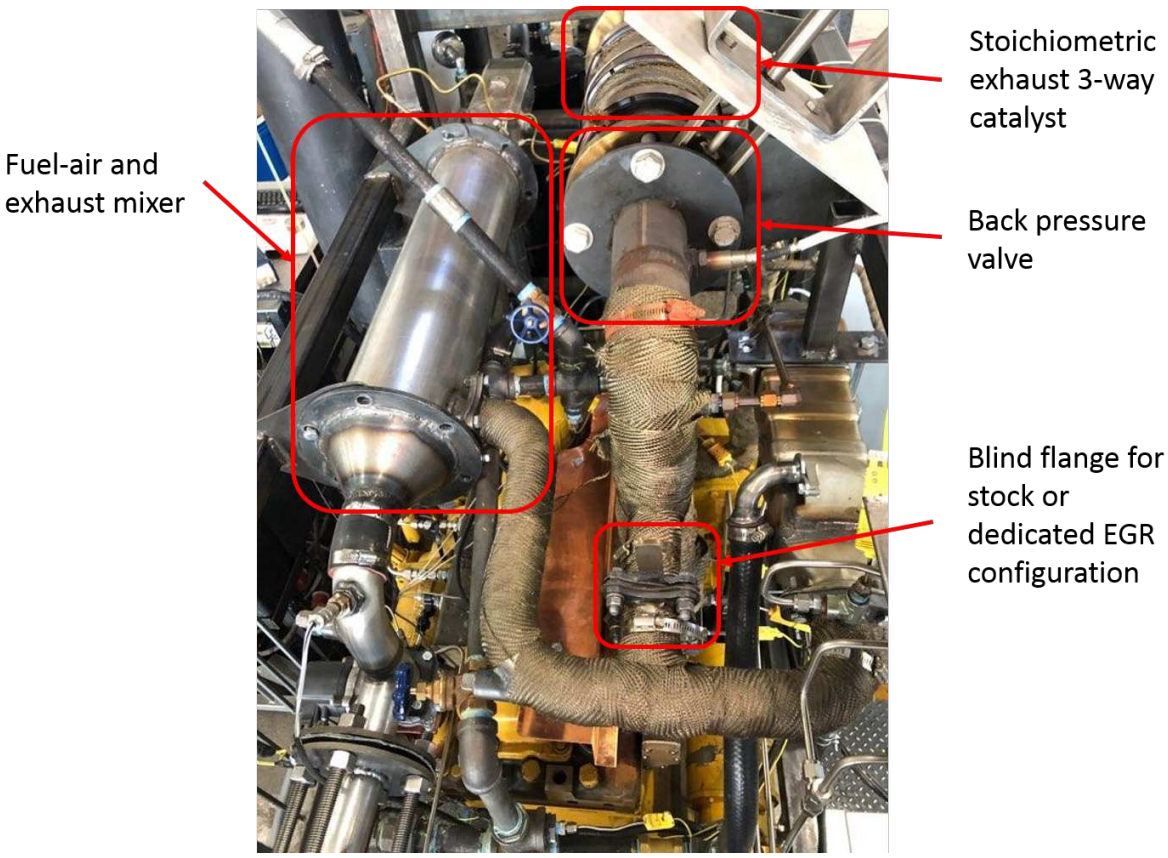

Figure A.17: Top side view of the G3304. EGR mixer, back pressure valve, NSCR catalyst, and flange used to convert the engine to dedicated EGR are highlighted.

Appendix B

G3304 Stock Configuration Knock Intensity and Knock Margin Characterization

Mentioned in numerous sections knock intensity (KI) served as a limit for possible engine operating points. A characterization of knock intensity in the G3304 engine was done qualitatively and quantitatively. The quantitative method was done using the knock intensity measurement technique outlined by Wise as cited in Chapter 4 section 10. Qualitative characterization was done by recording audio files of different levels of engine knock and matching them to calculated KI. While operating without EGR the G3304 engine was brought to conditions as outlined in TableB.1 Spark timing was advanced from 30 °bTDC, nominal timing for the G3304, until audible knock was distinguishable while standing next to the engine. All operating conditions shown in Table B.1 were held constant while advancing spark timing. While advancing spark timing is not the only means to achieve engine knock (increasing manifold air temperature and increasing BMEP are others) this determined to be the easiest method to do so. Audible knock could be heard at a spark timing of 59 °bTDC. At this spark timing individual cylinder knock events during a 500 cycle window were recorded and are shown in FigureB.1. Cycles showing a higher knock intensity experienced a heavier knocking event and from examining the results of Figure B.1 it can be seen that different cylinders have varying levels of KI. The frequency and magnitude of events appear to be chaotic, but cylinder 3 had the highest KI of any cylinder followed by cylinder 1, 4, and finally cylinder 2. Integration of cycle KI over a 200 cycle window gives a single value to quantify KI. From the data collected and shown for audible knock in Figure B.1 KI values for audible knock in cylinders 1, 3, 4, and 2 were 493, 216, 72, and 35, respectively. Figure B.2 shows the varying levels of KI for each cylinder during the 200 cycle window. Further insight into audible knock for the G3304 can be done by examining the in-cylinder pressure trace for a single knock event. Cylinder 3, cycle 201 from Figure B.1 had the highest cycle KI of any cycle observed. Cylinder pressure

Table B.1: Engine operating conditions during G3304 knock intensity characterization

Engine Speed	1480 rpm
Engine Torque	290 N-m
BMEP	5.2 bar
IMAP	11.97 psia
IMAT	47.9 °C
JW Inlet Temp	93.7 °C
JW Outlet Temp	99.5 °C
Spark Duration	150 μs
Spark Timing	Varied

as a function of crank angle during that cycle is shown in blue pressure trace of Figure B.3. The crank angle fraction between spikes in pressure observed correlates to the knock frequency of the engine. After audible knock was recorded the spark timing was retarded until only slight audible knock could be heard. KI values for each cylinder were recorded and the highest intensity was given the label light knock. The highest KI was seen in cylinder 1 with a value of 111. Spark timing was again retarded until only small knock events were able to be observed in cycles over a 200 cycle window. The highest KI at this condition was 40 and was found in cylinder 1. Figure B.4 shows cycle knock intensity for audible, light, incipient, and no knock tests. After consideration it was deemed that knock slightly about incipient levels was acceptable but levels approaching light knock were not. So the KI threshold for KI for the G3304 was set at a value of 50. Immediately following the knock characterization a set of tests was conducted to find the knock margin of the G3304 engine at rated power conditions. Knock margin in this work is defined as the number of crank angle degrees spark timing can be advanced from nominal timing before a KI of 50 is found in any cylinder. It was appropriate during this testing to also find the amount of spark timing retard until exhaust port temperatures were no longer acceptable. Based on discussion with engine industry advisors the limit for exhaust port temperature was set at a value of 750 °C. With these two limits set the engine was brought to rated power conditions and variables such as intake manifold temperature, jacket water outlet temperature, engine speed, and engine torque were all

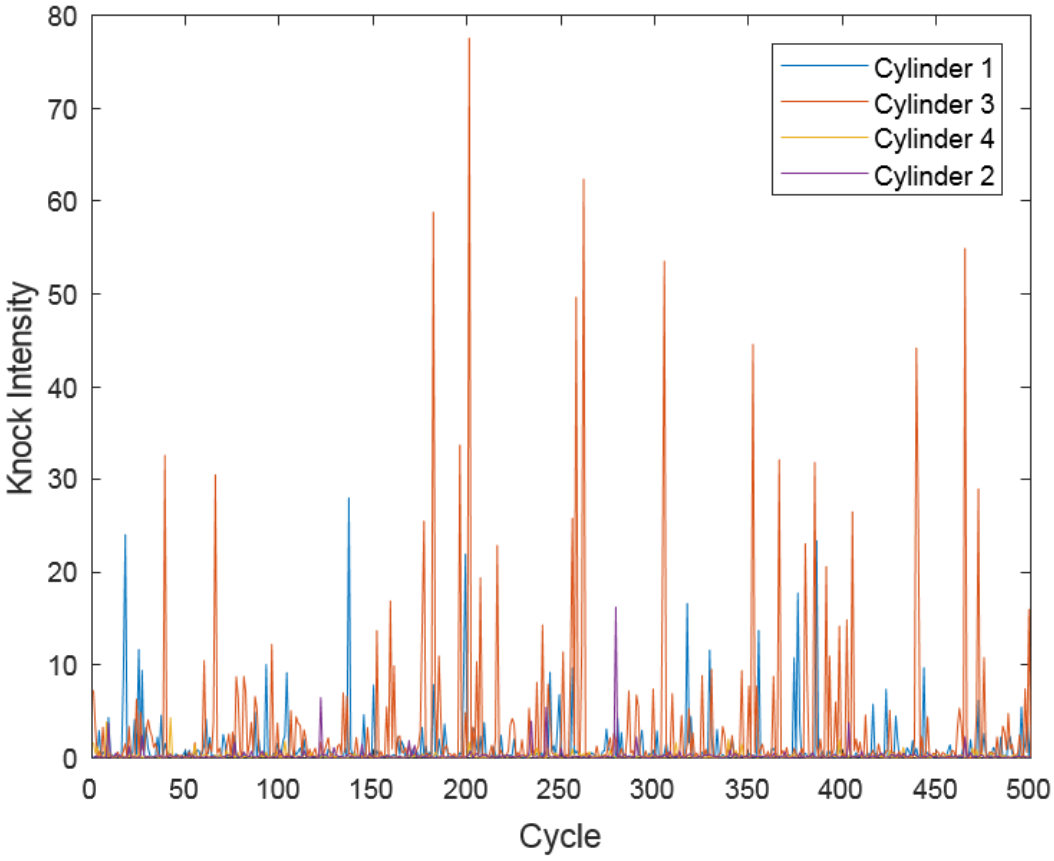

Figure B.1: Individual cylinder knock intensity as a function for individual cycles while operating at conditions of TableB.1 and a spark timing of 59 °bTDC.

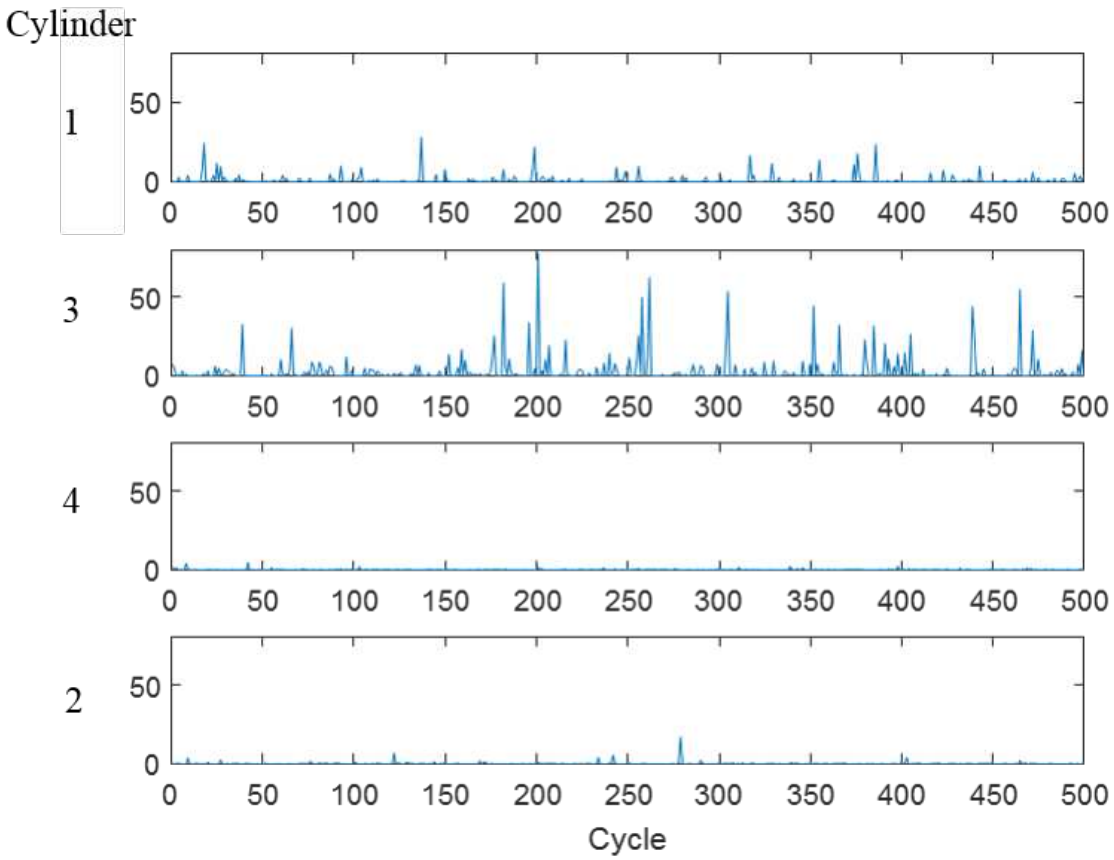

Figure B.2: Individual cylinder knock indensity integrated over a 200 cycle window.

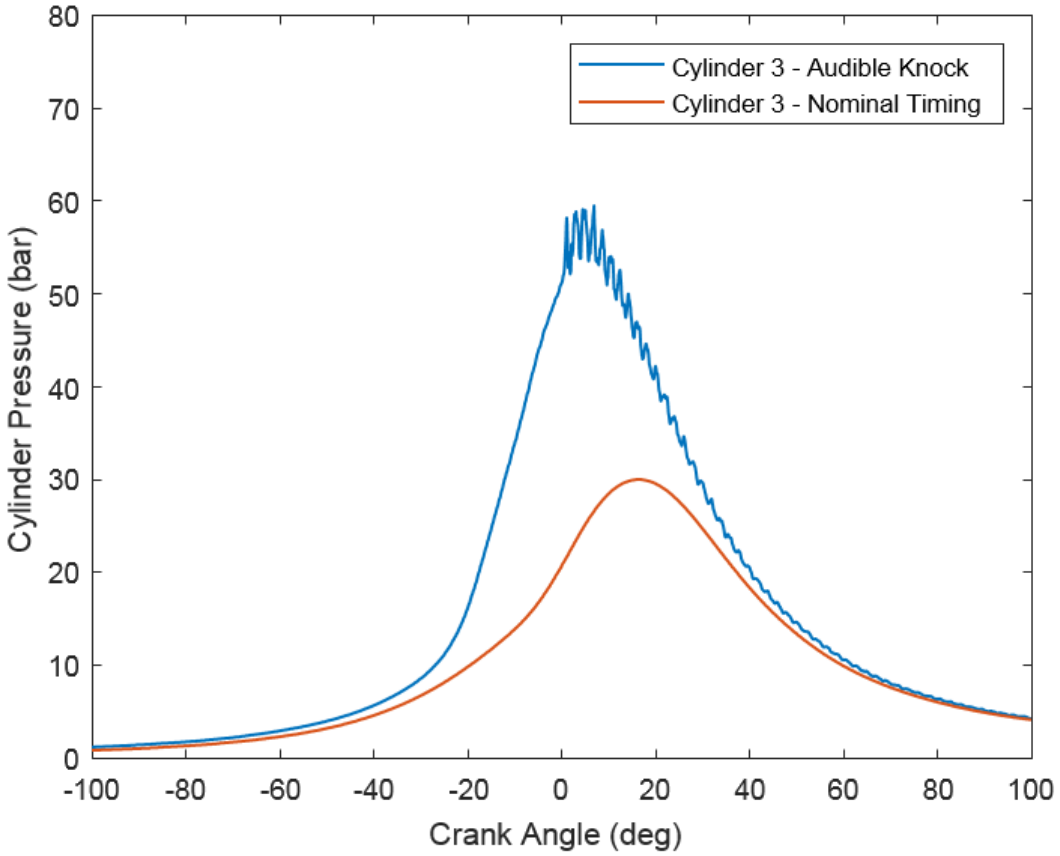

Figure B.3: G3304 cylinder 3 pressure as a function of crank angle degree. The orange pressure trace represents cylinder pressure while the engine was operating at conditions of TableB.1 and a spark timing of 30 °bTDC. The blue trace represents cylinder pressure while the engine was operating at similar conditions but with a spark timing of 59 °bTDC.

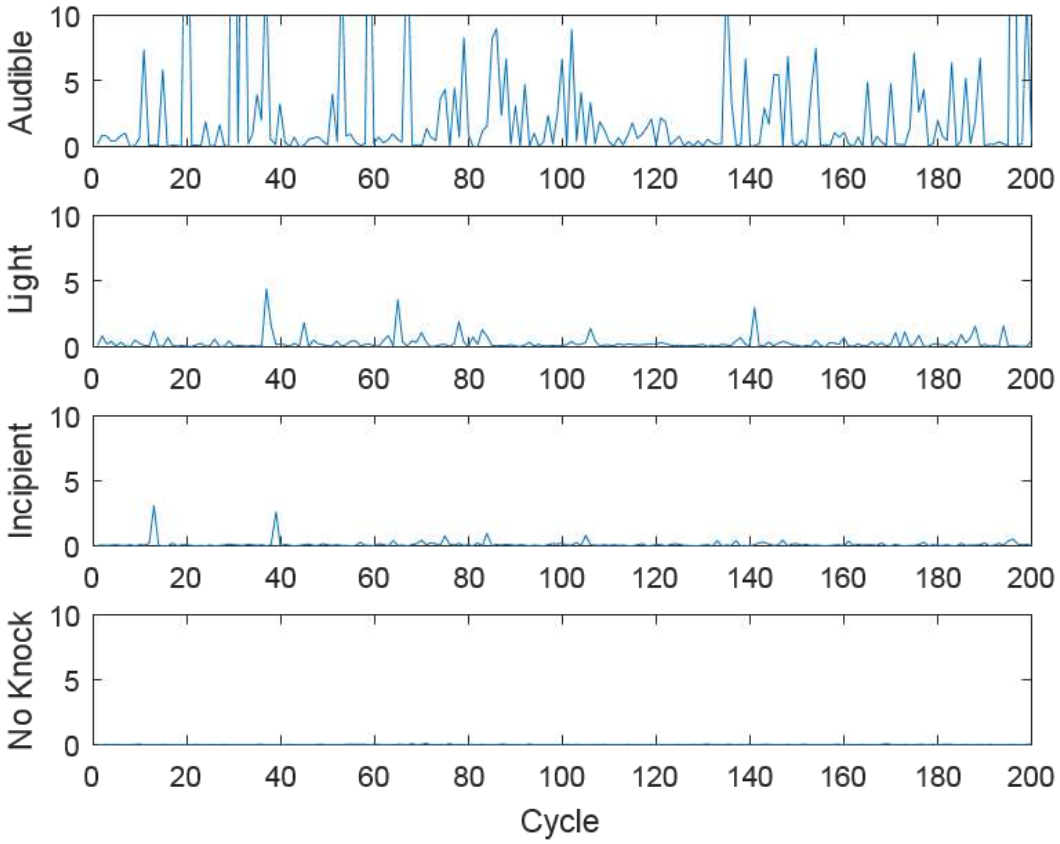

Figure B.4: Audible, light, incipient, and no knock KI values determined during the knock characterization work. Audible knock was found in cylinder 3 while light and incipient knock KI values were taken from cylinder 1

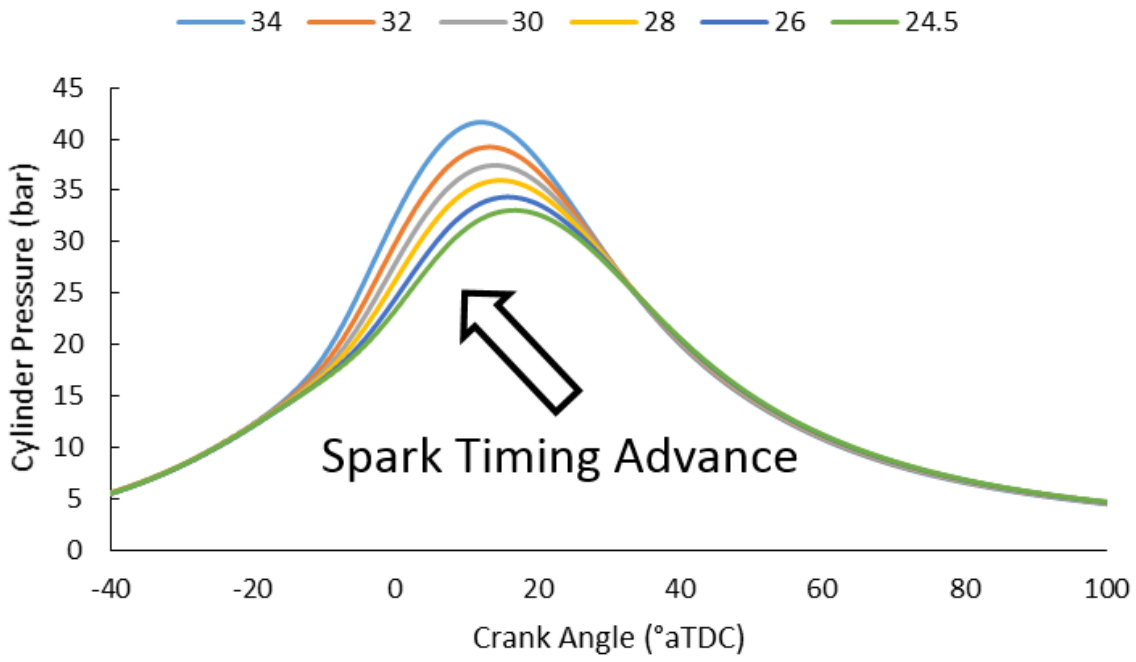

Figure B.5: A 500 cycle average cylinder pressure trace as a function of spark timing at rated engine power of 71 kW. Cylinder pressure shown comes from cylidner 3 of the engine.

held constant. To maintain rated power output while spark timing was changed the intake manifold pressure was allowed to change. From a nominal spark timing of 30 °bTDC spark timing was able to be advanced by 4 crank angle degrees before the KI limit of 50 was met. Spark timing was then retarded until the exhaust port temperature limit was found. A spark timing of 24.5 °bTDC was the most retarded timing found before temperatures surpassed 750 °C. Figure B.5 shows a 500 cycle average cylinder pressure trace (cylinder 3) for each spark timing considered in the knock and exhaust temperature margin tests. Spark timing was incremented by 2 crank angle degrees between 34 and 26 °bTDC and by 1.5 crank angle degrees between after 26 °bTDC. Figure B.6 shows the exhaust port temperatures at each of the exhaust port thermocouple locations at a spark timing of 24.5 °bTDC. The exhaust port temperature of cylinder 3 proved to limit the amount of spark retard possible as the temperature measured was 745 °C. Upon further observation of the exhaust port temperatures (lower 4 temperatures marked) shown in Figure B.6 variation in port temperatures is seen. Two comments can be made about this variation. First, is that the dedicated

cylinder (cylinder 1) does not share an exhaust manifold with the other three cylinders and the location of the thermocouple tip is further downstream of the exhaust valve than cylinders 2-4. The engine was operating without dedicated EGR in this test. The G3304 engine valve timing likely includes a slight valve overlap, that is both the intake and exhaust valves are open for a few crank angle degrees. In practice valve overlap allows for improved scavenging of exhaust products by allowing fresh air-fuel to push out the burned gas products. Some of the fresh-air fuel which is at a much lower temperature that combustion products (in this test intake manifold temperature was 30 °C) short circuits or passes directly through the cylinder. The exhaust port thermocouple tips are closer to the exhaust valves in cylinder 2-4 and are cooled more by the short circuited fresh-air fuel than the thermocouple tip of cylinder 1. This accounts for increased exhaust port temperatures seen in cylinder one across every test conducted in this work. Second, even variation in exhaust port temperatures of cylinders 2-4 can be seen. Spark timing was held constant across all cylinders during these tests but slightly differing duration of combustion in cylinders led to different exhaust port temperatures. Analysis of combustion data revealed that the location of the 90% mass burn fraction location was 32.5°, 25°, and 29° aTDC for cylinders 3, 4, and 2, respectively. The location of 90% mass fraction burned location correlates well to the varying exhaust port temperatures observed. As outlined in Chapter 5 section 3 it is assumed that air and fuel are well mixed prior to entering the intake manifold so differing air-fuel ratios in cylinder seems likely to be the cause of the difference in combustion duration. Upon discussion with industry advisors it was theorized that since the intake manifold design of the G3304 may be introducing different levels of turbulence in each cylinder, resulting in different combustion duration. A final note about the temperature measured downstream of the exhaust manifold in cylinders 2-4. That measurement was made to understand exhaust temperatures that may be entering a turbocharger. Again, exhaust temperature of 802 °C is higher due to the explanation given above. Finally, at each test point the fuel methane number was calculated at an MWM methane number of 72, and the fuel composition from which that methane number was derived did not change.

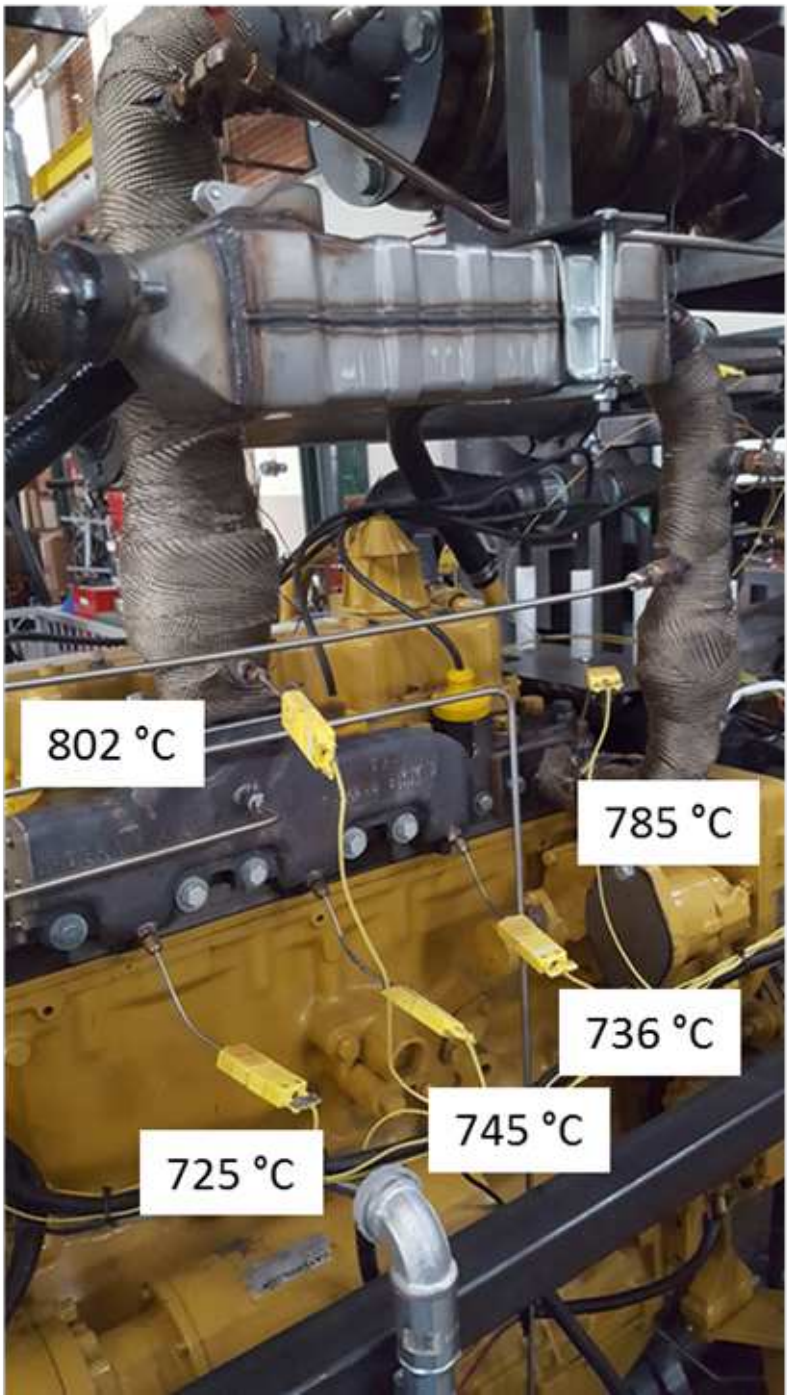

Figure B.6: A 500 cycle average cylinder pressure trace as a function of spark timing at rated engine power of 71kW. Cylinder pressure shown comes from cylidner 3 of the engine.

Appendix C

Analysis of the necessity of an EGR mixer using a Fast NOx Analyzer

In Chapter 3 section 4 and Chapter 5 section 3 an EGR mixer designed specifically for dedicated EGR was discussed briefly. Based on work by SouthWest Research Institute cited in citation 14 of Chapter 3 an EGR mixer was designed to adequately mix fresh air-fuel and recirculated exhaust. Figure C.1 shows the design of EGR mixer used. Specific details of the design are as follows. Considering only the volume between outer flanges shown in part A of Figure C.1 and excluding the volume of the EGR piping the total volume of mixed air, fuel, and exhaust is 176.41 cubic inches. The distance between outer shell flanges is 23.75 inches with the diameter of the outer shell being 6 inches. The volume of the cylinder accumulating recirculated exhaust is 37.34 cubic inches, and considering only the distance between the flange near the inlet of the pipe and the end of the cylinder carrying EGR most near to the inlet of fuel-air the length of pipe is 19.75" and the diameter is 2.75". Twenty-four 9/32" holes were drilled in the cylinder accumulating recirculated exhaust. While reviewing results from Chapter 4 a question arose as to how well the EGR mixer was performing. Evaluation of the performance would be non-trivial due to the nature of the mixer. It was determined that a marker for adequate mixing of the EGR mixer would be high speed quantification of NO concentration in the recirculated exhaust and downstream of the EGR mixer. At rated speed conditions of 1800 rpm the frequency of exhaust valve opening of a four-stroke engine is 15 Hz. It was assumed this would be the frequency of exhaust pulses passing through the EGR piping. Analyzers commonly used such as a 5-gas rack or FTIR record gas composition in the 1-2 Hz range and the distance between the gas sample location and the analyzer made a 5-gas rack or FTIR unusable for analyzing the mixed air, fuel, and exhaust. For this reason a Fast NO_x analyzer was chosen to measure the post mixer NO concentration. Among many other analysis instruments the CSU Powerhouse analysis capabilities include Cambustion CLD500 fast

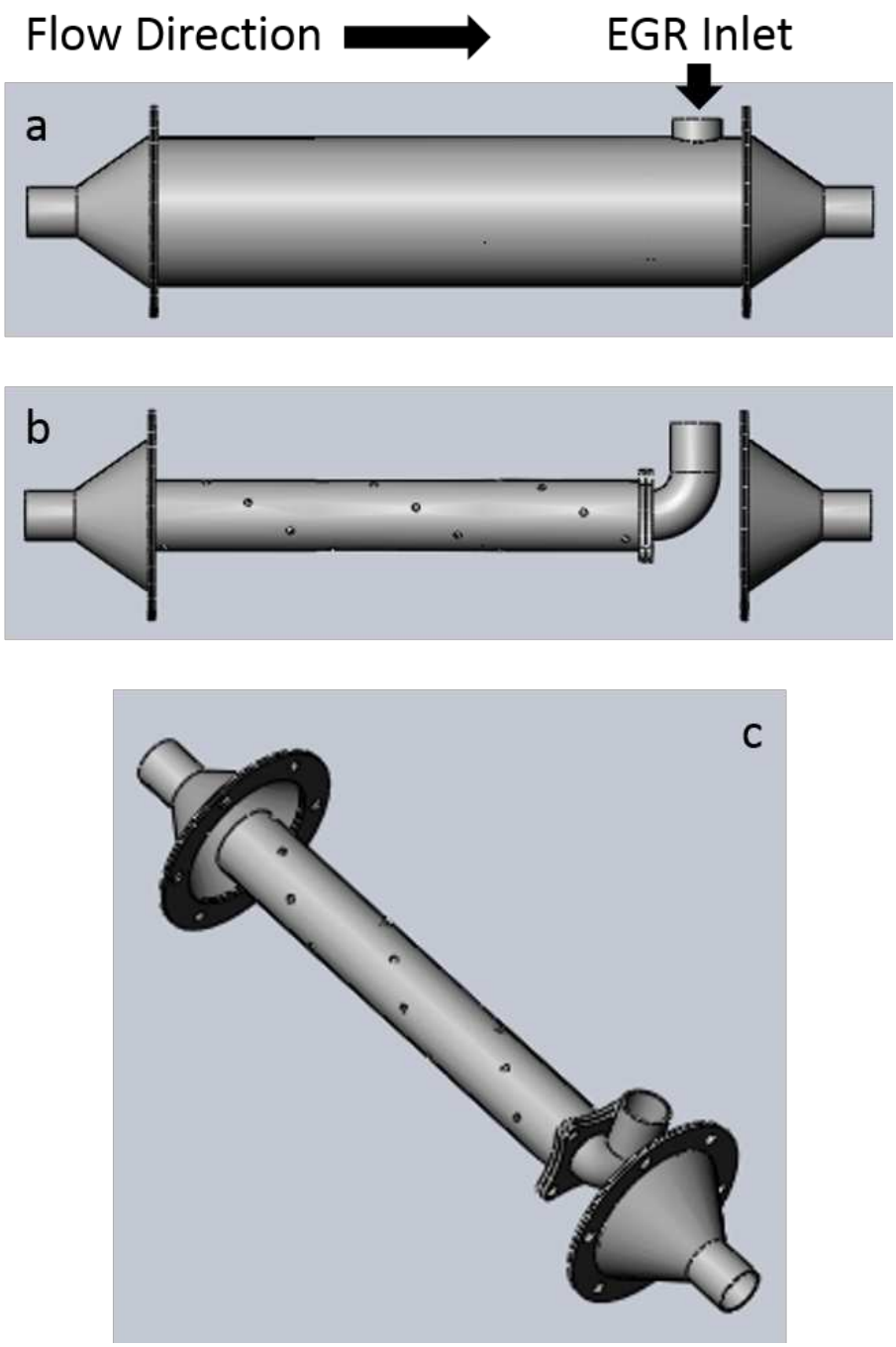

Figure C.1: SolidWorks model of the EGR mixer designed and used.

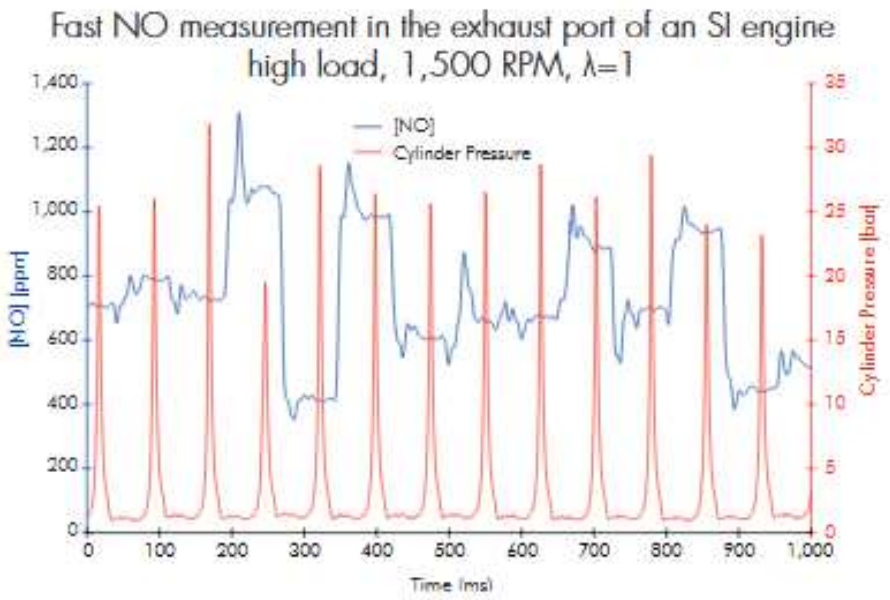

Figure C.2: Typical exhaust port measurement using a CLD Fast NO_x analyzer. This data is a sample provided by Cambustion and can be found (CITATION). The results are reasonable in a sense that after combustion events, shown by cylinder pressure spikes, the exhaust valve opens and an increase in NO is observed.

NO_x analyzer (owned by Dr. Anthony Marchese). The measurement technique for CLD500 is chemiluminescence, similar to that of a standard 5-gas rack. However, in comparison to a 5-gas rack the size of chemiluminescence detector is reduced so that it can be placed very close to the sample location. Depending on the probe length this results in a response time on the order of 500 to 125 Hz. Common practice when using a Fast NO_x analyzer is to place the sample probe very close to the cylinder exhaust valve. Per Cambustion literature a typical Fast NO_x measurement taken close to the exhaust valve would look something similar to what is seen in Figure C.2. High resolution measurement of NO concentration close to the cylinder exhaust port is not of interest in this work. Instead the sample probe was placed upstream and downstream of the EGR mixer. The analyzer has the ability to measure NO_2 and NO concentration, but was configured to measure NO concentration only. Along with commentary the following steps were taken in setup of the analyzer.

1. Multiple bottles of ultra high purity (UHP) nitrogen were purchased from AirGas and connected to the 'zero gas' and 'purge' connections on the back of the analyzer. In the main

user interface both sample heads were set to 'on' and 'purge'. The sample lines were purged with UHP nitrogen for approximately 4 hours.

2. A bottle of reference NO gas with a 2500 ppm concentration was purchased and plumbed to connections on the back of the analyzer. As a general rule, calibration gas concentration should be approximately double the highest expected measurement. However, the NO concentration was unknown so a 2500 ppm concentration of NO was chosen. Prior to calibration the calibration gas concentration must be updated to match the actual bottle concentration in the 'system' button on the main user interface.

3. Both sample heads were connected to the analyzer and set to 'on' and then 'calibrate' in the main user interface. After selecting 'on' for both sample heads the vacuum pumps will run for a short amount of time until satisfactory chamber pressure is met. It should be noted here that if a user only wants to use one sample head all of the other connections for the unused sample head on the back of the analyzer must be sealed in order for the chamber pressure requirement to be met.

4. If both sample heads pass the automatic calibration the main user interface will show the 'on' and 'sample' in green for each sample head. It is possible that one sample head may pass while the other may not. At times this did occur, but the reason for this was never found. It was also observed that near one of the sample heads what sounded like a gas leak could be heard. It was found that the gas coming from the leaking hose was UHP nitrogen and this did not affect the performance of that sample head.

5. Two bottles of known NO concentration were used to test the sample head measurements. The first bottle was a documented bottle of 996 ppm NO from AirGas. Both sample probes were connected to the bottle and gas was allowed to flow through each sample head. Sample head 1 measured 960 ppm and sample head 2 measured 999 ppm. After this a documented bottle of 49 ppm concentration of NO was connected to both sample heads. Sample head 1 measured 44 ppm while sample head 2 measured 37 ppm. Since the analyzer was cali-

brated on a 2500 ppm concentration of NO the lack of accuracy in low concentration seemed acceptable.

6. The fast NO_x analyzer does not have the capability to log data so the output signal from the analyzer was wired to an input on the Powerhouse high speed data acquisition system. This is the same system used to collect high speed in-cylinder pressure data.

Two engine operating points were selected during the EGR mixer evaluation. During the first, the engine was operating at 3.4 bar bmep, rated speed with conditions similar to that of the 3^{rd} factorial optimized conditions found in Table 4.7. Operating at these conditions provided the best possible combustion stability of the dedicated cylinder. If combustion stability was poor, it was theorized that this could lead to reduced mixing performance by the EGR mixer. The second operating point was again at 3.4 bar bmep, rated speed with all conditions similar to the 3^{rd} factorial optimization conditions except that the dedicated cylinder AFR was changed to 0.875 lambda. This was done to negatively impact COV of IMEP (combustion stability) in the dedicated cylinder and analyze how poor combustion would impact EGR mixing performance. At each of these points the fast NO_x sample probe was placed just downstream of the mixer, prior to the intake manifold and in the recirculated dedicated cylinder exhaust piping. Figure C.3 shows the sample probe installed downstream of the EGR mixer. In this specific test the dedicated cylinder exhaust is being analyzed by the Powerhouse low speed 5-gas rack emissions analyzer. When the fast NO_x analyzer was used to measured the NO concentration in dedicated cylinder exhaust these two sample lines were simply switched. Unfortunately, the raw fast NO_x data included signal noise. During commissioning of the engine, care was taken to eliminate signal noise on the high speed data acquisition system. Among other precautions, a wire between the engine and acquisition system was installed to provide a common ground. However, during these tests this was not adequate to eliminate signal noise. Figure C.4 shows cylinder pressure and post mixer NO concentration as a function of cylinder crank angle. Signal noise which is periodic in nature, occurring approximately every 180 crank angle degrees, is shown by sudden changes in measurement on the cylinder pressure and fast NO_x data. Two possible sources for this noise was identified. The first is that noise from the opening

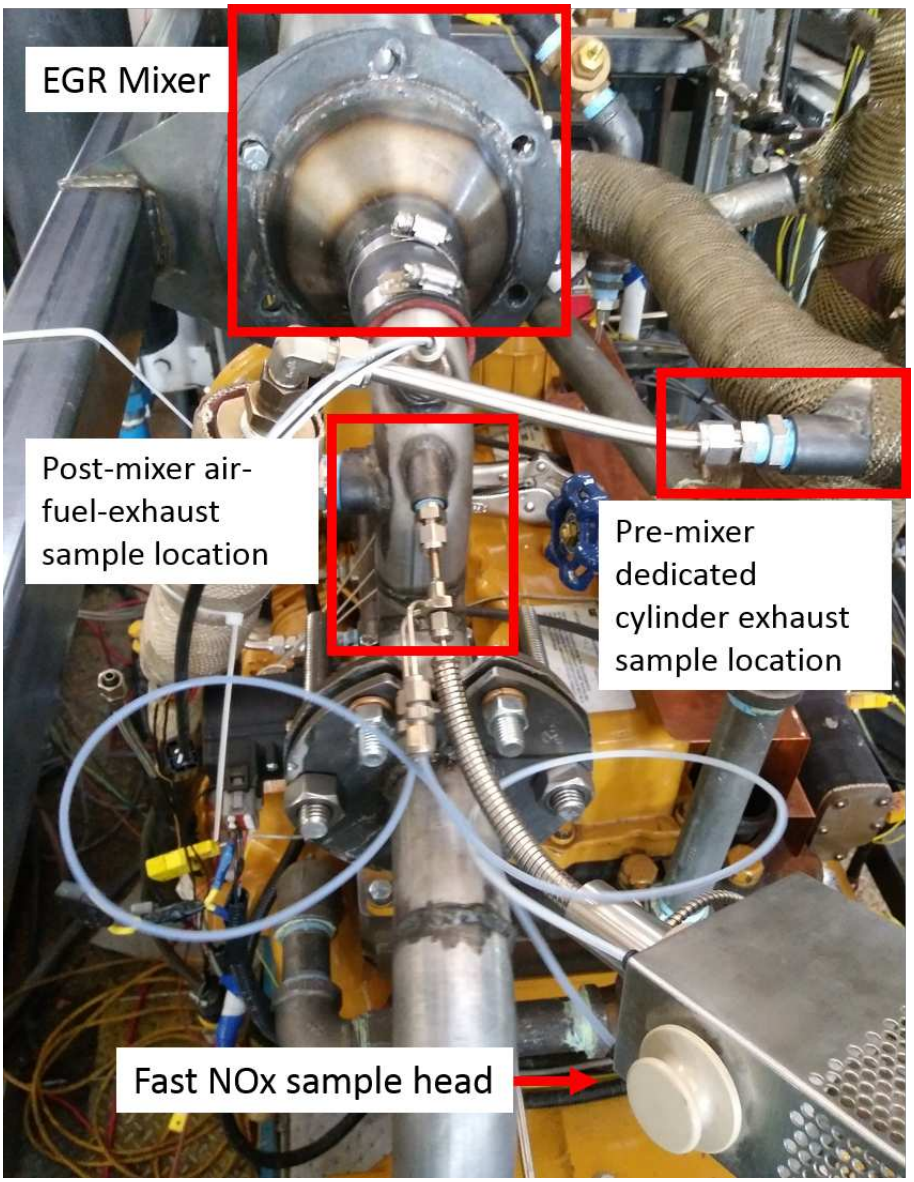

Figure C.3: Fast NO_x measurement on the G3304 engine. In this configuration the fast NO_x measurement is being made downstream of the mixer. Dedicated cylinder exhaust upstream of the mixer is being analyzed by the low resolution Powerhouse 5-gas rack.

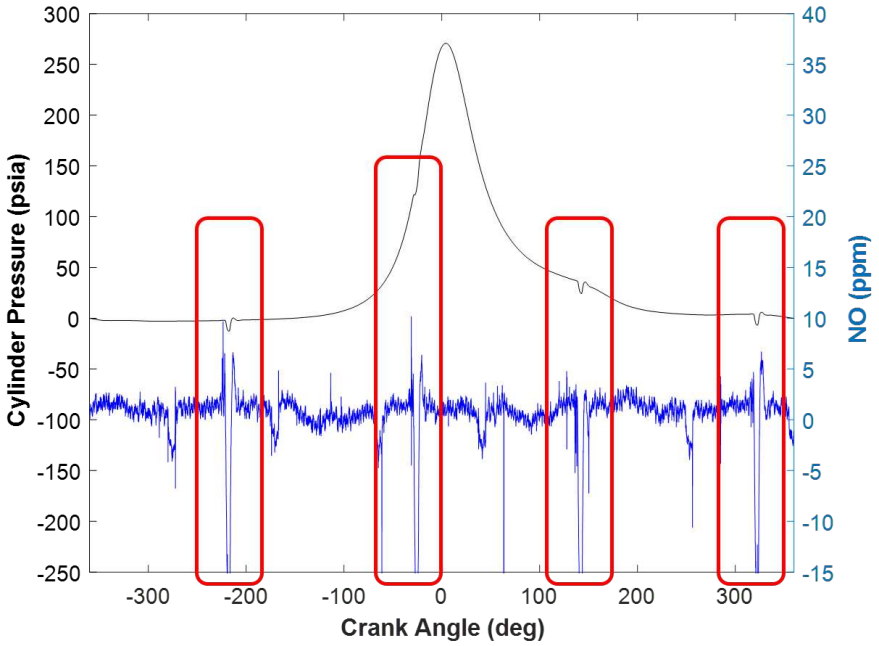

Figure C.4: Singal noise found in raw cylinder pressure and Fast NO_x data collected

or closing of intake or exhaust valves was causing this noise. The second is that something associated with the ignition system was causing this noise. Although the cause of the noise was never identified signal filtering was used to eliminate it. The Matlab rloess smoothing method was used to filter the fast NO_x data. Per Matlab documentation the rloess method is a local regression using weighted linear least squares and a 2nd degree polynomial model that assigns lower weight to outliers in the regression. The method assigns zero weight to data outside six mean absolute deviations. The smoothing span moving average was set to 10% of the entire data set. Prior to selecting the rloess function the Matlab lowpass filter was used in an attempt to eliminate noise from the data set. However, over wide range of frequencies examined the lowpass filter was not adequate to eliminate the signal noise. Figure C.5 shows the raw and filtered data for 5 full engine cycles while the analyzer sampled from the dedicated cylinder exhaust upstream of the EGR mixer. The engine was operating at conditions similar to 3^{rd} factorial optimized conditions. A comparison of this result from the sample results shown by Cambustion literature shown in Figure C.2 can be made but must be done so carefully. First, the expected spikes in NO seen in Figure C.2 which occur just after the exhaust valve opens are not observable in Figure C.5. This is likely due to the fact that NO

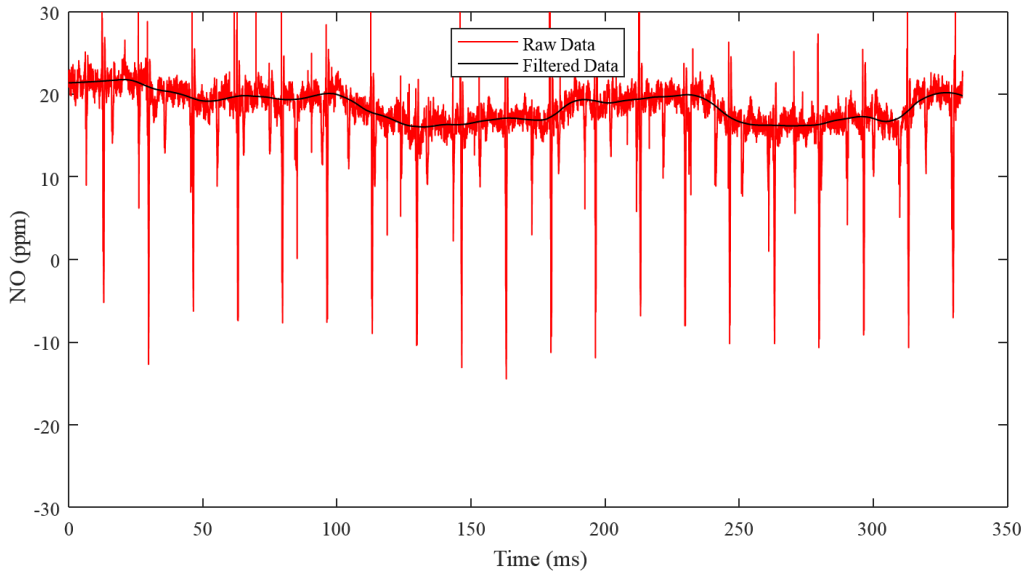

Figure C.5: Raw and Matlab 'rloess' filtered Fast NO_x data for 5 engine cycles while the engine was operating at conditions simlar to those found in Table 4.7. The sample location was upstream of the EGR mixer in the dedicated cylinder exhaust.

measurements are made far downstream of the exhaust valve. The pipe carrying exhaust from the dedicated cylinder to the mixer was two inches in diameter and the estimated distance between the dedicated cylinder exhaust valve and the fast NO_x sample location was approximately 38 inches. In this distance and considering the back pressure applied to the dedicated cylinder exhaust by the EGR mixer design the spikes of NO which signify pulses of exhaust are damped out. It should be noted that the EGR heat exchanger was also situated between the dedicated cylinder exhaust valve and the fast NO_x sample location. Figures C.6, C.7, and C.8 show the raw and filtered data of the pre-mixer poor combustion, post-mixer good combustion, and post-mixer poor combustion.

An understanding of the performance of the EGR mixer can be made by a direct comparison of the Matlab 'rloess' filtered fast NO_x data collected upstream and downstream of the EGR mixer. Figure C.9 shows this comparison over a 5 engine cycle range. The COV of IMEP of the dedicated cylinder for the pre and post mixer tests was 16.89 and 19.63, respectively, and the average COV of IMEP of the other cylinders was 10.07 and 9.65. The difference in average pre and post mixer NO concentration is due to the dilution of dedicated cylinder exhaust with fresh air-fuel mixture.

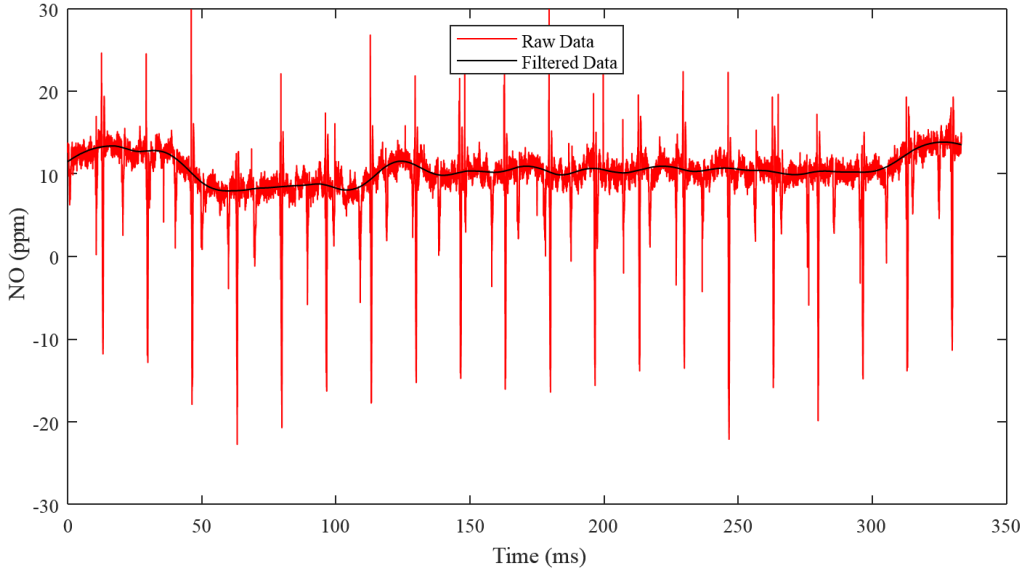

Figure C.6: Raw and Matlab 'rloess' filtered Fast NO_x data for 5 engine cycles while the engine was operating at conditions simlar to those found in Table 4.7 with the exception of the dedicated cylinder AFR which was set at lambda 0.875. The sample location was upstream of the EGR mixer in the dedicated cylinder exhaust.

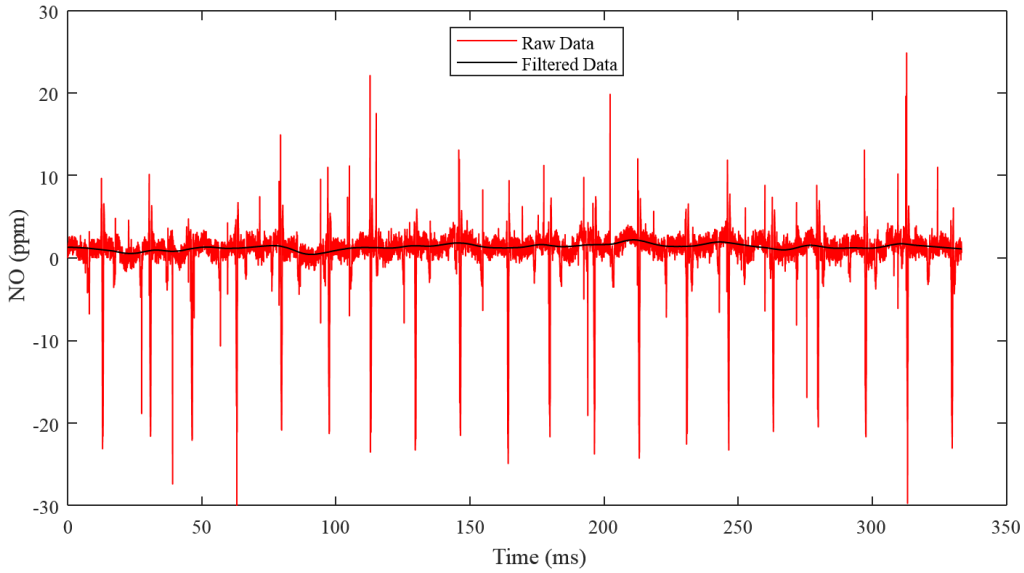

Figure C.7: Raw and Matlab 'rloess' filtered Fast NO_x data for 5 engine cycles while the engine was operating at conditions simlar to those found in Table 4.7. The sample location was downstream of the EGR mixer, just ahead of the throttle valve.

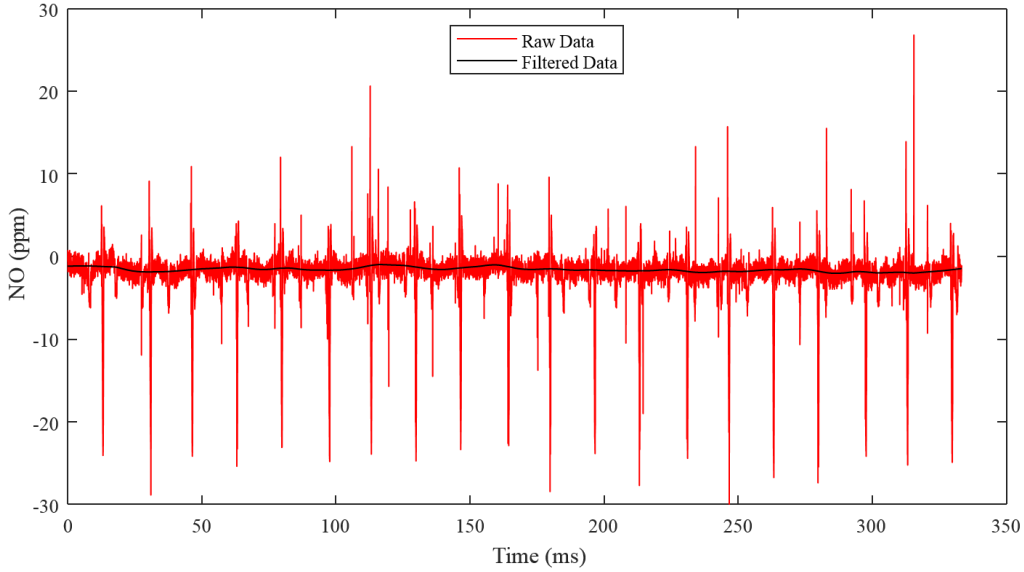

Figure C.8: Raw and Matlab 'rloess' filtered Fast NO_x data for 5 engine cycles while the engine was operating at conditions simlar to those found in Table 4.7 with the exception of the dedicated cylinder AFR which was set at lambda 0.875. The sample location was downstream of the EGR mixer, just ahead of the throttle valve.

It does appear that the EGR mixer dampens fluctuations in NO concentration present in post mixer measurements. Quantitatively, the standard deviation of the filtered data seemed like an acceptable method for analyzing the pre and post mixer data. One standard deviation for the pre-mixer data was calculated to be 1.6962 and one standard deviation for the post-mixer data was calculated to be 0.3400. This improvement does show that the EGR mixer used does improve mixing while using NO concentration as a surrogate for mixing. However, this result does not conclusively show that a mixer is or is not necessary for dedicated EGR since the engine was never run without a mixer. It does suggest that future work could include investigations on the design and necessity of a mixer. Figure C.10 shows the pre and post mixer results NO results while the engine was operating with poor combustion in the dedicated cylinder. The dedicated cylinder COV of IMEP was 35.59 and 27.50 for the post mixer and pre mixer tests, respectively. The standard deviation calculation showed that one standard deviation for the post mixer NO measurement was 0.2755, and one standard deviation for the pre mixer NO measurement was 1.4754.

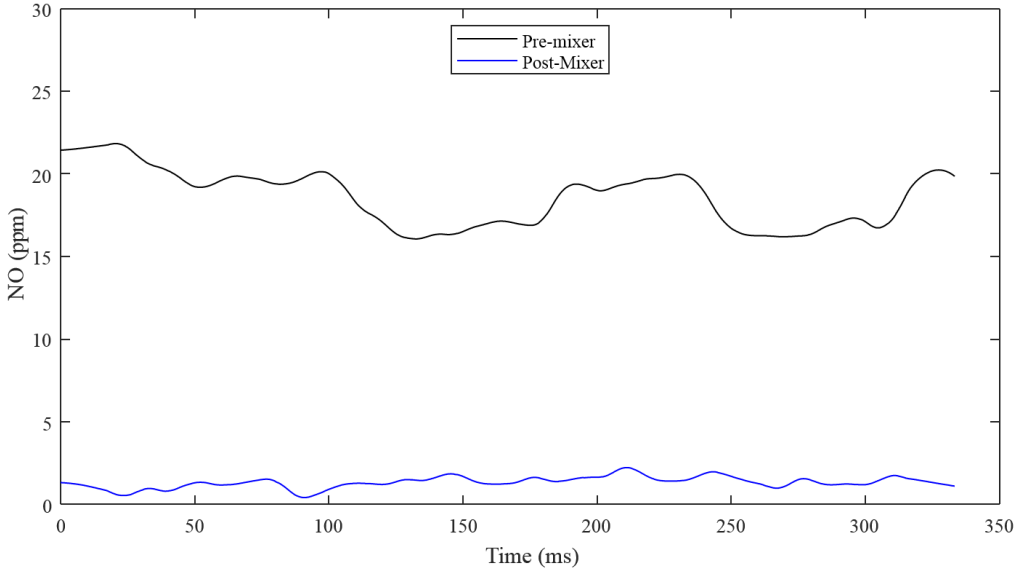

Figure C.9: A comparison of pre and post mixer fast NO_x measurements at a similar engine operating condition.

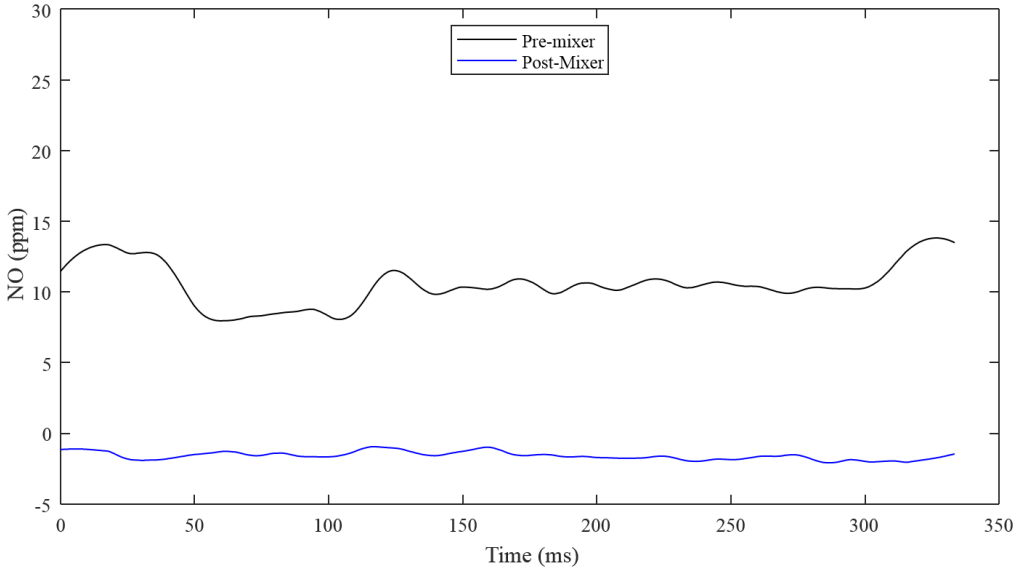

Figure C.10: A comparison of pre and post mixer fast NO_x measurements at a similar engine operating condition.

Appendix D

Daily Checkpoint Data

Prior to conducting any engine tests a industry advisors recommended setting up a common engine test to be conducted throughout the project. The purpose for this point was two fold. First, it was meant to track and assess the long term performance of the engine. If any undesired physical changes took place such as a shift in spark timing offset or a drift in sensor output repeating a common engine test would identify an issue. Second, it was meant to act as a go/no-go test prior to a test day. If gas composition shifted significantly such that the results of tests could be compared to others a daily checkpoint would identify this before any tests were conducted. The daily checkpoint was divided into engine control inputs and engine outputs. Table D.1 lists the engine variables that were directly controlled during the daily checkpoint and the target value for each variable. Other inputs to the daily checkpoint were not able to be controlled but were monitored. Table D.2 lists these uncontrolled but monitored inputs. The target values listed are the average of all individual (9 daily checkpoints) values collected, and in the third column a signal standard deviation is listed. The engine was operating without EGR during daily checkpoint tests. Given these inputs, engine outputs listed in Table D.3 and Table D.4 were logged to assess day-day and long term engine performance. While tracking these outputs during this work there were no daily checkpoints which exhibited outlying output variables.

Table D.1: Daily checkpoint engine input variables and targets

Variable	Target Value
Engine Speed	1800 rpm
Engine Torque	190 N-m
Stoichiometric Cylinder Spark Timing	-30°aTDC
Dedicated Cylinder Spark Timing	-30°aTDC
Stoichiometric Cylinder Spark Duration	150 μs
Dedicated Cylinder Spark Duration	150 μs
Stoichiometric Cylinder AFR	1.000 lambda
Dedicated Cylinder AFR	1.000 lambda
IMAT	25 °C
IMAP	8.5 psia
EGR Exhaust Temperature (post cooler)	105 °C
Jacket Water Inlet	80 °C
Jacket Water Outlet	87 °C
Throttle Position	50%
Boost Pressure	12 psia

Table D.2: Daily checkpoint engine input variables which were monitored but not controlled.

Variable	Average Value	σ_1
Natural Gas Fuel Temperature	26.4 °C	3.85
Fuel N_2 Mole Fraction	.043 %	0.05
Fuel CH_4 Mole Fraction	83.2%	2.25
Fuel CO_2 Mole Fraction	2.1 %	0.38
Fuel C_2H_6 Mole Fraction	11.8 %	1.92
Fuel C_3H_8 Mole Fraction	2.2 %	0.27
Fuel C_4H_10 (normal) Mole Fraction	0.2 %	0.13
Fuel C_5H_12 (normal) Mole Fraction	0.04 %	0.03
Fuel C_6H_14 (normal) Mole Fraction	0.006 %	0.01
Fuel Methane Number (MWM)	71	1.57
Fuel Heating Value	46625.8 kJ/kg	430.06
Ambient Temperature	70.8 °F	8.5
Ambient Pressure	12.31 psia	0.1
Ambient Humidity	26.9%	8.8

Table D.3: Daily checkpoint engine output data.

Variable	Average Value	σ_1
Natural Gas Flowrate	24.3 lb/hr	0.17
Dedicated Cylinder Exhaust Temperature	742 °C	6.9
Cylinder 2 Exhaust Temperature	704 °C	6.5
Cylinder 3 Exhaust Temperature	707 °C	3.4
Cylinder 4 Exhaust Temperature	696 °C	4.8
Pre Catalyst Temperature	522 °C	13.7
Mid Catalyst Temperature	589 °C	11
Post Catalyst Temperature	534 °C	10.8
CO_2 (Engine out)	9.73%	0.4
CO (Engine out)	1657 ppm	553
O_2 (Engine out)	0.17%	0.6
NO_x (Engine out)	2019 ppm	157
THC (Engine out)	899 ppm	11.7

Table D.4: Daily checkpoint engine output data.

Cylinder 1	Average Value	σ_1
10% Mass Fraction Burned	-3.69 °aTDC	0.46
50% Mass Fraction Burned	11.91 °aTDC	0.70
90% Mass Fraction Burned	30.45 °aTDC	1.20
0-10 Mass Fraction Burned	26.31 CA°	0.46
10-90 Mass Fraction Burned	34.14 CA°	0.83
COV IMEP	1.96%	0.95
COV Peak Cylinder Pressure (PCP)	11.99%	0.96
COV Location of Peak Pressure (LPP)	14.21%	0.37
Average PCP	340.53 psia	7.29
Cylinder 3	Average Value	σ_1
10% Mass Fraction Burned	-1.02 °aTDC	0.52
50% Mass Fraction Burned	16.58 °aTDC	0.49
90% Mass Fraction Burned	37.31 °aTDC	0.63
0-10 Mass Fraction Burned	28.98 CA°	0.52
10-90 Mass Fraction Burned	38.34 CA°	0.65
COV IMEP	2.70%	1.09
COV Peak Cylinder Pressure (PCP)	11.60%	0.58
COV Location of Peak Pressure (LPP)	14.95%	0.69
Average PCP	292.80 psia	3.06
Cylinder 4	Average Value	σ_1
10% Mass Fraction Burned	-3.29 °aTDC	1.06
50% Mass Fraction Burned	10.88 °aTDC	1.37
90% Mass Fraction Burned	27.81 °aTDC	1.45
0-10 Mass Fraction Burned	26.71 CA°	1.06
10-90 Mass Fraction Burned	31.10 CA°	0.54
COV IMEP	1.79%	1.19
COV Peak Cylinder Pressure (PCP)	12.49%	1.79
COV Location of Peak Pressure (LPP)	15.06%	1.83
Average PCP	356.73 psia	14.49
Cylinder 2	Average Value	σ_1
10% Mass Fraction Burned	-2.33 °aTDC	0.66
50% Mass Fraction Burned	12.85 °aTDC	1.12
90% Mass Fraction Burned	31.12 °aTDC	1.50
0-10 Mass Fraction Burned	27.67 CA°	0.66
10-90 Mass Fraction Burned	33.44 CA°	0.91
COV IMEP	2.14%	0.95
COV Peak Cylinder Pressure (PCP)	12.54%	0.66
COV Location of Peak Pressure (LPP)	13.99%	0.46
Average PCP	328.16 psia	11.24

Appendix E

Modified Aramco 2.0 Mechanism

After initially presenting the contents of Chapter 2 at the Western States Section of the Combustion Institute Spring 2018 Meeting the Aramco 2.0 mechanism used was modified to include the extended Zel'dovich chemical mechanism. Thermodynamic, gas transport, and chemistry files were updated. Forward and reverse chemical reactions were added and are described in Equations E.1 - E.6. The constants for each of the reaction rate coefficients of were taken from Chapter 5 in Turns [5].

$$O + N_2 \rightarrow N + NO \tag{E.1}$$

$$N + NO \rightarrow O + N_2 \tag{E.2}$$

$$N + O_2 \rightarrow O + NO \tag{E.3}$$

$$O + NO \rightarrow N + O_2 \tag{E.4}$$

$$N + OH \rightarrow H + NO \tag{E.5}$$

$$H + NO \rightarrow N + OH \tag{E.6}$$

Coefficiencts for thermodynamic properties of the molecules H, OH, N, N_2, O, O_2, and NO were taken from Appendix A, Table 13 in Turns. Gas transport data for the aforementioned molecules was found in the chemical kinetics mechanism GRIMech 3.0 and added to the Aramco 2.0 mechanism.

Appendix F

Dedicated EGR Research at SWRi

Prior to the literature review discussed in Chapter 3, to the authors knowledge there was no published research on the topic of dedicated EGR as applied to a multi-cylinder natural gas engine. However, in April of 2019 a publication by Southwest Research Institute researchers Robbie Mitchell and Michael Kocsis investigated the performance of dedicated EGR on a 12 L natural gas engine [24]. The experimental setup was similar to that presented in this work with the exception that two of six cylinder were modified to be dedicated cylinders for a 33%nominal EGR rate. The combustion recipe included a turbulent combustion chamber and a dual coil ignition system. Fuel composition was made up of 84.2% methane, 15%, and small amounts of propane for a methane number of 72.7. An similar EGR mixer was used and the engine and dedicated cylinder fuel delivery was the same as done in this dissertation work. The goal of this work was to show a improvement in engine efficiency using dedicated EGR. An engine speed and torque sweep that included idle and peak torque operating points was done to evaluate baseline engine performance. Using dedicated EGR improved 10-90% burn duration was not realized by increasing the amount of additional fuel added to the dedicated cylinders. The authors commented that since there was no improvement in burn rates from partial oxidation combustion products combustion duration was governed by in-cylinder turbulence. Higher engine loads tolerated EGR better than lower loads and at engine speeds near 1800 rpm all cylinders showed poor cylinder COV of IMEP. Issues with dedicated cylinder combustion stability were common. Conclusions from the author were first, that compression ratio of this engine could increase with dedicated EGR and second, that further investigation into dedicated EGR is needed with while making changes to the combustion chamber piston squish, ignition systems, and turbocharger.